WARWICK
THE UNIVERSITY OF WARWICK

A Thesis Submitted for the Degree of PhD at the University of Warwick

Permanent WRAP URL:
http://wrap.warwick.ac.uk/158722

Copyright and reuse:
This thesis is made available online and is protected by original copyright.
Please scroll down to view the document itself.
Please refer to the repository record for this item for information to help you to cite it.
Our policy information is available from the repository home page.

For more information, please contact the WRAP Team at: wrap@warwick.ac.uk

warwick.ac.uk/lib-publications

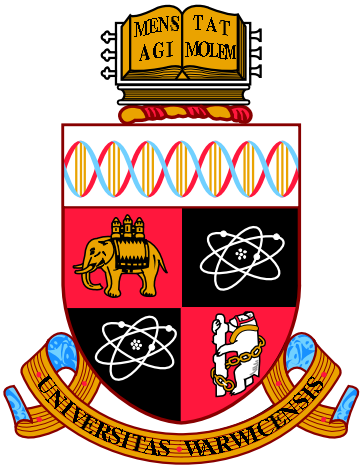

The Topology and Geometry of Liquid Crystals

by

Joseph Pollard

Thesis

Submitted to the University of Warwick

for the degree of

Doctor of Philosophy

Mathematics for Real World Systems CDT

December 2020

Contents

Acknowledgments

I would like to thank my supervisor Gareth Alexander for an enormous amount of guidance and support, and for putting up with me for three years. Over the years I have had many helpful discussions with my fellow PhD students Jack Binysh and Alex Houston, thanks to both of you. The fifth chapter of this thesis is a the result of collaborative work with Jack—many thanks for being such a pleasure to work with. I would also like to thank Robert MacKay and Randy Kamien for agreeing to be my examiners, and for their helpful suggestions.

Declarations

This thesis is submitted to the University of Warwick in support of my application for the degree of Doctor of Philosophy. It has been composed by myself and has not been submitted in any previous application for any degree. Parts of the material in this thesis have been published as follows:

1. Chapter 5 has been published as [BPA20].
2. Chapter 7 has been published as [PPČ+19].

Material from chapters 4, 6, 8, and 9 is being prepared for publication.

Abstract

Liquid crystals are materials that exhibit a number of fascinating properties, many of which have a geometric and topological flavour. Our understanding of liquid crystals often comes through the study of their topological defects, which has inspired new concepts of structural organization in soft matter. Topological and geometric methods have been fundamental to these developments. Today it is impossible to imagine any direction of the science of liquid crystals that does not actively use the concepts of topological defects: they play an essential role in fundamental theory and descriptions of such materials, and also underpin the promising new applications.

Varieties of liquid crystal with additional geometric structure are at the forefront of new applications. These materials include the chiral nematics, or cholesterics, and also the more recently discovered twist-bend nematics. It is known that chirality especially brings enormous richness, allowing for a wealth of new metastable states and textures. The defects in these classes of material have more structure than those in standard nematics, and include not just defects in the director, but defects in other directions associated to the director which nonetheless have a fundamental structural importance; these are the familiar lambda lines of cholesterics, and the beta lines in twist-bend materials which I describe for the first time. Despite their importance, defects in cholesteric materials are still poorly understood.

In this thesis I develop a theory of point and line defects in cholesterics using the mathematics of contact topology. I classify the structure of point defects by using singularity theory and contact topology; the classification shows a very good correspondence with experimental observations. Hedgehog point defects, ubiquitous in standard nematics, are energetically disfavoured in cholesterics due to being incompatibile with a single handedness. The same constraint applies to the boundary of a droplet with normal anchoring, which results in topologically-protected regions of reversed handedness in the boundary region. These 'twist solitons' are a novel type of topological defect in cholesterics, identified and studied here for the first time. This theory is applied to recent experiments to explain the stability of the novel structures observed in spherical cholesteric droplets. Additional textures with complex layered structures are examined from the perspective of contact topology. Convex surface theory aids visualisation of layered structures as well as helping to describe their properties. I give an overview of the structures that may occur based

on their layer topology, achieving a good correspondence with experiment.

Disclinations in cholesterics are studied using contact topology, and a full classification up to homotopy is obtained. The dichotomy between tight and overtwisted structures manifests itself in an interesting way for disclinations: the tight disclinations are exactly those not attached to positive strength lambda lines. While the overtwisted lines admit no new invariants, for these tight lines I identify a novel topological invariant, which has the form of a self-linking number. Orientable singular lines can be removed in a standard nematic, but the classification shows obstructions to doing this in a cholesteric which I use to explain certain experimentally-observed textures. This observation also leads to an experimentally-accessible method for generating metastable twist solitons in the bulk, as well as suggesting a novel method for generating Hopf solitons.

The topological invariants of nematics can be related to the zeros of a vector field orthogonal to the director. Using this approach, I study Hopf solitons in cholesteric droplets using the lambda lines, a novel perspective. The bend distortion of the director is a vector field that is always orthogonal to it; its zeros, the beta lines, have fundamental importance in the twist-bend nematic phase. I produce the first topological and geometric study of this phase, identifying various textures and defects, including Skyrmions, screw dislocations, and focal conics, by the structure of their beta lines. Hopf solitons in twist-bend materials appear not be stable; fundamental results in contact topological give insight into their process of removal, as well demonstrating that they are replaced with a twist soliton.

Finally, I develop a geometric theory of directors using Cartan's method of moving frames. As well as giving new insight into the director distortions and the relationships between them, this allows us to study the problem of reconstructing a director from its gradients, which has previously been solved in two dimensions but not three dimensions. This approach demonstrates the connection between directors and Lie theory, and suggests a description of directors in terms of their local symmetry groups.

Chapter 1

Liquid Crystals, Defects, and Topology

The term 'liquid crystals' encompasses a range of soft materials comprised of disk-like or rod-like molecules that exhibit a phase of matter with properties between those of liquid and a crystalline solid. Liquid crystals are soft and flow like a fluid, however they are not isotropic, but rather have a long range orientational order and exhibit elastic distortions that are analogous to those of a crystal when examined through under cross polarisers. There are several different mesophases of rod-like materials: the nematic phase is the most basic, however there also exist layered phases (smectics), chiral phases (cholesterics), and the twist-bend phases of banana-shaped molecules, each with their own rich set of behaviours with a geometric and topological flavour. The common feature of all these mesophases is the creation of long-range orientational order due to the alignment of the molecules along their long axes. A theoretical description of the material coarse-grains this picture by introducing a unit magnitude line field, the director, defined by the average local molecular alignment. This description places liquid crystals into a general class of materials known as ordered media, which also includes ferromagnets and superfluids.

Many liquid crystalline materials are optically active, with the image of a texture under cross polarisers determined by the orientation of the molecules. Optical microscopy reveals a wide array of colourful textures, fingerprint whorls, polarisations brushstrokes and confocal conics; all reflect the internal topological structure of the material. Liquid crystals offer a versatile setting for studying topological phenomena, often with relevance across multiple disciplines, including cosmological strings [CDTY91], biological tissues and morphogenesis [S$^+$91; Bou08], and magnetic Skyrmion textures [NFO$^+$17; AS17; MA16b].

The chiral phases of liquid crystals allow for the stabilisation of more interesting structures than those that occur in simple nematics, such as Hopfions and torons [AS16; AS17], and constellations of topological defects [PČM17; Pos18c]. The topological description of specifically chiral phases is lacking. There is a branch of mathematics, contact topology [Gei08], that deals with chiral structures. Using this language, we can study cholesteric liquid crystals from a topological perspective. We will see how structures in chiral liquid crystals also illustrate the beautiful mathematics of contact topology; this results in a back-and-forth between theory and applications, where the mathematical tools allow us to broaden our knowledge of the physics of these systems, and the physics in turn illustrates and enriches our understanding of the mathematics.

1.1 Topological Description of Ordered Media

The mathematical description of ordered media was given by Toulouse & Kléman in [TK76]; I will briefly review this theory and explain the problems that arise when trying to apply it to cholesterics, which will be partially addressed in later chapters. Many of the fundamental concepts explored in this thesis can be applied to other types of ordered media besides liquid crystals, most notably ferromagnets.

The ordered medium lives inside a physical domain M, a manifold, and there is also a manifold of internal states V, an abstract space that describes all possible values that the ordering may take. For physical systems M a surface in two dimensions, and a subset of Euclidean space (possibly with boundary) in three dimensions. The manifold V may in principle have any dimension, may not be connected, and may even fail to be orientable, depending on the order parameter. The medium itself is then described by a map $\Phi : M \to V$ that associates to each point in physical space the value of the order parameter at that point. For most systems we encounter in the real world it makes sense to demand something more of this map, for instance that it be smooth. For discussing certain systems, like cholesteric liquid crystals, it is also helpful to impose constraints on the gradients of the map.

Some examples help to fix ideas. At each point the ordering of a superfluid is given by a complex scalar, and it is therefore described by a smooth map $\psi : M \to \mathbb{C}$, the wave function. In some cases one may regard the wavefunction as having a fixed amplitude but arbitrary phase, so that the order parameter is really a map $\psi : M \to S^1$. At each point of a ferromagnetic material the magnetic moment can be described by a unit vector. Consequently, the magnetic ordering is described by

a map $\mathbf{m} : M \to S^2$, the magnetisation. Using the Euclidean metric we identify this with a section of the unit tangent bundle, a unit vector field. A liquid crystal is comprised of rod-like molecules can be described by a line at each point in space that gives the average orientation of the molecules, and thus is described by a map $\mathbf{n} : M \to \mathbb{RP}^2$; if it is possible to orient the rods, then the description is the same as a ferromagnet.

1.1.1 Topological Invariants

It is important to discuss situations where two different configurations of the order parameter are equivalent, e.g. if they are related by a global translation or rotation. For elastic materials like liquid crystals, it is natural to say that two different configurations Φ_0, Φ_1 of the ordered medium are equivalent if there exists a family $\Phi_t : M \to V$ of maps depending continuously[1] on a parameter t connecting them. Such a family is called a *homotopy*, and if such a family exists, the maps Φ_0, Φ_1 are called *homotopic*. When there is a fixed boundary condition, we call directors equivalent if they are *homotopic 'rel. boundary'*, i.e., there is a homotopy that leaves the boundary fixed. The space of homotopy classes of maps $M \to V$ is denoted $[M, V]$. Any quantities preserved by homotopy are called *topological invariants*, and they represent global features of the texture. A full set of topological invariants for the order parameter is equivalent to a complete specification of the set $\pi_0([M, V])$ of connected components of $[M, V]$[2]. It may also be interesting to determine if there are essentially different paths the material can take between configurations, which corresponds to a description of the fundamental group $\pi_1([M, V])$; I will not discuss this in this thesis.

Describing the full set of topological invariants is an important problem, as is identifying those invariants with physical structures and, if possible, energetics. For simple nematic liquid crystals the set of topological invariants is known and admits a description in terms of distortions of the director, see Chapter 2.

1.1.2 Defects

Classically a *defect* is a point where the order parameter map $\Phi : M \to V$ is undefined. The topology of M and the boundary conditions on Φ will often impose topological restrictions that imply there must exist at least some defects, and

[1] Or smoothly, or analytically; we will not overly concern ourselves with degrees of differentiability, and indeed for many of the questions we are concerned with it is reasonable to assume everything is analytic.

[2] $\pi_0(M)$ will not always have a group structures, but it does in certain cases, for instance when M is itself a group

changes in the topological invariants will also be mediated by the creation and annihilation of defects. The defects in a material texture are hugely important: they control strength or fragility [Tay34], determine elastic interactions [PSLW97; ŠRŽ+07], mediate self-assembly [MŠT+06; Muš17; WMB+16], and precipitate phase transitions [Abr57; Ber71; KT73; RL88; Kik07]. The widespread influence of defects derives from their high energetic cost, strong elastic distortions, and topological nature. This is especially true in liquid crystal materials, whose defects have often offered key insights and motivated the naming of textures.

In order to study the structure of defects, one measures the winding of the order parameter around an appropriately chosen contour that encloses the defect. Generally defects occur at points or along lines. For a line defect in three dimensions, we choose a closed curve surrounding the line and no other line defects; for a point defect, we choose a sphere surrounding the point and no other defects. Restricting the order parameter Φ to the given contour results in a map $S^1 \to V$ in the case of a line-like defect, and a map $S^2 \to V$ in the case of a point-like defect. Such maps are classified, up to a continuous deformation, by the homotopy groups $\pi_1(V), \pi_2(V)$ of the manifold of internal states. For example, for a simple vector field in three dimensions, where $V \cong S^2$, we have $\pi_1(V) = 0, \pi_2(V) = \mathbb{Z}$. The interpretation is that line defects will not occur, since they may be removed by 'escaping' along the line, replacing it with a closed orbit, while point defects may occur and are classified by an integer charge (although subtleties arise in chiral systems, see Chapter 8).

Arguably one should be more careful in the case of line defects, and use a torus surrounding the line to measure the winding along the line as well as around it. Using this method, the types of defects are given by homotopy classes of maps $T^2 \to V$. In particular we have $[T^2, S^2] \cong \mathbb{Z}$, so that directors that are fully orientable around the singularity line are classified by an integer, the winding around the singular line. As mentioned in the previous paragraph, these do not occur as stable defects. The class $[T^2, \mathbb{RP}^2]$ is more difficult to describe. Suppose we are given a map $f : T^2 \to \mathbb{RP}^2$, and assume that the map is nonorientable along a meridian, which is the relevant case for disclination. For this restricted class of maps, $[T^2, \mathbb{RP}^2]$ is isomorphic, as a set, to $\mathbb{Z}_4$ [Jän87]. I will review this work in more detail in Chapter 8. Note that the torus does not detect the ability to 'escape' along the line in the way the circle does. If we have an orientable line singularity of winding k and escape along it, we simply replace it with a closed orbit of 'winding' k, so that the homotopy class of the vector field on the surrounding torus is still locally determined by k. This is in fact detecting defects that are not in the director, but in any vector field orthogonal to the director. I will return to this idea in Chapter

2, and also Chapters 8 and 9 from the perspective of chiral liquid crystals.

The computation of the fundamental groups of V is easier when V is specified in terms of groups of continuous deformations that can act on the ordered medium. Suppose there is a Lie group $\mathcal{G}$ acting transitively on the order parameter space: that is, for any pair of elements v_1, v_2, there exists $g \in \mathcal{G}$ such that $g \cdot v_1 = v_2$, where $\cdot$ denotes the action. For any fixed value v_0 of the order parameter, there is a Lie subgroup $\mathcal{H}$ of $\mathcal{G}$ that fixes v_0. Call v_0 the *reference parameter*. We can then identify V with the quotient $\mathcal{G}/\mathcal{H}$ [Mer79]; note that $\mathcal{H}$ need not be a normal subgroup and consequently V need not be a group, but it will be a manifold with the quotient topology. Assuming we know the homotopy groups of $\mathcal{G}, \mathcal{H}$, we can compute the homotopy groups of V using the exact sequence

$$\cdots \to \pi_n(\mathcal{G}) \to \pi_n(V) \to \pi_{n-1}(\mathcal{H}) \to \pi_{n-1}(\mathcal{G}) \to \cdots . \tag{1.1}$$

1.1.3 Broken Symmetry

This approach to studying the topology, and especially the defects, of an ordered medium breaks down when considering ordered media with broken translational symmetry in the ground state. For these materials the structure is not captured by the value of the order parameter at a single point, we require information about the order parameter in at least an open neighbourhood. This problem with the naive generalisation of the theory to materials with broken symmetry has been understood for some time [Mer79], but few attempts have been made to address it.

For example, classically the order parameter for a cholesteric liquid crystal is taken to be an orthonormal frame, so that the symmetry group is $\mathcal{SO}(3)$ and the subgroup $\mathcal{H}$ is the dihedral group D_2, the group of symmetries of a brick [BDP$^+$78a]. Consequently, the quotient V is a space with $\pi_1(V) \cong \mathcal{Q}$ and $\pi_2(V) \cong 0$, where $\mathcal{Q}$ is the discrete quaternion group—this implies that there are no stable points defects in cholesterics. This is technically the case, but also somewhat misleading: point defects in the director are pinned to line defects in one other component of the frame. Moreover, cholesteric liquid crystals admit topological invariants, which have the flavour of a 'layer number' and exist purely as a consequence of their chirality and do not exist for standard nematics. This is not captured by the homotopy theory. For a second example, the requirement that the layers of two-dimensional smectic system be equally spaced implies that defects of winding larger than $+1$ cannot occur [Po1; CAK09], a fact that also cannot be determined through the standard homotopy theory alone. Similar complexities exist in three-dimensions [MAHK19].

Furthermore, when the material is biaxial, admitting physically-meaningful

directions different from the director but coupled to it, then the theory of homotopies through the director does not take these additional axes into account. This occurs in cholesterics, where the pitch axis defines an additional direction which we cannot manipulate independently from the director. It is possible that two configurations are related by a homotopy that does not create additional defects in the director, but not a homotopy that does not create additional defects in the other axes. This situation is of fundamental importance when trying to relate topology to energetics and fundamental physics in liquid crystal systems: creating defects in the pitch axis costs energy and also changes the texture in ways that are clearly observable in experiment.

The majority of this thesis is devoted to a more advanced topological and geometric description of such nematic materials, their invariants, and their defects.

1.2 The Physics of Liquid Crystals

In a continuum theory of a liquid crystal, we describe the material at each point in space by a line, which physically represents the average orientation of the molecules at that point. Consequently, the order parameter is a map $M \to \mathbb{RP}^2$ to the projective plane. Whenever the texture is orientable, meaning we can consistently assign an arrowhead to each line segment so that the resulting vector field is continuous, then we can instead describe the material by a unit vector field, equivalently a map $M \to S^2$. We call this vector field the *director*, and denote it by $\mathbf{n}$. In this thesis I will predominantly consider orientable textures, and thus adopt the description that uses the director rather than the Q tensor approach, an alternative method for describing general directors using a tensor $Q = \mathbf{n} \otimes \mathbf{n} - \frac{1}{3}I$. The topological tools that I will be using work in both cases, and I will make comments along the way as to the adaptions that must be made for nonorientable directors.

Defects in the director are places where the vector field $\mathbf{n}$ is undefined. It will often be convenient to write $\mathbf{n} = \mathbf{m}/\|\mathbf{m}\|$, for $\mathbf{m}$ a vector field (whose norm we do not control) which has zeros at the defect points. This approach makes it far easier to describe the local structure of the defects that can occur. The topology of $\mathbf{m}$ is the same as that of $\mathbf{n}$, however the gradients will of course be different.

The energy of a liquid crystal director is an elastic energy defined in terms of distortions away from a uniform state. Geometric elastic distortions pervade soft matter physics [Kam02], providing a common conceptual framework for understanding many different materials as well as numerous methods—including boundary conditions, substrate topography and surface curvature—for designing or con-

trolling properties and functionality [VI13; TLB+16; NV12; MVP+15; VAG+18; ENM+18; WB15; MWM17; AXZ+18]. For liquid crystals, the *Oseen–Frank free energy* is [Fra58]

$$E = \frac{1}{2}\int_M K_1(\nabla\cdot\mathbf{n})^2 + K_2(\mathbf{n}\cdot\nabla\times\mathbf{n}+q_0)^2 + K_3\left\|\nabla_{\mathbf{n}}\mathbf{n}\right\|^2 + K_4\nabla\cdot((\nabla\cdot\mathbf{n})\mathbf{n}-\nabla_{\mathbf{n}}\mathbf{n})\mu, \tag{1.2}$$

where M is the material domain, the K_i are elastic constants, q_0 is a constant that sets the handedness/chirality of the material, and μ is the volume form. The distortions that appear in the energy are called the *splay* $\nabla\cdot\mathbf{n}$, the *twist* $\mathbf{n}\cdot\nabla\times\mathbf{n}$, the *bend* $\nabla_{\mathbf{n}}\mathbf{n}$, and the *saddle-splay* $\nabla\cdot((\nabla\cdot\mathbf{n})\mathbf{n}-\nabla_{\mathbf{n}}\mathbf{n})$. See Fig. 1.1 for illustrations of these distortions. By the divergence theorem, the latter contributes to the energy only when M has a boundary. Typically the behaviour of the material at the boundary is prescribed, meaning the contribution is constant. For this reason it is often dropped from the energy functional, however there are valid reasons to keep it in: one can relate it to an additional term that is a bulk contribution [MA16b; Sel18]. In the absence of chirality, $q_0 = 0$, the ground state is given by a uniform director, e.g. $\mathbf{e}_z$, or any constant linear combination of the coordinate directions.

One often considers an approximation where $K_1 = K_2 = K_3$, the one-constant approximation. In this case, with $q_0 = 0$, the energy becomes

$$E = \frac{K}{2}\int_M \left\|\nabla\mathbf{n}\right\|^2\mu, \tag{1.3}$$

whose minimisers are harmonic vector fields. In the general case the energy landscape is not well understood.

A more geometric description of the liquid crystal director is presented by Machon & Alexander [MA16b; Mac16]. Consider a decomposition of the gradient tensor $\nabla\mathbf{n}$ into its irreducible components. There are two parts: the gradients of the director along itself, $\nabla_{\mathbf{n}}\mathbf{n}$, which we have already identified with the bend distortion, and the perpendicular gradients $\nabla_\perp\mathbf{n}$. If we choose a basis for the planes orthogonal to $\mathbf{n}$, this can be expressed as matrix,

$$\nabla_\perp\mathbf{n} = \frac{\nabla\cdot\mathbf{n}}{2}\begin{bmatrix}1 & 0\\ 0 & 1\end{bmatrix} + \frac{\mathbf{n}\cdot\nabla\times\mathbf{n}}{2}\begin{bmatrix}0 & -1\\ 1 & 0\end{bmatrix} + \Delta, \tag{1.4}$$

where the *umbilic tensor* Δ (Selinger calls it the *biaxial splay* [Sel18]) is the traceless, symmetric part, which is related to the saddle-splay. I will expand upon this description in Chapter 4.

Besides the standard nematic phase, there are other types of liquid crystal

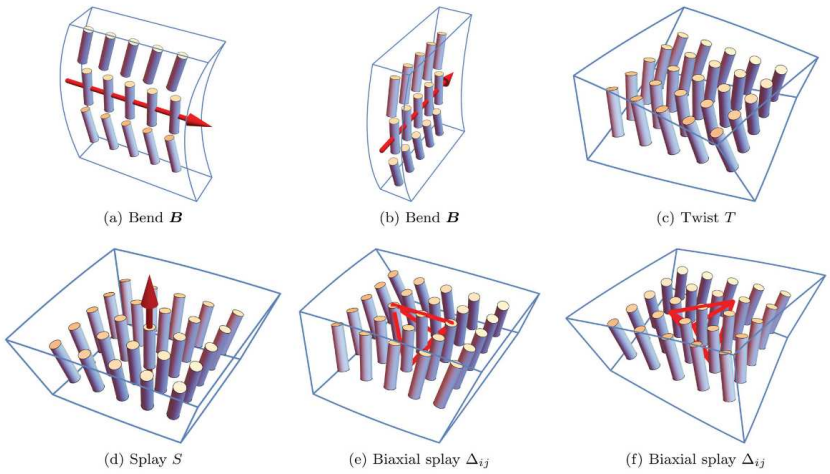

Figure 1.1: Schematic images of the liquid crystal distortions. In each case, the coloured rods represent the director. In (a,b) the red arrow indicates the direction of the bend vector field. Reproduced from [Sel18].

phase where the symmetry of the nematic phase is broken in some fashion. In the smectic phases, there is a broken translational symmetry as the molecules organise themselves into equally-spaced layers, determined by the level sets of a phase field. In a Smectic A material, the director is a small perturbation of the layer normal, while in a Smectic C it makes a constant angle with the layer normal. One may apply the naive generalisation of the defect classification, which suggests, among other things, that point defects in two dimensional smectics are classified by their winding number, a half integer. However, it is easily seen that the requirement that the layers be at a constant separation—something not taken into account by the naive homotopy theory—makes it impossible for defects of winding larger than +1 to occur [Po1]. Further complications arise in three dimensions, where the result of combining pairs of defects is path-dependent [MAHK19]. The homotopy classification of global textures fails as well, as two smectic directors that are homotopic as nematic directors may fail to be homotopic once the requirement of equally-spaced layers is imposed.

The two classes of material with broken symmetry that I will focus on in this thesis are the cholesterics and the twist-bend nematics. The former have been known for quite some time; indeed, the first example of a liquid crystal, discovered in 1888 by Friedrich Reinitzer, was the molecule cholesteryl benzoate, a chiral nematic from which the alternate name derives. A cholesteric is characterised by a nonzero q_0, which then determines a lengthscale $p = 2\pi/q_0$, the pitch. Physically q_0 is the 'chirality' of the material, and this manifests itself as an energetic preferrence

for nonzero twist. This results in cholesterics exibiting very different topology and geometry from standard nematics, leading to a variety of interesting new structures that may form, with the potential for novel applications. Moreover, if one makes the reasonable assumption that the twist is nowhere-zero throughout the material, and would prefer to stay that way, then the cholesteric texture may have additional homotopy invariants not present in a nematic.

We observe that the Frank energy for a cholesteric will be minimised, for any choice of elastic constants, by a unit vector field that is a curl eigenfield, $\nabla \times \mathbf{n} = -q_0\mathbf{n}$, and divergence free, $\nabla \cdot \mathbf{n} = 0$. Such vector fields are called *Beltrami fields*. The unit length Beltrami fields are exhaused by the family

$$\mathbf{n} = \cos(q_0 z)\mathbf{e}_x + \sin(q_0 z)\mathbf{e}_y, \tag{1.5}$$

where q_0 can be any integer, and consequently this director is the ground state of a cholesteric. In constrast to the uniform ground state of a nematic, this has nonzero twist, however the splay and bend do vanish. A consequence of chirality is the existence of an axis along which the twisting occurs, the *pitch axis*, and an associated lengthscale, the distance over which the material undergoes a full 2π rotation. In the cholesteric ground state, the pitch axis is the z-axis. Line defects can occur in this axis as well as the director. Because of the relationship between the pitch and the optical properties of the material, it is possible to see these lines in experiment. For a general texture, the pitch axis can be defined using the decomposition (1.4); it is the direction corresponding to the largest magnitude eigenvector of the tensor $\chi = J \circ \nabla_\perp \mathbf{n}$, where $J = \mathbf{n}\times$ is the tensor describing rotations around the director [BMČ$^+$14; EI14].

The standard homotopy classification of defects fails to fully describe the situation for cholesterics, largely due to the coupling between the director $\mathbf{n}$ and pitch axis $\mathbf{p}$. Following the prescription outlined in §1.1.2, one arrives at the quaternion group $\mathcal{Q}$ as the (non-abelian) fundamental group of the order parameter space [Mer79]. This group is generated by eight elements, $1, -1, i, -i, j, -j, k, -k$. The element 1 corresponds to corresponds to a singular line that can be removed by a small perturbation of the director, a χ line, which will replace with with a defect of type -1, a λ line (a defect in the pitch axis where the director is nonsingular) with integer winding. The elements i, j, k correspond to defects in a single one of of the axes $\mathbf{n}$, $\mathbf{p}$, and $\mathbf{n} \times \mathbf{p}$ while the other two are nonsingular, with the singular axis being such that it is nonorientable along a loop around the singularity. We adopt the convention that i denotes a disclination line, a defect in the director,

and j denotes a λ line with winding $\pm\frac{1}{2}$. I will sometimes label these lines with a half-integer describing the strength of the singularity, e.g. χ^{+1} denotes a singularity in the director with winding $+1$, while $\lambda^{-1/2}$ denotes a singularity in the pitch axis with winding $-\frac{1}{2}$.

The second homotopy group of the order parameter space is trivial, suggesting that there should be no stable point defects in a cholesteric. This is misleading: point defects in the *director* can occur, however there will be line defects (λ lines) in the pitch axis associated with them, so that overall there cannot be a point defect in the frame we have used to describe the material. In this thesis I will focus on the results of experiments by the Ljubjana group [PČM16; PČM17; Pos18c], which reveal a wealth of interesting defect structures in cholesteric droplets, including point defects of charge (winding) -2 and -3 that we would not expect to find in a standard nematic for energetic reasons. Much of the theoretical work in this thesis arises from an attempt to understand the various features of these droplets.

The cholesteric liquid crystal is similar in many ways to a chiral ferromagnet subject to the Dzyaloshinskii-Moriya interaction [Dzy58; Mor60], a system also described by the Hamiltonian (1.2) in the one-constant approximation with $q_0 \neq 0$, except the order parameter really is a vector field and not a line field, so that line defects do not occur. Consequently the topological and geometric theory developed here carries over to these magnetic systems. Indeed, since most of the numerical simulations are carried out using a vector field for the director and in the one-constant approximation, it's reasonable to expect that all the metastable structures explored in these thesis could be realised in the magnetic system as well. There are further connections to Beltrami fields that will be explored a little more in Chapters 3, 6, and 10.

Liquid crystals comprised of 'bent-core' molecules are a more recent discovery, and have been the subject of a flurry of experimental and theoretical work, see the review article [JLS18]. Informally speaking, these are materials with an energetic preference for a nonzero bend deformation, which in turn results in either a nonzero splay or nonzero twist deformation. Materials shaped like pizza wedges or peardrops have a preference for the splay-bend mode, while materials shaped like bananas have a preference for the twist-bend mode—the latter give rise to the twist-bend phase, and we call them twist-bend nematics. The latter differ from cholesterics in that they have no particular preference for either left-handed or right-handed twisting. The Oseen–Frank energy can be used to give a continuum theory of twist-bend materials by taking the bend elastic constant K_3 to be negative [Doz01]. An alternative describe employs a second vector field, the polarisation, which prefers to align with

the bend. I employ the latter, which I will discuss further in Chapter 5, as it is closer in spirit to the topological methods.

1.3 A Note on Numerics and Visualisation

To illustrate the constructions and ideas presented in this thesis, I have provided a large number of images from numerical simulations. I will briefly explain how these computations are carried out. All simulations were performed using gradient descent, and do not account for any hydrodynamics of the material. The material domain is a rectangular grid with constant lattice spacing. The derivatives of $\mathbf{n}$ are computed using a finite difference method, which is used to compute the molecular field. All simulations use a one-constant approximation, so the molecular field is

$$\frac{\delta E}{\delta \mathbf{n}} = \frac{K}{2}\left(\nabla^2 \mathbf{n} - 2q_0 \nabla \times \mathbf{n}\right), \tag{1.6}$$

as is obtained by computing the first variation of (1.2). The update step is $\mathbf{n}_t = \mathbf{n}_{t-1} + (\partial_t \mathbf{n}_{t-1}^{\perp})dt$, where dt is a constant timestep and the superscript $\perp$ denotes the removal of the component of the molecular field along the direction $\mathbf{n}_{t-1}$. Typically the timestep is $dt = 1.0$. In the case of twist-bend nematics I use a different energy functional—see Chapter 5—but the numerical approach is otherwise identical. Only in Chapter 9 do I employ the Q tensor approach in order to simulate cholesteric directors with disclination lines, impossible using a director field; the implementation of the numerical method is largely the same.

For simulations in a domain with boundary, for example a spherical droplet, normal anchoring on the boundary is imposed by applying mask to the molecular field, setting it 0 in any cell that lies outside the desired domain. For planar anchoring, we instead remove any component of the molcular field that points along the normal to the boundary. Although crude, this method results in numerical simulations that are sufficiently accurate for illustrating topological concepts, as evidenced by the good correspondence between simulatons and experiment shown in Chapters 7 and 9.

The output from the code is the director, as well as various quantities like the twist and bend that are derived from it. All visualisation of these quantities is done in Paraview [AGL05]. Three-dimensional visualisation of liquid crystal directors is not always easy, but various techniques have been developed for doing so, and I make use of many of them here. One method is to plot a Pontryagin–Thom surface—see Chapter 2—where one component of the director is fixed. The surface is coloured

according to the angle between the remaining two components, resulting in brush stroke patterns similar to those that can be imaged experimentally by exploiting the optical anisotropy of the material. In Chapter 3 I introduce some additional techniques for visualising the topological content of the director based on the theory of characteristic foliations and convex surfaces from contact geometry, and I also use these methods for visualisation in later chapters, as they give a good illustration of the layer structure of a material.

The director can be plotted on 2D slices, along with other scalar quantities such as the twist or the saddle-splay. For several applicayions we examine the zero sets of the bend or Δ—see Chapter 2 and 5 for a discussion of why this is useful—which is done by computing the norm and then plotting a surface where this is small, equal to some $0 < \epsilon \ll 1$. This often results in some strangely-shaped surfaces, so I have often made use of Paraview's line object to show the position of one of the zero lines when the contour would otherwise be unsuitable.

Chapter 2

Homotopy Invariants of Nematic Materials

2.1 Introduction

One of the fundamental problems in ordered media is the classification of mappings $\Phi : M \to V$ from the physical domain M into the order parameter space V up to an appropriate notion of equivalence. For a standard orientable liquid crystal director, i.e. a director describing a texture without disclination lines, the ordering is a mapping $\Phi : M \to S^{n-1}$, where $n = 2, 3$ is the dimension of space, and two liquid crystal directors are considered equivalent if they can be brought into alignment by means of a continuous deformation of the material, a homotopy of the director.

In three dimensions, unit vector fields, maps into S^2, and fields of planes can all be identified by using a Riemannian metric—a unit vector field picks out, at each point of space, a point on S^2, and also defines a smoothly varying collection of orthogonal planes. I will use the description of the director as a plane field extensively throughout this thesis.

In this section I will explain the homotopy classification of plane fields on closed 3-manifolds and on 3-manifolds with boundary. Using the obvious duality between plane fields and unit vector fields, we arrive at the homotopy invariants of nematic liquid crystal directors without defects. This is standard theory. My primary references are Geiges [Gei08] and Gompf and Stipsicz [GS99]. My aim is to present the classification in a general way, and then specialise to a concrete description that can be used in practice. A key observation is that these invariants can be expressed in terms of the zero link of a vector field everywhere orthogonal to the director, and consequently can be tied to physical objects which play a role

in energetics and can, at least in the case of λ lines, be seen in an experiment. I will also describe how this is extended to directors with some fixed defect set, and review the description of homotopy classes of nematic directors with disclination lines given by T. Machon [MA16a].

Breaking the symmetry of the nematic phase doesn't just affect the possible defects, but may also result in further homotopy invariants not accounted for by the theory of this chapter. This is the case for cholesteric liquid crystals, where the additional invariants take the form of a 'layer number' as explained in Chapter 3, for smectics [Po1], and for twist-bend nematics, Chapter 5.

2.2 Plane Fields

A *plane field* ξ on a 3-manifold M is a codimension 1 subbundle of the tangent bundle, that is, a choice of a plane $\xi_p \subset T_pM$ for each $p \in M$ such that the resulting field of planes varies smoothly. An orientable codimension 1 subbundle of the tangent bundle can be defined by a single partial differential equation. This equation is encoded by a differential 1-form η, a section of the cotangent bundle T_p^*M, and the plane field is its kernel $\xi = \{\eta = 0\}$. A Riemannian metric g on M allows us to identify sections of the tangent bundle, vector fields, with sections of the cotangent bundle, differential 1-forms. Given a vector field X, the corresponding 1-form is defined by the interior product $\omega = \iota_X g$, so that for any other vector field Y, $\omega(Y) = g(X, Y)$. Therefore, the sections of the plane field defined to be the kernel of ω are exactly those vector fields orthogonal to X.

We can identify a liquid crystal director $\mathbf{n}$ with a unit 1-form η using the Euclidean metric. The plane field ξ defined by η is the set of planes orthogonal to the director; in particular, we can define the plane field when the director is not orientable, but we will only be able to choose a defining 1-form locally, in the same way that we would only be able to define a local director. The description in terms of 1-forms and plane fields is then equivalent. We could even write the Frank energy using a 1-form,

$$E = \int_M \frac{K_1}{2}(\delta\eta)^2 + \frac{K_2}{2}(\star\eta \wedge d\eta + q_0)^2 + \frac{K_3}{2}\left\|\iota_{\mathbf{n}} d\eta\right\|^2 \mu, \tag{2.1}$$

although we gain nothing new from doing this. In general, it is easier to use the director field picture for visualisations and simulations while using the plane field picture for proofs and constructions. I will use them interchangably throughout this thesis.

Figure 2.1: An illustration of the plane field ξ associated to a director $\mathbf{n}$. (a) At each point, ξ is defined to be the orthogonal plane (grey) to the director (blue). $\mathbf{n}$ and ξ are shown for (b) the cholesteric ground state, and (c) a double-twist cylinder, whose axis is indicated by the green line.

Locally we can choose a right-handed basis $\mathbf{e}_1, \mathbf{e}_2$ of unit vector fields for the planes of ξ. The triple $\mathbf{e}_1, \mathbf{e}_2, \mathbf{e}_3 = \mathbf{n}$ is called a *distortion frame* for the director, as we can express the gradients of $\mathbf{n}$ in terms of quantities derived from the frame—this is described in more detail in Chapter 4. A distortion frame is evidently not unique, as we can rotate the pair $\mathbf{e}_1, \mathbf{e}_2$ around the director by any (perhaps spatially varying) angle θ to obtain another distortion frame. Generally we cannot choose a global distortion frame, and indeed the failure for a local frame to extend globally is related to a topological invariant of the plane field, discussed in the next section.

2.3 The Invariants Via Obstruction Theory

The earliest description of the homotopy classes of plane fields is via obstruction theory. By fundamental results in differential topology, every 3-manifold M can be viewed as a cell complex X. Given a pair of orientable plane fields ξ_0, ξ_1, we can always arrange for them to be homotopic over the 1-skeleton of this complex. By elementary obstruction theory, we have an obstruction $d^2(\xi_0, \xi_1) \in H^2(M, \pi_2(S^2)) \cong H^2(M, \mathbb{Z})$ to extending this homotopy over the 2-skeleton. Should this obstruction vanish, there is a further obstruction, $d^3(\xi_0, \xi_1) \in H^3(M, \pi_3(S^2)) \cong H^3(M, \mathbb{Z}) \cong \mathbb{Z}$, to extending it over the 3-skeleton. The classification of nonorientable plane fields is achieved by a similar approach, replacing S^2 with $\mathbb{RP}^2$. There are two cases to examine, although they are very similar. The first case is closed 3-manifolds, such as T^3 and S^3. For physical purposes the second case, where M is compact with boundary, is probably more important.

In liquid crystal theory it is more common to view these invariants through the lens of homotopy theory. I adopt the language of cohomology here for several reasons. Firstly, it often helps our understanding to see slightly different takes

on familiar problems, as it provides a new perspective. Secondly, the language of cohomology extends naturally to discuss more subtle invariants of vector fields and their closed orbits, for instance Morse–Novikov theory [Far03], Seiburg–Witten theory, and the Floer theories that have been employed to great effect in the study of 4-manifolds and plane fields with additional structure. Although I will not discuss these ideas further in this thesis, they have evident application to physical problems and can certainly be applied to the study of ordered media, and may be the subject of future work.

2.3.1 Closed Manifolds

The simplest way to compute the invariants of a plane field on a closed 3-manifold M is as follows. It is a classical result that the tangent bundle TM is trivial. Fix some trivialisation, which may come from a choice of orthonormal frame if a Riemannian metric is specified. Using a Riemannian metric, it is clear we can identify homotopy classes of plane fields ξ with homotopy classes of unit vector fields $\mathbf{n}$, the normal to the plane field. A unit vector field picks out, for every point in M, a point on the 2-sphere; consequently, we can identify homotopy classes of unit vector fields with maps $f : M \to S^2$ such that $\xi \cong f^*(TS^2)$. The standard homotopy-theoretic approach of classifying these maps involves looking at the homotopy groups $\pi_k(S^2), k > 0$. I adopt an alternative approach here, and relate the homotopy classes of maps into S^2 to the cohomology of M (with coefficients in the homotopy groups $\pi_k(S^2)$) via the following classic construction.

Theorem 2.1. *(Pontryagin–Thom Construction [Tho54; Pon55]) Homotopy classes of maps $f : M \to S^2$ are in a one-to-one correspondence with cobordism classes of framed links.*

For a full proof see [Mil65]. To understand this result, it is worth explaining at least part of the correspondence. Suppose we are given a map f. Choose a regular point p and a positively oriented basis $\mathfrak{b}$ of T_pS^2. The preimage of p is a link L in M, and the pullback of $\mathfrak{b}$ along f endows this link with a framing. Conversely, suppose we are given a framed link L. We can use the framing to trivialise a neighbourhood $N(L)$ of L as $N(L) \cong D^2 \times S^1$. Pick a point p on the sphere and let p^* denote the antipodal point. We construct a map f as follows: project the disk bundle onto the disk $S^2 - p^*$, where $0 \in D^2$ is identified with p, and extend f over the rest of M by mapping all of $M - N(L)$ to p^*.

Throughout this thesis I will give visualisations of directors based on Pontryagin–Thom (hereafter, PT) surfaces [CAA$^+$13; Ale18]. This involves plotting the set,

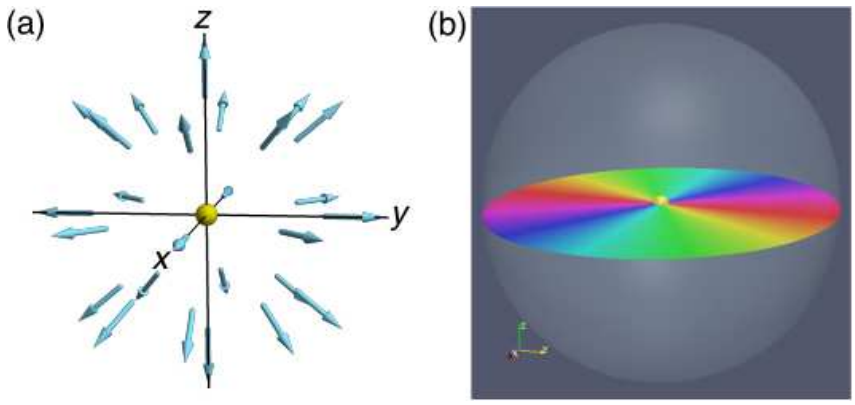

Figure 2.2: (a) Schematic director field of a radial point defect (yellow sphere). (b) Visualisation using the Pontryagin–Thom construction. The surface is the set of points where $n_z = 0$, coloured by the horizontal orientation. There are two full colour windings around the central point defect (yellow sphere) because of the apolar symmetry of nematics.

generically a surface, where one component of the director vanishes. The surface can then be coloured according to the angle between the remaining two components of the director. For example, in Fig. 2.2 we have a visualisation of a radial director $\mathbf{n} = \mathbf{e}_r$ in the sphere. Defects in the director will appear as points where the colouring is undefined. The brushes of colour wind around the defect point, whose topological charge is given by the number of full 2π windings.

Let $[L_\xi] \in H_1(M, \mathbb{Z})$ be the cobordism class of framed links corresponding to a plane field ξ. Then $d^2(\xi_0, \xi_1) = \mathcal{PD}[L_{\xi_0}] - \mathcal{PD}[L_{\xi_1}]$, where $\mathcal{PD}$ denotes the Poincaré duality $\mathcal{PD} : H_p(M, \mathbb{Z}) \to H^{3-p}(M, \mathbb{Z})$ between homology and cohomology. Moreover, we can write this as $d^2(\xi_0, \xi_1) = \frac{1}{2}(e(\xi_0) - e(\xi_1))$, where $e \in H^2(M, \mathbb{Z})$ denotes the Euler class of the vector bundle. The standard technical definition of the Euler class can be found in Bott & Tu [BT82], and I will give an equivalent definition in the next section which is more helpful to us in practice.

The manifolds we will be concerned with in practice have $H_1(M, \mathbb{Z}) \cong \mathbb{Z}^n$ for some n, and so the Euler class will be a tuple of integers representing how much 'charge' is carried by each of the generators of the first homology group. For example, suppose we have a triply-periodic director structure, which we can consequently assume lies in T^3. Let L be the preimage of some point on the sphere, with some framing. Then $L \in \pi_1(T^3) \cong \mathbb{Z}^3$. Components of L that are nullhomotopic do not count towards the Euler class. The remaining components are homotopic to either the x, y, or z axes. The framing assigns an integer to each component. The sum of these integers for, say, those components homotopic to the x axis gives the first

component in the tuple that represents the Euler class.

Initially this appears to be the whole story, however there is a subtlety. The description relies on the choice of trivialisation. It remains to understand this dependence, which leads us to an essentially three-dimensional obstruction. Firstly, recall the classical theorem that a homotopy class of maps $f : S^3 \to S^2$ is entirely determined by an element of $\pi_3(S^2) \cong \mathbb{Z}$ called the *Hopf invariant* [Hop31; Mil65]. We may define this as follows. Choose an area form Ω on the sphere. The pullback $f^*\Omega$ is a closed 2-form, and since $H^2(S^3, \mathbb{Z}) = 0$ there exists ω such that $f^*\Omega = d\omega$. Define

$$\mathcal{H}(f) = \int_{S^2} \omega \wedge d\omega. \tag{2.2}$$

This is independent of the choice of ω, for any other choice is of the form $\omega' = \omega + d\phi$ for some function ϕ, and the resulting integrand would differ from $\omega \wedge d\omega$ only by the form $d\phi \wedge d\omega$; Stokes' thereom implies the intergal of this term is zero. There is an alternative definition. Let p, q be two regular values of the map f, and let $K_1 = f^{-1}(p), K_2 = f^{-1}(q)$ be the preimages. The Hopf invariant is equal to their linking number, $\mathcal{H}(f) = \mathrm{Lk}(K_1, K_2)$. One can show (e.g., by the arguments in §17 of Milnor [Mil65]) that these definitions are equivalent, and moreover that $\mathcal{H}(f_0) = \mathcal{H}(f_1)$ if and only if the maps f_0, f_1 are homotopic. Consequently, we can make the identification $d^3(\xi_0, \xi_1) = \mathcal{H}(f_0) - \mathcal{H}(f_1)$ on S^3, where $f_i : S^3 \to S^2$ is the map associated to the plane field ξ_i.

To define the invariant in a more general setting, suppose that $d^2(\xi_0, \xi_1) = 0$. Then we may not just extend the homotopy between ξ_0 and ξ_1 over the 2-skeleton, but in fact over the complement of a single 3-ball D^3 in M. The equator of the 2-sphere S^2 bounds a disk D^2; similarly, the equator of S^3 bounds a 3-ball D^3. Let $\pi_\pm$ be the orthogonal projections (in $\mathbb{R}^4$) from the upper and lower hemispheres of S^3 onto the boundary disk D^3. We define $d^3(\xi_0, \xi_1)$ to be the Hopf invariant of the map $f : S^3 \to S^2$ defined as $f_0 \circ \pi_+$ on the upper hemisphere and $f_1 \circ \pi_-$ on the lower hemisphere.

2.3.2 Manifolds with Boundary

On a manifold with boundary the natural notion of a homotopy of plane fields is a homotopy 'rel. boundary', i.e. the plane field is fixed along the boundary and allowed to vary only in the interior. If the boundary is not fixed, we may as well remove it and regard the manifold as open: the homotopy classification of plane fields on open manifolds is due to Gromov [Gro69], and I will not explain it here since it is not a physically-meaningful situation.

We have the following relative variant of the Pontryagin–Thom construction on 3-manifolds M with boundary ∂M, which is proved using the same arguments as for closed manifolds. A modern proof can be found in Ref. [Etn13].

Theorem 2.2. *(Relative Pontryagin–Thom Construction) Let ξ_0 be a plane field defined near ∂M that extends as a nonsingular plane field over the interior. There is a one-to-one between homotopy classes of plane fields ξ on M that extend ξ_0 and the set of framed links in the interior of M up to framed cobordism.*

The description is otherwise the same as for the closed case.

The Euler class rel. boundary is constructed in the following fashion. Suppose we can trivialise ξ on the boundary. Then we can choose some nowhere vanishing section X, and extend this as a section X' over all of M. We can choose this extension so that it vanishes generically on some link L, such that the homology class $[L]$ is Poincaré dual to the relative Euler class. If we cannot trivialise ξ over the boundary, then any section X we choose on the boundary will vanish, generally at some set of points. The extension X' can still be chosen so that it vanishes generically along a link L. We then consider the homology class $[L]$ of this link, once we identify each component of the boundary with a point. Thus loops that extend from one boundary component back to itself are nullhomotopic.

2.3.3 Plane Fields with Singularities

Consider now a director that has a collection of defects, that may be both points and lines. Dual to this is a 'singular plane field', where at each nonsingular point of the director we have a codimension 1 plane in the tangent space, while at each singular point this degenerates to a 'codimension 0' subset of the tangent space. I will define singular plane fields more formally in Chapter 6.

By removing small disjoint open balls around each singular point and open tubes around singular lines in M, we can regard our singular plane field as being a plane field on a manifold with boundary $\hat{M}$. Then we can identify homotopies of singular plane fields that leave the defect set fixed with homotopy classes of plane fields on $\hat{M}$ rel. boundary. When it comes to homotopies of the plane field that may create, destroy, or decompose defects, it is better to discuss the situation locally around the point where this 'bad' behaviour occurs, and see how this modifies the possible sets of plane fields on the complement. This is a running theme through later chapters of this thesis.

2.4 Computation of the Invariants via Legendrian Vector Fields

2.4.1 Legendrian Vector Fields

I will now present a different method of calculating of the homotopy invariants that uses a link L that does not arise as the preimage of a regular value, but instead comes from the zero set of a vector field related to the director, a section of the bundle ξ. This approach is extremely helpful in practice, as it helps us connect topology to energetics. First we make a definition.

Definition 2.1. Fix a plane field ξ. A vector field X is called *Legendrian* if it is a section of the bundle $\xi \to M$.

Much of the discussion of the properties of Legendrian vector fields in the literature centres around their singularities, as discussed by Arnold [AGLV88], as well as their applications to the theory of waves and to general relativity [FS83]. Many properties of these vector fields remain unexplored: for instance, are their any dynamical properties of a vector field that prevent it from being Legendrian? We can observe that perturbing a Legendrian vector field by adding a small component along the normal to ξ results in a nonsingular vector field that is transverse to ξ, and certain properties of Legendrian vector fields can be deduced from properties of transverse vector fields, which have been studied [Goo85; Goo86; Hon98]. A specific investigation into Legendrian vector fields was carried out by Etnyre & Ghrist [EG99]. We will use a couple of results from this paper.

Proposition 2.1. *(Lemma 2.1 [EG99]) Locally, any Legendrian vector fields is 'quasi two-dimensional', that is, in a neighbourhood of a point there exists a coordinate system x, y, z and functions f_1, f_2, g such that any Legendrian vector field can be written $X = f_1\mathbf{e}_x + f_2\mathbf{e}_y - gf_2\mathbf{e}_z$. Moreover, any z-parameterised family of vector fields on $\mathbb{R}^2$ gives rise to a Legendrian vector field.*

Proof. Let U be a small open neighbourhood of a point. On U it is possible to find coordinates such that the plane field can be defined by the 1-form $\eta = dz + g(x, y, z)dy$, see [ET91] for a construction of these coordinates. We can then parameterise U as $\mathbb{R}^2 \times z$, $z \in \mathbb{R}$. The condition for $X = f_1\mathbf{e}_x + f_2\mathbf{e}_y + f_3\mathbf{e}_z$ to be a Legendrian vector field is then that $f_3 = -gf_2$, giving the desired construction. Moveover, if $X_z(x, y) = f_1(x, y, z)\mathbf{e}_x + f_2(x, y, z)\mathbf{e}_y$ is a z-parameterised family of vector fields on $\mathbb{R}^2$, we simply define the z component to be $-gf_2$ in order to obtain a Legendrian vector field. □

Given that the zero set of a 2-dimensional vector field will generically consist of points, it's clear that a Legendrian vector field will generically have a zero set consisting of lines. For a formal proof we invoke the transversality theorem.

Proposition 2.2. *(Proposition 2.2 [EG99]) The zero set of a generic Legendrian vector field X is smooth, finite, embedded link L_X, which is transverse to ξ except at finitely many points, which we call Legendrian points.*

Let us examine the degenerate points where transversality of the link fails more closely, following [EG99]. There are two kinds of bifurcation that may occur in a linearised two-dimensional flow, and these may be characterised by the behaviour of the eigenvalues λ_x, λ_y of the flow. In one case, both eigenvalues are real and one of them changes sign as the bifurcation parameter is varied; this is a *saddle-node bifurcation*. In a saddle-node bifurcation, a previously nonsingular vector field nucleates a pair of singularities of opposite index. Otherwise, λ_x, λ_y are complex conjugate and their mutual real part changes sign as the bifurcation parameter varies; this is a *Hopf bifurcation*. In this type of bifurcation, a node switches its stability by emitting a periodic orbit. The former describes a Legendrian vector field close to a generic Legendrian point, while the latter describes a point where the profile of the singular line changes stability.

Let K be a component of L_X and $p \in K$ a point where transversality fails. In a neighbourhood U of p, choose the coordinates given by Proposition 2.1, such that the origin of these coordinates corresponds to p. First we will look at the saddle-node bifurcation. Choose the x, y coordinates so that the x-direction corresponds to the eigenvector associated to λ_x. The saddle-node bifurcation is locally given by the Legendrian vector field

$$X = \lambda_x x \mathbf{e}_x + (z - ay^2)\mathbf{e}_y - g(x, y, z)(z - ay^2)\mathbf{e}_z, \tag{2.3}$$

in these coordinates, where $a \neq 0$ is a parameter. The curve of fixed points is the set $x = 0, z = ay^2$, a parabola. Furthermore, this system has a family of hetroclinic orbits that connect one branch of the parabola to the other. For a Legendrian vector field, these hetroclinic orbits will always exist close to the Legendrian point.

Now we turn to the Hopf bifurcation. This is easier to describe in terms of polar coordinates r, θ associated to x, y,

$$X = (zr + ar^3)\mathbf{e}_r + \omega \mathbf{e}_\theta - g(x, y, z)\omega \mathbf{e}_z, \tag{2.4}$$

where ω is the angular velocity and $a \neq 0$ is a parameter. Solving for $(zr + ar^3)$

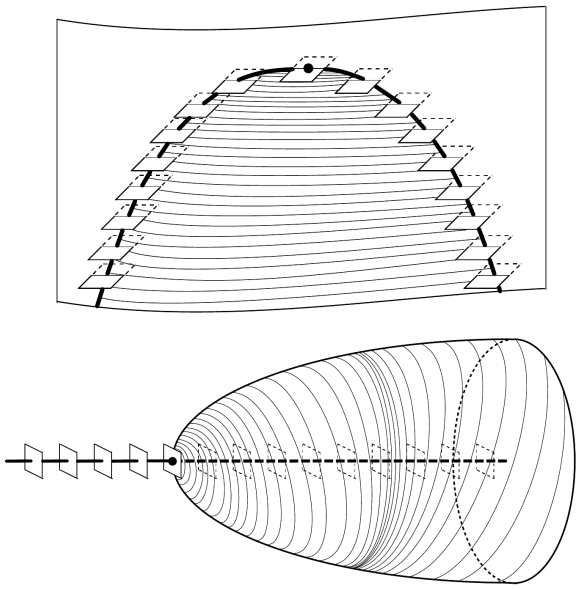

Figure 2.3: Diagrams illustrating the saddle-node (top) and Hopf (bottom) bifurcations in Legendrian vector fields. The solid black line is the zero link of the Legendrian vector field, the black dot indicates the point where the bifurcation occurs. In the case of a saddle-node bifurcation, there are flowlines of the Legendrian vector field connecting the two branches of the zero line, and the black dot is a Legendrian point, where the tangent vector to the zero link lies in the plane field itself. In the Hopf bifurcation, there is a cone that attracts orbits of the Legendrian vector field. Figure reproduced from Ref. [EG99].

gives a paraboloid $r = \sqrt{-z/a}$, which is either attracting or repelling for the orbits of X according to the sign of a. The paraboloid in this example is fibred by orbits of X, and although we may not have this fibration in general, the attracting/repelling paraboloid will always exist and orbits will spiral around it.

The zero link L_X of a Legendrian X is oriented in the following manner. Fix a Riemannian metric and let ν denote the field of planes orthogonal to some component K_j of L_X. The gradients of a Legendrian vector field determine a map $\nabla X : \nu \to \xi$, and generically this will be an isomorphism. Orient K_j so that the isomorphism is orientation perserving. Associated to any Legendrian X is a connection 1-form ω on the plane field ξ, defined as follows. Firstly, for a fixed Riemannian metric we have an orthogonal frame defined on the complement of the zero set of X, $\mathbf{e}_1 = X/\left\|X\right\|, \mathbf{e}_2 = \mathbf{n} \times \mathbf{e}_1, \mathbf{e}_3 = \mathbf{n}$. The connection 1-form is defined, for any vector field Y, by $\omega(Y) = g(\nabla_Y \mathbf{e}_1, \mathbf{e}_2)$[1]. We can also use this connection

[1]As ω is a connection 1-form on a rank 2 bundle it reduces to a scalar for dimensional reasons, much as it would if it were a connection on the tangent bundle to a surface.

form to orient L_X: we orient each component K_j so the vector field dual to the connection form ω winds around it in an anti-clockwise fashion.

The curvature 2-form of the connection is $\Omega = d\omega$. Let S be an oriented surface with boundary ∂S, which may be empty, and such that S intersects L_X transversally in its interior. The Gauss–Bonnet–Chern theorem implies that

$$\int_{\partial S} \omega - \int_S \Omega = 2\pi \sum_j s_j \mathrm{Int}(K_j, S). \tag{2.5}$$

The quantity $\mathrm{Int}(K_j, S)$ is the signed number of intersections of K_j with S, where an intersection contributes $+1$ if the tangent vector to K_j points out from the surface there, and -1 if it points into the surface at the intersection point. This quantity is the Euler class of ξ evaluated on $[S]$,

$$\int_{\partial S} \omega - \int_S \Omega = 2\pi e(\xi)[S]. \tag{2.6}$$

We remark that $e(\xi)[S]$ may be computed from the director $\mathbf{n}$ in the following manner. Firstly, suppose that the set of points where $\mathbf{n}$ is tangent to S is a collection of closed curves—this is the generic situation, so we can assume this holds after a small perturbation of S. Then we can divide S into two sets, S^+ and S^-, consisting of the points where $\mathbf{n}$ points out of an in to the surface respectively. Then $\chi(S) = \chi(S^+) + \chi(S^-)$, and $e(\xi)[S] = \chi(S^+) - \chi(S^-)$.

This description also works for Legendrian line fields, such as the eigendirections of the tensor Δ, which need not be orientable. For a more detailed description of this case and the (minor) modifications that must be made, see Ref. [MA16b]. Although I will make use of the tensor Δ when discussing cholesterics, where its relationship with the pitch axis makes it a logical choice, when Legendrian vector fields are needed I will primarily use the bend vector field, especially in Chapter 5.

It is interesting that (2.6) leads to new expressions for the writhe of closed integral curves of the director in terms of the Euler class. Let K be such a closed integral curve. Define the twisting number of K with respect to a frame $\mathfrak{f} = \{\mathbf{e}_1, \mathbf{e}_2, \mathbf{n}\}$ to be $\mathrm{Tw}(K, \mathfrak{f}) = \int_K \omega(\mathbf{n})$. The writhe of the curve is defined by [Cv̆61; Ful71],

$$\mathrm{Wr}(K) := \mathrm{SL}(K, \mathfrak{f}) - \mathrm{Tw}(K, \mathfrak{f}). \tag{2.7}$$

Then (2.6) implies that,

$$\mathrm{Wr}(K) + \int_S \Omega = \overline{\mathrm{SL}}(K), \tag{2.8}$$

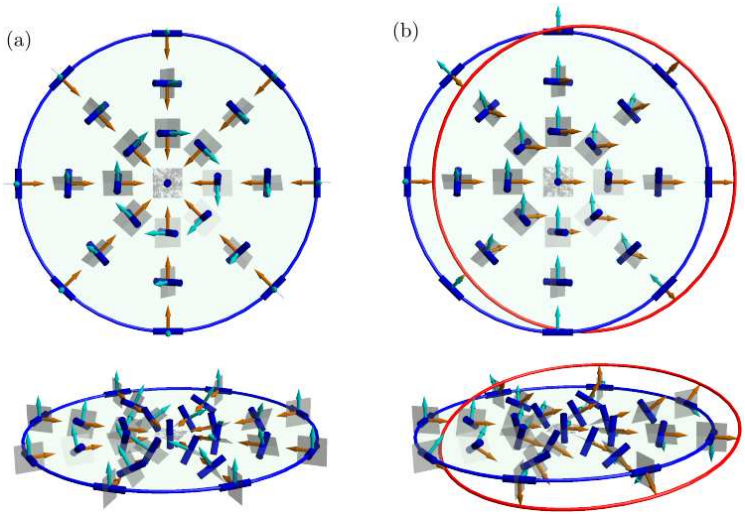

Figure 2.4: Illustration of the transverse self-linking number associated to a closed integral curve of the director field, here a planar circle (blue). (a) The Frenet-Serret framing with the normal (direction of the bend) in orange and the binormal in cyan. The self-linking number of the closed integral curve with this framing is zero but the frame has a singularity at the centre of the disc. (b) A trivialisation of the orthogonal plane field over the disc induces a framing of the closed integral curve with self-linking -1 (illustrated using the red curve displaced from K along a basis vector of the trivialisation); this is the transverse self-linking number of the curve.

where S is a Seifert surface for K and $\overline{\mathrm{SL}}(K)$ is the transverse self-linking number of K, the self-linking number with respect to a framing that extends over S without singularities. This is illustrated in Fig. 2.4 for the simplest example of a planar circle bounding a disc. It is independent of the choice of S, provided that $H_2(M, \mathbb{Z}) = 0$.

2.4.2 The Euler Class

The connection between generic Legendrian vector fields and the topological information carried by ξ follows from a similar argument as the Poincaré–Hopf theorem. The zero link L_X of a Legendrian X is equal to the intersection between X and the zero section of ξ, which is Poincaré dual to the Euler class. Consequently the Euler class is determined by counting the zeros of X with multiplicity. Let K_j denote the jth component of the zero link L_X of X, and let s_j denote the winding of X around this component. Ignoring the multiplicity for a moment, we see that K_j is an oriented submanifold and consequently carries a homology cycle γ_j. The count of these cycles, adding back the multiplicity s_j, gives the homology cycle γ carried

by L_X,

$$\gamma = \sum_j s_j \gamma_j, \tag{2.9}$$

where s_j is the multiplicity of the line, equivalently the winding of X around the line.

Proposition 2.3. *Let $\gamma \in H_1(M, \mathbb{Z})$ be the homology cycle carried by the link L_X. Then $e(\xi) = \sum_j s_j \mathcal{PD}[\gamma_j]$.*

This explains why the standard homotopy theory approach tells us that point defects cannot exist in cholesterics. We have described our cholesteric using a local frame $\mathbf{e}_1, \mathbf{e}_2, \mathbf{n}$, where $\mathbf{e}_1, \mathbf{e}_2$ span the plane field orthogonal to $\mathbf{n}$, i.e. are Legendrian vector fields, with $\mathbf{e}_1$ being the pitch axis. We can assume without loss of generality that they are generic. Suppose we have a point defect in the director. We can surround it by a sphere S. Then $e(\xi)[S]$ is equal to twice the charge of the defect. Whenever this is nonzero, γ must be a nontrivial cycle, i.e., generic Legendrian vector fields must have zero lines whenever there are nontrivial defects in the director. This implies that defects in cholesterics sit at the confluence of λ lines, whose specific structure is related not just to the homotopy type of the defect, but its diffeomorphism type, or local symmetry group, see Chapter 7.

2.4.3 Three-dimensional Invariant

Now we turn to the 3-dimensional invariant. Relating this to Legendrian vector fields is not so easy, and requires a little set up. Firstly, it helps to give a completely different description of the invariant, following Gompf & Stipsicz [GS99]. We will assume that $e(\xi)$ is a torsion class, although the constructions do work (with modification [GS99]) in the general case. In particular, this happens when $e(\xi)$ vanishes, for example when the material domain can be compactified to S^3, a fundamental example that we should bear in mind throughout the following discussion.

It is a classical result that any closed 3-manifold bounds a compact 4-manifold W, e.g., S^3 bounds the 4-ball. An *almost complex structure (ACS)* on a 4-manifold W is a map $J : TW \to TW$ with $J^2 = -I$. Given a plane field ξ we obtain an ACS on ξ using rotations around the director, $J = \mathbf{n}\times$. We can trivialise a small neighbourhood of the boundary of W as $M \times [0, 1]$. We obtain an ACS, which I will also call J, by making it equal to J on $\xi \subset TW$, and defining $J\mathbf{n} = \mathbf{e}_t$, for t the coordinate on $[0, 1]$. This makes ξ the set of complex tangencies to the boundary. There is an obstruction to extending this ACS over W, which arises in the same

fashion as the obstruction to a nonsingular extension of a vector field defined near the boundary of a manifold: it is related to the Euler/Chern class.

Another classical result tells us we can relate the Chern class $c_1(J) \in H^2(W, \mathbb{Z})$ of an ACS J to properties of a *closed* 4-manifold W. Concretely,

$$\theta(J) = c_1(J)^2 - 2\chi(W) - 3\sigma(W) = 0. \tag{2.10}$$

where $\chi(W)$ is the Euler characteristic and $\sigma(W)$ is the signature of the 4-manifold W. This is a consequence of the Hirzebruch signature theorem [HH58]. The square of $c_1(J)$ means taking the intersection product $\smile : H_2(W, \mathbb{Z}) \times H_2(W, \mathbb{Z}) \to H_4(W, \mathbb{Z}) \cong \mathbb{Z}$ of $c_1(J)$ with itself, and then pairing with the fundamental class $[W, \partial W]$ to obtain an integer.

When W is compact with boundary, the intersection pairing is not defined in general, and some technical considerations are required. I will not dwell on these here, and we will assume that this intersection pairing can be defined; see Gompf & Stipsicz [GS99] for details. On the 3-sphere, the most important case for our application, many of the subtleties vanish and the definition of the intersection pairing is simple, see the description given by Etnyre & Ghrist [EG02a]. When $M = S^3$, then W is the 4-ball, whose Euler class is $+1$ and whose signature vanishes.

Assuming we have defined the intersection pairing, the quantity $\theta(\xi) := c_1(J)^2 - 2\chi(W) - 3\sigma(W)$ gives an obstruction to extending J over the interior of W—if it does not vanish, we cannot extend. Then $\theta(\xi)$ is a homotopy invariant.

Theorem 2.3. *(Theorem 11.3.4 [GS99]) The invariant $\theta(\xi)$ depends only on (M, ξ), and reverses sign if the orientation of M is reversed.*

Before moving on to the relationship with Legendrian vector fields, let's first try to get a better understanding of how θ fits into the picture we have of liquid crystal textures. When we wish to measure the defect charge carried by some defects in a nematic, we surround them with a 2-sphere. The director then gives us a map $S^2 \to S^2$. Up to homotopy, such maps are characterised by the degree, as we have discussed. In order to extend the director from the boundary over the interior so that it is nonsingular, the degree must vanish; otherwise the degree gives the amount of charge that must be carried by any singularities in the interior. Globally, a director on S^3 determines a map $S^3 \to S^2$, which we can imagine as a director in a four dimensional physical space defined near the boundary of some 4-ball, which we are trying to extend over the interior of the 4-ball. The role of the degree is now played by the square of the Chern class of the almost complex structure J defined by the director. The Hirzebruch signature theorem plays the role of the Poincaré–

Hopf theorem, which tells us that to extend J over the interior without 'defects', we must have $c_1(J)^2 = 2$; the difference then gives the 'defect charge' carried by that particular director.

Now we wish to construct a variant of $\theta(\xi)$ in terms of the zero link of a Legendrian vector field. Let $\Gamma \in H_2(W, \partial W, \mathbb{Z})$ be a relative cycle whose boundary cycle $\partial\Gamma$ is carried by a link $L \subset M$, and let $\mathfrak{f}$ be a framing on L. We can define the self-intersection number of Γ relative to $\mathfrak{f}$ by glueing handles onto W according to the framing on the link on its boundary to obtain a 4-manifold $\hat{W}$, and then extending Γ to a cycle Γ' in $H_2(\hat{W}, \mathbb{Z})$ whose intersection number makes sense. Loosely speaking, this extension involves gluing surfaces onto the boundary components of Γ in a way prescribed by the framing to obtain a closed surface. We denote the resulting self-intersection number as Γ^2. It depends on both Γ and $\mathfrak{f}$, however, when $[\partial\Gamma]$ is a torsion class the invariant depends only on $[\Gamma]$ [GS99].

Now we suppose that Γ is a relative cycle whose boundary $[\partial\Gamma]$ is Poincaré dual to the Euler class $e(\xi)$ of our plane field, i.e is equal to γ, for γ the homology cycle carried by the zero link of some Legendrian vector field X. Gompf & Stipsicz prefer to discuss this in terms of spin structures, which on a closed 3-manifold are equivalent to trivialisations of the tangent bundle. A Legendrian vector field determines a trivialisaton of ξ, and hence of M, on the complement of its zeros, which can be extended over all of M when the Euler class of ξ vanishes[2]. Let $\mathfrak{s}$ be the spin structure determined by X. We define the invariant

$$\Theta(\xi, \mathfrak{s}, \mathfrak{f}) = \Gamma^2 - 2\chi(W) - 3\sigma(W), \tag{2.11}$$

which *a priori* depends on both the particular choice of spin structure and the framing. Again, when $e(\xi)$ is not a torsion class one needs to be more careful with this definition, but we are discounting this case. The intersection number Γ^2 is essentially the self-linking number of L with respect to the framing $\mathfrak{f}$. Concretely, if K_j are the components of L, and X has winding s_j—so that $[\gamma] = \sum_j s_j[\gamma_j]$, for γ_j the cycle carried by K_j—then we define

$$\Gamma^2 := \sum_j s_j^2 \mathrm{SL}(K_j, \mathfrak{f}) + \sum_{i \neq j} s_i s_j \mathrm{Lk}(K_i, K_j). \tag{2.12}$$

Therefore, Θ is essentially determined by the linking number of the zeros of a Legendrian vector field. Importantly, Θ is a homotopy invariant. The following theorem arises from Theorem 11.3.16 of Gompf & Stipsicz [GS99], applied specifically to

[2]More generally, when the Euler class is nonzero but has torsion, then if each zero has even multiplicty we can extend the spin structure over them uniquely using the belt-trick.

the case $M = S^3$, although I emphasise that it holds more generally for closed 3-manifolds with the additional complexities previous hinted at.

Theorem 2.4. *Two plane fields ξ_0, ξ_1 on S^3 are homotopic if and only if $\theta(\xi_0) = \theta(\xi_1)$, and also if and only if $\Theta(\xi_0, \mathfrak{s}, \mathfrak{f}) = \Theta(\xi_1, \mathfrak{s}, \mathfrak{f})$ for some (and hence every) spin structure $\mathfrak{s}$ and framing $\mathfrak{f}$.*

The definition of Θ bears resemblance to the definition of the Hopf invariant in terms of the linking of preimages. Theorem 2.4 implies that it must capture the same $\pi_3(S^2)$ obstruction that the Hopf invariant does, however $\Theta(\xi, \mathfrak{s}, \mathfrak{f})$ does not need to be equal to the Hopf invariant of ξ even if we are careful about our choice of spin structure. Since Theorem 2.4 holds for any spin structure (trivialisation), so we may as well fix it to be the standard coordinate trivialisation, with Hopf invariant 0. It remains to determine the framing that this imposes on the zero link.

Consider the following example. Start with an example of a meron on a cylinder $D^2 \times [0,1]$, as described by the vector field $r(R-r)\mathbf{e}_\theta + (R-2r)\mathbf{e}_z$, for r, θ polar coordinates on the disk and z the coordinate on $[0,1]$. Now embed this into S^3 as a solid torus, gluing the endpoints of the cylinder together with a map that twists $H > 0$ times in a right-handed sense. The resulting configuration extends globally over the 3-sphere and has Hopf invariant H; such 'axially-symmetric' Skyrmion textures were used by Sutcliffe in numerical investigations of Hopfions in the Skyrme–Faddeev model [Sut07]. It is clear that we can choose a Legendrian vector field for this director with a single zero line of winding $+2$[3], whose profile rotates H times between $\mathbf{e}_r$ and $\mathbf{e}_\theta$. The trivialisation of S^3 determined by this Legendrian vector field is the trivialisation with Hopf invariant H, which corresponds to the zero framing on the link. With respect to the coordinate trivialisation, the framing is the one with self-linking number H.

More generally, and provided that the zero link of a Legendrian X is really generic—has transverse intersection with the zero section of ξ—we define the self-linking number using the isomorphism $\nu \to \xi$ determined by ∇X. The set of such isomorphisms has the homotopy type of a circle, so that the variation of the isomorphism as we move along the line defines a map $K \to S^1$. This map has a degree, and we define the framing so that $\mathrm{SL}(K)$ is equal to this integer. Given a metric g, we can compute this quantity directly. Consider the total rotation

$$\mathrm{rot} = \int_{K'} g(\mathbf{e}_2, \nabla \times \mathbf{e}_1), \tag{2.13}$$

[3] If this is not clear, see the discussion of the Lutz twist in §3.8.1 of Geiges [Gei08].

where $\mathbf{e}_1 = X/\|X\|, \mathbf{e}_2 = \mathbf{n} \times \mathbf{e}_1$, and K' is the pushoff of K along the zero framing. Part of this rotation is a Berry phase ψ equal to the area on the unit sphere that is bounded by the curve swept out by $\mathbf{n}$ as we move along the line. Then $\mathrm{rot} - \psi = 2\pi \mathrm{SL}(K)$.

I emphasise that while this invariant captures the same obstruction as the Hopf invariant, they need not be equal.

For further examples of Θ_0 and also the related invariant θ, consider the director in S^3 given by the actual Hopf fibration[4]. The orthogonal plane field ξ_0^+ is the set of complex tangencies to S^3 regarded as the unit sphere in $\mathbb{C}^2$ with its usual complex multiplication. Consequently the Chern class of the induced almost complex structure is the same as the Chern class of the complex structure on $\mathbb{C}^2$: it vanishes [EG02a]. Thus $\theta(\xi_0^-) = -2$, however ξ has Hopf invariant $+1$. We can also consider the Hopf fibration with Hopf invariant -1, ξ_0^-, which has $\theta(\xi_0^-) = +2$—to see this, we appeal to the fact that θ changes sign under an orientation reversing diffeomorphism of S^3, which would carry ξ_0^+ into ξ_0^-. We can compute Θ_0 using the λ lines. In each texture there are two λ^{+1} lines, forming the Hopf link with linking number $+1$ for ξ_0^+ and linking number -1 for ξ_0^-. Therefore, we have $\Theta_0(\xi_0^+) = +2$ and $\Theta_0(\xi_0^-) = -2$, again distinguishing the textures. This example shows that even for a single plane field the values of $\mathcal{H}(\xi), \theta(\xi)$, and $\Theta_0(\xi)$ can all differ, despite all being homotopy invariants characterising the same obstruction $\pi_3(S^2) \cong \mathbb{Z}$.

The Hopf invariant can also be computed from the zero link of a Legendrian vector field X using the associated connection ω introduced earlier in this section. I follow the description given previously by Machon & Alexander [MA16b; Mac16], adapted to the case of a Legendrian vector field rather than a line field. We continue to assume that our material domain is $M = S^3$ and the director $\mathbf{n}$ is free of defects. Let α be a globally-defined connection on the plane field ξ dual to $\mathbf{n}$, which exists as the Euler class vanishes. This computes the Hopf invariant via the Chern–Simons integral

$$\mathcal{H}(\mathbf{n}) = \frac{1}{4\pi^2} \int_M \alpha \wedge d\alpha. \tag{2.14}$$

We wish to understand what happens when we replace α with the connection ω derived from a Legendrian vector field X, which vanishes along a link L. Given a global trivialisation of ξ, we can write $\omega = d\theta + \alpha$[5], for θ the angle between X and

[4]Looking ahead slightly to Chapter 3, we can say that this is the Reeb field of the standard tight contact form on S^3.

[5]If we follow Machon & Alexander and use a Legendrian line field, such as that defined by an eigendirection of the umbilic tensor Δ, then there is a factor of 2 in front of α which propagates through the following formulas and has a major impact on the final expression.

$\mathbf{n} \times X$. This allows us to write

$$\frac{1}{4\pi^2}\int_{M-L} \omega \wedge d\omega = \mathcal{H}(\mathbf{n}) + \frac{1}{4\pi^2}\int_{M-L} d\theta \wedge d\alpha, \tag{2.15}$$

where we have used the fact that L has measure zero to identify the integral of $\alpha \wedge d\alpha$ over the complement of L with the Hopf invariant. Let N_i be a small neighbourhood of the ith component K_i of L, and let $N = \bigcup_i N_i$. We can use Stokes' theorem to write,

$$\int_{M-N} d\theta \wedge d\alpha = \sum_i \int_{\partial N_i} \alpha \wedge d\theta. \tag{2.16}$$

Each N_i is diffeomorphic to a torus—we can assume they all have radius r, for some fixed small $r > 0$. We can choose a longitude for each torus that has zero linking with K_j. Along each meridian ω will be approximately constant and equal to its value on the umbilic line. Meanwhile, $d\theta$ is constant along the longitude. Its integral around the meridian is equal to $2\pi s_j$, where s_j is the strength of the zero. Using these facts and taking the limit as $r \to 0$ gives,

$$\lim_{r\to 0} \sum_i \int_{\partial N_i} \alpha \wedge d\theta = 2\pi \sum_i s_i \int_{K_i} \omega. \tag{2.17}$$

We observe that,

$$\int_{K_i} \omega = \int_{S_i} \Omega + 2\pi \sum_j s_j \mathrm{Lk}(K_i, K_j), \tag{2.18}$$

where S_j is a Seifert surface for K_j. Then we can apply Gauss–Bonnet–Chern theorem (2.6) to eliminate the integral over Ω, yielding,

$$\frac{1}{4\pi^2}\int_{M-L} \omega \wedge d\omega = \mathcal{H}(\mathbf{n}) + \frac{1}{2\pi}\sum_i \int_{K_i} \omega - \sum_i e(\xi)[S_i] + \sum_{i,j} s_j \mathrm{Lk}(K_i, K_j). \tag{2.19}$$

The latter two terms cancel. Rearranging the formula then gives us an expression for the Hopf invariant,

$$H = \frac{1}{4\pi^2}\int_{M-L} \omega \wedge d\omega - \frac{1}{2\pi}\int_L \omega. \tag{2.20}$$

Note that this is very different to the formula given by Machon & Alexander [MA16b; Mac16] for the Hopf invariant in terms of a Legendrian line field, which contains additional terms that cancel here.

When M is a manifold with boundary, the zero set of a Legendrian vector field will not always lie in the interior, but will often connect to the boundary; in

particular, if we are looking at a manifold with boundary obtained by removing an open neighbourhood of a defect set, we will certainly have zero lines intersecting the boundary. Both the Hopf and Gompf invariants may still be computed by calculating the self-linking of the zero set of a Legendrian vector field rel. boundary. For examples of this process in textures with nontrivial Hopf invariant in cholesteric droplets, see Chapter 9. In this case, linking relative to the boundary implies we are free to move the endpoints of any curve that lie in a boundary component around on that boundary component. An arc whose endpoints both lie in the same component is nullhomotopic—two arcs that each have an endpoint in the same boundary component are never linked.

2.5 Homotopy Invariants of Nonorientable Textures

In the previous sections in this chapter we assumed that the director could be oriented, so that it determined a map $M \to S^2$. More generally, the director determines a map $M \to \mathbb{RP}^2$, the projective plane. When there are no defects, we may pull back to a double cover and apply the standard homotopy theory there. This may not preserve the more complicated topology that can occur in systems with broken symmetry, but is sufficient to capture the standard nematic textures.

When there are defects, we must pullback to a branched cover as described by Machon & Alexander [MA14; MA16a]. I review the classification here, focussing on just the case $M = S^3$, and will extend the discussion to cholesteric textures in Chapter 8. Let $\mathbf{n}$ be a director with point defects at the points of $\mathcal{P}$, and nonorientable disclinations along a set $\mathcal{L} = \{L_1, \ldots, L_m\}$. Here, each L_j is either a single knot, or else it is a non-split link[6]. The homotopy classes of directors $\mathbf{n}$ with this fixed defect set are given by elements of

$$\bigoplus_{p\in\mathcal{P}} \mathbb{Z} \oplus \bigoplus_{L\in\mathcal{L}} (\mathbb{Z} \oplus H_1(\Sigma(L))), \tag{2.21}$$

modulo the equivalence $\mathbf{n} \mapsto -\mathbf{n}$ [MA16a]. The manifold $\Sigma(L)$ is the double cover of S^3 branched over the link L. The factors of $\mathbb{Z}$ correspond to the integer charge associated to either a point defect, or a non-split link, while the factor $H_1(\Sigma(L))$ counts topologically-distinct textures on the link complement. The number of such textures is then determined by $|H_1(\Sigma(L))|$, a quantity known as the link determinant—this can also be computed from the Alexander polynomial $A(t)$ of the knot [Ale28], with $|H_1(\Sigma(L))| = |A(-1)|$.

[6] That is, a link that contains no component that is unlinked from the rest of the components.

If $\mathcal{L} = \{K\}$, for a single knot K, then distinct nematic textures on the complement of K correspond to entangling the knot with a Skyrmion tube [MA16a]. If K is the unknot, the Alexander polynomial is constant and equal to 1, which implies that, up to continuous deformation, there is a single texture on the complement of the unknot. One cannot entangle this with a Skyrmion. To see this, consider the texture on $\mathbb{R}^3$ that contains an unknotted disclination line in the xy plane and a tube of skyrmions running along the z axis. Take a sphere surrounding the disclination line. The presence of the Skyrmion implies that the sphere carries 'charge' $+1$. Once we compactify to get a texture on S^3, the vanishing Euler class on S^3 implies that there must be an additional defect to balance out the $+1$ charge. In Chapter 8 I will show that there are many more topologically distinct textures once we bring chirality into the picture, even when the defect set is simply the unknot. I give a more in-depth discussion of the homotopy classes of nonorientable textures in that chapter.

Chapter 3

Contact Topology and Geometry

3.1 Introduction

In this chapter I review material on contact topology, which I will apply to the study of chiral liquid crystals in later chapters. The idea of chirality, or handedness, was best expressed by Kelvin: "I call any geometrical figure, or group of points, 'chiral', and say that it has chirality if its image in a plane mirror, ideally realized, cannot be brought to coincide with itself." Contact topology is the study of plane fields that are always turning with a constant sense of handedness.

The first mention of contact geometry occurs in the work of Sophus Lie [Lie72], who introduced the idea of a contact tranformation for studying solutions to systems of differential equations. The Hamiltonian formalism of classical mechanics is based around symplectic topology, the even-dimensional analogue of contact topology, but admits a reformulation in terms of contact geometry once one takes an explicit time-dependence into account [Arn89], in effect adding an additional dimension. Russian mathematician V.I. Arnold was a vocal proponent of the importance of contact topology and geometry in physics, even arguing that "Contact geometry is all geometry" [Arn90b]. The appearance of contact topology in thermodynamics goes back to the original formulation of Gibbs, who recognised, without stating it explicitly, that each material corresponds to a Legendrian hypersurface in a certain contact manifold, with curves on those hypersurfaces being the possible trajectories of the system [Arn90a]. Important results in geometric optics, such as Hugyens' principle on the propogation of wave fronts, have a contact geometric interpretation [Gei06; Gei08]. One of Arnold's many contributions to the field was the classifi-

cation of the generic singularities of Legendrian curves [AGLV88], which leads to an understanding of the cusps and perestroikas that occur in wave fronts and optical caustics. More recently, in the work of Etnyre & Ghrist [EG00a; EG00b; EG02b], contact topology has been applied to fluid dynamics via the relation between the Reeb fields of contact structures and Beltrami fields, which I will discuss further in §3.11 below. For a more detailed historical review and list of applications see the review article by Geiges [Gei06].

The goal is to describe in reasonable detail the three-dimensional theory of contact structures, so that this theory may be extended and applied to the study of chiral materials such as ferromagnets and cholesteric liquid crystals, a novel application of these ideas. Many of the basic theorems are directly applicable to liquid crystals, giving us methods of constructing directors with predefined properties, of examining the topological structure of a system by means of projections onto families of surfaces, and proofs of the existence or non-existence of additional topological invariants associated to chiral materials. Even in cases where the theory may not be applied directly, it provides fresh perspectives and insights that motivate future study. In later chapters the basic results described in this chapter are extended to 'singular' contact structures, so that we may bring a discussion of defects under the umbrella of contact geometry.

Throughout this chapter I present proofs or proof sketches of certain theorems—usually taken from the literature, although I have tried to include my own insights and understanding of the problems where possible—in cases where it is enlightening to see them. However, the primary focus is on understanding the connection between the ideas of contact topology and what one might see in a numerical simulation or experimental image of a cholesteric material, in which case the rule that a picture is worth a thousand equations certainly applies. With this in mind, I have included numerous images of simulations of cholesteric liquid crystals to aid the reader in understanding the theory. Since we will always be working with a unit vector field in Euclidean space, it is also helpful to see some of the proofs presented in geometric terms via the introduction of a distortion frame, e.g. when discussing Gray Stability in §3.4.

3.2 Foliations and Contact Structures

Recall from §2.2 that an orientable plane field ξ on a 3-manifold M can be defined by the kernel of a 1-form η. The 3-form $\eta \wedge d\eta$ is a top form, and hence can be identified with a scalar. If $\eta \wedge d\eta = 0$, the plane field is a *foliation*, while if $\eta \wedge d\eta \neq 0$,

it is a *contact structure*. If we fix a Riemannian metric g these conditions can be written in terms of the twist of the unit normal $\mathbf{n}$ to the planes of ξ, $g(\mathbf{n}, \nabla \times \mathbf{n}) = 0$ and $g(\mathbf{n}, \nabla \times \mathbf{n}) \neq 0$ respectively. A contact structure is *positive* if the twist is positive and *negative* if the twist is negative; equivalently, if the orientation induced by the volume form $\eta \wedge d\eta$ is the same as (positive) or opposite to (negative) the orientation of the manifold. A pair (M, ξ) where M is a manifold and ξ a fixed contact structure on M is commonly referred to as a *contact manifold*.

These conditions can be stated in terms of the space of sections $\Gamma\xi$ of ξ, the vector fields that lie everywhere tangent to the planes. Let X, Y be a local basis of vector fields for $\Gamma\xi$. The Lie bracket $[X, Y]$ is also a section of ξ if and only if $g(\mathbf{n}, \nabla \times \mathbf{n}) = 0$. A plane field satisfying $[X, Y] \in \Gamma\xi$ for every $X, Y \in \Gamma\xi$ is called *involutive*. We say that ξ is *integrable* if we can find a family of embedded surfaces such that ξ is everywhere the tangent space to these surfaces.

Theorem 3.1. *(Frobenius Integrability Theorem [Dea40; Cle66]) A plane field is integrable if and only if it is involutive.*

Thus a foliation defines a partition of space into submanifolds, called *leaves*. Foliations are the natural model for smectic liquid crytals [Po1; MAHK19], where the director is normal to a family of layers.

A contact structure is a 'maximally nonintegrable' plane field, where the Lie bracket of a pair of sections is *never* a section. The geometric consequence of this condition is that the planes of a contact structure ξ must always be twisting away from one another. This can be made more precise with a geometric intepretation. Choose a Riemannian metric g. Let $\mathbf{n}$ be the unit normal to ξ, and let $\mathbf{e}_1, \mathbf{e}_2$ be a local orthonormal basis for ξ. Denote by ψ_t the flow of $\mathbf{e}_1$, and let $\theta(t)$ be the angle between $(\psi_{-t})_*\mathbf{e}_2$ and $\mathbf{n}$, that is

$$\cos\theta(t) = \frac{g((\psi_{-t})_*\mathbf{e}_2, \mathbf{n})}{\|(\psi_{-t})_*\mathbf{e}_2\|} \tag{3.1}$$

Then ξ is a positive contact structure if and only if $\dot{\theta}(t) > 0$, and a negative contact structure if and only if $\dot{\theta}(t) < 0$, for all $p \in M, t \in \mathbb{R}$. It can easily be checked—see Chapter 4—that the twist is $g(\mathbf{n}, \nabla \times \mathbf{n}) = \dot{\theta}(0)$. One can interpret this as the instantaneous angular velocity of the planes induced by the flow along $\mathbf{e}_1$. The sign of the twist correponds to the direction of rotation: positive twist corresponds to a left-handed sense of rotation, while negative twist corresponds to a right-handed sense of rotation. It follows that aplane field ξ is contact if and only if, for every Legendrian vector field X, the flow ϕ_t of X acts to rotate the planes of ξ in a

constant sense.

This sense of handedness means that contact structures are the natural mathematical structure for representing chiral materials with a line or vector order parameter, such as cholesteric liquid crystals.

Finally, we observe that contact structures have no local invariants, only global ones.

Theorem 3.2. *(Darboux Normal Form) Let ξ be a (positive) contact structure. At each point there is open ball U around that point and coordinates (x, y, z) on that open ball such that $\xi|_U$ is defined by $\eta = dz + \frac{1}{2}(xdy - ydx)$.*

This is analagous to a similar theorem about local normal forms for symplectic structures—too wit, that locally a sympletic form on a $2n$-manifold can be written as $\Omega = \sum_j dx_j \wedge dy_j$, for coordinates $(x_1, \ldots, x_n, y_1, \ldots y_n)$ on some open ball—and proved in the same fashion. The Darboux normal form $\eta = dz + xdy - ydx$ is also sometimes written as $dz + xdy$ or $dz - ydx$; these are completely equivalent.

3.3 Contact Vector Fields

When describing a mathematical structure it is important to understand the maps between two instances of the structure, and in particular the automorphisms of a given instance. A diffeomorphism ϕ of a manifold M which preserves a contact structure ξ on M, $\phi^*\xi = \xi$, is called a *contactomorphism*. Such maps do not generally preserve contact forms, but they do always rescale them, $\phi^*\eta = \lambda\eta$ for some function $\lambda > 0$. A contactomorphism which preserves a fixed contact form η for ξ is called *strict* for that form. As the composition of two contactomorphisms is again a contactomorphism, we obtain a Lie subgroup of the diffeomorphism group of the manifold called the contactomorphism group, $\mathcal{C}(M, \xi)$. The contactomorphism group is a diffeomorphism invariant of the contact structure, but not a homotopy invariant. Similarly, we obtain the strict contactomorphism group $\mathcal{SC}(M, \eta)$ of a contact form.

Associated to any contact form η is a special vector field R, the *Reeb field*, defined uniquely by the equations $\iota_R\eta = 1, \iota_R d\eta = 0$, whose flow then gives a strict contactomorphism of η. The uniqueness follows from the fact that $d\eta$, being nonzero when restricted to the kernel of η, must have a one-dimensional kernel; the first condition then fixes a single vector spanning this kernel. The Reeb field satisfies $\mathcal{L}_R\eta = d\iota_R\eta + \iota_R d\eta = 0$, and consequently preserves the contact form.

The Lie algebra of the contactomorphism group is the space of all vector fields X whose flows are contactomorphisms of ξ. For a given contact form η, these

satisfy $\mathcal{L}_X\eta = \lambda\eta$ for some function λ. These are called *contact vector fields*—for example, the Reeb field is a contact vector field with $\lambda = 0$. Fix a contact form η defining ξ. Any contact vector field X_H can be associated to a function H via the following relationships,

$$\eta(X_H) = H, \qquad \iota_{X_H} d\eta = dH(R)\eta - dH, \tag{3.2}$$

where R is the Reeb vector field of η. Conversely, any function H gives rise to a contact vector X_H field by solving the above equations; H is the *contact Hamiltonian* of X_H. Conseqently, we can identify contact vector fields with smooth functions on the manifold. Since contact vector fields are the infinitesmal generators of contactomorphisms, we see the Lie algebra of the contactomorphism group is equivalent to the algebra $C^\infty(M)$ of smooth functions on M.

Since we are concerned with contact structures on subsets of Euclidean space where the contact form, dual to the director, has unit length, it makes sense to express the above conditions in terms of the gradients of a unit 1-form η, or equivalently the director $\mathbf{n}$. Choose a local orthonormal basis $\mathbf{e}_1, \mathbf{e}_2$ of sections of ξ. Let $\mathbf{b}$ be the bend vector field, β its dual 1-form, and κ its norm, and let q be the twist of $\mathbf{n}$. Using the formula $d\eta = qe^1 \wedge e^2 + \eta \wedge \beta$ (see Chapter 4) and the above pair of equations, we can express any contact vector field X_H in terms of the director and the bend. We start with the Reeb field,

$$R = \mathbf{n} + \frac{1}{q} J\mathbf{b}, \tag{3.3}$$

where $J = \mathbf{n}\times$ is an almost complex structure on ξ that rotates a section ninety degrees anticlockwise around the director. It is interesting to observe that this has no component along the normal direction to the integral curves of $\mathbf{n}$, and that it agrees with $\mathbf{n}$ only when the bend vanishes—this essentially gives a topological definition for the 'β lines' that are the primary subject of Chapter 5, as long as the twist is nonzero.

For any nonzero function f, we can rescale η to obtain another contact form $\bar{\eta} = f\eta$ defining the same contact structure. The Reeb field of this rescaled form is

$$\bar{R} = \frac{1}{f}\mathbf{n} + \frac{1}{f^2 q} J(\mathbf{b} + \nabla f). \tag{3.4}$$

Thus $\mathbf{n}$ directs the Reeb flow of some contact form defining the same contact structure if and only if there exists a function $f > 0$ such that $\mathbf{b} + \nabla f$ is colinear with $\mathbf{n}$. By Proposition 2.1, in a neighbourhood of any point we can find an adapted coordi-

nate system x, y, z so that the bend is a 1-parameter family of 2-dimensional vector fields. In order for $\mathbf{n}$ to be a Reeb field associated to the same contact structure, these vector fields must be the gradients of a 1-parameter family of functions.

We can also extend this formula to contact vector fields. Write $X_H = X_1\mathbf{e}_1 + X_2\mathbf{e}_2 + X_3\mathbf{n}$ for a contact field. The coefficient of $\mathbf{n}$ must be H, as determined by $\eta(X_H) = H$. The remaining two terms are obtained from plugging our ansatz into $\iota_{X_H} d\eta = dH(R)\eta - dH$,

$$\begin{aligned} X_1 &= -\frac{1}{q}(\nabla_2 H + H\mathbf{b}\cdot\mathbf{e}_2), \\ X_2 &= \frac{1}{q}(\nabla_1 H + H\mathbf{b}\cdot\mathbf{e}_1). \end{aligned} \tag{3.5}$$

Grouping terms, we find the formula for a general contact vector field,

$$X_H = HR - \frac{1}{q}(J\nabla H). \tag{3.6}$$

3.4 Gray Stability

In this section I describe an early result in contact topology, the Gray Stability Theorem [Gra59]. Although this result is very simple, it has important applications to cholesterics: it implies that homotopies of contact structure give rise to isotopies, and hence that diffeomorphism invariants of contact *structures* are of no particular relevance[1]. This is explained in the recent paper of Machon [Mac17]. I will review it briefly for completeness, more details can be found in the cited reference. I follow the proof in Geiges [Gei08], which uses the Moser trick to simplify the original proof of Gray [Gra59], but give the statements a geometric flavour in order to arrive at the form given by Machon [Mac17].

Theorem 3.3. *(Gray Stability Theorem) Let ξ_t be a smooth family of contact structures on a closed 3-manifold M. There exists an isotopy ψ_t such that $\xi_0 = \psi_t^*\xi_t$.*

Proof. Let $e_t^3 = \eta_t$ be the unit 1-form defining ξ_t, and choose a local orthonormal pair of 1-forms e_t^1, e_t^2 whose dual vector fields span ξ_t. In general, the isotopy we hope to construct cannot be chosen so that $\psi_t^*\eta_t = \eta_0$, as there is no reason it should preserve lengths. Instead, we hope to find an isotopy so that $\psi_t^*\eta_t = \lambda_t\eta_0$, for some family of strictly positive functions λ_t. Differentiating both sides with respect to t

[1] Although the strict contactomorphisms are tied to geometric quantities and connected to the structure of layers in the cholesteric, see Chapter 10

and rearranging terms, we need to solve

$$\psi_t^*(\dot{\eta}_t + d(\iota_{X_t}\eta_t) + \iota_{X_t}d\eta_t) = \psi_t^*(\mu_t\eta_t) \tag{3.7}$$

for a time dependent vector field X_t whose flow defines the isotopy ψ_t, and we have defined $\mu_t := \frac{d}{dt}(\log\lambda_t)\circ\psi_t^{-1}$. If we can write down the vector field X_t, we then can uniquely integrate to get the flow ψ_t, so it is enough to find X_t.

Suppose $X_t \in \xi_t$. Then (3.7) would be satisfied if $\dot{\eta}_t + \iota_{X_t}d\eta_t = \mu_t\eta_t$. If we apply this to the Reeb field R_t of η_t, we see that this will be satisfied by $\mu_t = \dot{\eta}_t(R_t)$.

Write $X_t = X_1(t)\mathbf{e}_1(t) + X_2(t)\mathbf{e}_2(t)$ and $\dot{\eta}_t = \sum_i Y_i e^i$. Then to solve (3.7) X_t must satisfy

$$\dot{\eta} + q(X_1e^2 - X_2e^1) - \beta(X)\eta = \mu\eta, \tag{3.8}$$

where every term is understood to depend on t. From this, we deduce that $Y_1 - qX_2 = 0$ and $Y_2 + qX_1 = 0$. Consequently, the isotopy is generated by the time-dependent vector field

$$X_t = \frac{1}{q_t}J\dot{\mathbf{n}}_t. \tag{3.9}$$

□

One may also obtain (3.9) by taking an appropriate limit in the Ericksen–Leslie equations for the hydrodynamics of liquid crystals [Mac17].

The proof applies to nonorientable contact structures as well. This can also been seen by performing the calculations locally in charts where the director is orientable, and noting the flow field X_t remains unchanged if we send $\mathbf{n}$ to $-\mathbf{n}$ (since J will also change sign), so that the conclusion holds globally. The vector field X_t we have chosen is not the unique solution of (3.7), as we can add any contact vector field Y_t to X_t, although this will result in a different function μ_t.

The actual flow field is easily determined once we precribe $\dot{\mathbf{n}}_t$. Suppose the system evolves under the Euler–Lagrange equations of the Frank free energy (1.2). Assume a one elastic constant approximation, so that

$$\dot{\mathbf{n}} = K(\nabla^2\mathbf{n} - 2q_0\nabla\times\mathbf{n})^\perp, \tag{3.10}$$

where $\perp$ denotes projection into the planes orthogonal to $\mathbf{n}$. Using the equation $\mathbf{n}\times\nabla\times\mathbf{n} = -\nabla_{\mathbf{n}}\mathbf{n}$, we deduce that the flow field is

$$X_t = \frac{1}{q}(\mathbf{n}\times\dot{\mathbf{n}}) = \frac{K}{q}(J\nabla^2\mathbf{n} + 2q_0\mathbf{b}), \tag{3.11}$$

where q is the twist of $\mathbf{n}$. For another example, consider the following 1-parameter family

$$\mathbf{n}_t = \sin\left(\frac{\pi t}{2}\right)\mathbf{e}_z + \cos\left(\frac{\pi t}{2}\right)(\cos(z)\mathbf{e}_x - \sin(z)\mathbf{e}_y)\,, \tag{3.12}$$

with $t \in [0,1)$ that interpolates between the cholesteric ground state and the heliconical state. We compute that $q_t = \cos^2\left(\frac{\pi t}{2}\right)$ and $\dot{\mathbf{n}}_t = \frac{\pi}{2}(\cos\left(\frac{\pi t}{2}\right)\mathbf{e}_z - \sin\left(\frac{\pi t}{2}\right)(\cos(z)\mathbf{e}_x - \sin(z)\mathbf{e}_y))$, so the flow field is

$$X_t = -\frac{\pi}{2}\sec^2\left(\frac{\pi t}{2}\right)(\sin(z)\mathbf{e}_x + \cos(z)\mathbf{e}_y). \tag{3.13}$$

The isotopy in question solves the equation $\partial_t\phi_t = X_t(\phi_t)$. Using the fact that $\sec^2(t) = \partial_t \tan(t)$, we conclude that

$$\psi_t(x,y,z) = \left(h_1 - \tan\left(\tfrac{\pi t}{2}\right)\sin(h_3), h_2 - \tan\left(\tfrac{\pi t}{2}\right)\cos(h_3), h_3\right), \tag{3.14}$$

for some time-independent functions h_1, h_2, h_3. Using the fact that ψ_0 should be the identity map, we find $h_1 = x, h_2 = y, h_3 = z$.

An immediate consequence of Gray Stability is that there are no 1-parameter families of non-isotopic contact structures, and hence any homotopy invariants of contact structures must be discrete. This contrasts with the homotopy invariants of foliations which may be continuous, and indeed a continuous invariant (the 'Godbillon–Vey number' [GV71; RW73; Mac20a; Mac20b]) does exist. For liquid crystals there is a further consequence, the preservation of the layer structure [Mac17]. Suppose that the cholesteric director at time 0 is tangent to some foliation $\mathcal{F}_0$ defined by a 1-form α_0. The leaves of this foliation are the 'layers'. Then $\alpha_0(\mathbf{n}_0) = 0$. This implies that, for all t, $\alpha_0(\psi_{t*}\mathbf{n}_t) = 0$. Furthermore, if we define $\alpha_t(X) := \alpha_0(\psi_{t*}X) = \psi_t^*\alpha_0$, then clearly $\mathbf{n}_t$ lies in the kernel of this 1-form, and moreover the 1-form defines a foliation $\mathcal{F}_t$ isotopic to $\mathcal{F}_0$.

The preservation of the layer structure leads to an instability, the Helfrich–Hurault instability, which involves the buckling of the cholesteric layers under an applied electromagnetic field [Hel71; Hur73] or mechanical strain [CM73]. We simulate the effect of an applied field by applying a sinusiodal perturbation to a cholesteric ground state on $T^2 \times [0,1]$ with one full 2π twist along the z direction, but q_0 chosen so that the equilibrium number of twists is three. The layers buckle, Fig. 3.1. The colours shown in the figure indicate the dot product between the director and the normal to the slice, with blue being negative and yellow positive. The black lines, where the director is planar, give a good idea of the geometry of the layers.

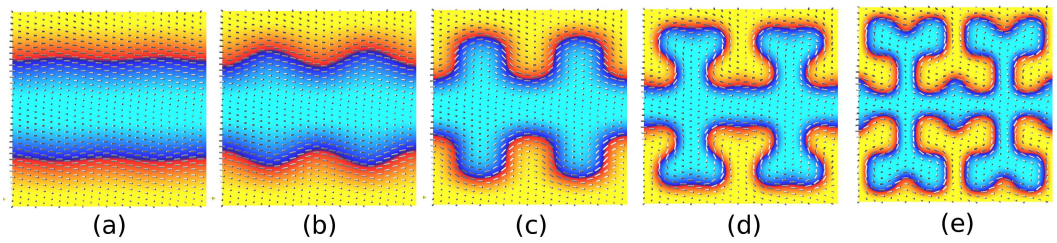

Figure 3.1: The Helfrich–Hurault instability. (a) A frustrated cholesteric ground state with a sinusoidal perturbation, shown on a slice across the domain. (b-e) Evolving this state over time under the gradient dynamics of the Frank energy causes the layers, whose geometry is indicated by the black line where the director lies in the plane of the slice, to buckle.

3.5 Confoliations, and the Perturbation of Foliations into Contact Structures

In Chapter 2 I described the homotopy classes of plane fields in terms of the Euler class and the Hopf invariant. When considering plane fields with additional structure, such as contact structures or foliations, it is natural to ask whether there are additional homotopy invariants. There is a foliation in every homotopy class of plane fields, and moreover foliations satisfy an h-principle: if two foliations are homotopic as plane fields, they are homotopic as foliations [EB16][2].

For contact structures, one has various proofs of existence of at least one contact structure on any closed 3-manifold, for instance one due to Martinet [Mar71], and a later result due to Thurston & Winklenkemper [TW75]—see §4.1 and §4.4 of [Gei08]. In addition to these existence results, there is the Lutz–Martinet theorem.

Theorem 3.4. *(Martinet [Mar71], Lutz [Lut71]) There is a contact structure in every homotopy class of plane fields.*

The proof is by first establishing the existence of a single contact structure, and then applying a type of surgery called the Lutz twist (see §3.8.1) to modify its homotopy class.

It is interesting to consider the question of how one may obtain a contact structure from a foliation. There are two physical reasons to ask this question. The first is to ask how one may interpolate between a region in which the twist is nonzero, and a region where it vanishes, e.g. because of imposed boundary conditions. This arises when discussing cholesteric droplets with normal anchoring, as in Chapter 7.

[2]This is one of many notions of homotopy for foliations; other notions, such as foliated concordance, admit additional homotopy invariants, e.g. the Godbillon–Vey invariant.

The other is when considering phase transitions. Consider a material that exhibits both a smectic phase and a cholesteric phase, with some critical temperature T_c at which the former transitions into the latter. For $T < T_c$ the system may be described by a foliation, while for $T > T_c$, the system is described by a contact structure. Matters are complicated by the fact that for a real material both the foliation and the contact structure will exhibit disclinations and dislocations, but let us ignore this for now. As we pass through the phase transition, the material must undergo a homotopy between a foliation and a contact structure. The question of how this happens, and how (or if) invariants of foliations are converted into invariants of contact structures, is then a relevant one. Materials in which this transition exists exhibit a 'twist-grain boundary' (TGB) phase. This phase is characterised by a series of smectic blocks that rotate as one moves along some helical axis that is orthogonal to the layer normals. In between the 'grains', or blocks of smectic layers, one has screw dislocations forming where the twist is localised. One can imagine that, as the temperature increases, the twist diffuses out from the screw dislocations until the entire material has nonzero twist distortion.

In a seminal work, *Confoliations* [ET91], Eliashberg & Thurston discuss the question of perturbing foliations into contact structures. To this end, they introduce the concept of a *confoliation*, a plane field defined by 1-form η with $\eta \wedge d\eta \geq 0$. The part where $\eta \wedge d\eta > 0$ is the contact part, the part where $\eta \wedge d\eta = 0$ is the foliated part.

The first use of confoliations, discussed in §1 of *Confoliations* [ET91], is to examine whether or not it is possible for a plane field to be contact in the neighbourhood of an integral leaf; said differently, we ask for a unit vector field that is the normal to some surface S but has nonzero twist away from S. A fundamental obstruction to doing this occurs when S is a sphere. This theorem is very important and has numerous applications in cholesteric materials. To aid in understanding it I will give two proofs of this fact, one that is taken directly from *Confoliations* [ET91], and a proof of my own based on the divergence theorem.

Theorem 3.5. *(Reeb Stability Theorem for Confoliations) Let ξ be a germ along $S^2 \times 0$ of a confoliation on $S^2 \times \mathbb{R}_+$ that has $S \times 0$ as an integral leaf. Then ξ is a foliation diffeomorphic to the foliation whose leaves are $S^2 \times z$, $z \in \mathbb{R}_+$.*

Proof. (Proof 1) The proof of Eliashberg & Thurston is based on the idea of holonomy maps. Suppose we have a plane field on $S \times \mathbb{R}$ which is transversal to the lines $p \times \mathbb{R}$ for $p \in S$, where S is any surface. This plane field ξ can be viewed as a $\mathcal{G}$-connection on bundle bundle $S \times \mathbb{R}$, where $\mathcal{G}$ is the group of diffeomorphisms

of the fibre $\mathbb{R}$. The curvature Ω of this connection is a 2-form on S valued in diffeomorphisms of $\mathbb{R}$ that can be computed as follows: for any pair of vector fields X_1, X_2, $\Omega(X_1, X_2)$ is the component of the Lie bracket $[X_1, X_2]$ that points along the fibre, see Fig. 3.2. Let D be a disk in S with boundary γ. We define $\int_D \Omega$ to be equal to the holonomy diffeomorphism along γ, see Fig. 3.2. We see that $\int_D \Omega = \mathrm{id}$ for a foliation and $\int_D \Omega < \mathrm{id}$ for a positive contact structure, where id denotes the identity diffeomorphism. The non-strict inequality holds for a positive confoliation. Moreover, the integral can be reduced to an integral over the boundary via the 'non-commutative Stokes theorem,'

$$\int_D \Omega = \int_{\partial D} \xi, \tag{3.15}$$

where we are regarding ξ as a connection form and $\Omega = d\xi$.

Now specialise to the case where $S = S^2$ is a sphere, and ξ is a germ along S of a confoliation with S as an integral leaf. Let D^+, D^- be the upper and lower hemisphere, with shared boundary ∂D. This boundary is oriented one way if we consider it as the boundary D^+, and the opposite way if we consider it as the boundary of D^-. Computing the holonomy of the confoliation ξ over the disks D^+, D^-, we obtain the inequalities $\int_{D^+} \Omega \leq \mathrm{id}$ and $\int_{D^-} \Omega \geq \mathrm{id}$; consequently, the holonomy diffeomorphism around ∂D must be the identity, and hence ξ is a foliation. Since it is assumed transverse to the lines $p \times \mathbb{R}$ everywhere, it must be diffeomorphic to the foliation by spheres. □

Proof. (Proof 2) Suppose for a contradiction that ξ is contact in a region $S^2 \times (-\delta, 0)$ of a sphere $S \cong S^2 \times 0$, but tangent to S itself. Let B be the ball bounded by S, which we can assume without loss of generality is centred on the origin. We can extend ξ over $B - 0$ so that it is contact everywhere in the interior. Pick a contact form η for ξ, and let R be the Reeb field of η. We observe two things about R. Firstly, since it is transverse to the contact planes, it is transverse to the sphere $S' = S \times -\epsilon$ for some $\delta > \epsilon > 0$. Secondly, on the ball B' bounded by S' minus the origin ξ is contact and R preserves the volume form $\eta \wedge d\eta$, for we have

$$\mathcal{L}_R \eta \wedge d\eta = d(\eta(R) d\eta + \eta \wedge \iota_R d\eta) = 0. \tag{3.16}$$

Pick any Riemannian metric g whose volume form is $\eta \wedge d\eta$ (such metrics are easily seen to exist, see §3.11.1). We can extend R over the origin so that it is zero there.

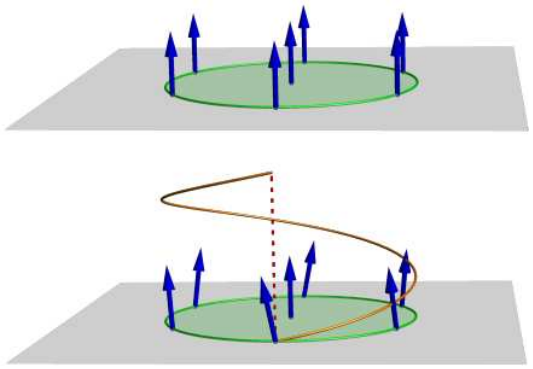

Figure 3.2: Schematic illustration of the twist as a holonomy. (Top) When the twist vanishes the director coincides with the normal to a surface and is perpendicular to the boundary of any disc lying in the surface. (Bottom) When the twist is non-zero and the director is no longer the surface normal, the disc boundary can be lifted along the surface normal to give an open curve, again perpendicular to the director. The distance between the end points gives a measure of the twist.

The divergence theorem implies that

$$\int_{B'} \text{div } R = \int_{S'} g(R, N), \tag{3.17}$$

where N is the unit normal to S'. Since R is transverse to S', the right-hand side of this equation is nonzero. As R is divergence free the left hand side vanishes. We have found our contradiction. Since ξ is a confoliation, it cannot have regions of opposite handedness and since we have just shown it cannot be contact in a neigbourhood of S, it must be a foliation. □

A corollary of Theorem 3.5 is that one cannot modify a foliation near a point to make it contact in a neighbourhood of that point. This has consequences for the textures produced by certain experimental techniques [CAA$^+$13; AS16; AS17; TS19]. It also has consequences for cholesteric droplets with normal anchoring, implying the existence of some boundary region where the director cannot be a contact structure, which I will discuss further in Chapters 6, 7, and 9. Physical materials are not constrained to satisfy the confoliation condition and can exhibit regions of reversed (i.e., different from the energetically preferred) handedness rather than being a foliation in a neighbourhood of the boundary, which is indeed what happens.

Using the idea of holonomy, one can prove that there is no obstruction to producing confoliations that are contact in a neighbourhood of an integral leaf whenever that leaf is not a sphere, but a surface of positive genus. We can realise the

genus g surface Σ_g as a cell complex with a single 0-cell and 2-cell, and $2g$ 1-cells $a_1 \dots a_g, b_1 \dots, b_g$

Theorem 3.6. *(Proposition 1.3.13 [ET91]) Let f_j, h_j be germs of diffeomorphisms of $\mathbb{R}$ whose commutators satisfy $[f_1, h_1] \circ \cdots \circ [f_g, h_g] \leq id$. There exists a germ of a confoliation on $\Sigma_g \times \mathbb{R}_+$ that has $\Sigma_g \times 0$ as an intergal leaf, is otherwise contact, and such that the holonomy diffeomorphisms along a_j, b_j are f_j, h_j for each $j = 1, \dots, g$.*

The consequence of this theorem is that it is possible to expel regions of reversed handedness in, for example, toroidal droplets with normal anchoring. I will discuss this issue, along with the situation for planar anchoring on the boundary, in Chapter 6. An example of the bounary behaviour on $T^2 \times [0, 1]$, with coordinates x, y on T^2 and z on $[0, 1]$, is given by $\eta = \sin\left(\frac{\pi z}{2}\right) dz + \cos\left(\frac{\pi z}{2}\right) (\cos(z)dx + \sin(z)dy)$. This has $T^2 \times 1$ as an integral leaf, and is contact otherwise.

In §2 of [ET91] Eliashberg & Thurston prove their main result on the perturbation of foliations into contact structures.

Theorem 3.7. *Let $\mathcal{F}$ be any C^1 foliation that is not diffeomorphic to the foliation of $S^2 \times S^1$ by spheres. Then $\mathcal{F}$ can be perturbed into a contact structure.*

Consequently there is no global obstruction to making a foliation into a contact structure by an arbitrarilly small change, however Theorem 3.5 implies that this cannot be done by modifications in a neighbourhood of a point, i.e. it must be nonlocal.

3.6 Characteristic Foliations

A useful technique for studying properties of plane fields is to describe them in a neighbourhood of a surface. This is already sufficient to pick up topological information such as the Skyrmion charge, via Eq. (2.6). When dealing with contact structures specifically one can say a little more about the structure near to a surface, which is useful for many constructions, but in fact the ideas of this section can be applied to general plane fields.

Let S be a surface embedded in a contact manifold (M, ξ). The contact structure induces a singular foliation S_ξ on S by setting $S_\xi = TS \cap \xi$. Singularities occur at points where ξ is tangent to S, and hence the singular set is at least codimension 1. It is evident that a small perturbation of S will result in the singular set becoming codimension 2, so we will assume this is the case. The foliation S_ξ is called the *characteristic foliation* induced on S.

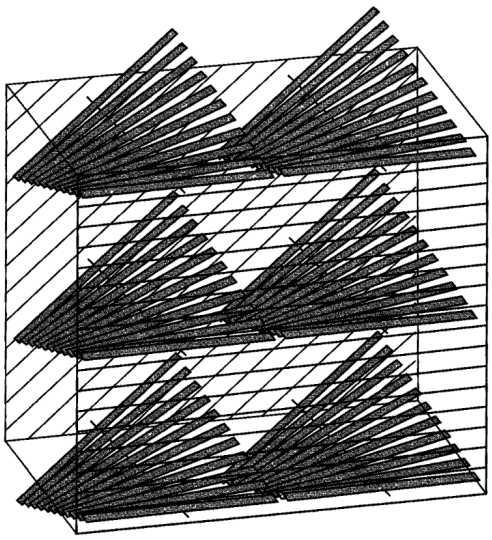

Figure 3.3: A contact structure carves a set of lines into a family of surfaces, and the contact condition implies that these lines rotate like a propeller. Figure reproduced from [ET91].

Eliashberg & Thurston [ET91] offer an alternative interpretation of the contact condition based on the characteristic foliation. We can identify a neighbourhood of S with $S \times [-1, 1]$, where S itself is $S \times 0$. The characteristic foliation on S is a set of lines and the contact condition implies these lines must constantly rotate like a propeller as we move along the $[-1, 1]$ direction, Fig. 3.3.

Let x, y be local coordinates on S and denote by z the coordinate on $[-1, 1]$. We can choose a contact form η for ξ that is decomposed as $\eta = \beta_z + u_z dz$, where β_z is a family of 1-forms and u_z a family of functions on S. In terms of the vector field $\mathbf{n}$ orthogonal to ξ (in some metric), this decomposition is nothing more than writing $\mathbf{n} = \mathbf{n}_\perp + \mathbf{n}_{||}$, where $\mathbf{n}_\perp$ is the projection of $\mathbf{n}$ onto S and $\mathbf{n}_{||}$ is the part of $\mathbf{n}$ orthogonal to S. The characteristic foliation is directed by a vector field X satisfying $\beta_0 = \iota_X \Omega$, where Ω is any area form on the surface; alternatively, it is directed by the vector field orthogonal to $\mathbf{n}_\perp$ in the metric induced on the surface by the ambient metric.

The contact structure can be reconstructed (in a neighbourhood of S) from the characteristic foliation, and the resulting contact structure along the surface is unique up to homotopy, as the following lemma shows.

Lemma 3.1. *Let ξ_0, ξ_1 be two contact structures inducing the same characteristic foliation on a surface S. Then ξ_0, ξ_1 are homotopic in a neighbourhood of S.*

Proof. We may choose contact forms $\eta_i = \beta_i + u_i dz$, $i = 0, 1$, defining ξ_i in a

neighbourhood $S \times [-1,1]$ of S, where $\beta_0 = \beta_1$ whenr estricted to $z = 0$. The functions u_i satisfy

$$u_i d\beta_i + \beta_i \wedge du_i - \beta_i \wedge \dot{\beta}_i > 0. \tag{3.18}$$

This equations remains true when we restrict to $z = 0$, where $\beta_0 = \beta_1 = \beta$. The lemma follows from observing that, for fixed β, the space of solutions to this equation is convex, so that there exists a line u_t of functions connecting u_0 and u_1, which induces a line of contact forms η_t connecting η_0 to η_1. □

Moreover, the condition that must be satisfied by a foliation on S in order that it be the characteristic foliation of some contact structure is very mild. Let $\mathrm{div}_\Omega X$ denote the divergence of a vector field X with respect to the area form Ω.

Lemma 3.2. *(Lemma 4.6.3 [Gei08]) Let $\mathcal{F}$ be a singular foliation on S. It is the characteristic foliation induced on S by some contact structure defined on a neighbourhood of S if and only if there exists an area form Ω and a vector field X directing $\mathcal{F}$ such that $div_\Omega X$ is nonzero at every point where $X = 0$.*

Proof. Set $u = \mathrm{div}_\Omega X$ and suppose this does not vanish at the zeros of X. Let $\beta = \iota_X \Omega$ be the 1-form defining the foliation $\mathcal{F}$. As S is an orientable surface we can choose a 1-form γ with singularities at the same points as β such that $\beta \wedge \gamma \geq 0$, with equality only at the singular points; for example, we may choose a metric on the surface, let Y be the vector field orthogonal to X, and set $\gamma = \iota_Y \Omega$.

Now we define $\beta_z = \beta + z(du - \gamma)$, and set $\eta = \beta_z + udz$. We compute that

$$\eta \wedge d\eta|_{z=0} = (u^2 \Omega + \beta \wedge \gamma) \wedge dz, \tag{3.19}$$

and this is positive because $\beta \wedge \gamma$ vanishes only at points where u does not, and whenever u vanishes, we have $\beta \wedge \gamma > 0$.

Conversely, suppose that $\eta = \beta_z + u_z dz$ defines a contact structure ξ in a neighbourhood of S. The vector field directing the characteristic foliation can be defined by $\iota_X \Omega = \beta_0$, for some area form Ω. At any point p where $X = 0$, $\xi_p = T_p S$. We must have $d\eta|_\xi > 0$, so that $d\eta|_S$ is positive at the point p, and therefore $(d\eta|_S)_p = d\beta_0 = (\mathrm{div}_\Omega X)\Omega \neq 0$. □

In terms of a director field, this construction is as follows. Let X be vector field whose divergence is nonzero at each point where X vanishes, and let Y be the orthogonal vector field to X for some choice of metric on S. Then the divergence u of Y is nonzero at its singular points. The director is

$$\mathbf{n} = Y + z(\nabla u - X) + u\mathbf{e}_z. \tag{3.20}$$

These constructions can be generalised to situations where the director must be unit length, Chapter 4, and where the director may have defects on the surface, Chapter 6.

When considering surfaces in a cholesteric material, one quantity of interest is the value of the Euler class of the director evaluated on that surface, which computes the Skyrmion charge. Suppose the characteristic foliation induced on some surface S is generic, so that each singularity has winding ± 1 and the Jacobian is non-degenerate at every singular point—we can arrange this by a perturbation of S. Since each singularity occurs at a point where the unit normal $\mathbf{n}$ to the contact structure is orthogonal to the surface, we can associate to them a sign: positive if $\mathbf{n}$ agrees with the normal to the surface there, and negative if it is opposite to the normal to the surface. Let $\mathbf{e}_\pm$ denote the number of positive/negative singularities of winding $+1$ (elliptic singularities), and $h_\pm$ denote the number of positive/negative singularities of index -1 (hyperbolic singularities). Set $d_\pm = \mathbf{e}_\pm - h_\pm$.

Proposition 3.1. *(Proposition 3.1.1 [Eli92])*

$$d_\pm = \frac{1}{2}(\chi(S) \pm e(\xi)[S]) \tag{3.21}$$

Proof. Let $\mathbf{n}$ be unit normal to the contact structure. We can partition S into the sets S^+ (resp. S^-) when $\mathbf{n}$ points out of (resp. into) the surface, and a set of closed curves Γ where $\mathbf{n}$ is tangent to the surface. Assume that the characteristic foliation is oriented by a vector field X that points transversally out of S^+—that we can arrange this is proved in §3.9 but it essentially follows from genericity of the desired properties.

It is clear that $\chi(S) = \chi(S^+) + \chi(S^-)$, and that $e(\xi)[S] = \chi(S^+) - \chi(S^-)$. We may compute $\chi(S^\pm)$ using the Poincaré–Hopf index theorem applied to the vector field $X|_{S^\pm}$. As elliptic points have index $+1$ and hyperbolic points have index -1, this calculation yields $\chi(S^\pm) = \mathbf{e}_\pm - h_\pm = d_\pm$. The result follows. □

This result is essentially the Gauss–Bonnet–Chern theorem that was discussed in Chapter 2. Using this equation we can deduce the Skyrmion charge from examining the characteristic foliation induced on a surface in a cholesteric, and with care we can use Theorem 3.2 to design cholesteric directors with the desired Skyrmion charge. Characteristic foliations exist on a surface in any manifold with any plane field, not just a contact structure, although they will obey different properties. Eq. (3.21) always holds for a generic surface.

3.7 Characteristic Foliations on Surfaces Dividing Regions of Opposite Handedness

For applications to liquid crystals it is not enough to study just contact structures, we must also understand the degeneracies that can occur in them. The most obvious degeneracy is the presence of singularities, the subject of Chapters 6 and 8. Another possible degeneracy is the existence of regions where the handedness of the contact structure reverses. Although this comes with an energy penalty, real materials do exhibit such regions, and indeed their existence can be forced by imposing certain boundary conditions, as implied by Theorem 3.5, and they can also be generated in the bulk, Chapter 8. The existence of these regions is of central importance for the stability of the structures formed in cholesteric droplets, a discussed in Chapters 7 and 7.

Let us consider the characteristic foliation induced on a surface that separates a region of left-handedness from a region of right-handedness in a material, in order to get a better idea of the structure of the director near these regions. For a generic surface of this type, the local structure of the characteristic foliation can be deduced from known results on the normal forms of plane fields. Let ξ_1, ξ_2 be generic germs of plane fields. Two such germs are called *topologically equivalent* if there is a homeomorphism f of $\mathbb{R}^3$ that maps curves tangent to ξ_1 into curves tangent to ξ_2—equivalently, $f^*\xi_2 = \xi_1$. This obviously defines an equivalence relation. The equivalence classes are known:

Theorem 3.8. *(Theorem F.1 [Zhi93]) The germ of a generic plane field is topological stable and topologically equivalent to the kernel of one of the following germs of 1-forms,*

1. $\eta_1 = dz + xdy$,
2. $\eta_2 = dz + x^2dy$,
3. $\eta_3 = dz + (xz + x^2y)dy$,
4. $\eta_4 = dz + (xz + x^3/3 + xy^2)dy$.

The first normal form is contact: it is the local model for a contact structure that comes from the Darboux theorem. The remaining three cases all describe regions of opposite handedness seperated by a surface along which the handedness vanishes. These interfaces are the zero level sets of the functions x, $z + 2xy$, and $z + x^2 + y^2$, respectively a flat plane, a saddle, and a parabola. Note that there is no particular reason these should correspond to any kind of curvature of an interface.

Let ξ be a plane field and S denote a surface across which the handedness of ξ reverses. By the above theorem, for any generic point $p \in S$ there exists some open neighbourhood and a coordinate system on that neighbourhood for which ξ is defined by one of the 1-forms (2-4). Case (2) is 'more generic' than cases (3) and (4), and occurs when ξ is transversal to S in a neighbourhood of the point being considered. In the latter cases transversality is violated only at the point p, see §2.2 of the book by Zhitomirskiĭ [Zhi93]. One may consider further degeneracies, where transversality is violated along lines, but these will be even less likely to occur and are 'topologically unstable', in the sense that small perturbations will destroy this property. In cases (3) and (4), the characteristic foliation induced by ξ on the surface Σ will have an isolated singular point at p, which is hyperbolic for (3) and elliptic for (4).

Let us examine the characteristic foliations induced on the surface S where twist vanishes for each model (2-4). In case (2), this surface is the set $x = 0$, and the characteristic foliation consists of straight lines in the y direction. The other two cases are more interesting. First consider case (4). Here S is the set $z + x^2 + y^2 = 0$. Let $\beta = \eta_4|_S$. We easily compute that $\beta = -2xdx - (2y + 2x^3/3)dy$. The vector field X directing the characteristic foliation on S is $X = -(2y + 2x^3/3)\mathbf{e}_x + 2x\mathbf{e}_y$. Clearly a relabelling of the coordinate system in a neighbourhood of the zero reduces this to $-y\mathbf{e}_x + x\mathbf{e}_y$, which is a vector field with everywhere vanishing divergence (in the old coordinate system, the divergence still vanishes at the origin). A similar computation shows the same behaviour for (3), where the vector field directing the characteristic foliation on the set $z+2xy = 0$ is directed by $X = -2(x+x^2y)\mathbf{e}_x+2y\mathbf{e}_y$, which again has vanishing divergence at the origin. This is in constrast to Theorem 3.2, which implies that such singularities are exactly those which cannot occur in a contact structure. Interestingly, the same behaviour occurs in the characteristic foliation on a surface intersecting a defect, see Chapter 6.

A simple example on $T^2 \times [-1, 1]$ is given by the 1-form

$$\eta = \cos(z^2)dx - \sin(z^2)dy. \tag{3.22}$$

This is a positive contact structure when $z > 0$ and a negative contact structure when $z < 0$. At each point on the surface $z = 0$ the plane field defined by η_{rev} looks like the normal form (2). This example illustrates an important point: the set where the twist vanishes need not be an integral leaf of the plane field. It is also straightforward to construct examples where this is the case: by Theorem 3.6 we can construct both a positive and a negative confoliation on $T^2 \times [0, 1]$ that have

$T^2 \times 0$ as an integral leaf but oriented opposite ways, and then glue these together along said leaf to obtain our example.

We can ask what might force a region of reversed handedness to be metastable in a cholesteric even when its presence is not forced by topological constraints. We expect that if all that is required to remove the region is a local modification to the director, then it will not be stable, so a possible route to stability is to force the presence of regions of reversed handedness that require nonlocal modifications to remove. Theorem 3.2 implies that a surface with characteristic foliation containing a singularity with vanishing divergence must intersect a region of reversed handedness. We can certainly perturb a characteristic foliation on a single surface to remove such a singularity, but in a large domain this may only result in moving the 'bad' singularity somewhere else—said differently, the property of being the kind of characteristic foliation that may occur in a contact manifold is generic for a single foliation, but not generic in a one-parameter family. In Chapter 8 I give an experimentally-accessible example where the removal of regions of reversed handedness requires modifying the director along a closed curve, which provides a method by which these regions of reversed handedness could be studied further.

3.8 Tight and Overtwisted Contact Structures, and the Relationship With Skyrmions

In Chapter 2 we saw that there were two invariants that determined the homotopy class of the plane field, and that these invariants could be related to physical properties of a liquid crystal material via the λ lines and β lines. Now I discuss topological information that is of a purely contact-topological nature. The foundational paper of Bennequin [Ben83] illustrates the existence of such contact invariants: he defines two contact structures on $\mathbb{R}^3$ that belong to the same homotopy class of plane fields, and then proves they are not homotopic as contact structures. The ideas of Bennequin were greatly expanded on by Eliashberg [Eli89], who made precise the notion of an overtwisted disk and separted contact structures into two classes: those that possess an overtwisted disk, the *overtwisted* contact structures, and those that do not, the *tight* contact structures.

Consider the following contact form on $\mathbb{R}^3$, given in cylindrical coordinates r, θ, z,

$$\eta^{\text{ot}} = \cos(r)dz + r\sin(r)d\theta \tag{3.23}$$

This defines the *standard overtwisted contact structure* ξ^{ot}. The disk $D^{\text{ot}} = \{z =$

$0, r \leq \pi\}$ is the *standard overtwisted disk*. We see that the boundary of this disk is a Legendrian curve (i.e., a curve tangent to the contact planes) of ξ^{ot}, and that the contact planes are tangent to the disk only at the origin. The characteristic foliation is radial, with singularities at the origin and at every point along the boundary. A small perturbation of the interior of the disk produces a characteristic foliation with a spiral singularity whose integral curves asymptote on the boundary of the disk, which is a limit cycle, Fig. 3.4. The leaves of the characteristic foliation on the perturbed disk are given in polar coordinates by $\theta = -2 \log \sin r$ [Bla10].

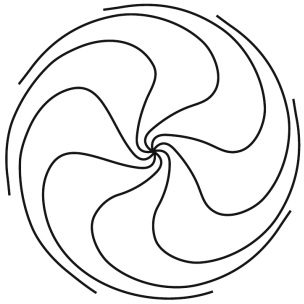

Figure 3.4: The characteristic foliation on an overtwisted disk. Reproduced from [Bla10].

An *overtwisted disk* in a contact structure ξ is a disk D whose boundary is a Legendrian curve and such that there is a contact embedding of a neighbourhood of D into the standard overtwisted contact structure. It is in fact enough for the Legendrian boundary of the disk D to have Thurston–Bennequin number equal to 0. This follows from the so-called Bennequin inequalities, which I describe in the next section.

3.8.1 Overtwisted Contact Structures

The importance of the tight-overtwisted dichotomy lies in the following theorem of Eliashberg.

Theorem 3.9. *(Eliashberg's h-principle for overtwisted contact structures [Eli89]) If two overtwisted contact structures are homotopic as plane fields, they are homotopic as contact structures.*

This theorem asserts that there are no additional homotopy invariants associated to overtwisted contact structures. The technique used to prove the Lutz–Martinet theorem always produces an overtwisted contact structure, and therefore that theorem is more precisely stated as there being an overtwisted contact structure in every

homotopy class of plane fields—Eliashberg's result asserts that this object is unique up to homotopy. As we will see, it is not the case that there is a tight contact structure in every homotopy class of plane fields. The theorem is also not constructive, and does not tell us how the homotopy might be performed in a real material. This is a running theme in the topological results throughout this thesis, and discussing how these processes interact with energetics is an important open problem.

The value of the Euler class on D, equivalently the Skyrmion number, is easily read off from Eq. (3.21), $e(\xi)[D] = +1$. This implies the disk is pierced by a single generic λ^{+1} line. The standard overtwisted disk (3.23) is recognisably a Skyrmion, a disk where the director moves from pointing out from the disk at the centre to pointing into the disk at the boundary, corresponding to a radial coordinate $0 \leq r \leq \pi$, with the director tangent to the disk at $r = \pi/2$. The inner part, $0 \leq r \leq \frac{\pi}{2}$, is a meron, and also defines an overtwisted texture (as the boundary is a Legendrian curve of Thurston–Bennequin number 0, which makes it overtwisted by the Bennequin Inequalities given below). Consequently, every cholesteric texture that contains a meron or Skyrmion is overtwisted. One should be careful about making the converse statement, as overtwisted disks may be embedded in the material in a strange fashion and one would not generally identify the resulting disk with a meron or Skyrmion.

One can 'spoil' a tight contact structure by inserting a tube of overtwisted disks along a positively transverse curve. This is effected by a type of surgery called the *Lutz twist*. A neighbourhood of a curve K that is positively transverse to a contact structure is contactomorphic to the kernel of $dz + r^2 d\theta$. We remove this neighbourhood and replace it with the kernel of

$$\eta = h_1(r)d\theta + h_2(r)dz \tag{3.24}$$

where h_1, h_2 are functions that satisfy the following conditions:

1. $h_1(r) = -1$ and $h_2(r) = -r^2$ near $r = 0$,
2. $h_1(r) = 1$ and $h_2(r) = r^2$ near $r = 1$,
3. (h_1, h_2) is never parallel to (h_1', h_2') for $r \neq 0$.

This surgery is the *half Lutz twist*. The first two conditions determine the topological properties of the surgery; the final condition ensures the resulting plane field is a contact structure. In effect, one inserts a tube of merons along K. A Legendrian vector field that is constant on the boundary of the torus extends over the interior with a single zero of winding $+2$, oriented along $-\mathbf{e}_z$: consequently, the surgery

doesn't just make the contact structure overtwisted, but also modifies the Euler class by $-2\mathcal{PD}[K]$. One can instead insert a tube of Skyrmions, which makes the contact structure overtwisted but does not change the Euler class. This surgery, the *full Lutz twist*, uses (3.24), but with $h_1(r) = 1$ and $h_2(r) = r^2$ near $r = 0$ as well as $r = 1$, with a full rotation in between. To modify the Hopf invariant, we pick a nullhomotopic link L and perform the Lutz twist along this link, whose linking number will then represent the Hopf invariant.

In §6.4.3 I will define a singular variant of the half Lutz twist which describes how this process might occur in a real material. This will be effected by a homotopy rather than a surgery, but of course it must be a homotopy through 'singular contact structures'.

3.8.2 Tight Contact Structures

The homotopy classification of tight contact structures is far more subtle than that of the overtwisted structures, and has a deeper relationship with the topology of the underlying manifold. The first manifold whose tight contact structures were understood was S^3: up to homotopy, there is a single left-handed and a single right-handed tight contact structure which can be defined by taking the planes orthogonal to the left- and right-handed Hopf fibrations of S^3. We can view S^3 as the group $\mathcal{SU}(2)$ with associated Lie algebra $\mathfrak{su}(2)$ generated by a trio of vector fields $\mathbf{e}_1, \mathbf{e}_2, \mathbf{e}_3$ satisfying $[\mathbf{e}_i, \mathbf{e}_j] = \epsilon_{ijk}\mathbf{e}_k$ [Mil76]; each of these vector fields is orthogonal to a 'pure double-twist' contact structure, and in fact these three contact structures are all homotopic to the one given by the Hopf fibration. Stereographic projection onto $\mathbb{R}^3$ produces the contact structure defined by

$$\eta^{\text{std}} = dz + xdy. \tag{3.25}$$

This is the *standard tight contact structure*. Of course, this contact structure cannot be realised in flat space with only twist distortions, which is demonstrated in Chapter 4. There is a sense in which S^3 is the 'natural' geometry for the double-twist distortions of the cholesteric phase due to the neatness of its Lie bracket identities [SWM83].

Also interesting from the point of view of liquid crystal physics is the classification of tight contact structures on $\mathbb{T}^3$, performed independently by Giroux [Gir00] and Kanda [Kan97]. There is a single 1-parameter family of tight contact structures,

all in the zero homotopy class of plane fields, defined by the 1-forms

$$\eta_q = \cos(qz)dx - \sin(qz)dy. \tag{3.26}$$

The handedness is given by the sign of the integer $q \in \mathbb{Z} - 0$. Astute readers will recognise the cholesteric ground state, where q is the layer number; these contact structures are also evidently homotopic, and hence isotopic, to the heliconical director discussed in Chapter 5, the ground state for twist-bend nematics. On $T^2 \times [0,1]$ the classification of tight contact structures, completed by Giroux [Gir00] and Honda [Hon00a], is far more complicated. The proofs of these classification theorems are instructive, and I will sketch them in a later section once the appropriate machinery has been developed.

3.9 Convex Surfaces, Dividing Curves, and Tomography

In the previous section I introduced the dichotomy between tight and overtwisted contact structures. The latter features correspond to merons and Skyrmions, and we have a good idea how to detect these in liquid crystal textures by studying either the β lines or the λ lines, and the characteristic foliation. In this section I describe a refinement of the theory of characteristic foliations from §3.6, the theory of convex surfaces. These surfaces are used to simply the task of classifying tight contact structures, and easily detect merons and Skyrmions.

3.9.1 Convex Surfaces

A surface S is called *convex* if there is a contact vector field transverse to it, although in practice this is perhaps the least helpful criterion for determining convexity. Suppose X_H is a contact vector field transverse to S. We can define a set $C_H = \{X_H \in \xi\} = \{H = 0\}$, the *characteristic hypersurface* of X_H. For a generic contact vector field, where H is transverse to the zero section, C_H is a nonsingular hypersurface, X_H is tangent to C_H and directs the characteristic foliation induced on C_H by ξ [Etn04a]. Any surface that intersects C_H transversally is convex.

There are more useful criteria for determining whether a surface is convex. A vector field X on a surface S is called *Morse–Smale* if the following conditions hold:

1. X has finitely many singularities and closed orbits, all of which are non-degenerate (i.e., the Hessian matrix at the singular point is non-degenerate),

2. The flow of any point p under X converges to either a singular point or periodic orbit in both forward and backward time,

3. There are no trajectories connecting saddle points.

We say a foliation $\mathcal{F}$ directed by a vector field X on S *admits a dividing curve* if there exists a set Γ of embedded circles such that

1. Γ is transverse to $\mathcal{F}$,

2. There is an area form Ω on S such that $\operatorname{div}_\Omega X \neq 0$ on $S - \Gamma$,

3. X points out of S^+ along Γ, where $S^\pm = \{p \in S \mid \pm \operatorname{div}_\Omega X > 0\}$.

These conditions are then equivalent to convexity.

Theorem 3.10. *Let S be either a closed surface or a compact surface with Legendrian boundary inside a contact manifold. The following are equivalent:*

1. *S is convex,*

2. *The characteristic foliation on S is directed by a Morse–Smale vector field X,*

3. *The characteristic foliation on S admits a dividing curve.*

For a proof see §4.8 of Geiges [Gei08]. In particular, since Morse–Smale vector fields are generic, it is not hard to see that convex surfaces are also generic: if S is any surface, then either S is convex or we can perturb it a small amount to make it so. Given a fixed contact vector field X_H with Hamiltonian H the dividing curve induced on any surface S transverse to the flow of X_H to is $S \cap C_H$.

Close to a convex surface, the contact structure has a nice form.

Proposition 3.2. *Let S be a convex surface in a contact manifold (M, ξ). Then there exists a neighbourhood of S diffeomorphic to $S \times [-1, 1]$ such that ξ is defined by a vertically-invariant (i.e. independent of z) contact form $\eta = \beta + u dz$ on this neigbourhood.*

Proof. Use the contact vector field transverse to S to define the trivialisation of $S \times [-1, 1]$, so that the contact vector field is $\mathbf{e}_z$ in this trivialisation. Then the fact that ξ is preserved by the flow of $\mathbf{e}_z$ implies that it can be defined by a contact form η which does not depend on z. □

The utility of convex surface theory rests in the fact that the topology of the contact structure close to the surface can be deduced completely from the dividing curve. I will describe this presently. Firstly, it is convenient to find a nice way of constructing the dividing curve in practice. The following proposition, originally due to Giroux [Gir91], provides such a method. Fix a metric and let $\mathbf{n}$ be the unit normal to the contact planes. Let S be a convex surface with normal N, and $\mathcal{F}$ the characteristic foliation on S.

Proposition 3.3. *If the set of points* Γ *where* $\mathbf{n}\cdot N = 0$ *is a curve, which generically it will be, then it divides* $\mathcal{F}$*.*

Given a numerical simulation of a director field, or a reconstructed director field from an experiment, we can easily study the topology near a surface by simply plotting the function $\mathbf{n}\cdot N$ over that surface. This gives a neat tool for visualising cholesteric directors and their layer structure, as in Fig. 3.1. An alternative construction, as implied by the definition of the dividing curve, is to take the divergence of the vector field $N \times \mathbf{n}$ and let Γ be the set where this vanishes, which will generically be a set of curves.

Now I will explain how the structure of the dividing curve may be used to study the topology of contact structure ξ. The key observation is that the contact structure only depends on the dividing curve, not the particular characteristic foliation.

Lemma 3.3. *(Giroux Flexibility [Gir91]) Let* S *be a convex surface with transverse contact vector field* V*, characteristic foliation* $\mathcal{F}_0$*, and dividing set* Γ*. Let* $\mathcal{F}_1$ *be another singular foliation on* S *divided by* Γ*. Then there is an isotopy* ϕ_t*,* $t \in [0,1]$*, of* S *such that*

1. ϕ_0 *is the identity and* $\phi_t|_\Gamma$ *is the identity for all* t *(i.e., the dividing curve is fixed),*
2. $\phi_t(S)$ *is transverse to* V *for all* t*,*
3. $\phi_1(S)$ *has characteristic foliation* $\mathcal{F}_1$*.*

This lemma is related to classification results about Morse–Smale vector fields in two dimensions [OS98]: the diffeomorphism type of the characteristic foliation is determined by the dividing curve. The fact that the topology of a liquid crystal director near to a surface can be reduced to a discussion about the set of lines where the director is tangent has been recognised previously [ČŽ12].

Any leaf of the characteristic foliation is a Legendrian arc. In light of Giroux Flexibility, we might imagine that we can realise many more curves as Legendrian curves, or leaves in the characteristic foliation after some isotopy. This is indeed the case.

Lemma 3.4. *(Legendrian Realisation Principle [Gir91]) Let S be a convex surface and C a collection of curves on S. Suppose further that C is transverse to Γ and is nonisolating, i.e. each connected component of $S-C$ has nonempty intersection with Γ. Then there is an isotopy, as in Giroux flexibility, such that $\phi_t(C)$ is Legendrian.*

Moreover, we may compute the invariants of the Legedrian curve directly from the dividing set. Suppose a Legendrian knot L lies on a surface S. We may define the *twisting number of L relative to S*, $\mathrm{tw}(L,S)$, to be the twisting of the contact planes of ξ along L measured with respect to the framing induced on L by S; if S is a Seifert surface for L, then this is exactly the linking number of L with respect to the contact framing, the Thurston–Bennequin number. More generally, the twisting number describes the number of cholesteric layers which the curve L passes through, as discussed below in §3.9.2.

Proposition 3.4. *(Giroux [Gir91]) Let L be a Legendrian curve on a convex surface S with dividing set Γ. Then $tw(L,S) = -\frac{1}{2}|L \cap \Gamma|$. In particular, if S is a Seifert surface for L then this computes the Thurston–Bennequin number.*

Note: one reverses the sign of the twisting number when ξ is a negative rather than a positive contact structure, i.e. $\mathrm{tw}(L,S) = \frac{1}{2}|L \cap \Gamma|$.

In light of the relationship between curves C on the surface, the dividing curve, and the twisting number, we have the following theorem that allows us to deduce overtwistedness from the structure of the dividing curve alone.

Theorem 3.11. *(Giroux's Criterion [Gir91]) Let S be a closed convex surface in a tight contact manifold. If the genus of S is positive, the dividing curve on S has no nullhomotopic components; if the genus of S is zero, the dividing curve is connected. If S is instead a compact surface with Legendrian boundary in a tight contact manifold, then the dividing curve has no nullhomotopic components in the interior of S; any components are either homotopically essential, or are arcs connecting the boundary to itself.*

Proof. (Sketch) The 'only if' follows from the Legendrian realisation principle, as well as the computation of the twisting number of a Legendrian curve on a convex surface. If Γ contains a nullhomotopic component, which consequently bounds a

disk D, then one may choose a closed curve in the interior of D which intersects no component of Γ and use the Legendrian realisation principle to realise it as a Legendrian unknot, which has twisting number zero since it does not intersect the dividing curve. As the Thurson–Bennequin number vanishes, D is an overtwisted disk. The 'if' direction follows from constructing explicit models, see Ref. [Gir91] for the details. □

Now we see the connection between dividing curves and Skyrmions. Let S be a plane orthogonal to a tube of merons. The tube of merons is defined by the property that $\mathbf{n}$ points along the axis of the tube down the middle and rotates by $\pi/2$ as it moves to the boundary. Consequently, the set $\mathbf{n} \cdot N = 0$, where N is the normal to S, contains the boundary of the meron tube. Of course it is not necessary that S intersect the tube orthogonally, it suffices for it to intersect transversally; we can still use the Legendrian realisation principle to find the intersection between the boundary of the tube and S. The same argument works for Skyrmions and other structures that contain a tube of overtwisted disks: provided we choose a surface intersecting the tube transversally, we pick up the existence of an overtwisted disk by looking at the dividing curve.

Another important theorem, which essentially follows from Eq. (3.21) and Giroux's criterion, is the following set of bounds on the Euler class in a tight contact manifold.

Theorem 3.12. *(Bennequin Inequalities [Ben83; Eli92; ET91]) If S is either a closed surface of positive genus in a tight contact manifold, or a compact surface with Legendrian boundary, then*

$$e(\xi)[S] \leq -\chi(S). \tag{3.27}$$

Further, if $S = S^2$, then

$$e(\xi)[S] = 0. \tag{3.28}$$

When dealing with a negative contact structure one has $e(\xi)[S] \geq \chi(S)$ instead.

There is also a version of the Bennequin inequalities that applies to nullhomotopic Legendrian (tangent to the contact planes) and transverse knots, which is easily proved by choosing a Seifert surface from the knot, expressing the invariants of the knot in terms of quantities on the surface, and then applying the previous theorem. These knot invariants are defined as follows. For a transverse K, the plane field $\xi|_S$, for S a Seifert surface, is trivial. We may push K in the direction of any nonzero section X of $\xi|_S$ to produce a new knot K'. We then define the *transverse*

self-linking number $\overline{\mathrm{SL}}(K)$ of K to be the linking number of K with K'; this does not depend on the Seifert surface as long as $H_2(M) = 0$.

Pushing a Legendrian K (which we assume is closed but need not be nullhomotopic) along the unit normal $\mathbf{n}$ to ξ, we obtain another knot K'. The *Thurston–Bennequin* number $\mathrm{tb}(K)$ is the linking number of K and K', and computes the number of full rotations the director makes as we move around the curve K, to which it is orthogonal. Again, the restriction of ξ to a Seifert surface S for K is trivial, and we may choose a trivialisation X. The *rotation number* $\mathrm{rot}(K)$ is the number of times the tangent vector to K rotates relative to X, and again this is independent of S as long as $H_2(M) = 0$.

Theorem 3.13. *(Bennequin Inequalities for Knots) Let K be a knot bounding an embedded surface S in a tight contact manifold (M, ξ). If K is transverse to ξ, then*

$$\overline{SL}(K) \leq -\chi(S), \tag{3.29}$$

and if K is Legendrian, then

$$tb(K) + |rot(K)| \leq -\chi(S). \tag{3.30}$$

One may combine these inequalities with expressions for the Euler class in terms of various geometric quantities, e.g. Eq. (2.6) in Chapter 2, to produce bounds on these quantities in a tight contact manifold. I will not make further use of this idea here, and will focus on the applications of Giroux's criterion for the visualisation of cholesteric directors.

Later on in this thesis I will study cholesteric directors on manifolds with boundary, with the director either tangent (planar anchoring) or orthogonal (normal anchoring) to the boundary. In the case of planar anchoring, it is possible for such directors to be contact over the entire manifold, see Chapter 6. Therefore, we would like to know how to apply convex surface theory in this case, and in particular how to think about the boundary itself using these tools.

Let M be a manifold with boundary, and let $\mathrm{Tight}(M, \mathcal{F})$ be the set of all isotopy classes of tight contact structures that induce the characteristic foliation $\mathcal{F}$ on the boundary. We would like to know how exactly this class depends on $\mathcal{F}$. The answer, unsurprisingly, it is that it hardly depends on $\mathcal{F}$ at all.

Proposition 3.5. *Let $\mathcal{F}_0, \mathcal{F}_1$ be singular foliations on ∂M divided by the same curve Γ. Then Tight$(M, \mathcal{F}_0) \cong$ Tight$(M, \mathcal{F}_1)$*

See Ref. [Etn04a] for a proof. This result has consequences for cholesteric directors

in domains with planar anchoring, where the director is not fixed on the boundary but allowed to vary in the plane. Changes in the possible tight fillings for the interior will only occur when the singular points in the foliation change. To make this result fully general we will need to extend it to contact structures with defects, an exercise that will be carried out in Chapters 6 and 8.

Tight contact structures on balls with a fixed boundary condition were classified by Eliashberg [Eli92]. A modern proof can be found in §4.10 of Geiges [Gei08].

Lemma 3.5. *Let M be either the unit ball B, or the annulus $S^2 \times [0,1]$. Any two tight contact structures defining the same characteristic foliation on the boundary of M are isotopic rel. boundary; that is, Tight$(M, \mathcal{F})$ consists of a single point.*

If one has a cholesteric droplet with anchoring that is not too strong, so that the director need not be either tangent or orthogonal on the boundary, then this lemma implies that the director is determined up to homotopy by the homotopy class of the characteristic foliation on the boundary.

Now let us examine convex torii. This will allow us to study tight contact structures on $T^2 \times [0,1]$ and $D^2 \times S^1$, both of which correspond to physically-realisable domains. By Giroux's criterion, the dividing curve on a convex torus must consist of some number of homotopically essential curves; by orientability, there are an even number of them. Via an isotopy, we can assume all curves are linear of some fixed slope $-s$, $s > 0$; by which I mean their tangent vectors are $\mathbf{e}_x - s\mathbf{e}_y$.

A convex torus is said to be in *standard form* if the dividing curve consists of $2k$ lines of fixed rational slope $s \leq 0$, and the characteristic foliation is as shown in the right panel of Fig. 3.5. Such a torus can be produced by perturbting a non-convex surface where the characteristic foliation is by lines of slope s, for example a torus $T^2 \times z$ in T^3 with the contact structure defined by the cholesteric ground state. The perturbation involves pushing 'down' along some of the leaves and 'up' along others, more concretely, we take the surface of constant z', where $z' = \sin(y - zx)$. It's clear we can produce more than two dividing curves by pushing up/down in more places.

3.9.2 The Dividing Curve and Cholesteric Layers

Let us briefly examine the relationship between characteristic foliations, dividing curves, and the cholesteric layers. Typically the layers are thought of as surfaces to which the director is tangent, with their normal direction being aligned with the pitch axis; the surfaces of constant z coordinate are the layers in the ground state.

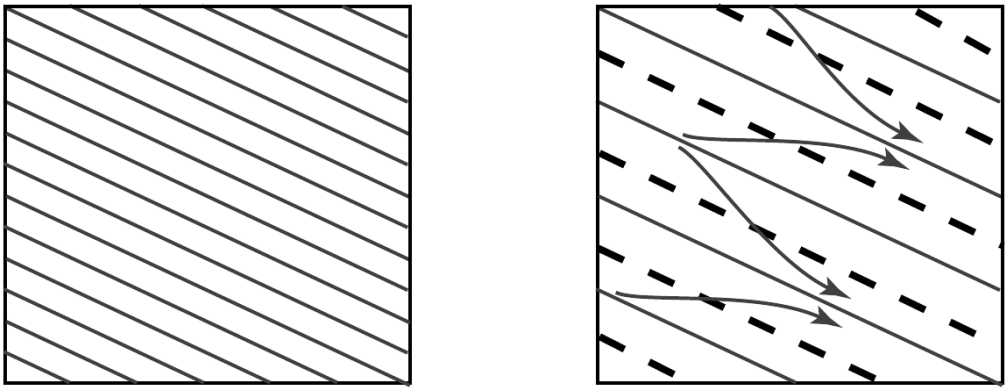

Figure 3.5: Left: a characteristic foliation on the torus by straight lines of fixed slope $s \in \mathbb{Q}$. Right: after a small perturbation, we produce a convex torus in standard form, where the dividing curves have slope s. Figure reproduced from [Etn04a].

This requires a geometric description. For the purposes of this discussion we will adopt a topological approach and not consider directors, but rather the Reeb field R of the contact form η dual to the director; recall the deviation between this direction and the director is determined by the bend. The *layers* in this system are the leaves of a singular foliation $\mathcal{F}$ to which R is tangent.

The following two propositions are very straightforward, but I was unable to find a reference in the literature.

Proposition 3.6. *Let S be a convex surface in a contact manifold (M, ξ). There exists a singular foliation $\mathcal{F}$, a collection of curves Γ, and a contact form η in a neighbourhood $S \times [-1, 1]$ of S with the following properties*

1. *$\xi = ker\ \eta$,*
2. *The connected components of the set $\Gamma \times [-1, 1]$ are leaves of $\mathcal{F}$,*
3. *The Reeb field R of η is tangent to $\mathcal{F}$.*

Proof. As S is convex, in a neighbourhood of S ξ can be defined by a vertically-invariant contact form $\eta = \beta + udz$, with Reeb field R, such that the set $\Gamma = \{u = 0\}$ divides the characteristic foliation induced on S. Then we have

$$d\eta = ud\beta + du \wedge dz. \tag{3.31}$$

In particular, along the set where $u = 0$ we must have $du(R) = 0$ and $dz(R) = 0$, i.e., R is tangent to the level set $u = 0$, and hence the surfaces $\Gamma \times [-1, 1]$. Since $d\beta$

is a top form on the surface, then away from the set of points where either $u = 0$ or $du = 0$ we can find a 1-form ω such that $ud\beta = du \wedge \omega$, so that away from the points where u or du vanish, we have $d\eta = du \wedge (\omega + dz)$. Then we conclude that $du(R)$ also vanishes on the complement of the set $du = 0$—this implies R is tangent to the level sets of u—and also $\omega(R) = -dz(R)$ on this set. At the isolated points where $du = 0$, $R = \pm\mathbf{e}_z$. Thus R is everywhere tangent to the sets $\{u = c\} \times [-1, 1]$, which define a singular foliation with singularities $p_j \times [-1, 1]$, for p_j the non-regular points of the function u. □

Giroux's Criterion also has an expression in terms of layers. Suppose the Reeb field R of is tangent to some singular foliation $\mathcal{F}$ whose singular set consists of a link L, which will necessarily be closed orbits of R.

Proposition 3.7. *Let S be a closed convex surface of positive genus inside M. If $S \cap L$ is empty, then the contact structure ξ defined by η is tight in a neighbourhood of S.*

Proof. Let X_0 direct the characteristic foliation induced by ξ on S, and let $\mathcal{G} = \mathcal{F} \cap S$ be the characteristic foliation induced by $\mathcal{F}$ on S. After a small perturbation of S which does not effect the conclusion of the proposition, we can assume that $\mathcal{G}$ has only isolated singularities. The Reeb field R of η is tangent to S along a set of curves Γ that divide the foliation directed by X_0. As R is also tangent to $\mathcal{F}$, it follows that Γ consists of leaves of the foliation $\mathcal{G} = \mathcal{F} \cap S$. Suppose that ξ is overtwisted in a neighbourhood of S. Then, by Giroux's criterion, Γ must have a nullhomotopic component, and so $\mathcal{F} \cap S$ has a closed nullhomotopic leaf. I claim that this implies $S \cap L$ is nonempty, which is contradiction, so ξ must be tight close to S. It remains to prove this claim.

Firstly, as S is convex we can homotope ξ to a contact structure ξ' defined by a contact form η' that is vertically-invariant, and the characteristic foliation of this contact form is still divided by Γ. The vertically-invariant property means that ξ' descends to a contact structure on $S \times S^1$. We construct a singular foliation $\mathcal{F}'$ on $S \times S^1$ as in Proposition 3.6, to which the Reeb field R' of η' is tangent. If Γ has a closed nullhomotopic component, then there is a singular point of the characteristic foliation of η' in the interior of this component of Γ, which corresponds to a closed orbit of R' and a singular line of $\mathcal{F}'$.

Thus the disk D bounded by this component of Γ has $e(\xi')[D] \neq 0$. As ξ is homotopic to ξ', we must also have $e(\xi)[D] \neq 0$. By the description of Legendrian vector fields in Chapter 2, in particular the Gauss–Bonnet–Chern theorem, this

implies that the singular link of $\mathcal{F}$ has nonempty intersection with D and hence with S. □

In particular, the link L must pierce any overtwisted disks. This supports our intuition that meron and Skyrmion tubes should contain a λ line, or β line (see Chapter 5 for the latter).

Note that we have not proved the converse, that ξ is tight in a neighbourhood of S implies $S \cap L$ is nonempty. This is not true: to see this, take a Darboux ball for the contact structure that is centred on a point of the singular link, and choose a closed surface of positive genus contained in this ball that also intersects the singular link transversally. By genericity, we may perturb this surface slightly to make it convex. Since this surface lies entirely in a Darboux ball the contact structure will be tight in a neighbourhood of the surface, and but it does intersect the singular link by design.

The idea of contact forms whose Reeb fields are tangent to foliations is an interesting one, and worth pursuing further for applications to liquid crystals, as well as being an interesting subclass of contact forms in its own right. Some speculative work in this direction is presented in Chapter 10.

3.9.3 Bypasses and Dislocations

Honda has introduced a helpful technqiue for manipulating the dividing curve on convex surfaces inside tight contact manifolds.

Definition 3.1. Let S be a convex surface in a contact manifold with dividing curve Γ. Let α be a Legendrian arc on S that intersects Γ in three points p_1, p_2, p_3, where p_1, p_3 are the endpoints of α. A *bypass* is a convex half-disk D such that $D \cap S = \alpha$ and $\mathrm{tb}(\partial D) = -1$.

See Fig. 3.6(a,b) for a picture of the bypass attachment. If S is then isotoped over D, the dividing set changes: the number of components is reduced by 2. A bypass is, in a sense, the smallest unit of change that can occur when isotoping a convex surface. Bypasses are a technical tool used in the proofs which I will not give in detail. However, it is useful to introduce the concept because of how it relates to edge dislocations in cholesterics, and the study of changes in the structure of cholesteric layers.

There are two kinds of bypasses where all three points p_1, p_2, p_3 lie on the same component of the dividing curve. They are shown in Fig. 3.6(c). One is trivial, and attaching a bypass does not change the structure of the dividing set. The second

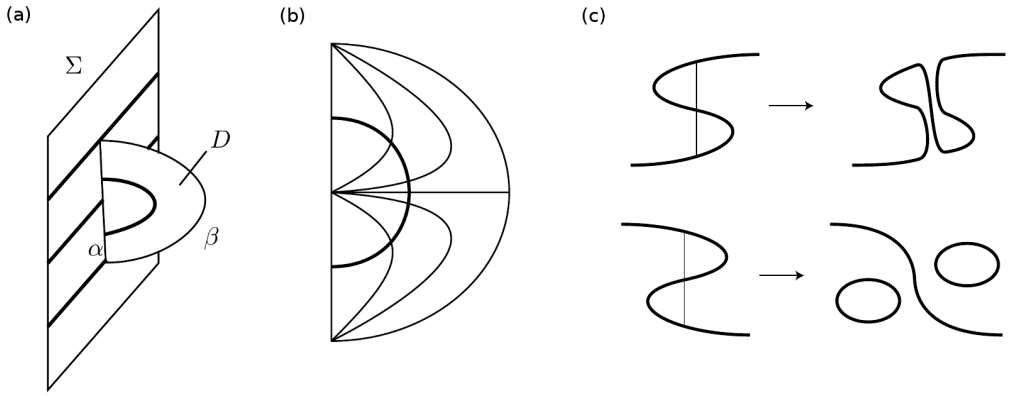

Figure 3.6: (a) A schematic diagram of a bypass along the attachment arc α, with the dividing curve being denoted by the thick black lines. (b) The characteristic foliation (thin lines) and dividing curve (thick line) induced on the half disk. (c) Top: trivial bypass attachment that has no effect on the dividing curve. Bottom: The 'bad' bypass attachment which produces a nullhomotopic component of the dividing set, and consequently reveals the presence of an overtwisted disk. All panels reproduced from [Etn04a].

is forbidden in a tight contact structure, as it creates nullhomotopic components of the dividing curve that indicate the presence of overtwisted disks. Both pictures assume the normal to the surface is pointing out of the page; if this is not the case, we reverse the meaning of the images.

A sudden change in the number of cholesteric layers is called an edge dislocation. A dislocation is not a singularity in the cholesteric director—these are called disclinations and are treated in Chapter 8—but rather in the pitch axis. Consequently, they are associated to the presence of λ lines. By analogy with the cholesteric ground state, we can define the *layer number* of a cholesteric texture to be the twisting number of some Legendrian arc that is transverse to the planes orthgonal to the pitch axis. Via Proposition 3.4, this twisting number can be computed by counting the intersection of the arc with the dividing curve on a suitably-chosen convex surface. Thus, by sliding a surface through the material in such a way that it is transverse to the layers, we pick up information about the number of layers, and detect dislocations by changes in the number of components of the dividing curve.

Let us consider a simple texture where the cholesteric layer number changes, as shown in Fig. 3.7(a). For $y < 0$, the texture undergoes three full rotations, while for $y > 0$, it undergoes only two. Fig. 3.7(b,c) show the dividing curve on two surfaces intersecting the layers transversally. As we move over the λ line (blue tube), the number of components in the dividing curve changes by 2. By

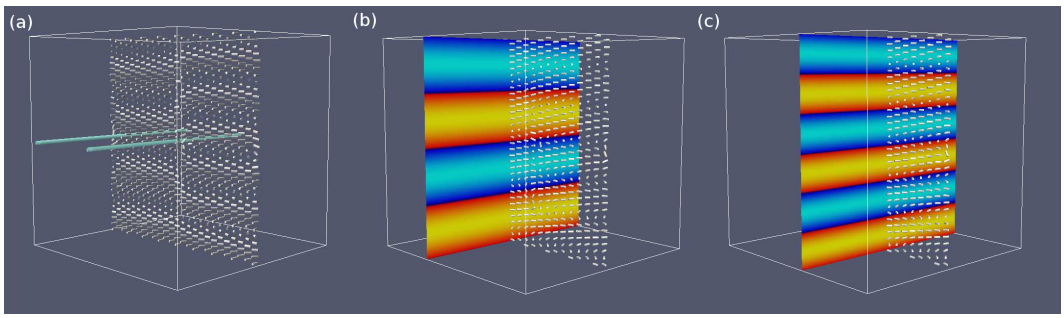

Figure 3.7: A change in the layer number of a cholesteric corresponds to a change in the number of components of the dividing curve on appropriately chosen convex surfaces. (a) A typical cholesteric texture on $T^2 \times [0,1]$ where the layer number changes as one passes through the surfaces $y = 0, \pi$. These changes are indicated by the presence of λ lines (blue tubes). Panel (b) and (c) show the dividing curves on surfaces that lie on either side of one of the λ lines. In panel (b) the dividing curve has four components, indicating that there are two full twists, while in panel (c) there are six components, indicating three full twists.

examining the characteristic foliation and the dividing curve we can explicitly see there is a possibility of adding a bypass which lowers the layer number, Fig. 3.8. The characteristic foliation on this half disk has the structure suggested by the schematic in Fig. 3.6.

In this example it is rather easy to see the change in layer number without resorting to an examination of bypasses. In later sections we will study textures in cholesteric droplets, where analogues of the layer number can be computed. Here, it is often not so quite so easy to read off the layer number by examining the director, and so techniques involving convex surfaces become more useful.

3.9.4 Tomography

While the work of Honda is largely centred around a 'cut-and-paste' theory of contact structures based on bypasses and manipulations of the dividing curve, Giroux adopts a different approach, focussing on the characteristic foliations traced out on a 1-parameter family of surfaces that span the system [Gir00]. A second-hand account of the ideas and results of Giroux, which has the advantage of being in English, is given in §4.9 of Geiges [Gei08].

Tomography can be used to obtain a coarse view of topological structures in chiral materials. Much of the topological information that is extracted from examining the 'film' of characteristic foliations and dividing curves made by a family of surfaces can be got at via other means, most notably looking at the zeros of a

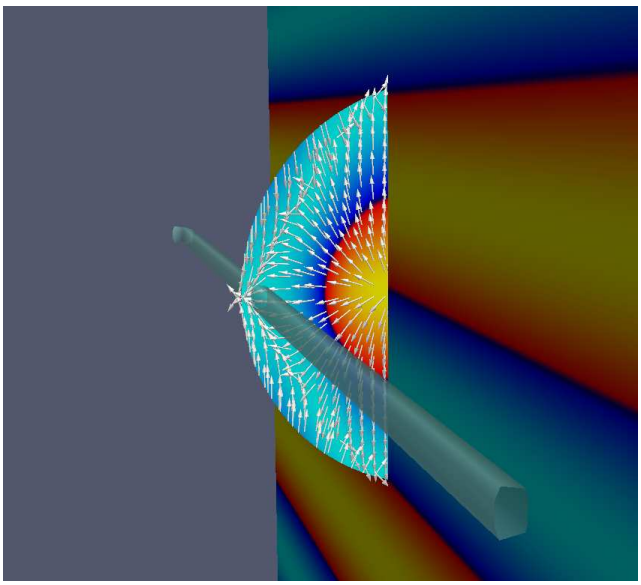

Figure 3.8: A half-disk attached to the surface shown in Fig. 3.7(c). The λ line is shown as a blue tube. Compare the characteristic foliation and dividing curve on the half-disk with the schematic in Fig. 3.6

Legendrian vector field, which also connects the information to energetics, however it can still aid us in visualising the structure of complex textures. In this section I will give a few simple examples to illustrate the concept, as well as the notion of a bypass introduced in the previous section. Once a theory of singularities in contact structures is developed, as will be done in Chapter 6, it becomes possible to apply tomography to a broader variety of systems, and we will see further examples in later chapters.

A central result underpinning tomography is the following uniqueness lemma. Since I will be using the result and similar results in later chapters I give a proof, taken from Geiges [Gei08].

Lemma 3.6. *(Uniqueness Lemma [Gir00; Gei08]) Let S be a closed surface and let ξ_0, ξ_1 be two contact structures on $S \times [0,1]$ with the following properties:*

1. *The characteristic foliations induced by ξ_0, ξ_1 on the boundary coincide.*
2. *Each $S \times z$ is convex for both contact structures, and there is a smoothly varying family of curves Γ_z that divides the characteristic foliations of both ξ_0 and ξ_1 on $S \times z$.*

Then ξ_0, ξ_1 are homotopic rel. boundary.

Proof. We can choose contact forms $\eta^i = \beta^i_z + u^i_z dz$ defining ξ_i. Set $A^i = u^i_z d\beta^i_z + \beta^i_z \wedge (du^i_z - \dot{\beta}^i_z)$. The contact condition implies these are positive functions. By convexity, we can choose functions v^i_z that vanish at first order on Γ_z and satisfy $B^i = v^i_z d\beta^i_z + \beta^i_z \wedge dv^i_z > 0$, which follows from Proposition 3.2. As v^i_z vanish at the same order on Γ_z, then for each z the function v^0_z/v^1_z extends to a function on all of $S \times z$, not just on $(S \times z) - \Gamma_z$.

An easy computation shows that we can replace β^1_z with $(v^0_z/v^1_z)\beta^1_z$ while keeping η^1 contact, which doesn't change the characteristic foliation induced on any $S \times z$ and is clearly homotopic to the original η^1, and after doing this we can take $v^0_z = v^1_z =: v_z$.

Now define $\eta^i_t = \beta^i_z + ((1-t)u^i_z + t\lambda v_z)dz$, for $\lambda > 0$ a positive constant. This is contact for all $t \in [0,1]$ provided that λ is sufficiently large. The 1-form $\eta_s = (1-s)\eta^0_1 + s\eta^1_1$ is also contact for all $s \in [0,1]$ provided λ is sufficiently large.

The desired homotopy between η^0 and η^1 is given by taking η^0_{3t} for $t \in [0, 1/3]$, η_{3t-1} for $t \in [1/3, 2/3]$, and η^1_{3-3t} for $t \in [2/3, 1]$. This homotopy is stationary on $S \times 0$ and $S \times 1$, and therefore gives a homotopy between ξ_0 and ξ_1 rel. boundary. □

The key ingredient of this proof is the existence of a smoothly varying family of curves that divides both characteristic foliations. Essentially, prescribing such a family of curves completely determines a contact structure on a family of surfaces. Discontinuous changes in the structure of the dividing curve are taken care of by considering bypass attachments. It's worth mentioning the following variant on this lemma, which deals with existence rather than the uniqueness of a contact structure inducing a particular set of characteristic foliations. I was unable to find a statement and proof of this lemma in the literature, however it is very simple.

Lemma 3.7. *(Existence Lemma) Let S be a compact surface, possibly with boundary. Suppose we are given a family $\mathcal{F}_z$, $z \in [0,1]$, of smooth singular foliations on S and a smoothly varying family of curves Γ_z such that Γ_z divides $\mathcal{F}_z$ for each z. Then there exists a contact structure ξ on $S \times [0,1]$ inducing the characteristic foliation $\mathcal{F}_z$ on each $S \times z$.*

Proof. Fix an area form Ω on S, choose a smoothly-varying set of vector fields X_z directing $\mathcal{F}_z$, and define $\beta_z = \iota_{X_z}\Omega$. By Proposition 3.2 we can choose functions v_z, depending smoothly on z, that vanish at first order on Γ_z and satisfy $A_z := v_z d\beta_z + \beta_z \wedge dv_z > 0$ for each z.

Let $\eta = \beta_z + v_z dz$. On $S \times [0,1]$, we have

$$\eta \wedge d\eta = (A_z - \beta_z \wedge \dot{\beta}_z)dz. \tag{3.32}$$

As $S \times [0,1]$ is compact, $\beta_z \wedge \dot{\beta}_z$ is bounded, $|\beta_z \wedge \dot{\beta}_z| < K_1$ say, where $K_1 > 0$ is a constant independent of z. We must also have $A_z > K_2 > 0$, where K_2 is some other positive constant. If $K_2 - K_1 > 0$, then η is certainly a contact form. Otherwise, consider rescaling v_z by a constant λ. Then $A_z \mapsto \lambda A_z$, and we may replace K_2 with λK_2. Thus for λ sufficiently large, we will have $\lambda K_2 - K_1 > 0$, and η will be contact. □

Now we will look at examples of complex textures whose structure is illuminated by tomography. Let K be a nullhomotopic knot or link in T^3, with solid angle function ω; for an introduction to solid angle and its use in defining directors with specific behaviour along knots, see Refs. [BA18; Bin19]. We define a director in a tube of radius R around K

$$\mathbf{n} = \sin\left(\frac{\pi r}{2R}\right)\cos(q_0 z + \omega/2)\mathbf{e}_x + \sin\left(\frac{\pi r}{2R}\right)\sin(q_0 z + \omega/2)\mathbf{e}_y + \cos\left(\frac{\pi r}{2R}\right)\mathbf{e}_z, \quad (3.33)$$

where $r(x,y,z)$ denotes distance from K. We extend this over the rest of the domain by letting it be equal to the cholesteric ground state there. This defines an overtwisted contact structure with a tube of merons along the link K.

Fig. 3.9 shows a texture obtained by initialising a simulation with (3.33), taking K to be a Hopf link, and allowing it to relax using gradient descent with the cholesteric Frank energy. We cosider the torii $x \times T^2$ and view the dividing curve as we allow x to slide from 0 to 2π. At 0, the dividing curve has four components, panel (a). Coming forward slightly, the surface touches the meron tube and the structure of the dividing curve changes, panel (b), resulting in a nullhomotopic component that indicates, via Giroux's criterion, the presence of the overtwisted disk. The change in the dividing curve indicates the presence of a bypass for the convex surface shown in (a), transforming it into that shown in (b). There is a second bypass, which results in the characteristic foliation of (c); here, there are two nullhomotopic components of the dividing curve, indicating that we are now intersecting the meron tube in two places. As we continue sliding the torus forwards, the dividing curve undergoes the inverse transformations, finally returning to the case where it has four homotopically-essential components.

A similar series of transformations occurs when we construct a texture using the same initialisation but take K to be a trefoil knot, see Fig. 3.10. In Fig. 3.11, we examine one convex surface (panel (e) in Fig. 3.10) in the trefoil texture for the possibility of a bypass. We see (indicated in green) a region of the dividing curve as shown in the bottom panel of Fig. 3.6(c). This allows for a 'bad' bypass attachment that would be forbidden in a tight contact structure. There is a Legendrian arc

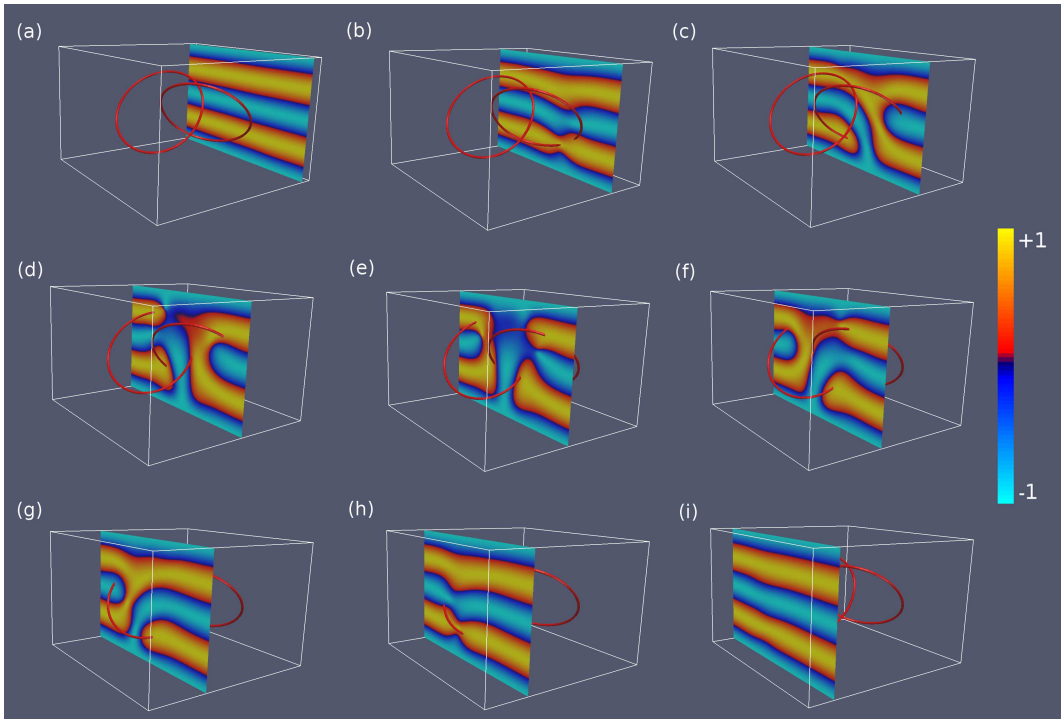

Figure 3.9: A director in T^3 containing two tubes of merons that form a Hopf link. The initialisation is given by Eq. (3.33). As we slide a convex torus through the material, the structure of dividing curve changes, allowing us to see passage across the meron as a series of edge dislocations, and also detecting the presence of overtwisted disks.

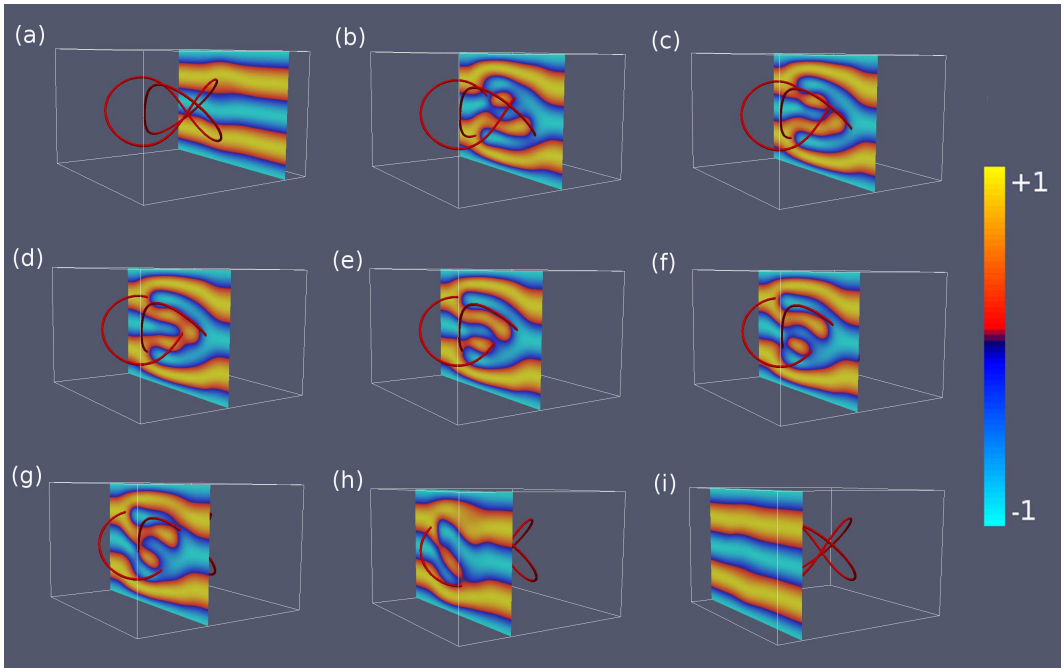

Figure 3.10: A director in T^3 containing a tube of merons that form a trefoil knot. The initialisation is given by Eq. (3.33). In panel (a), the dividing curve has four components; in panel (d), it has only two, showing that we have passed through an edge dislocation. Panels (b,f) show a dividing curve with a nullhomotopic components, indicating an overtwisted disk as per Giroux's criterion.

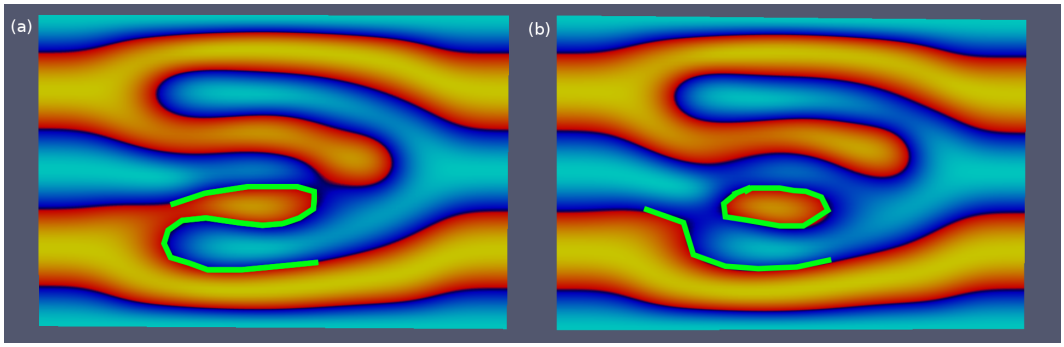

Figure 3.11: Closer view of panels (e) and (f) from Fig. 3.10. There is a 'bad' bypass that may be attached along a Legendrian arc transverse to the green curve in panel (a). Isotoping along the bypass results in panel (b), and the creation of a nullhomotopic component of the dividing curve, which indicates the presence of an overtwisted disk.

intersecting the green section of curve in three places. Attaching a bypass along this arc and isotoping along it results in a new dividing curve with a nullhomotopic component.

3.10 On the Classication of Tight Contact Structures

3.10.1 Tight Contact Structures on the 3-Torus

Now let us turn to the classification of tight contact structures via convex surface theory. First, I will sketch the classification on $\mathbb{T}^3$, and the formalisation of the idea of 'layer number' that comes from our intuition about the cholesteric ground state. We begin with the following lemma, which is due to Kanda [Kan97].

Lemma 3.8. *There is a unique tight contact structure on $D^2 \times S^1$ whose convex boundary in standard form has a dividing curve with two components and slope $\frac{1}{q}$, $q > 0$; this contact structure ξ_q is defined by $\eta_k = \cos(qz)dx - \sin(qz)dy$.*

Proof. Evidently the given contact form η_q defines a contact structure with the appropriate boundary condition, so it suffices to demonstrate uniqueness. Let S be the boundary of the solid torus, and D a meridonal disk. Using the Legendrian realisation principle, we may realise ∂D as a Legendrian curve with Thurston–Bennequin number -1. Perturbing D slightly, we may assume it convex, and since $\mathrm{tb}(\partial D) = -1$ the dividing curve must have a single component. Moreover this component must connected the boundary to itself, otherwise we could apply the Legendrian realisation principle again to find an overtwisted disk. Thus there is, up to isotopy, a unique contact structure in a neighbourhood of D.

The dividing curve uniquely determines the contact structure in a neighbourhood of S as well, and consequently we find that there is a unique contact structure in a neighbourhood of $S \cup D$ determined by the dividing curve on the boundary. What is left is a ball $B \subset D^2 \times S^1$, so we can apply Lemma 3.5 to conclude that there is a unique extension over the interior. □

Note that this shows that any Legendrian curve with Thurston–Bennequin number q has a neighbourhood diffeomorphic to $\eta_q = \cos(qz)dx - \sin(qz)dy$. My reason for giving this argument here is that it will reappear in Chapter 8, where it will be applied to the characterisation of disclination lines in cholesterics.

The layer number is a homotopy invariant, indeed the only homotopy invariant. Let ξ_q be the contact structure on T^3 defined by η_q.

Theorem 3.14. *(Classification Theorem [Kan97]) The contact structures ξ_q on $\mathbb{T}^3$ are not homotopic for distinct q. Every tight contact structure on $\mathbb{T}^3$ is homotopic to one of the ξ_q.*

The proof strategy is to look at nullhomotopic Legendrian curves, and demonstrate that the Thurston–Bennequin number of such curve in ξ_q is at least q (at most $-q$ for right-handed contact structures), with the minimum being achieved by a curve with tangent vector $\mathbf{e}_z$. The uniqueness lemma 3.8 implies the contact structure is unique in a neighbourhood of such a curve, and convex surface theory methods are used to extend this over the rest of the domain.

This theorem implies that the creation of an edge dislocation cannot occur in the cholesteric ground state without the simultaneous creation of regions of reversed handedness. To see this, observe that if we create an edge dislocation in the state η_q, we can move the two λ lines shown in Fig. 3.7 opposite ways around along an incompressible torus, and annihilate them again on the other side. The result of this homotopy would be to carry η_q into η_{q+1}; however, Theorem 3.14 implies we cannot do this through a homotopy through contact structures, and therefore the creation of the edge dislocation must not be possible via a homotopy through contact structures. We can also see this by noting that the edge dislocation state shown in Fig. 3.7 is actually overtwisted, see also Fig. 5.14.

3.10.2 Tight Contact Structures on Toric Annuli

In [Hon00a; Hon00b], Honda classifies tight contact structures on a variety of manifolds: $T^2 \times [0,1]$, $D^2 \times S^1$, lens spaces $L(p,q)$, twisted torus bundles $T^2 \times_\phi S^1$, and products of a genus g surface and a circle $\Sigma_g \times S^1$. It is the first two spaces that

really interest us, being physically-realisable domains. In particular, $T^2 \times [0,1]$ with some fixed boundary condition represents the cell used in a typical experimental set up (although the experimental cell will not generally have periodic boundary conditions). I will not give full details of the classification theorem here, and most of the technical results are far beyond the scope of this thesis, however it is instructive to examine the basic definitions and to state the classification theorem.

First, introduce some notation. Denote by T_z the slice $T^2 \times z$. We can assume that the boundary torii T_0 and T_1 are convex, and the dividing curve and characteristic foliation are placed in standard form. Via an action of the group $\mathrm{SL}(2,\mathbb{Z})$, we may assume the boundary component T_0 has a dividing curve with $2n_0$ components of slope -1, while the boundary torus T_1 has a dividing curve with $2n_1$ components of slope $-\frac{p}{q}$, where $p \geq q > 0$ have no common divisors. More generally, given a convex torus T_z whose dividing curves are linear curves, we denote the slope by s_z.

Given a slope s of a line in T^2, we associate it with the standard angle $\alpha(s) \in \mathbb{RP}^1$. A slope is said to be between s_1 and s_0 if $\alpha(s_1) \leq \alpha(s) \leq \alpha(s_0)$; said differently, if we view the slopes as being points on the projectivised unit circle, then a slope is between s_0 and s_1 if it is clockwise of s_0 and anti-clockwise of s_1. A tight contact structure ξ on $T^2 \times [0,1]$ is called *minimally twisting* if the slope on every convex torus T_z is between s_1 and s_0.

Recall we can associate to $-\frac{p}{q}$ its continued fraction expansion

$$-\frac{p}{q} = r_0 - \cfrac{1}{r_1 - \cfrac{1}{r_2 - \cdots \frac{1}{r_k}}} \tag{3.34}$$

where each integer $r_i \leq 2$, unless $p = q = 1$. Then, assuming a tight contact structure on $T^2 \times [0,1]$ with convex boundary with 2 dividing curves on each boundary component in the form discussed above, we have the following classification theorem.

Theorem 3.15. *The classification of tight contact structures on $T^2 \times [0,1]$ is as follows:*

1. *There are exactly $|(r_0+1)(r_1+1)\ldots(r_{k-1}+1)r_k|$ tight contact structures with minimal twisting.*

2. *For each integer $n > 0$ there are exactly two tight contact structures ξ with $n\pi \leq \beta(\xi) \leq (n+1)\pi$.*

It is worth mentioning the classification of tight contact structures on solid torii as well, which is also due to Honda [Hon00a].

Theorem 3.16. *There are exactly* $|(r_0+1)(r_1+1)\cdots(r_{k-1}+1)r_k|$ *tight contact structures with minimal twisting on* $D^2 \times S^1$ *inducing a dividing slope on the convex boundary with two components of slope* $-\frac{p}{q}$.

3.11 Contact Geometry: Beltrami Fields, and the Etnyre–Ghrist Correspondence

In this section I will discuss the more geometric aspects of contact structures. My primary reference is the monologue by Blair [Bla10]. The essential idea is that the 2-form $d\eta$ endows the contact planes ξ with a symplectic structure, which in turn implies the existence of a Riemannian metric that is, in a sense, compatible with the contact structure in the same way that one can construct metrics compatible with symplectic structures. These compatible metrics can be seen as metrics for which the gradient tensor of the director is reduced to only the essential parts.

First I will recall a few facts about Riemmanian metrics for readers who are unfamiliar with the concept. The metric g determines a map $\star : \bigwedge^p \to \bigwedge^{3-p}$ on the exterior algebra that takes p-forms into $(3-p)$-forms, the *Hodge star*, and this map satisfies $\star^2 = I$. The Hodge star satisfies the relationship

$$g(\alpha, \beta)\mu = \alpha \wedge \star\beta \tag{3.35}$$

for any pair of p-forms α, β, where μ is the volume form of g. This relationship uniquely determines the Hodge star, and may consequently be taken as a definition of it. In particular, if one expresses g as a matrix $g = [g_{ij}]$ with respect to a coordinate basis, the entries s_{ij} for the matrix form of $\star$ are $g_{ij}\sqrt{|g|} = s_{ij}$.

Using the Hodge star, we can define a *codifferential* $\delta = \star d \star$ that maps p-forms to $(p-1)$ forms. When applied to a 1-form η dual to a vector field $\mathbf{n}$, we have $\delta\eta = \operatorname{div} \mathbf{n}$, so that δ generalises the divergence operator. Using the exterior derivative and the codifferential, we define the *Laplace–Beltrami operator* of g[3],

$$\Delta_g = d\delta + \delta d. \tag{3.36}$$

The Hodge decomposition theorem generalises the Helmholtz decomposition. It states that any p-form η can be written

$$\eta = \alpha + \beta + \gamma, \tag{3.37}$$

[3]One should note this is different from the Böckner Laplacian $\nabla^*\nabla$, although they are related.

where α is closed, β is coclosed ($\delta\beta = 0$), and γ is harmonic. On a compact manifold, a 1-form is harmonic if and only if it is both closed and coclosed. When applied to vector fields on $\mathbb{R}^3$ this simply says we can write the vector field as the sum of a curl-free part and divergence-free part, the Helmoholtz Theorem.

3.11.1 Compatible Metrics

The relationship between the contact condition and Riemannian geometry is explained by the following lemma. Since I will use and generalise this lemma later on in Chapter 6, I present two proofs of it here. The first is taken from §9.4 of Farber [Far03], the second is based on the proofs in §4.2 of the monologue by Blair [Bla10] and more easily generalisable to the singular case.

Lemma 3.9. *Let α be a nonzero 1-form and β a nonzero 2-form such that $\alpha\wedge\beta > 0$. There exists a Riemannian metric g such that $\star_g\alpha = \beta$.*

Proof. (Proof 1) We can work in coordinate charts $\{U\}$. We can choose this system of charts so that on each set U in the cover there is a coordinate basis of 1-forms dx_1, dx_2, dx_3 such that $dx_1 = \alpha|_U$ and $dx_1 \wedge dx_2 \wedge dx_3 > 0$. We can write

$$\beta|_U = a_1 dx_2 \wedge dx_3 + a_2 dx_1 \wedge dx_3 + a_3 dx_1 \wedge dx_2, \tag{3.38}$$

and by assumption we have $a_1 \neq 0$. Define a set η_i of 1-forms by setting $\eta_1 = \alpha$ and

$$\eta_i = dx_i + (-1)^i \frac{a_i}{a_1} dx_1, \tag{3.39}$$

for $i = 2, 3$. Then $\alpha|_U = \eta_1, \beta|_U = a_1\eta_2 \wedge \eta_3$. Define a Riemannian metric g_U by taking $\eta_1, a_1\eta_2, \eta_3$ to be an orthonormal basis. Then $\star_{g_U}\alpha|_U = \beta|_U$, and the volume form is $(\alpha \wedge \beta)|_U$.

Now we have to glue these metrics together. Choose a partition of unity f_U subordinate to the open cover and fix some volume form μ, and then define a metric by $g(X, Y)\mu = \sum_U f_U g_U(X, Y)(\alpha \wedge \beta)|_U$ for vector fields X, Y. The volume form of this metric is $\mu_g = a\mu$ for some function $a > 0$, and we have

$$\star_g\alpha = a\beta. \tag{3.40}$$

It remains to rescale g by a factor a^{-2}, which will rescale the star operator by a factor of a^{-1}, yielding the desired metric. □

Proof. (Proof 2) Let ξ denote the kernel of α. Since $\beta|_\xi$ is nonzero by assumption, its kernel must be one-dimensional. Let R be the vector field in this kernel such

that $\alpha(R) = 1$. Since R is transverse to ξ, we can choose a Riemannian metric h such that R is the unit normal to ξ in this metric. Let $\mathbf{e}_1, \mathbf{e}_2$ be a local orthonormal basis for ξ. Let A be the matrix with entries $A_{ij} = \beta(\mathbf{e}_i, \mathbf{e}_j)$, $i = 1, 2$. Then A is a skew symmetric matrix with nonzero eigenvectors. A well-known fact about such matrices is that they admit a polarisation: there is a positive-definite symmetric matrix G and an orthogonal matrix F such that $A = FG$. Let $g'(\mathbf{e}_i, \mathbf{e}_j) = G_{ij}$. This defines an inner product on the planes of ξ. Extend g' to a metric g that agrees with h in the direction R. This g is the desired Riemannian metric. □

An immediate corollary of this lemma is the existence of *compatible metrics* for contact forms, by taking $\beta = d\alpha$ for α a contact form.

Theorem 3.17. *Let η be a contact form with Reeb field R defining a contact structure ξ. Then there exists a Riemannian metric g and a $(1,1)$ tensor $J : TM \to TM$ such that $\star_g d\eta = \eta$, $J = -I + \eta \otimes R$, and $g(X, JY) = d\eta(X, Y)$ for all vector fields X, Y.*

The second proof shows we can view the space of the compatible metrics as the image of a projection operator on the space of Riemannian metrics, see Blair [Bla10][4]. Using the expression for the Reeb field of a contact form in terms of the director, Eq. (3.3), we can construct the metric that results from applying this projection to the Euclidean metric. Let h be the Euclidean metric. We define a new metric k by

$$k(X, Y) = h(-X + \eta(X)R, -Y + \eta(Y)R) + \eta(X)\eta(Y). \tag{3.41}$$

In the orthonormal basis $\mathbf{e}_1, \mathbf{e}_2, \mathbf{n}$, this is given by the matrix

$$k = \begin{bmatrix} 1 & 0 & \frac{b_2}{q} \\ 0 & 1 & -\frac{b_1}{q} \\ \frac{b_2}{q} & -\frac{b_1}{q} & 1 + \frac{\kappa^2}{q^2} \end{bmatrix} \tag{3.42}$$

where we have written the bend as $\mathbf{b} = b_1\mathbf{e}_1 + b_2\mathbf{e}_2$, q is the twist of $\mathbf{n}$ and κ is the norm of the bend in the Euclidean metric. Now we must polarise $d\eta$ on ξ. The matrix referred to as A in the proof of Lemma 3.9 is

$$A = \begin{bmatrix} 0 & q \\ -q & 0 \end{bmatrix}, \tag{3.43}$$

[4] I am using slightly different conventions to this reference. There, compatible metrics are referred to as associated metrics, and they satisfy $\star d\eta = 2\eta$.

in the basis $\mathbf{e}_1, \mathbf{e}_2$, which is a k-orthonormal basis for ξ. Polarisation gives

$$G = \begin{bmatrix} q & 0 \\ 0 & q \end{bmatrix}, \qquad F = \begin{bmatrix} 0 & 1 \\ -1 & 0 \end{bmatrix}. \tag{3.44}$$

Thus the compatible metric g that results from applying the projection onto the space of compatible metrics to the Euclidean metric h is

$$g = \begin{bmatrix} q & 0 & b_2 \\ 0 & q & -b_1 \\ b_2 & -b_1 & 1 + \frac{\kappa^2}{q} \end{bmatrix} \tag{3.45}$$

as a matrix with respect to the frame $\mathbf{e}_1, \mathbf{e}_2, \mathbf{n}$. As a sanity check, note that if η is the cholesteric ground state the Euclidean metric is already compatible with η and indeed the projection has no effect in this case. The difference between this metric and the Euclidean metric is a measure of the failure of a cholesteric director to be a global minimum of the Frank energy. Further, suppose we have a homotopy η_t of unit contact forms. Then we can find a moving frame $\mathbf{e}_1(t), \mathbf{e}_2(t)$ that is an orthonormal (with respect to the Euclidean metric) basis for the contact structure ξ_t defined by η_t, and we can choose this pair of vector fields so that they also depend smoothly on t. Since the bend and twist depend smoothly on t, the construction just outlined produces a smooth family g_t of metrics such that, for each t, g_t is compatible with $\mathbf{n}_t$ – although this construction produces a matrix for g_t that is expressed with respect to a time-varying basis, the metric itself is obviously independent of the choice of basis, so this family is well-defined.

With respect to a compatible metric, the twist is constant, the splay and bend vanish, and all that is left is the deviatoric part of $\nabla\mathbf{n}$, the tensor Δ.

3.11.2 Beltrami Fields

Using compatible metrics, we can demonstrate the connection between contact geometry and fluid dynamics first explored in [EG00a]. Recall that Euler's equations for an incompressible flow u on a Riemannian 3-manifold (M, g) are

$$\begin{aligned} \partial_t u + \nabla_u u &= -\nabla p, \\ d\iota_u \mu &= 0, \end{aligned} \tag{3.46}$$

where μ is the volume form of the manifold and p is the pressure. Suppose u does not depend on time t. Fundamental solutions to the Euler equations are given by vector fields satisfying $d\iota_u\mu = 0$ and $\operatorname{curl} u = \lambda u$ for some function λ. Such a

vector field is called a *Beltrami field* on (M, g). By a slight abuse of notation, I will call any vector field that is parallel to its curl for *some* Riemannian metric g and some proportionality factor λ (a positive function) a Beltrami field, and this is the convention I will use throughout—such a field always preserves some volume form, but need not preserve the volume form of g. Some authors also use the terms 'curl eigenfield' (generally when λ is a constant) or refer to such fields as 'force-free'.

The following theorem connects Beltrami fields to contact geometry.

Theorem 3.18. *(Etnyre–Ghrist Correspondence [EG00a]) There is a one to one correspondence between nonsingular Beltrami fields on M, and the Reeb fields of contact forms.*

Proof. Given a contact form η with Reeb field R, we have already shown the existence of a metric which makes R Beltrami, so it remains to give the other half of the correspondence. Let R be a Beltrami field with respect to some metric g, curl $R = \lambda R$ for some function $\lambda > 0$. Define $\eta = \iota_R g$. The condition on R translates to $\star_g d\eta = \lambda\eta$, which implies that $\eta \wedge d\eta = \frac{1}{\lambda} \|\eta\|_g^2$, and consequently η is a contact form. The Reeb field of η is $\|R\|^{-2} R$, so rescale η by $\|R\|^{-2}$ to obtain a contact form whose Reeb field is R. □

This theorem allows methods from contact topology to be brought to bear on problems in fluid dynamics, see the original papers of Etnyre & Ghrist [EG00a; EG02b; EG00b] for a general survey. One major result that can be proved this way is that every Beltrami field on a closed manifold must have a closed orbit, a consequence of the proof of the Weinstein conjecture in dimension 3 by Taubes [Tau07]. In general the closed orbits of a Beltrami field can be extremely complicated, supporting knots and links of all possible types [EG00b], even when one insists that the field is Beltrami with respect to the Euclidean metric [EPS15].

The difference between a vector field for which $\mathbf{n} \cdot \nabla \times \mathbf{n} \neq 0$ and a vector field which is Beltrami (with some proportionality factor λ) with respect to some metric is a subtle one. If we don't worry about the divergence vanishing, then a vector field being Beltrami with respect to some metric is equivalent to there being a metric for which its bend vanishes, i.e. there is a metric for which its integral curves are geodesics, and this in turn must be equivalent to it being the Reeb field of a contact structure via the Etnyre–Ghrist correspondence. One can prove a variant of the Etnyre–Ghrist correspondence for 'contact structures with singularities', and we will see that the difference between singular vector fields where $\mathbf{n} \cdot \nabla \times \mathbf{n} \neq 0$ away from the singular point and Beltrami fields has an impact on the singularities that can occur.

One can also consider *weakly compatible metrics* [EKM12], where the Reeb field R of η is orthogonal to ξ and has length ρ, and furthermore $\star_g d\eta = \lambda\eta$, for a pair of positive functions ρ, λ. Then R is still a Beltrami field, with curl $R = \lambda R$, although R may not be divergence-free. As we argued at the beginning of this chapter, in order for $\mathbf{n}$ to be the normalisation of some Reeb field of the orthogonal contact structure ξ, the bend of $\mathbf{n}$ had to be gradient like. If $\mathbf{n}$ is the normalisation of a Reeb field with respect to some weakly compatible metric of η, $\mathbf{n} = R/\rho$, then we see that

$$\nabla_{\mathbf{n}}\mathbf{n} = -(\nabla \log \rho)^{\xi}, \tag{3.47}$$

where X^{ξ} denotes the component of the vector field X that is tangent to ξ. This allows us to find the following condition for when $\mathbf{n}$ is the normalisation of a Beltrami field.

Proposition 3.8. *Let* $\mathbf{n}$ *be a director in Euclidean space with non-vanishing twist, with dual 1-form* η *and orthogonal plane field* ξ*. The following are equivalent*

1. $\mathbf{n}$ *is the normalisation of the Reeb field* $\bar{R}$ *associated to some contact form* $\bar{\eta}$ *defining* ξ*,*
2. *There exists a contact form* $\bar{\eta}$ *defining* ξ *such that the Euclidean metric is weakly compatible with* $\bar{\eta}$ *defining* ξ*,*
3. *There exists a function* f *such that the bend of* $\mathbf{n}$ *is equal to* $-(\nabla f)^{\xi}$*.*

Proof. We have just seen that (2) implies both (1) and (3). That (3) implies (1) was argued in §3.3. If (1) holds, then the Reeb field of $\bar{\eta}$ is orthogonal to ξ, and hence the Euclidean metric must be weakly compatible with $\bar{\eta}$, showing (2). □

Not all vector fields that are chiral, satisfying $\mathbf{n} \cdot \nabla \times \mathbf{n} \neq 0$ with respect to some metric, are Beltrami, parallel to their curl for some metric. Taubes' proof of the Weinstein conjecture implies every Beltrami field on a 3-manifold has a closed orbit [Tau07]. Therefore, we can produce an example of a vector field that is chiral but not Beltrami by finding a vector field transverse to a contact structure without closed orbits. Consider the contact structure defined by $\eta = \cos(z)dx - \sin(z)dy$ on T^3. The vector field[5]

$$X = \cos(z)\mathbf{e}_x - \sin(z)\mathbf{e}_y + \sqrt{2}\cos(z)\mathbf{e}_z, \tag{3.48}$$

is evidently transervse to this contact structure, as $\eta(X) = 1$. The torii $z = 0, \pi$ are invariant under the flow of X, and every orbit on these torii is dense and consequently

[5]This example is taken from an answer to a MathOverflow question.

not closed. Every other integral curve limits on the torii $z = 0, \pi$ in forward and backward time, and hence these orbits are also not closed. Therefore, this vector field is chiral but not Beltrami.

Chapter 4

Geometric Description of Liquid Crystals, and Reconstruction Problems

4.1 Introduction

Several classical problems in differential geometry involve determining the necessary and sufficient information to construct a geometric object. The Frenet–Serret theorem proves that a space curve is determined by its curvature and torsion, while the Gauss–Cadazzi equations show that an embedded surface can be reconstructed from knowledge of its first and second fundamental forms. In this chapter we consider a similar geometric reconstruction problem, that of constructing a liquid crystal director $\mathbf{n}$ from knowledge of its gradient tensor $\nabla\mathbf{n}$. This problem was solved in two dimensions by Niv & Efrati in a recent paper [NE18], which I recap in §4.2. In this chapter I solve the problem in three dimensions, demonstrating that, in general, the gradient tensor does not contain sufficient information and we need additional information about the gradients of the bend vector field $\mathbf{b}$ in order to solve the reconstruction problem. My approach uses classical differential geometry as well as Cartan's theory of moving frames, and helps connect the problem to Lie theory and fundamental symmetries of liquid crystal directors.

4.2 The Geometric Reconstruction Problem for Directors on Surfaces: A Review

4.2.1 The Reconstruction Method of Niv and Efrati

To motivate my construction, I first review the reconstruction formula for a director in two dimensions [NE18]. Given any director $\mathbf{n}$ on a surface S with Riemannian metric g of Gaussian curvature K there is a unique unit vector $\mathbf{n}_\perp$ orthogonal to it such that the pair $\mathbf{n}, \mathbf{n}_\perp$ form a right-handed basis. Let $\eta, \eta_\perp$ denote the differential 1-forms dual to $\mathbf{n}, \mathbf{n}_\perp$. The derivatives of $\mathbf{n}$ decompose as

$$\nabla \mathbf{n} = \big(\kappa\eta + s\eta_\perp\big) \otimes \mathbf{n}_\perp, \tag{4.1}$$

where κ is the curvature of the integral curves of $\mathbf{n}$ (and magnitude of the bend $\mathbf{b} = \nabla_{\mathbf{n}}\mathbf{n}$) and $s = \nabla\cdot\mathbf{n}$ is the splay. We read off the connection 1-form $\omega = \kappa\eta + s\eta_\perp$. The curvature 2-form is $\Omega = d\omega = d\kappa \wedge \eta + \kappa d\eta + ds \wedge \eta_\perp + s d\eta_\perp$, and the Gaussian curvature is $K = -\Omega(\mathbf{n}, \mathbf{n}_\perp)$. Using the formula $\Omega(X, Y) = X(\omega(Y)) - Y(\omega(X)) - \omega([X, Y])$ for the curvature form, we write this as

$$K = \nabla_{\mathbf{n}_\perp}\kappa - \nabla_{\mathbf{n}} s + \kappa\eta\big([\mathbf{n}, \mathbf{n}_\perp]\big) + s\eta_\perp\big([\mathbf{n}, \mathbf{n}_\perp]\big). \tag{4.2}$$

Since the connection is torsion free $[\mathbf{n}, \mathbf{n}_\perp] = \nabla_{\mathbf{n}}\mathbf{n}_\perp - \nabla_{\mathbf{n}_\perp}\mathbf{n} = -\kappa\mathbf{n} - s\mathbf{n}_\perp$, which leads to the geometric compatibility equation [NE18],

$$K = -s^2 - \kappa^2 - \nabla_{\mathbf{n}} s + \nabla_{\mathbf{n}_\perp}\kappa. \tag{4.3}$$

The reconstruction problem in two dimensions is to find a director field given (generic) splay and bend functions, s and κ. The geometric compatibility condition (4.3) is key to solving it. Let J denote the almost complex structure on the tangent space which is compatible with the metric (for example, if g is the Euclidean metric then $J\mathbf{e}_x = \mathbf{e}_y$ in a local coordinate system x, y). Then, by noting that $\mathbf{n}_\perp\cdot\nabla\kappa = (J\mathbf{n})\cdot\nabla\kappa = -\mathbf{n}\cdot J\nabla\kappa$, we can rewrite the compatibility condition (4.3) as

$$\mathbf{n}\cdot\big(\nabla s + J\nabla\kappa\big) = -K - s^2 - \kappa^2. \tag{4.4}$$

Using the given splay and bend functions we can define the orthonormal frame,

$$\mathbf{e}_1 = \frac{\nabla s + J\nabla\kappa}{|\nabla s + J\nabla\kappa|}, \qquad\qquad \mathbf{e}_2 = J\mathbf{e}_1, \tag{4.5}$$

and the compatibility condition gives the component of the director along $\mathbf{e}_1$; the component along $\mathbf{e}_2$ follows from normalisation, $|\mathbf{n}| = 1$. Explicitly we have the reconstruction formula

$$\mathbf{n} = -\frac{s^2 + \kappa^2 + K}{|\nabla s + J\nabla\kappa|}\,\mathbf{e}_1 \pm \sqrt{1 - \frac{(s^2 + \kappa^2 + K)^2}{|\nabla s + J\nabla\kappa|^2}}\,\mathbf{e}_2. \tag{4.6}$$

The sign choice is not arbitrary: only one of the branches yields the correct director [NE18]. To resolve the ambiguity we compute the splay and bend of the director and choose the sign so that they agree with s and $\kappa\mathbf{n}_\perp$. It is interesting to note that the reconstruction formula is purely algebraic, which contrasts with the reconstruction of space curves and surfaces in $\mathbb{R}^3$, both of which require solving a differential equation.

The unresolved part of the reconstruction is the identification of the allowed set of functions that can represent the splay and bend of a director field. The geometric compatibility equation (4.4) implies that the functions s and κ must satisfy the necessary condition

$$|\nabla s + J\nabla\kappa| \geq s^2 + \kappa^2 + K. \tag{4.7}$$

On a flat surface ($K = 0$) both s and κ must vanish at any points where $\nabla s + J\nabla\kappa = 0$, which is equivalent to the Cauchy–Riemann equations for $s + i\kappa$; it follows that s and κ cannot be the real and imaginary parts of a holomorphic function. However, the constraint represented by the necessary condition (4.7) is stronger than this and it is currently not known what the set of allowed splay and bend functions is.

4.2.2 Coframes and Structure Functions

As a precursor to considering the corresponding compatibility and reconstruction problems in three dimensions, I now describe how the two-dimensional case fits into a more general picture. Any frame $\{\mathbf{e}_1, \mathbf{e}_2\}$ on the surface is completely determined by its *structure functions* c_{ijk}, determed by the Lie bracket of the frame components [Car37; Car45; Olv95]. In two dimensions we require only one Lie bracket, $[\mathbf{e}_1, \mathbf{e}_2]$, to compute the Lie bracket of any pair of vector fields, and there are two structure functions, c_{121} and c_{122}. The Lie bracket is itself a vector field and hence can be expressed as a linear combination of the basis vectors

$$[\mathbf{e}_1, \mathbf{e}_2] = c_{121}\mathbf{e}_1 + c_{122}\mathbf{e}_2, \tag{4.8}$$

which defines the structure functions. When the frame is orthonormal the structure functions determine the metric tensor though their relationship with the connection 1-form. We can write the components of the connection 1-form $\omega_j^k = \sum_i \omega_{ij}^k \mathbf{e}^i$ as

$$\omega_{ij}^k = \mathbf{e}_k \cdot \nabla_{\mathbf{e}_i} \mathbf{e}_j = \frac{1}{2}(c_{ijk} + c_{kij} + c_{kji}). \tag{4.9}$$

For the particular choice $\mathbf{e}_1 = \mathbf{n}$ and $\mathbf{e}_2 = \mathbf{n}_\perp$, the structure functions also determine the gradient tensor $\nabla \mathbf{n}$, with $\kappa = -c_{121}$ and $s = -c_{122}$. Computing the curvature 2-form Ω in terms of the structure functions and making these identifications leads to (4.3). The condition (4.7) translates to

$$|\nabla c_{122} + J\nabla c_{121}| \geq c_{121}^2 + c_{122}^2 + K. \tag{4.10}$$

4.3 Distortion Frames and Structure Functions in Three-Dimensions

Let $\mathbf{n}$ be a unit vector field in $\mathbb{R}^3$ with the Euclidean metric, $J = \mathbf{n}\times$, and let ξ be the orthogonal plane field. Now that we have an extra dimension there is freedom in the choice of basis for ξ. A *distortion frame* for $\mathbf{n}$ is a trio of orthogonal, unit vector fields $\mathbf{e}_1, \mathbf{e}_2, \mathbf{e}_3$ where $\mathbf{e}_3 = \mathbf{n}$ is the director and $\mathbf{e}_1, \mathbf{e}_2$ are sections of ξ such that $\mathbf{e}_2 = J\mathbf{e}_1$. The non-uniqueness of the distortion frame reflects an $\mathcal{SO}(2)$ gauge freedom: we can rotate the pair e_1, e_2 by any position-dependent angle θ to obtain a new frame. It will not always be possible to define the distortion frame globally due to the topological obstructions discussed in Chapter 2, however we can always cover the space with charts in which the frame can be locally defined.

For biaxial materials there is an obvious choice for the distortion frame, with $\mathbf{e}_1, \mathbf{e}_2, \mathbf{e}_3$ corresponding to the three molecular axes. In cholesterics and twist-bend materials, it is natural to align $\mathbf{e}_1$ with the pitch axis in the former case, and the normal to the integral curves of $\mathbf{n}$ in the latter. The distortion frame is then defined everywhere except at defects in $\mathbf{n}$ and a set of lines, the λ lines of cholesterics and the β lines (see Chapter 5) of twist-bend nematics.

The structure functions c_{ijk} of a distortion frame are defined by the same equations as in three dimensions,

$$[\mathbf{e}_i, \mathbf{e}_j] = \sum_k c_{ijk} \mathbf{e}_k. \tag{4.11}$$

We now have three brackets giving a set of nine structure functions, which satisfy

$c_{jjk} = 0$ and $c_{ijk} = -c_{jik}$. It is often more convenient to work with the dual coframe $e^1, e^2, e^3 = \eta$ rather than the frame. The structure functions can also be determined from the derivatives of the coframe elements,

$$de^k = \sum_{i<j} -c_{ijk} e^i \wedge e^j. \tag{4.12}$$

To relate the structure functions to the gradients of the director we use the formula (4.9) for the connection and compare with the decomposition of the gradient tensor (1.4). This leads to

$$\begin{aligned} s &= c_{131} + c_{232}, \\ q &= -c_{123}, \\ \mathbf{b} &= c_{133}\mathbf{e}_1 + c_{233}\mathbf{e}_2, \\ \Delta_1 &= \frac{1}{2}\left(c_{131} - c_{232}\right), \\ \Delta_2 &= \frac{1}{2}\left(c_{231} - c_{312}\right). \end{aligned} \tag{4.13}$$

Note also that $-c_{231}$ and $-c_{312}$ are twists of the vector fields $\mathbf{e}_1$ and $\mathbf{e}_2$ respectively. If we take $\mathbf{e}_1$ to be the normal to the integral curves of the director, then the structure function c_{133} is equal to the curvature κ of the integral curves of $\mathbf{n}$, while their torsion is $\tau = \frac{1}{2}(c_{231} + c_{312} - c_{123})$. We can express the torsion in terms of gradient tensor of the director via the formula [RW73]

$$\mathbf{b} \cdot \nabla \times \mathbf{b} = -\kappa^2 \left(\tau + \frac{1}{2}q + \Delta_2\right). \tag{4.14}$$

To obtain this formula, we simply note that both sides of the equation evaluate to $-\kappa^2 c_{231}$.

The gradients of the director are evidently independent of the choice of distortion frame, however the structure functions are not. The formulas for the structure

functions $\bar{c}_{ijk}$ of a new frame $\bar{\mathbf{e}}_1 = \cos\theta \mathbf{e}_1 + \sin\theta \mathbf{e}_2, \bar{\mathbf{e}}_2 = J\bar{\mathbf{e}}_1$ are

$$\begin{aligned}
\bar{c}_{121} &= \cos\theta(c_{121} - \nabla_1\theta) + \sin\theta(c_{122} - \nabla_2\theta),\\
\bar{c}_{122} &= -\sin\theta(c_{121} - \nabla_1\theta) + \cos\theta(c_{122} - \nabla_2\theta),\\
\bar{c}_{123} &= c_{123},\\
\bar{c}_{131} &= \cos^2\theta c_{131} + \sin^2\theta c_{232} + \sin\theta\cos\theta(c_{231} - c_{312}),\\
\bar{c}_{132} &= \cos^2\theta c_{132} - \sin^2\theta c_{231} - \sin\theta\cos\theta(c_{131} - c_{232}) - \nabla_3\theta,\\
\bar{c}_{133} &= \cos\theta c_{133} + \sin\theta c_{233},\\
\bar{c}_{231} &= \cos^2\theta c_{231} - \sin^2\theta c_{132} - \sin\theta\cos\theta(c_{131} - c_{232}) + \nabla_3\theta,\\
\bar{c}_{232} &= \cos^2\theta c_{232} + \sin^2\theta c_{131} - \sin\theta\cos\theta(c_{231} - c_{312}),\\
\bar{c}_{233} &= -\sin\theta c_{133} + \cos\theta c_{233}.
\end{aligned} \tag{4.15}$$

Or, in terms of director gradients,

$$\begin{aligned}
\bar{c}_{123} &= q,\\
\bar{c}_{131} &= \frac{s}{2} + \cos 2\theta\Delta_1 + \sin 2\theta\Delta_2,\\
\bar{c}_{132} &= -\tau - \frac{q}{2} + \cos 2\theta\Delta_2 - \sin 2\theta\Delta_1 - \nabla_{\mathbf{n}}\theta,\\
\bar{c}_{133} &= \cos\theta c_{133} + \sin\theta c_{233},\\
\bar{c}_{231} &= \tau + \frac{q}{2} + \cos 2\theta\Delta_2 - \sin 2\theta\Delta_1 + \nabla_{\mathbf{n}}\theta,\\
\bar{c}_{232} &= \frac{s}{2} - \cos 2\theta\Delta_1 - \sin 2\theta\Delta_2,\\
\bar{c}_{233} &= -\sin\theta c_{133} + \cos\theta c_{233},
\end{aligned} \tag{4.16}$$

where Δ_1, Δ_2 are the components of Δ in the original frame. This gives the transformation rule $\bar{\Delta}_1 = \cos 2\theta\Delta_1 + \sin 2\theta\Delta_2, \bar{\Delta}_2 = \cos 2\theta\Delta_2 - \sin 2\theta\Delta_1$ for these components.

4.4 The Compatibility Conditions in Three-Dimensions

In two dimensions, there is a single compatibility condition that couples the structure functions to the curvature. In three dimensions, there are nine compatibility conditions, six of which derive from the flatness of Euclidean space, and three of which derive from the Leibniz identity for the Lie bracket, or in the dual picture the property $d^2 = 0$ of the exterior derivative—these do not arise in two dimensions because a 2-form is already a top form, and hence we get $d^2\alpha = 0$ 'for free', for any

1-form α. In three dimensions,

$$\begin{aligned} 0 = d^2 e^k = &- c^k_{12}\left(c^1_{13} + c^2_{23}\right) + c^k_{13}\left(c^1_{12} - c^3_{23}\right) \\ &+ c^k_{23}\left(c^2_{12} + c^3_{13}\right) - \nabla_{\mathbf{e}_1} c^k_{23} + \nabla_{\mathbf{e}_2} c^k_{13} - \nabla_{\mathbf{e}_3} c^k_{12}, \end{aligned} \tag{4.17}$$

for $k = 1, 2, 3$, and e^k the components of the distortion coframe. I refer to (4.17) as the *algebraic compatibility conditions*. Via (4.13), we can interpret the constraint $d^2 e^3 = 0$ in terms of the gradients of the director. Notice that

$$d\eta = q e^1 \wedge e^2 + \eta \wedge \beta, \tag{4.18}$$

where β is the 1-form dual to the bend $\mathbf{b}$ of the director; in terms of the dual vector fields, this expression is $\nabla \times \mathbf{n} = q\mathbf{n} + \mathbf{n} \times \mathbf{b}$. The algebraic compatibility condition expresses the formula,

$$L_{\mathbf{n}} q + qs - d\beta(\mathbf{e}_1, \mathbf{e}_2) = 0. \tag{4.19}$$

To write this in terms of the dual vector fields we compute the divergence of $\nabla \times \mathbf{n}$, which must vanish. This gives us the equivalent vectorial expression,

$$\mathbf{n} \cdot \nabla q + qs - \mathbf{n} \cdot \nabla \times \mathbf{b} = 0, \tag{4.20}$$

which can also be expressed purely in terms of the director field,

$$\nabla \cdot \big[\mathbf{n}\big(\mathbf{n} \cdot \nabla \times \mathbf{n}\big)\big] = \mathbf{n} \cdot \nabla \times \big[(\mathbf{n} \cdot \nabla)\mathbf{n}\big]. \tag{4.21}$$

The other algebraic compaitibility conditions express the same constraint on the gradients of $\mathbf{e}_1$ and $\mathbf{e}_2$.

To obtain the other compatibility conditions, we generalise the approach used for two dimensions. In three dimensions, the curvature 2-form has components

$$\Omega^k_j = d\omega^k_j + \sum_i \omega^k_i \wedge \omega^i_j = \frac{1}{2} \sum_{il} R^k_{ilj} e^i \wedge e^l, \tag{4.22}$$

where R^k_{ilj} are the components of the Riemann tensor. After applying the symmetries of this tensor, we are left with six independent components, each of which vanishes in Euclidean space. providing six geometric compatibility conditions. In terms of the structure functions and the connection, these are

$$R^l_{ijk} = \nabla_j \omega^l_{ik} - \nabla_i \omega^l_{jk} + \sum_m c_{ijm} \omega^l_{mk} - \omega^m_{jk} \omega^l_{im} + \omega^m_{ik} \omega^l_{jm}. \tag{4.23}$$

If we take the distortion frame to be the Frenet–Serret frame, then we can write six independent components of the Riemann tensor as

$$R^1_{122} = \nabla_{\mathbf{e}_2}\omega^2_{11} - \nabla_{\mathbf{e}_1}\omega^2_{21} - \left(\omega^2_{11}\right)^2 - \left(\omega^2_{21}\right)^2 - \frac{s^2}{4} - \frac{q^2}{4} + \frac{1}{2}|\Delta|^2 - q\tau, \tag{4.24}$$

$$R^1_{133} = \nabla_{\mathbf{e}_1}\kappa - \nabla_{\mathbf{n}}\left(\frac{s}{2} + \Delta_1\right) - \left(\frac{s}{2} + \Delta_1\right)^2 - \Delta_2^2 + \frac{q^2}{4} - \kappa^2 + 2\tau\Delta_2, \tag{4.25}$$

$$R^2_{233} = \nabla_{\mathbf{n}}\left(\Delta_1 - \frac{s}{2}\right) - \left(\frac{s}{2} - \Delta_1\right)^2 - \Delta_2^2 + \frac{q^2}{4} + \kappa\omega^2_{21} - 2\tau\Delta_2, \tag{4.26}$$

$$R^1_{123} = \nabla_{\mathbf{e}_1}\left(\Delta_2 - \frac{q}{2}\right) - \nabla_{\mathbf{e}_2}\left(\frac{s}{2} + \Delta_1\right) + 2\omega^2_{11}\Delta_1 + 2\omega^2_{21}\Delta_2 + \kappa q, \tag{4.27}$$

$$R^2_{123} = \nabla_{\mathbf{e}_1}\left(\frac{s}{2} - \Delta_1\right) - \nabla_{\mathbf{e}_2}\left(\Delta_2 + \frac{q}{2}\right) + 2\omega^2_{11}\Delta_2 - 2\omega^2_{21}\Delta_1, \tag{4.28}$$

$$R^2_{133} = -\nabla_{\mathbf{n}}\left(\Delta_2 + \frac{q}{2}\right) - s\left(\Delta_2 + \frac{q}{2}\right) - 2\tau\Delta_1 + \kappa\omega^2_{11}. \tag{4.29}$$

In two-dimensions there is a single curvature, the Gaussian curvature, that encapsulates all information contained in the Riemann tensor. The generalisation of the Gaussian curvature to higher-dimensions is the sectional curvature,

$$K_{ij} = -\Omega^j_i(\mathbf{e}_i, \mathbf{e}_j) = -R^j_{iji} = 0, \tag{4.30}$$

with $K_{ij} = K_{ji}$ and $K_{jj} = 0$. In flat space they each vanish. In terms of the structure functions,

$$\begin{aligned} K_{ij} = \nabla_{\mathbf{e}_i} c_{ijj} + \nabla_{\mathbf{e}_j} c_{jii} + \sum_k \frac{1}{2} c_{ijk}\left(-c_{ijk} + c_{jki} + c_{kij}\right) \\ - \frac{1}{4}\left(c^2_{ijk} - (c_{jki} - c_{kij})^2\right) - c_{kii}c_{kjj}. \end{aligned} \tag{4.31}$$

To fully capture the Riemann tensor, we also need to know the sectional curvatures of plane sections spanned by, for example $\mathbf{e}_3$ and $\frac{1}{\sqrt{2}}\mathbf{e}_1 + \mathbf{e}_2$. These can be easily computed via the change of basis formulae for the structure functions.

An equivalent expression of the sectional curvature constraints is $\mathrm{Ric}_j = 0$, where $\mathrm{Ric}_j = \frac{1}{2}\sum_i K_{ij}$ are the diagonal elements of the Ricci tensor Ric. This form of the geometric compatibility conditions is the simplest to interpret in terms of the gradients of the director. The condition $\mathrm{Ric}_3 = 0$ yields a well-known relationship between splay, twist, $|\Delta|^2$ and the saddle-splay that is used in constructing the Frank free energy [MA16b; Sel18]:

$$\frac{1}{2}s^2 + \frac{1}{2}q^2 - \mathrm{Tr}\Delta^2 = \nabla \cdot [s\mathbf{n} - \mathbf{b}] \tag{4.32}$$

The equations $K_{12} + K_{13} = 0$ and $K_{12} + K_{23} = 0$ express the same relationships between the distortions of the vector fields $\mathbf{e}_1$ and $\mathbf{e}_2$ respectively.

We can also obtain the algebraic compatibility conditions from the metric tensor: they are equivalent to the Bianchi identities, which is unsurprising, since the Bianchi identities are themselves derived using the Leibniz formula.

There is one additional geometric quantity of interest. Consider the field of planes ξ orthogonal to the director. As a subbundle of the tangent bundle, there is an induced metric g obtained by restricting the Euclidean metric to ξ. When the twist of $\mathbf{n}$ vanishes $\mathbf{n}$ is the normal to a family of surfaces, and in this case the metric g is just the induced metric on these surfaces, the first fundamental form. Even when the twist does not vanish we may still regard g as being the 'first fundamental form' of the director, in the same way that the symmetric part of $\nabla_\perp \mathbf{n}$ plays the role of the second fundamental form.

The curvature K_ξ of g may be computed via an orthonormal basis for ξ in the same fashion as the curvature of a surface, using the formulae of §4.2. In terms of the structure functions of an orthonormal frame $\mathbf{e}_1, \mathbf{e}_2$ for ξ, we have $K_\xi = -(c^1_{12})^2 - (c^2_{12})^2 + \nabla_{\mathbf{e}_1} c^2_{12} - \nabla_{\mathbf{e}_2} c^1_{12}$. This quantity is independent of the choice of distortion frame. Using the formula (4.31) for the sectional curvature K_{12}, we can express this in terms of the other structure functions,

$$K_\xi = c_{131}c_{232} + \frac{1}{4}c_{123} + \frac{1}{2}c_{123}\left(c_{123} - c_{231} - c_{312}\right) - \frac{1}{4}\left(c_{231} - c_{312}\right)^2. \tag{4.33}$$

If the director is normal to a family of surfaces, which occurs precisely when $c_{123} = 0$, then $K_\xi = c_{131}c_{232} - \frac{1}{4}(c_{231} - c_{312})^2$ is the intrinsic curvature of those surfaces. If we choose $\mathbf{e}_1, \mathbf{e}_2$ to diagonalise the shape operator $\nabla_\perp \mathbf{n} = \frac{s}{2} I + \Delta$, then the second term vanishes. For this choice of frame, we may identify c_{131}, c_{232} with the principal curvatures of the surface, and hence their product K_ξ is the Gaussian curvature of the surfaces orthogonal to the director.

For a general director we can still choose $\mathbf{e}_1, \mathbf{e}_2$ so as to diagonalise $\frac{s}{2} I + \Delta$, and regard these directions as 'directions of principal curvature'. Let us define $\kappa_1 = c_{131}, \kappa_2 = c_{232}$ to be the values of these structure functions in this particular choice of basis, and call these the 'principal curvatures' of ξ. We have $c_{231} = c_{312}$ in this basis, so the twists of the principal directions are the same. Define $q' = -c_{231}$ to be equal to the twist of $\mathbf{e}_1$ and $\mathbf{e}_2$. Then we may write

$$K_\xi = \kappa_1\kappa_2 + \frac{3}{4}q^2 + -qq'. \tag{4.34}$$

4.5 Geometric Reconstruction in Three-Dimensions

The problem of reconstructing a director is not as simple in three dimensions as in two, and there is no obvious 'correct' way to go about it. For completeness I describe here four methods for reconstructing the director when one is provided with vector quantities, and three methods for reconstruction when one is only provided with scalar quantities. The latter all require us to know at least one of the structure functions c_{121}, c_{122}, which can be computed via the divergence or curl of the bend. It is interesting that while these distortions do not play a role in the energy they are nonetheless required for reconstructing the director unless we are given a vector quantity.

4.5.1 Reconstruction via the Helmholtz Theorem

A classical result, the Helmholtz Theorem, implies we can reconstruct the director $\mathbf{n}$ on a compact region U with boundary ∂U provided we know the curl and splay of $\mathbf{n}$ in U, as well as the director itself on the surface ∂U. Concretely, we have

$$\mathbf{n} = -\nabla \int_U \frac{\nabla \cdot \mathbf{n}}{4\pi|\mathbf{r}' - \mathbf{r}|} d\mathbf{r}' + \nabla \times \int_U \frac{\nabla \times \mathbf{n}}{4\pi|\mathbf{r}' - \mathbf{r}|} d\mathbf{r}'. \tag{4.35}$$

4.5.2 Reconstruction Using the Bend Vector Field

Suppose we are given only the bend vector field $\mathbf{b} = b_x\mathbf{e}_x + b_y\mathbf{e}_y + b_z\mathbf{e}_z$. The director satisfies the PDE $\nabla_{\mathbf{n}}\mathbf{n} = \mathbf{b}$, which translates into a set of coupled PDEs for the components of $\mathbf{n}$. These can be solved directly by integration.

4.5.3 Reconstruction Using the Bend and Curl

We can combine the previous two reconstruction methods if we are given both the curl $\mathbf{c} = \nabla \times \mathbf{n} = c_x\mathbf{e}_x + c_y\mathbf{e}_y + c_z\mathbf{e}_z$ and bend $\mathbf{b} = b_x\mathbf{e}_x + b_y\mathbf{e}_y + b_z\mathbf{e}_z$. Then $\nabla \times \mathbf{n} = q\mathbf{n} + \mathbf{n} \times \mathbf{b}$ gives us a formula for the components of $\mathbf{n} = n_x\mathbf{e}_x + n_y\mathbf{e}_y + n_z\mathbf{e}_z$,

$$\begin{aligned} c_x &= qn_x + (n_y b_z - n_z b_y), \\ c_y &= qn_y + (n_z b_x - n_x b_z), \\ c_z &= qn_z + (n_x b_y - n_y b_x). \end{aligned} \tag{4.36}$$

These are linear equations, and can be solved in the standard way, by inverting a linear system:

$$\mathbf{c} = \begin{bmatrix} q & b_z & -b_y \\ -b_z & q & b_x \\ b_y & -b_x & q \end{bmatrix} \mathbf{n} \tag{4.37}$$

This gives us $\mathbf{n}$ in terms of q and the (known) components of the curl and bend, provided we can invert the matrix. For this to be possible it suffices that its determinant is nonzero, which translates to the condition

$$q(q^2 + \mathbf{b} \cdot \mathbf{b}) \neq 0. \tag{4.38}$$

Note that we cannot invert the matrix if $q = 0$, so this method does not work for any smectic director. Provided this constraint holds, the director is

$$\mathbf{n} = \frac{1}{q(q^2 + \mathbf{b} \cdot \mathbf{b})} \begin{bmatrix} b_x^2 + q^2 & b_x b_y - q b_z & b_x b_z + q b_y \\ b_x b_y + q b_z & b_y^2 + q^2 & b_y b_z - q b_x \\ b_x b_z - q b_y & b_y b_z + q b_x & b_z^2 + q^2 \end{bmatrix} \nabla \times \mathbf{n}. \tag{4.39}$$

If the twist q is not specified then this gives us the director in terms of the unknown q. However, we can determine q either from $\mathbf{n} \cdot \mathbf{n} = 1$, or by computing $\mathbf{n} \cdot \nabla \times \mathbf{n}$. Unlike the previous two reconstruction methods, this method does not require computing any integrals or solving differenital equations.

4.5.4 Reconstruction Using an Arbitrary Section of ξ

Suppose we are given a unit vector field $\mathbf{e}_1$ with the assurance that $\mathbf{e}_1 \in \Gamma\xi$, i.e., $\mathbf{n}$ lies in the planes orthogonal to $\mathbf{e}_1$. Suppose further we are given the splay s and curvature κ of the director, and these are not constant.

Let E denote the subbundle of the tangent bundle consisting of the planes orthogonal to $\mathbf{e}_1$. Is is equipped with a metric g, the restriction of the Euclidean metric to this bundle. We can compute the curvature K of E by choosing any orthonormal basis of sections and computing it directly from the structure functions of this frame, as in the two-dimensional case—for the purposes of this computation we regard E as a rank 2 bundle over $\mathbb{R}^3$ equipped with the restriction $[\cdot, \cdot]_E$ of the Lie bracket to E, so that the bracket $[\cdot, \cdot]_E$ of any two sections has no component along $\mathbf{e}_1$. Then, using the same reasoning as in the two-dimensional case, we must have $\mathbf{n} \cdot (\nabla s + J \nabla \kappa) = -K - s^2 - \kappa^2$, where $J = \mathbf{e}_1$ and ∇ denotes the connection of the metric g on E, *not* the connection of the Euclidean metric. Much like the curvature K, this connection can be computed using the structure functions of an

orthonormal basis of sections of E.

With this formula, we may reconstruct $\mathbf{n}$ using the same method as outlined in §4.2, so this gives us a purely algebraic formula for reconstructing the director. We can regard this as a variant of the Helmholtz Theorem method: it sufficies to specify the splay and the bend vector field, which will give us both the curvature κ and the direction $\mathbf{e}_1$.

4.5.5 Reconstruction Using the Structure Functions and Compatibility Conditions

For the first method that does not require specifying a vector field, we consider the problem of reconstructing a director from a set c_{ijk} of structure functions. The structure functions c_{121}, c_{122} cannot easily be recovered from the gradients of a director, and consequently this approach requires more information than is contained in the usual gradients. However, for biaxial materials where the components $\mathbf{e}_1, \mathbf{e}_2$ of the distortion frame have physical meaning, and also for cholesteric and twist-bend materials where $\mathbf{e}_1$ may be aligned respectively with the pitch axis and the bend, all the structure functions may be obtained provided that one knows the gradients of each component of the frame.

Suppose then that the nine structure functions c_{ijk} are specified. The unknown frame $\mathbf{e}_1, \mathbf{e}_2, \mathbf{e}_3 = \mathbf{n}$ with structure functions c_{ijk} can be expressed in terms of the coordinate frame $\mathbf{e}_{x_j}$ using a matrix R, so that $\mathbf{e}_i = \sum_j R_{ij}\mathbf{e}_{x_j}$. To reconstruct the director, it suffices to find the entries of R.

Define a tensor D by $D^k_{ijl} = \nabla_l c_{ijk}$, where the gradient is taken along the coordinate direction $\mathbf{e}_{x_l}$. The algebraic and geometric compatibility conditions yield linear equations for the entries R_{ij} in terms of this tensor D. Firstly, we rewrite the algebraic compatibility conditions as

$$\sum_{i<j,l} \epsilon_{ijl} \left(\nabla_{\mathbf{e}_l} c_{ijk} - c_{ijk} s_l \right) = 0, \tag{4.40}$$

for each $k = 1, 2, 3$, where ϵ_{ijl} is the Levi-Civita tensor, and for compactness we have written the divergence of the vector field $\mathbf{e}_k$ as $s_k = \sum_i c_{iki}$. Expressing $\mathbf{e}_l$ in terms of R we rewrite this as $\sum_{i<j,l,m} \epsilon_{ijl} R_{lm} D^k_{ijm} = A_k$, where we have defined $A_k = \sum_{i<j,l} \epsilon_{ijl} c^k_{ij} s_l$. Then we expand out the sum over i, j, l to obtain the equations

$$\sum_m R_{3m} D^k_{12m} + R_{2m} D^k_{31m} + R_{1m} D^k_{23m} = A_k. \tag{4.41}$$

For the geometric compatibility conditions, we first define $B^l_{ijk} = -2 \sum_m c_{ijm} \omega^l_{mk} -$

$\omega^m_{jk}\omega^l_{im} + \omega^m_{ik}\omega^l_{jm}$. Then the vanishing of the components of the Riemann tensor implies, through Eq. (4.23)

$$\sum_m R_{jm}\left(D^m_{ikl} + D^m_{lik} + D^m_{lki}\right) - R_{im}\left(D^m_{jkl} + D^m_{ljk} + D^m_{lkj}\right) = B^l_{ijk}. \tag{4.42}$$

Together, Eqs. (4.41) and (4.42) give a set of nine linear equations for the nine functions R_{ij}. We observe that every one of the 27 independent components of D plays a role in these equations, and consequently we cannot eliminate the functions c_{121}, c_{122} from these equations alone. We can invert this system of linear equations to get an expression for the R_{ij} in terms of the known quantities D^l_{ijk}, A_k, and B^l_{ijk}.

4.5.6 Reconstruction Using the Compatibility Conditions and Projections

Suppose we know the scalar quantites $s, q, |\Delta|$, $\mathbf{n}\cdot\nabla\times\mathbf{b}$ and $\nabla\cdot\mathbf{b}$. Suppose further that ∇s and ∇q are not zero, and are nowhere colinear.

Then the geometric compatibility conditions, in the form of Eq. (4.32), give the projection of the director onto the vector ∇s,

$$\mathbf{n}\cdot\nabla s = \nabla\cdot\mathbf{b} + \frac{q}{2} - \frac{s}{2} - |\Delta|^2, \tag{4.43}$$

while the algebraic compatibility condition Eq. (4.20) gives the projection onto the vector ∇q,

$$\mathbf{n}\cdot\nabla q = \mathbf{n}\cdot\nabla\times\mathbf{b} - qs. \tag{4.44}$$

Define $\bar{\mathbf{e}}_1 = \frac{\nabla s}{|\nabla s|}$ and $\bar{\mathbf{e}}_2 = \frac{\nabla q}{|\nabla q|}$. Since we know the projection of $\mathbf{n}$ on these two unit vector fields, we can compute the component in the orthogonal direction $\bar{\mathbf{e}}_1\times\bar{\mathbf{e}}_2$, and hence reconstruct the director.

Alternatively, if the structure functions are the structure functions of the Frenet–Serret frame, the the sectional curvature K_{23} gives the projection of the director on the vector $\nabla\left(\frac{s}{2} - \Delta_1\right)$, while the component R^2_{133} of the Riemann curvature tensor gives the projection on $\nabla\left(\frac{q}{2} + \Delta_2\right)$. Assuming these directions are neither zero nor colinear, we can use them to reconstruct the director via the above process.

4.5.7 Reconstruction via the Characteristic Foliation

Fix a surface S in $\mathbb{R}^3$. We know from Chapter 3 that the director $\mathbf{n}$ is determined, up to continuous deformation, by the characteristic foliation it induces on the surface

S in a neighbourhood of S. We will see here that if we specify just two structure functions we can reconstruct both the characteristic foliation and the director. This requires knowing these structure functions with respect to a carefully chosen frame, however.

Choose a family of surfaces that foliate the domain on which the director is to be reconstructed. It is simplest to take these surfaces to be surfaces of constant z coordinate, which I denote S_z, however any family of surfaces can be used, and other choices may be useful for particular problems. Let $\mathbf{n}_\perp$ denote the unit vector that directs the projection of the director into the surfaces, which is defined everywhere except at points where the director is normal to the surfaces. Let $\mathbf{e}_1$ be the unit vector directing the characteristic foliation. Then the vector fields $\mathbf{e}_1, \mathbf{n}_\perp$ are an orthonormal frame for the surface S_z, and hence can written as $\mathbf{n}_\perp = \cos(\psi)\mathbf{e}_x + \sin(\psi)\mathbf{e}_y$ and $\mathbf{e}_1 = -\sin(\psi)\mathbf{e}_x + \cos(\psi)\mathbf{e}_y$, for some function ψ which we must determine.

We compute that $\nabla \times \mathbf{e}_1 = -\dot{\psi}\mathbf{e}_1$, where the overdot denotes differentiation with respect to z. Consequently $\mathbf{e}_1 \cdot \nabla \times \mathbf{e}_1 = -\dot{\psi}$. In terms of the structure functions of the frame the twist of $\mathbf{e}_1$ is $-\bar{c}^1_{23}$, so we see that ψ solves the differential equation $\dot{\psi} = \bar{c}^1_{23}$. Solving this differential equation only determines ψ up to a function $\psi_0(x, y)$ of x and y alone, which we can compute if we have fixed the director along S_0.

Now we have determined the direction of the projection of the director into each surface S_z, and it remains only to determine the z-component. Write $\mathbf{n} = \cos(\phi)\mathbf{e}_z + \sin(\phi)\mathbf{n}_\perp$ and $\mathbf{e}_2 = \mathbf{n} \times e_1 = \cos(\phi)\mathbf{n}_\perp - \sin(\phi)\mathbf{e}_z$ for some function ϕ that completely determines the director.

To relate ϕ to the structure functions, we must compute the Lie brackets between elements of this frame. Write $[\mathbf{n}_\perp, \mathbf{e}_1] = f_1\mathbf{n}_\perp + f_2\mathbf{e}_1$ for the Lie bracket between these vector fields on the surface. Note that this bracket has no component in the z-direction as $\mathbf{n}_\perp, \mathbf{e}_1$ span integral surfaces. We compute that $[\mathbf{n}_\perp, \mathbf{e}_1] = -\partial_x\psi\mathbf{e}_x - \partial_y\psi\mathbf{e}_y$, which leads to

$$\begin{aligned} f_1 &= -\cos(\psi)\partial_x\psi - \sin(\psi)\partial_y\psi, \\ f_2 &= \sin(\psi)\partial_x\psi - \cos(\psi)\partial_y\psi. \end{aligned} \tag{4.45}$$

The interpretation of f_1, f_2 is the same as for structure functions in two dimensions, as explained in §4.2: $-f_1$ is the curvature of the integral curves of $\mathbf{n}_\perp$, while $-f_2$ is the divergence of $\mathbf{n}_\perp$. It is worth noting that if we wished to instead prescibe f_1 and f_2, we could use this to reconstruct $\mathbf{n}_\perp$ without using the structure function $\bar{c}^1_{23}$ by

applying the method of Niv & Efrati for two-dimensional reconstruction outlined in §4.2.

Next we compute $[e_1, e_3]$. To do this we use $[\mathbf{n}_\perp, \mathbf{e}_1]$ and two other brackets, $[\mathbf{n}_\perp, \mathbf{e}_z] = -\dot{\psi}\mathbf{e}_1$ and $[\mathbf{e}_1, \mathbf{e}_z] = \dot{\psi}\mathbf{n}_\perp$. From this we determine that $\bar{c}^1_{13} = -f_2 \sin(\phi)$. Consequently, whenever $f_2 \neq 0$ we can write

$$\mathbf{n} = \sqrt{1 - \left(\frac{\bar{c}^1_{13}}{f_2}\right)^2}\,\mathbf{e}_z - \frac{\bar{c}^1_{13}}{f_2}(\cos(\psi)\mathbf{e}_x + \sin(\psi)\mathbf{e}_y). \tag{4.46}$$

There are two choices for the sign of the square root: only one sign will yield the correct director. We then have a geometric reconstruction formula similar to that derived by Niv & Efrati [NE18] for the two dimensional director.

4.6 Director Distortions and Lie Groups

In this section I will examine a few classes of directors—namely those with pure distortions, uniform distortions, and quasi-uniform distortions—from the perspective of Lie algebras and groups. There is some overlap between this section and a recent preprint of Sadoc *et al.* [SMS20], however I emphasise that the Lie group perspective I adopt here is a novel approach to the problem.

4.6.1 Curvature of Pure Distortions

When the structure functions of a distortion frame $\mathbf{e}_1, \mathbf{e}_2, \mathbf{e}_3 = \mathbf{n}$ are constant, they describe a Lie algebra. It is a well-known fact that every Lie algebra uniquely determines a homogeneous space, a Lie group [Car04]. Such groups are abstract spaces where the given structure functions could be realised, even if they cannot not be realised in Euclidean space. The curvature of these Lie groups—which, following Milnor [Mil76], can be computed from the structure constants of the Lie algebra using Eq. (4.31)—gives insight into what curvature is required to realise the particular choice of distortion modes, while the group itself describes the natural symmetries associated to the distortion mode. We can use this to understand the curvature associated to pure splay, twist, bend, or biaxial splay distortions. Moreover, certain Lie groups admit a projection into flat Euclidean space, allowing us to realise the idealised texture as a frustrated texture in Euclidean space.

Firstly, consider a director with constant nonzero twist q, but vanishing splay, bend, and biaxial splay. This requires the structure functions $c_{123} = -q$, $c_{231} = c_{312}$, with c_{121}, c_{122} left undetermined and all other structure functions vanishing. A

minimal model for this has $c_{121} = c_{122} = 0$ and either $c_{231} = -q$ or $+q$. The former choice yields the Lie algebra of $SU(2)$, the 3-sphere, and the set of vector fields described previously by Sethna *et al.* [SWM83] which, when projected into Euclidean space, give the familiar double-twist director. The latter choice gives the Lie algebra of the group $SL(2,\mathbb{R})$, which consists of real, traceless 2×2 matrices. The group can be identified with the unit sphere in the $(2,2)$ anti-de Sitter spacetime, that is, $\mathbb{R}^4$ equipped with the pseudometric with signature $(1,1,-1,-1)$, as opposed to $SU(2)$ which is the unit sphere in the Euclidean metric. This texture is an alternative realisation of 'double-twist' where the twisting in the orthogonal directions has the opposite sense of handedness to the twisting in the director: see Ref. [SMS20] for a further discussion of this example.

One may also take $c_{231} = c_{312} = 0$ for a 'single twist' director, which describes the Lie algebra of the Heisenberg group. This group has a natural coordinate parameterisation x, y, z in which the director is given by

$$\mathbf{m} = \mathbf{e}_z + x\mathbf{e}_y - y\mathbf{e}_x, \tag{4.47}$$

which, after normalisation in the Euclidean metric, $\mathbf{n} = \mathbf{m}/|\mathbf{m}|$, is the standard example of local twist, see for example Selinger [Sel18]. This vector field is also recognisable as the Darboux normal form in contact topology [Gei08].

Sadoc *et al.* conjucture that a positive Ricci curvature along one direction is a necessary condition for a pure nonzero twist state [SMS20]. This conjecture is correct and follows immediately from a computation of $\mathrm{Ric}_3 = \frac{1}{2}K_{13} + K_{23}$, which in a pure twist case is simply equal to $q^2/4$, so that the Ricci curvature along the director is always positive as long as the twist is nonzero.

Next consider pure splay. This requires $c^1_{131} = c_{232} = s/2$, and we may take all other structure functions equal to zero for a minimal model. The resulting Lie group is consequently a space of constant negative curvature [Mil76]. Even if we allow ourselves maximum freedom, with c_{121}, c_{122} free and $c_{231} = c_{312}$ to ensure the vanishing of Δ, then the compatibility equations (4.31) imply that all sectional curvatures will still be negative. Pure bend requires c_{133}, c_{233} nonzero. If we take $c_{121} = c_{233}$ and $c_{122} = -c_{133}$, and similarly we find the curvature is negative. In two dimensions it is also true that constant, nonzero pure bend and pure splay directors can only occur on a negatively-curved space, as follows from (4.3).

Finally, we ask for the possibility of pure $\Delta \neq 0$. We can assume without loss of generality that Δ is diagonal, so this mode of distortion requires $c_{231} = c_{312}$ and $c_{131} = -c_{232}$. Setting all other structure functions equal to zero gives a space where

the curvature of planes orthogonal to the director is positive, whereas the curvature of planes containing the director is negative, suggesting this is the natural form of curvature associated to this distortion.

4.6.2 Uniform Directors

The next simplest question to ask is when it is possible to have a director with at least uniform distortions, i.e., constant splay, twist, bend, and Δ. It is known that all such directors are given by the heliconical director [Vir19],

$$\mathbf{n} = \cos(\theta)\mathbf{e}_z + \sin(\theta)(\cos(qz)\mathbf{e}_x \pm \sin(qz)\mathbf{e}_y), \tag{4.48}$$

for some choice of θ, q constant. This encapsulates both the cholesteric ground state ($\theta = \pi/2$) and the nematic ground state ($\theta = 0$) as limits.

I now provide an alternative argument for this classification based on the framework described in this chapter. In the language used here, the condition of being a uniform director is equivalent to having constant structure functions. Using the compatibility conditions, we can examine which sets of constant c_{ij}^k are permissable. Any set of structure functions satisfying the algebraic compatibility conditions defines a Lie algebra, and conversely every Lie algebra gives rise to a frame satisfying the algebraic compatibility conditions. Satisfying the geometric compatibility conditions as well is then equivalent to the Lie group associated to the Lie algebra having a flat metric. This Lie group, taken along with rotations and about the director $\mathbf{n}$ and the nematic symmetry $\mathbf{n} \mapsto -\mathbf{n}$, can be seen as the symmetry group of the texture described by $\mathbf{n}$.

Three-dimensional Lie algebras have been classified up to isomorphism [PSWZ76]. Up to this equivalence, the only Lie algebras giving rise to flat Lie groups are the trivial algebra with all Lie brackets being equal to zero, which corresponds to the coordinate basis of $\mathbb{R}^3$, and the algebra defined by the brackets $[\mathbf{e}_1, \mathbf{e}_2] = 0, [\mathbf{e}_3, \mathbf{e}_1] = \mathbf{e}_2, [\mathbf{e}_2, \mathbf{e}_3] = \mathbf{e}_1$, which is the Lie algebra of the Euclidean group $E(2)$, the group of rigid motions of the Euclidean plane. A concrete realisation of the latter as a set of vector fields in Euclidean space is given by

$$\begin{aligned} \mathbf{e}_1 &= \cos(z)\mathbf{e}_x + \sin(z)\mathbf{e}_y, \\ \mathbf{e}_2 &= \sin(z)\mathbf{e}_x - \cos(z)\mathbf{e}_y, \\ \mathbf{e}_3 &= \mathbf{e}_z. \end{aligned} \tag{4.49}$$

Any combinations of these three vector fields with constant coefficients, e.g. the

heliconical director, or those involving rescalings of the coordinate directions, e.g. $z \mapsto qz$ for a nonzero integer q, will also give a distortion frame with constant structure functions. The classification of Lie algebras then proves that, up to a coordinate parameterisation, these are the only possible cases.

4.6.3 Quasi-Uniform Directors

Pedrini & Virga [PV20] define quasi-uniform directors to be those whose distortions are in constant proportion to one another. This is equivalent to the structure functions being of the form $c_{ijk} = f a_{ijk}$, for f a function and a_{ijk} constant. One can construct examples by assuming that a_{ijk} are the structure constants of a Lie algebra. Let $\mathbf{e}_i$ be the distortion frame, and suppose that c_{ijk} are the structure functions of this frame. Denote by $K_{ij}(a)$ the sectional curvatures of the Lie group whose Lie algebra has structure constants a_{ijk}. The compatibility conditions for c_{ij}^k then reduce to a set of differential equations that serve as compatibility conditions for the function f,

$$\begin{aligned} a_{23k}\nabla_{\mathbf{e}_1} f + a_{31k}\nabla_{\mathbf{e}_2} f + a_{12k}\nabla_{\mathbf{e}_3} f = 0, \\ K_{ij}(a) + a_{ijj}\nabla_{\mathbf{e}_i} f + a_{jii}\nabla_{\mathbf{e}_j} f = 0, \end{aligned} \tag{4.50}$$

for i, j, k running from 1 to 3. One may then determine those choices of Lie algebra for which the above equation is possible to solve, which give necessary and sufficient conditions for the existence of a frame with these structure functions. For example, consider the Lie algebra with the only nonzero structure constants $a_{23}^1 = a_{31}^2 = 1$ defined by the vector fields (4.49). The compatibility conditions (4.50) for the function f reduce to $\partial_x f = \partial_y f = 0$, and therefore we may choose f to be any function of z alone. The frame giving rise to the structure functions c_{ijk} is:

$$\begin{aligned} \mathbf{e}_1 &= \cos g(z)\mathbf{e}_x + \sin g(z)\mathbf{e}_y, \\ \mathbf{e}_2 &= \sin g(z)\mathbf{e}_x - \cos g(z)\mathbf{e}_y, \\ \mathbf{e}_3 &= \mathbf{e}_z, \end{aligned} \tag{4.51}$$

where $\partial_z g = f$. As before, any unit director which is a constant combination of these three vector fields will be quasi-uniform, e.g. a quasi-uniform heliconical director $\mathbf{n} = \cos(\theta)\mathbf{e}_z + \sin(\theta)(\cos g(z)\mathbf{e}_x \pm \sin g(z)\mathbf{e}_y)$ with θ constant. These then give examples of quasi-uniform directors with twist and bend distortions that vary in the z direction according to f, but still have vanishing splay.

More generally, if the Lie algebra can be reduced to a form where the

structure functions a_{ijj} vanish, then we see that it is impossible for there to be a quasi-uniform corresponding to this Lie algebra unless the Lie algebra itself is flat. These algebras are the unimodular Lie algebras [Mil76], and the two flat unimodular algebras are, as we have already noted, $\mathbb{R}^3$ and the Euclidean group $E(2)$ which determine the nematic and the cholesteric/heliconical states respectively. Any quasi-uniform diretor corresponding to the latter is defined by a taking a constant combination of the vectors in the frame (4.51).

When a Lie group is not unimodal, it has a basis $\mathbf{e}_j$ such that

$$\begin{aligned}[\mathbf{e}_1, \mathbf{e}_3] &= A\mathbf{e}_1 + B\mathbf{e}_2, \\ [\mathbf{e}_2, \mathbf{e}_3] &= C\mathbf{e}_1 + D\mathbf{e}_2,\end{aligned} \tag{4.52}$$

for constants A, B, C, D such that $A+D = 2$ [Mil76]. The second set of conditions in (4.50) then imply that $K_{12}(a) = 0$, which is satisfied when $B = -C$, and further that $A(\nabla_3 f - A) = D(\nabla_3 f - D) = 0$, which implies that either one of A, D vanishes, or that $A = D = 1$, and that $\nabla_3 f$ is constant and nonzero. Moreover, the first set of conditions imply that f is constant along $\mathbf{e}_1, \mathbf{e}_2$. Since the curl of the $\mathbf{e}_3$ direction vanishes, we can assume that it is the gradient of a function h. The vector fields $\mathbf{e}_1, \mathbf{e}_2$ must be a pair of orthogonal vector fields orthogonal to ∇h. As $[\mathbf{e}_1, \mathbf{e}_2]$ vanishes the level sets of h must be flat, so we may take $\mathbf{e}_3 = \mathbf{e}_z$, and consequently these cases all reduce to the case of a uniform director.

Thus we have shown that, when the a_{ijk} are chosen to be the structure constants of a Lie algebra, then the only possible quasi-unfiform directors are those in the family (4.51).

More options are possible if we allow for singularities in the director, or for the function f to have singular behaviour. For instance, the director $\mathbf{n} = \cos(\phi)\mathbf{e}_z + \sin(\phi)\mathbf{e}_r$ in cylindrical coordinates, which has $\mathbf{n}_\perp = \mathbf{e}_r$ and $\mathbf{e}_1 = r\mathbf{e}_\theta$, is a quasi-uniform pure-splay texture provided that $0 \leq \phi \leq \pi/2$ is constant, in which case we have structure functions $c_{121} = -\frac{1}{r}\cos(\phi), c_{131} = \frac{1}{r}\sin(\phi)$, with the others vanishing. The function f here is $1/r$, which becomes undefined along the z axis. Quasi-uniform pure-bend states can be defined similarly, by $\mathbf{n} = \cos(\phi)\mathbf{e}_z + \sin(\phi)\mathbf{e}_\theta$, for $0 \leq \phi \leq \pi/2$ constant.

Chapter 5

The Topology and Geometry of Twist-Bend Nematics

5.1 Introduction to Twist-Bend Nematics

Fresh perspectives invariably accompany the discovery of a new phase: The recent discovery of the twist-bend nematic phase [C$^+$11; B$^+$13; C$^+$13] invites fresh consideration of nematic geometry and topology. The twist-bend nematic is a fluid mesophase in which the nematic orientation exhibits a heliconical modulation with nanoscale pitch and modest cone angle [JLS18]. It occurs in compounds with a bent core architecture (banana molecules) and is characterised by a preferred state of non-zero bend distortion [Doz01; SDS13]. Thus the geometry of bend is a natural vehicle for describing the structural degeneracies and defects of the twist-bend nematic that equally applies quite generally to any material with orientational order.

A common feature of many materials are structural degeneracies along lines or curves, with examples including flux lines in superconductors [Abr57], fluid vortices [Irv18], nodal lines in optical beams [DKJ$^+$10], C lines in electromagnetic fields [Nye83], defect lines in liquid crystals [dGP95] and umbilic lines in general [MA16b]. In many instances these lines are fundamental to the organisation and properties of the entire material, simultaneously characterising it and offering a mechanism for controlling and engineering specific responses. In this chapter I consider a new line-like geometric degeneracy associated to zeros of the bend in a unit vector field, called β lines. These lines occur in all materials with vector or orientational order, such as liquid crystals and ferromagnets, but have added significance when there is an energetic preference for non-zero bend, and in such materials β lines are a new type of topological defect.

This is joint work with J. Binysh, part of which appears in Refs. [Bin19; BPA20].

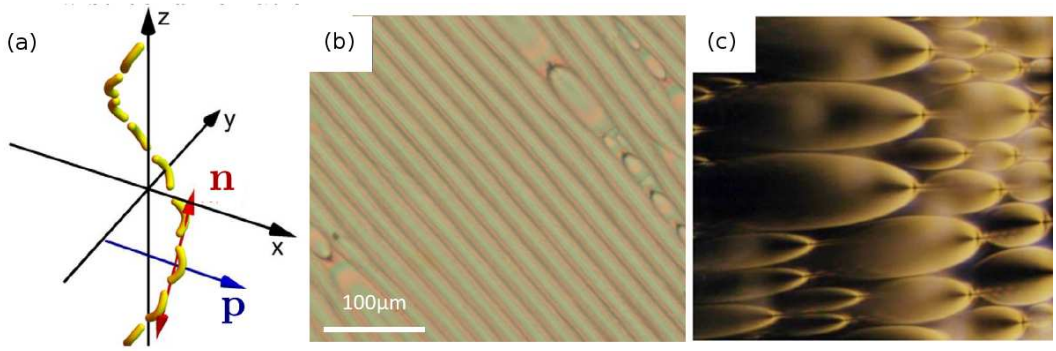

Figure 5.1: (a) Liquid crystal materials with banana-shaped molecules can form twist-bend nematic phases. The optimal way of packing banana-shaped molecules is to stack them into helices, forming the heliconical ground state (5.1), with director $\mathbf{n}$ and polarisation $\mathbf{p}$. (b) Experimental image of stripe patterns forming in the twist-bend phase of CB7CB. The director close to these stripes can be described by heliconical ground state, where the stripes themselves are level sets of the z coordinate. There are also focal conic domains. (c) A larger focal conic domain in CB7CB. Panels reproduced from [JLS18].

The ground state of the twist-bend nematic is

$$\mathbf{n}_{\text{hel}} = \cos(\phi)e_z + \sin(\phi)\mathbf{n}_{\text{chol}}, \tag{5.1}$$

the *heliconical director*, so called because its integral curves are helices. Here, $\mathbf{n}_{\text{chol}}$ is the cholesteric ground state with some helical pitch $\frac{2\pi}{q}$, and $\phi \in (0, \pi/2)$ is the helical cone angle; observe that the limit $\phi \to 0$ takes us to the uniform state, while $\phi \to \frac{\pi}{2}$ recovers the cholestric ground state. It is easy to compute the splay, twist, and bend $\mathbf{b}$,

$$\begin{aligned} \nabla \cdot \mathbf{n} &= 0, \\ \mathbf{n} \cdot \nabla \times \mathbf{n} &= -q\sin^2(\phi), \\ \mathbf{b} &= q\sin(\phi)\cos(\phi)(-\sin(qz)e_x + \cos(qz)e_y). \end{aligned} \tag{5.2}$$

It is a little premature to call (5.1) *the* heliconical director: in fact there are two textures that might reasonably be referred to by that name, depending on the sign of q. As well as nonzero bend, the heliconical director also has nonvanishing twist everywhere, and consequently we see in twist-bend nematics the similar preference for chirality in the ground state. However, the presence of multiple ground states

with opposite handedness implies that there is no preference for the sign of the chirality, and thus we might expect energetically stable textures with regions of reversed handedness separated by domain walls, as described in §3.7.

The heliconical ground state of the twist-bend nematic has one-dimensional periodic spatial modulation. On scales large compared to the heliconical pitch, its elastic deformations and hydrodynamic modes are the same as those of a smectic [Kam96; P$^+$16; MD16], as is the case also for cholesterics [RL11]. The polarisation is a non-hydrodynamic mode [P$^+$16]. As such, many calculations from the literature on smectics can be applied directly to give a coarse description of the energetics of defects and textures in twist-bend nematics, when the latter are closely similar to known smectic textures. Our focus will be on describing these states from the twist-bend perspective where they may be visualised as disruptions to the family of helices which make up the director integral curves.

The energetics of the twist-bend phase may be described by a Frank free energy with negative bend elastic constant [Doz01], or alternatively via the following energy functional [SDS13]

$$F_{\mathrm{tb}} = \int_M \frac{K}{2} \|\nabla \mathbf{n}\|^2 + \frac{C}{2} \|\nabla \mathbf{p}\|^2 - \lambda \mathbf{p} \cdot \mathbf{b} + \frac{U}{2}(1 - \|\mathbf{p}\|^2)^2 \mu. \tag{5.3}$$

This is the approach originally suggested by Meyer for describing spontaneously modulated splay and bend phases and adopted by the Kent State group [SDS13]. This description makes use of two vector fields, the director $\mathbf{n}$ which keeps track of the orientation of the long axis of the banana, and the polarisation $\mathbf{p}$ which specifies the orientation of the banana in the plane orthogonal to $\mathbf{n}$. The coupling $-\mathbf{p} \cdot \mathbf{b}$ between polarisation and bend results in an energetic preference for nonzero bend distortion, and finally U, which imposes a preference for the polarisation to be unit length; one may instead enforce the condition that $\mathbf{p}$ is unit length as is done for the director, and one may also choose to enforce that $\mathbf{n} \cdot \mathbf{p} = 0$, although the latter makes it difficult to define the core of a defect, which would normally consist of the region where $\mathbf{n} \cdot \mathbf{p} \neq 0$. The condition for a pair $\mathbf{p}, \mathbf{n}$ to be a minimiser of (5.3) is obtained by taking the derivatives of the functional with respect to both $\mathbf{n}$ and $\mathbf{p}$, which yields

$$\begin{aligned} \frac{\delta F_{\mathrm{tb}}}{\delta \mathbf{n}} &= \left[K\nabla^2 \mathbf{n} + \lambda \left(\nabla_{\mathbf{p}} \mathbf{n} - (\nabla \cdot \mathbf{n})\mathbf{p} - \nabla_{\mathbf{n}} \mathbf{p}\right)\right]^{\perp} = 0, \\ \frac{\delta F_{\mathrm{tb}}}{\delta \mathbf{p}} &= C\nabla^2 \mathbf{p} + \lambda \mathbf{b} + U(1 - \|\mathbf{p}\|^2)\mathbf{p} = 0, \end{aligned} \tag{5.4}$$

where $\perp$ denotes projection into the planes orthogonal into $\mathbf{n}$. There are four positive

parameters in the energy: K, a single elastic constant for the director, C, an elastic constant for the polarisation, λ, which sets the strength of the coupling between polarisation and bend, and finally U, which provides a preference for the polarisation to be unit length. The energy (5.3) does not have a unique ground state: rather, either of the two heliconical directors minimises the energy, with polarisation set to be the unit vector in the direction of bend in each case. Substituting (5.1) into (5.4) tells us what values the parameters should take in terms of the elastic constants in order for the energy to be minimised,

$$\frac{C}{K} = \frac{\sin^4(\phi)}{\cos(2\phi)}, \qquad \frac{\lambda}{K} = \frac{q}{2}\tan(2\phi). \tag{5.5}$$

I emphasise that the focus here is on geometric and topological properties of the director field, which are largely insensitive to the exact form of the free energy and have general applicability for typical values of material constants.

5.2 Profiles of Bend Zeros

Let us first describe some properties of bend. The bend vector field and its relationship with the other gradients of the director is described in Chapter 4. Here we are most interested in the fact that bend is a Legendrian vector field, orthogonal to the director. In particular, the set of points where it vanishes is one-dimensional and forms a collection of fundamental curves in the material that are characteristic of the director field. They are points of inflection of the integral curves of $\mathbf{n}$, where the curvature vanishes; I call them β lines in an informal analogy with the λ lines of cholesterics, to which they may be considered 'cousins'. These β lines are the locus of inflection points in the director integral curves; as a director integral curve intersects a β line, the curvature of the director integral curve vanishes. In addition to their geometric significance, β lines also carry topological data about the director field and are themselves topological defects in any material where the bend is naturally nonzero, for example the twist-bend nematics.

When discussing Legendrian vector fields in §2.4 I remarked that generically the zero set would not be transverse to the plane field, but rather would be tangent to it at isolated points—these are points where $\mathbf{n}\cdot\mathbf{j} = 0$, where $\mathbf{j}$ denotes the tangent to the line. Generically these are associated with a change in the profile of the β line from a $+1$ to a -1 winding, a saddle-node bifurcation. We can also have changes in stability where a β line whose profile is that of a stable node switches to one whose profile is an unstable node. Here, I will give a simple construction of two linearised

directors and associated linearised bend vector fields that exhibit the saddle-node and Hopf bifurcations.

The first step is to construct a linearised bend vector field from a director, which allows us to relate the gradients of the director to the profile of a β line. I will follow the constructions given in [Bin19]. Throughout this section, let s denote the splay, q the twist, $\mathbf{b}$ the bend, and Δ the deviatoric part of the gradients of a director $\mathbf{n}$ with orthogonal plane field ξ. In order to study the Legendrian points, it suffices (essentially by Proposition 2.1) to study the parts of the gradient of bend that themselves lie in the plane ξ, which we will denote $\nabla^{\xi}\mathbf{b}$. We could also look at the gradients in the plane orthogonal to the β line itself. Moreover, to get an idea of the linear behaviour along a β line when can take a local coordinate system x, y, z about a point on the β-line where x, y are orthogonal to the line at that point and z is tangent to it, as in Proposition 2.1. Working sufficiently locally, we can can assume that the coordinate directions e_x, e_y agree with the eigendirections of Δ, so that $\Delta_2 = 0$. It then suffices to compute $B = \nabla^{\xi}\mathbf{b}|_{\beta \text{ line}}$, and the linearised bend $\tilde{\mathbf{b}}(x, y) = B[x, y]^T + O(z)$. From now on, all quantities are understood as being resticted to the β line.

A direct calculation shows that $\nabla^{\xi}\mathbf{b} = (\nabla^{\xi}\mathbf{n})^2 + \nabla_{\mathbf{n}}\nabla^{\xi}\mathbf{n}$. This leads to

$$B = \begin{bmatrix} s^2/4 + s|\Delta| + |\Delta|^2 - q^2/4 + \nabla_{\mathbf{n}}\Delta + \nabla_{\mathbf{n}}s & -qs/2 - \nabla_{\mathbf{n}}q/2 + |\Delta|\theta' \\ qs/2 + \nabla_{\mathbf{n}}q/2 + |\Delta|\theta' & s^2/4 - s|\Delta| + |\Delta|^2 - q^2/4 - \nabla_{\mathbf{n}}\Delta + \nabla_{\mathbf{n}}s \end{bmatrix}, \tag{5.6}$$

see [Bin19] for details of the calculation. The above equation contains a mysterious quantity, θ'. In a local trivialisation, we can write

$$\Delta = \begin{pmatrix} \Delta_1 & \Delta_2 \\ \Delta_2 & -\Delta_1 \end{pmatrix} = \sqrt{-\det\Delta} \begin{pmatrix} \cos\theta & \sin\theta \\ \sin\theta & -\cos\theta \end{pmatrix}. \tag{5.7}$$

Then we define $\theta' = d\theta(\mathbf{n})$, which captures the change in the rotation of the eigenvectors as we move along the director.

For a selection of local profiles for bend based on setting all but one of the gradients of $\mathbf{n}$ to zero along the bend line, see Fig. 5.2. When constructing linearised bend vector fields with the desired gradients, we will not try to choose values for the gradients so that they come from a realistic director field, i.e., we won't worry about the compatiblity conditions between the gradients (see Chapter 4). The idea is to get an idea of what sort of changes in the deformations lead to a Legendrian point, and a rough idea of the structure of bend around such points, rather than give concrete constructions.

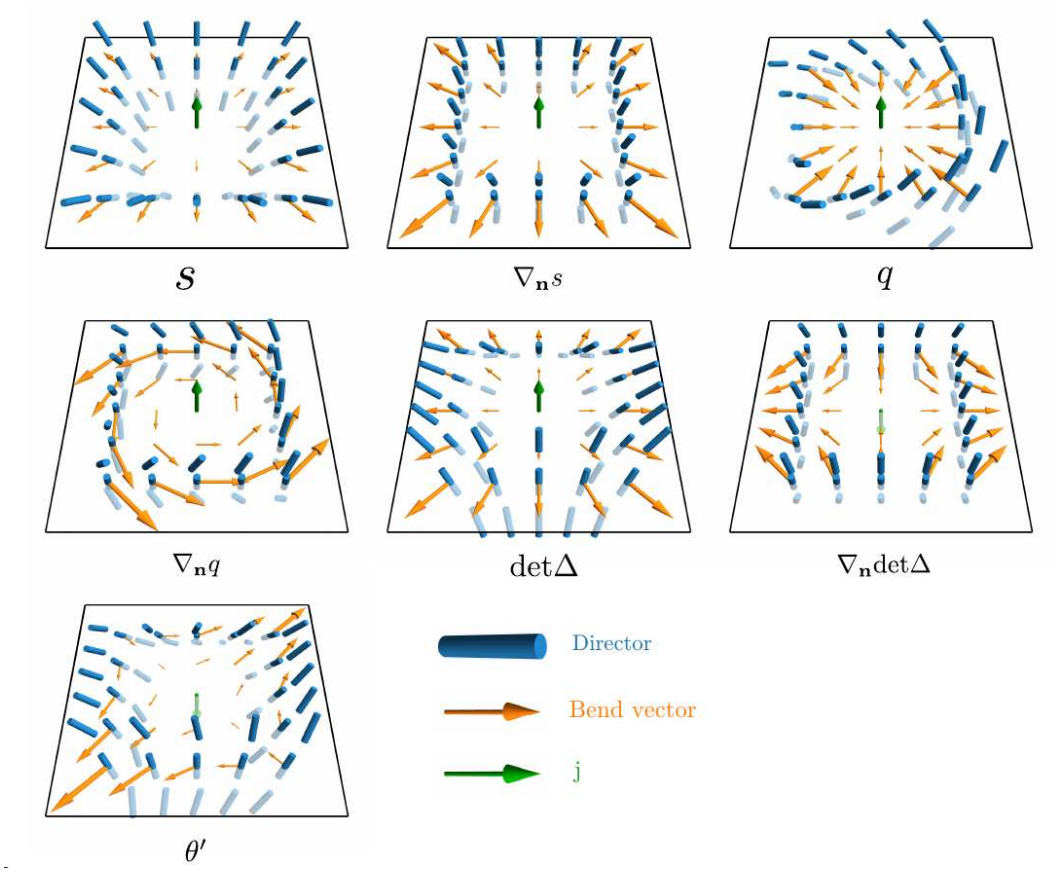

Figure 5.2: The profiles of a β line that are associated to each distortion of the director that plays a role in the linearised bend vector field. In all by the final panel, only the associated mode is nonzero; in the final panel, we require $|\Delta| \neq 0$ in order for θ' to be defined. Figure reproduced from [Bin19].

The eigenvectors of the linearised bend can be written as $\lambda^{\pm} = \frac{1}{2}(T \pm \sqrt{T^2 - 4D})$, where T is the trace and D the determinant of the matrix B. Recall that a saddle-node bifurcation involves a matrix with two real eigenvalues and one eigenvalue changing sign as a parameter is varied, while the Hopf bifurcation requires a complex conjugate pair of eigenvectors to pass transversally though zero.

We can construct a saddle-node bifurcation in bend by taking $|\Delta|, \theta' > 0$, setting all other parameters to zero. Then $T = 2|\Delta|^2$, $D = |\Delta|^2(|\Delta|^2) - \theta'^2)$. Fix $|\Delta|$ and treat θ' as the parameter. The eigenvalues are

$$\lambda_{\pm} = |\Delta|^2 \pm \theta', \tag{5.8}$$

and one will change sign as θ' passes through $|\Delta|^2$. In Fig. 5.3(a) the director and

bend are shown on a slice for $|\Delta|^2 = 3$ and several different values of θ'. This shows a change in the profile from an unstable node to a saddle, crossing a Legendrian point in the process. This bifurcation gives the local structure around a generic Legendrian point, and generic Legendrian points generically occur in β lines, so we expect to see such points in all situations where we have not programmed in a high degree of symmetry by our choice of director.

The Hopf bifurcation occurs in the linear system given by the matrix

$$\begin{bmatrix} a & -1 \\ 1 & 0 \end{bmatrix}, \tag{5.9}$$

where once again we have a parameter $a \in \mathbb{R}$. This is the linearised Van der Pol oscillator. Replicating this in bend is simple. Take $\nabla_{\mathbf{n}} s$ to be the parameter, $\nabla_{\mathbf{n}} \Delta = -\frac{1}{2} \nabla_{\mathbf{n}} s$, and $\nabla_{\mathbf{n}} q = 2$. Set all other parameters to zero. Then the linearised bend field is exactly the linearised Van der Pol oscillator with parameter $a = \nabla_{\mathbf{n}} s$, and the bifurcation occurs as this crosses 0. For a more realistic plot, one may also take $s = 2|\Delta|$ to be small but nonzero. This bifurcation is shown in Fig. 5.3(b). We see it does not correspond to a Legendrian point, only a change of stability for the zero of bend. Hopf bifurcations in the β-line profile arise quite naturally when one creates a meron by trying to remove a +1-winding singular line in the director via an escape into the third dimension. This process is discussed at length in Chapter 8.

5.3 Two-dimensional Vortex-Like Structures

Twist-bend materials capture the geometry of both cholesterics and smectics. In this section and the following section, we will focus on the nematic geometry, studying merons and Skyrmions and the twist-bend phase. These are vortex-like distortions of the material. Merons and Skyrmions in twist-bend phases are similar to merons and Skyrmions in the cholesteric phase, as discussed in Chapter 3. A surface S intersecting a single Skyrmion in a plane field ξ has $e(\xi)[S] = +2$, and consequently must be pierced by two generic β lines, or a single degenerate β line. A meron is a fractionalisation of a Skyrmion, and therefore an example of a structure with a single β line with charge +1. The local structure of such a cholesteric meron is given in cylindrical coordinates r, θ, z by

$$\eta = \cos(r) dz + r \sin(r) d\theta. \tag{5.10}$$

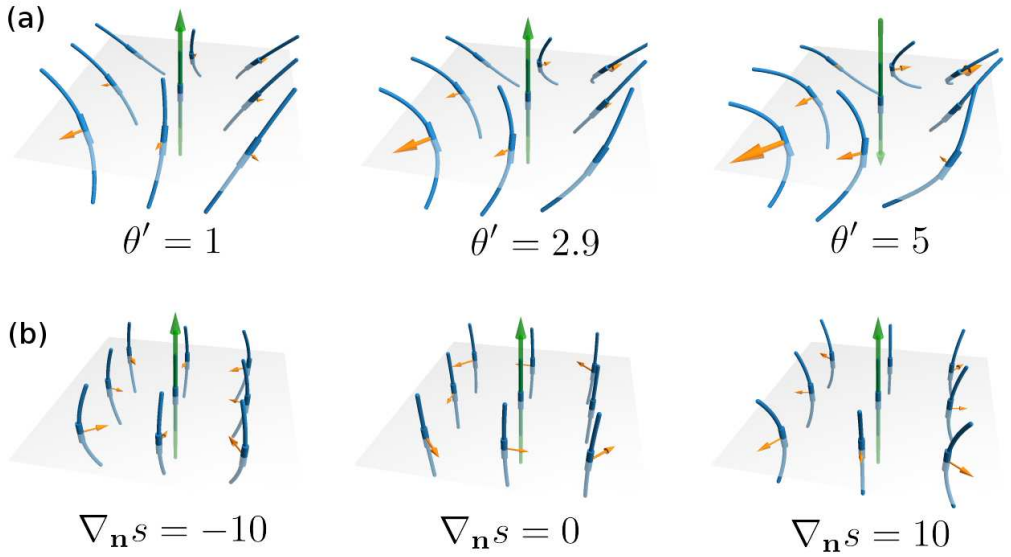

Figure 5.3: The two generic bifurcations occuring in families of two-dimensional vector fields arise as changes in stability for bend zeros. (a) The saddle-node bifurcation controlled by the parameter θ', as discussed in the text. The β line changes from unstable to half-stable, passing through a Legendrian point in the process. (b) The Hopf bifurcation, controlled by the change in the splay along the director, as discussed in the text. The line switches from being stable to unstable, emitting a closed orbit in the process as in the Van der Pol oscillator. There is no Legendrian point here. In all cases the director and its integral curves are shown in blue, the bend vector field in orange, the tangent to β line in green, and the values of the control parameter are shown beneath the panels.

The bend of this director is $\mathbf{b} = -\frac{\sin^2(r)}{r}\mathbf{e}_r$, which vanishes along $r = 0$. A meron constructed in this way is shown in Fig. 5.4(a). One can also produce a type of meron where the director winds by -1 rather than $+1$ around the central axis of the meron, Fig. 5.4(b); this is still represented by a single $+1$ β line. We can use the meron to get a feel for the 'footprint' of a β line, the size of the region over which the polarisation $\mathbf{p}$ deviates from being orthogonal to the director, as a function of the parameter $\frac{K}{\lambda}$; this is shown on slices in Fig. 5.4(c). In these panels, $\frac{K}{\lambda}$ is equal to 1 in the leftmost panel and doubles each panel as we move to the right, showing a linear scaling in the footprint.

Skyrmions are constructed in the same fashion, but with $r \in [0, \pi]$ instead. One then matches on to the uniform heliconical background state, which results in a director than can be used to initialise a simulation. As the Skyrmion charge of a single Skyrmion is $+2$, a Skyrmion will contain two generic β lines, one with

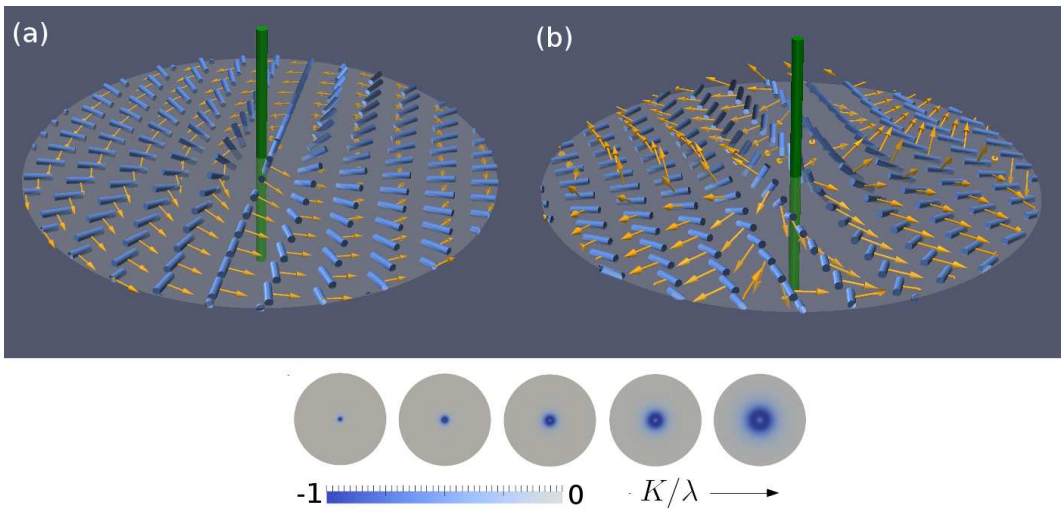

Figure 5.4: Merons in twist-bend nematics. (a) A meron with a winding +1 and (b) a meron with winding −1. In each case the β line has winding +1, and the director is orthogonal to an overtwisted contact structure. By comparison with the local profiles in Fig. 5.2, we see that the profile of the +1 winding meron is associated with splay and twist distortions in the director, while the −1 winding meron is associated with the director distortion $|\Delta|$. In each case, the bend zeros are shown in green, the director in blue, and the bend in orange. Bottom: a plot of $\mathbf{n} \cdot \mathbf{p}$ on a slice through the meron of +1 winding indicates that each β line corresponds to a region where the polarisation is not orthogonal to the director, resulting an energy penalty. The size of the region grows as a function of $\frac{K}{\lambda}$—in the images shown, $\frac{K}{\lambda}$ is equal to 1 in the leftmost panel and doubles each panel as we move to the right.

winding +1 and the other with winding −1, Fig. 5.5(a). We have numerically checked metastability of the Skyrmion for heliconical far-field angle $\theta \in [0.1, 0.5]$ and elastic constants $U/C \in [0.1, 0.5]$ in simulations performed in a box with height chosen to match one pitch length and with periodic boundary conditions.

One can also form lattices of Skyrmions, Fig. 5.5(b,c).

5.4 Three-dimensional Vortex-Like Structures

The structures discussed in the previous section are all quasi two-dimensional, in that they consist of straight tubes whose properties are essentially determined by a transverse slice, and moreover the β lines are tangent to the director. This is a highly nongeneric situation. We can also construct merons and Skyrmions which have an essentially three-dimensional character, laying along curves in three-dimensional space. Tying these curves into knots and links can produce textures with nontrivial

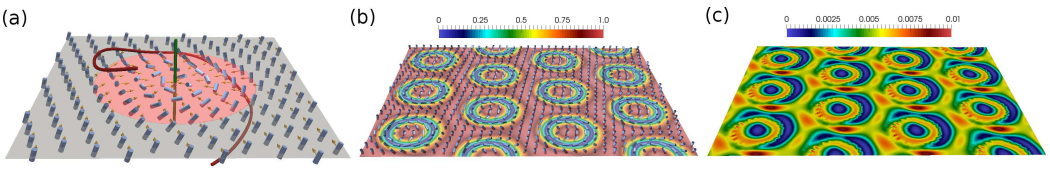

Figure 5.5: (a) A single Skyrmion in a twist-bend phase is characterised by two β lines, one with $+1$ winding (green) and one with -1 winding (red), for a total Skyrmion charge (value of the Euler class on a surface transverse to the axis of the Skyrmion) of 2. The red disk indicates the size of the Skyrmion region. (b) A hexagonal lattice of Skyrmions, where the colours indicate the magnitude of the e_z component of the director. (c) The same Skyrmion lattice, but where the colours now indicate the magnitude of the bend vector field. In each case the director is shown as blue cylinders, and the bend vector field as orange arrows.

Hopf invariant, which too have an essentially three-dimensional character. Over 100 molecules are known to form twist-bend phases [JLS18], with typical pitches on the nanometre scale. The short pitch means that the textures with fully three-dimensional tubes of merons and Skyrmions, such as those produced in [TS19], are currently experimentally inaccessible, as the techniques used to generate them in cholesterics do not work at such small scales. Nonetheless, we can generate and examine such textures numerically.

5.4.1 Meron Tubes

To produce knotted tubes of merons, we employ the same construction as in §3.9.4. Given a knot K, one may locally construct a texture with K as a β line using the director

$$\mathbf{n} = \cos\left(\frac{\pi r}{2R}\right)\mathbf{e}_z + \sin\left(\frac{\pi r}{2R}\right)\left[\cos\phi\,\mathbf{e}_x + \sin\phi\,\mathbf{e}_y\right], \tag{5.11}$$

on a tube of radius R around K, where r is the radial distance from K and $\phi = qz + \frac{\omega_K}{2}$, for ω_K the solid angle function of the knot [BA18]. Close to the knot the solid angle function agrees with the angular coordinate in a local cylindrical coordinate system, so this construction generalises the meron director (5.10). The director (5.11) is extended by taking it to be the heliconical ground state outside this tube. An example, where K is the 4_1 knot, is shown in Fig. 5.6(a). It is easy to extend this to a general link: we simply peform the construction along each component of the link separately. Along the β line itself the director is oriented along the z axis, and it rotates through an angle of $\frac{\pi}{2}$ as we move outwards; this implies there were will be at least two Legendrian points. Such knotted tubes of merons,

also called 'heliknotons', have recently been constructed in cholesterics [TS19]. In Chapter 8 I give an alternative construction of linked meron tubes in cholesterics which produces textures very similar to those in [TS19], where the β lines are without Legendrian points, but also not along an arbitrary link. Of course this construction can be adapted to twist-bend phases as well.

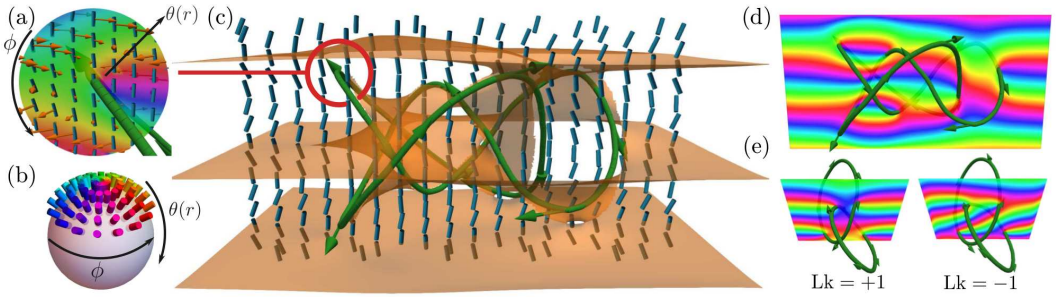

Figure 5.6: Knotted β line meron textures in twist-bend nematics. (a–d) shows a β line tied into a figure-eight knot, embedded in heliconical background. The local structure of the director (a, b) is an escape-up meron containing a single β line (colour denotes helical phase ϕ). In (c) level sets (orange) show $\phi = 0$, and in (d) we show ϕ on a cross-sectional slice through the entire knot. This construction generates any knot or link; in (e) we show β lines tied into Hopf Links with linking numbers ± 1, and their distinct helical phase fields. Figure reproduced from [BPA20].

5.4.2 Hopfions

For the purposes of this section, a 'Hopfion' will be any liquid crystal texture with nonzero Hopf invariant; for technical purposes, the 'Hopf invariant' is the quantity obtained by computing either the self-linking number of the zero set of the (Legendrian) bend vector field as described in §2.4, or the linking number of two preimages, which captures the same information as the usual Hopf invariant in S^3; see Chapter 2 for the details.

Stable Hopfions are impossible in a nematic described by the Frank energy (1.2) with one elastic constant, a result known as the Derrick–Hobart theorem [Hob63; Der64]. The energy E in this case is just the L^2 norm of the gradient tensor $\nabla \mathbf{n}$. A necessary condition for a particular director to be stable with respect to the energy E is that the second variation of the energy is non-negative. Suppose $\mathbf{n}$ has nonzero energy, and contains a spatially localised structure like a Hopfion. We may rescaling the spatial coordinates by a factor of λ, which corresponds to a shrinking of the spatially localized hopfion structure. A simple calculation given in Ref. [Der64] shows that such a dilation always reduces the energy E, and that the

second variation of the energy of $\mathbf{n}$ is negative. The conclusion is that any Hopfion we may initialise will shrink in size until it is gone, a fact that can be reproduced in numerical simulations.

There are two obvious ways to try and get around the Derrick–Hobart theorem. If there is an inherent length scale in the material, such as that provided by the pitch length in a cholesteric, this acts to prevent expansion or contraction by setting a preferred size for the Hopfion. When the material is confined in a domain with fixed boundary conditions, anisotropy of the elastic constants also serves to introduce a lengthscale which aids stability. The first experimental realisations of Hopfions in cholesteric liquid crystals appear in Ref. [CAA$^+$13], and in the further work of Ackerman and Smalyukh [AS16; AS17], which I will briefly describe. The domain for these experiments is a slab which we roughly identify with $\mathbb{R}^2 \times [0, 1]$, where physically the boundary consists of glass slides. The experiments impose normal anchoring on the boundary and a uniform far-field for the director, so we may compactify and regard them as taking place in S^3. A cholesteric liquid crystal is first prepared in a twist-free state where the director is $\mathbf{n} = \mathbf{e}_z$. Due to the optical Fréedericksz transition, the liquid crystal director will align according to its coupling with the optical-frequency electric field of the laser beam, a fact which is exploited in the experiment by using optical tweezers moved in a circular pattern to produce $H = \pm 1$ hopfions whose preimages form the Hopf link, where the sign is determined by the direction of rotation. One can also produce examples of Hopfions with more complicated linking of preimages and/or with Hopf invariants larger than 1 in magnitude, see [AS17].

If shrinking is not energetically favourable, the only mechanism by which a Hopfion may be destroyed is via a homotopy producing and annihilating a pair of defects, which in turn creates or destroys a λ line. This proceedure can be effected in a cholesteric without introducing regions of opposite handedness via the 'singular Lutz twist' that will be described in Chapter 6. The simplest case is when this homotopy occurs along a closed integral curve of the director. In order for the singular Lutz twist to work, this integral curve must be transversally hyperbolic; it possesses both a nonempty stable and a nonempty unstable manifold. If one attempts to create a pair of Morse defects along an orbit with $+1$ winding, one of those defects will always be achiral, and the result of performing the singular Lutz twist will be to replace the λ line with a region of reversed handedness, which is energetically disfavourable in a cholesteric, suggesting that this mode of decomposition is inaccessible. One can of course convert between $+1$ and $_1$ winding orbits via a homotopy, but this has its own energtic costs associated to it. By the fact that

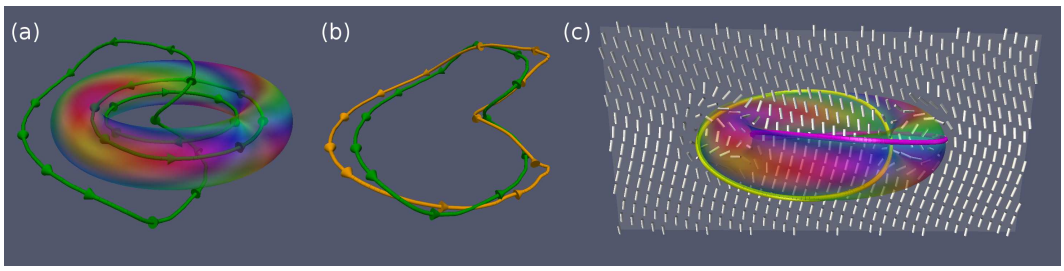

Figure 5.7: A Hopfion in a twist-bend nematic phase. (a) The β lines (green) are show with orientation vector $\mathbf{j}$. The surface shown is the set where the z component of the director vanishes. This torus structure is indicative of the Hopf texture. There are three β lines, but computing the linking number of these lines results in zero, as the two 'planar' β lines have opposite linking with the fully three-dimensional line. Instead, the Hopf invariant manifests through the self-linking number of the three-dimensional β line, which is shown alongside its pushoff (orange) in panel (b). (c) One may also compute the Hopf invariant by looking at preimages. Here we show the set of points where $\mathbf{n} = \pm\mathbf{e}_x$ as yellow and magenta lines. Clearly they form the Hopf link. The director (white) is also shown on a slice.

Hopfion structure are stable in cholesterics, we can conclude that these energetic costs must be greater than simply tolerating the distortions associated with the λ lines.

Due to the stability of Hopfions in cholesterics and the similarities between twist-bend nematics and cholesterics, it is natural to ask whether they can be stabilised in twist-bend materials as well. Numerical explorations suggest that Hopfions in twist-bend nematics are unstable, decaying not by shrinking, but by the collapse mechanism just described; that said, we have not performed a complete parameter sweep, so it is possible there exist regions of parameter space where stability can be achieved.

Fig. 5.7(a) shows a realisation of a Hopfion in a twist-bend nematic before its collapse. This is initialised using the Hopf fibration director field [CAA+13]. Notice there is not a single β line, but rather three. Two of these lines are planar, and they are topologically redundant, as the Hopf invariant is given purely by the self-linking number of the fully three-dimensional β line, which is shown in Fig. 5.7(b) (green) along with its pushoff (orange); the latter is constructed as described in §2.4. One can also see the nontrivial Hopf invariant by looking at a pair of preimages, Fig. 5.7(c).

The collapse of the structure in Fig. 5.7 is shown in Fig. 5.8, from left to right. Initially, the torus that represents the Hopfion 'pinches off'. In terms of the preimages, this involves the two components of the link coming together. Their

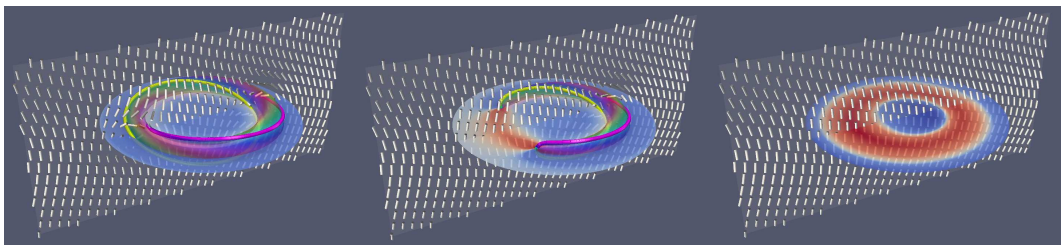

Figure 5.8: The observed decay of a Hopfion in a twist-bend phase is not through shrinking as it would be in a nematic phase, but through the creation of point defects, as is necessary to change topological invariants. The decay process is shown from left to right. The preimages of $\mathbf{n} = \pm\mathbf{e}_x$ are shown as yellow and magenta lines; in the second panel, they meet at the point defects. The director is shown as white cylinders of a cross-section, which illustrates that there is a periodic orbit of the director, around which the winding is +1. The twist of the director is shown on another cross section. Initially it is everywhere negative (blue), but after the decay process there is a toriodial region of positive twist (red) left behind.

collision occurs at exactly the moment an index 0 point defect, with local structure A_2 (see Chapter 6), is created. This defect splits into a pair of ± 1 charge defects which move in opposite directions around the loop, removing the preimages as they go. When they reach one another again they annihilate, and the result is a removal of the Hopfion and the return to (what appears to be) a uniform state. This process is described in greater detail in Chapter 6. A feature of the Hopf texture used to initialise this simulation is that there is a closed periodic orbit of the director, which sits at the centre of the torus structure shown in Fig. 5.7. The winding of the director around this orbit is +1. When the point defects are created, it is in fact this orbit they are erasing. Because the orbit has winding +1, one of the created defects must be of hedgehog type. I show in Chapter 6 that such defects are fundamentally achiral, sitting on an interface between regions of opposite handedness. A region of 'reversed handedness' connects the two defects, grows as they move around the periodic orbit, and is left behind when they annihilate again. Thus the result of the decay process is to replace the Hopfion with a toroidal region of left-handedness in an otherwise right-handed background, as seen in the final panel of Fig. 5.8.

This is our first example of an energetically stable 'twist solition'. The theorem of Lutz & Martinet (Theorem 3.4) implies there is a contact structure in every homotopy class of plane fields, so this region is not topologically protected and can be removed; however, removing it is a nonlocal process. More examples of twist solitions in the cholesteric phase are given in Chapters 7 and 8.

5.5 Smectic-Like Structures

In addition to the vortex-like structures examined in the previous two sections, which are classically cholesteric structures, we can define twist-bend analogues of smectic structures. In a smectic A (SmA) material the director is normal to a family of surfaces, and hence defines a (singular) foliation. Moreover, such materials have a constant layer spacing, so the foliation is a *measured foliation* [FLP79; Po1]: there is a nonzero measure on the space of arcs transverse to the leaves which is invariant under deformations of the arcs that leave the endpoints fixed; the idea being that this measure gives the 'distance between leaves' is independent of the choice of arc used to measure the distance. Foliations by closed 1-forms are always measured, and we will usually assume the smectic director is $\mathbf{a} = \nabla\phi / \|\nabla\phi\|$, for some function ϕ called the smectic phase field[1].

In the chiral smectic A phase (SmA*) the director makes a constant angle with the layer normal $\mathbf{a}$, and the direction of deviation from the layer normal rotates as one moves transverse to the layers, causing the integral curves of the director to become helices transverse to the layers. The one-dimensional periodicity of the heliconical phase leads to a general correspondence with the elasticity of smectics and so a description in terms of 'smectic-like' phase fields, and a coarse-grained theory of twist-bend nematics that makes analogy with the smectic case. The heliconical phase $\phi = qz$ in the heliconical ground state is the same as the phase in the mass-density wave of the smectic ground state. Other smectic phase fields—corresponding to screw dislocations, edge dislocations, TGB phases, focal conics, etc.—lend themselves to analogous twist-bend states with the same helical phase field and provide examples of smectic-like defects in twist-bend nematics.

Let us describe a construction of a twist-bend director from a foliation defined by the level sets of ϕ. Suppose we can find an orthonormal basis $\mathbf{e}_1, \mathbf{e}_2$ for the layers which is parallel transported along the smectic director $\mathbf{a}$, i.e., $(\nabla_{\mathbf{a}}\mathbf{e}_1)\cdot\mathbf{e}_2 = 0$. Then the director

$$\mathbf{n} = \cos(\theta)\mathbf{a} + \sin(\theta)(\cos(\phi)\mathbf{e}_1 + \sin(\phi)\mathbf{e}_2) \tag{5.12}$$

defines a twist-bend texture templated on the smectic state with phase field ϕ. The cone angle θ should be constant outside a small region around the singular lines of the smectic, and should vanish along those lines. Away from singular lines, we can find local coordinates x, y, z where the layer normal is $\mathbf{e}_z$, and therefore this

[1] Technically, the smectic director is actually assumed to be a perturbation of the layer normal, as making it equal to the layer normal results in infinite enegry states, but we will not worry about this here.

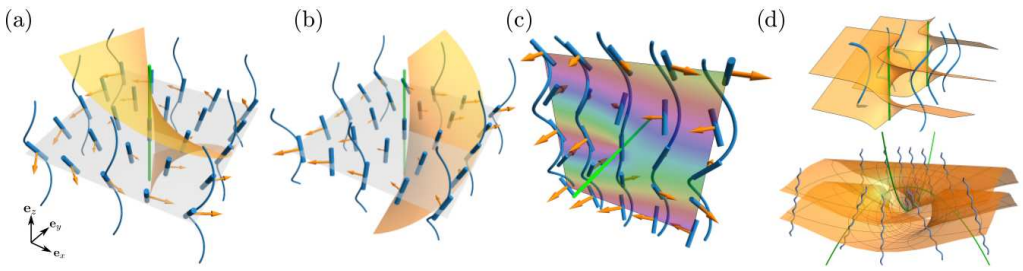

Figure 5.9: A selection of smectic-like textures in twist-bend nematics. (a,b) Local structure of β lines with winding $+1$ and -1 respectively, with the local director structure that of a screw dislocation. The orange surfaces are level sets of the smectic phase field ϕ for the screw dislocation. (c) Edge dislocation. (d) Twist-grain boundary. (e) Focal conic. In each case the β lines are indicated by the green tubes, the director by blue rods, and the bend vector field by orange arrows.

construction is locally equivalent to the heliconical ground state, while encoding the global geometry of the smectic state it is modelled on.

There is an alternative description, which I describe informally here. Suppose we are given a singular foliation $\mathcal{F}$ defined by a closed 1-form $\alpha = d\phi$, and a pair of transverse sections $\mathbf{e}_1, \mathbf{e}_2$ with the following properties: (1) neither $\mathbf{e}_1$ nor $\mathbf{e}_2$ vanish at any point, and (2) there exists a closed 2-form Ω, positive on each nonsingular leaf L of $\mathcal{F}$, such that both $\mathbf{e}_1$ and $\mathbf{e}_2$ preserves the area form $\Omega|_L$ on every nonsingular leaf L. Then $\cos(\phi)\mathbf{e}_1 + \sin(\phi)\mathbf{e}_2$ is a contact form, and by Lemma 6.3 from Chapter 6, its Reeb field is tangent to $\mathcal{F}$. Define a director as in (5.12). Then the Reeb field of the dual 1-form is still tangent to $\mathcal{F}$, however the director is transverse to the foliation by construction; since the director and Reeb field are nowhere colinear, Eq. (3.3) implies that the bend is nonzero away from the singularity in $\mathcal{F}$. These singularities are places where the Reeb field and the director are colinar, and hence these are exactly the β lines.

Using this construction we can easily produce analogues of classical structures from smectic physics in bent-core materials. The singularities in these textures are of a different character than the vortex-like distortions described in §5.3 and §5.4. See Fig. 5.9 for a selection of such structures. All the textures described in this section belong to the zero homotopy class of plane fields, and are overtwisted contact structures in that class. Despite this, they nonetheless have interesting geometry and are energetically metastable, i.e., they don't immediately collapse to a trivial plane field.

5.5.1 Screw Dislocations

Our first example of a smectic-like defect is the screw dislocation, for which we consider the texture

$$\mathbf{n} = \cos\theta(r)\,\mathbf{e}_z + \sin\theta(r)\big[\cos\phi\,\mathbf{e}_x + \sin\phi\,\mathbf{e}_y\big], \tag{5.13}$$

where $\phi = qz + s\arctan(y/x)$, with $s \in \mathbb{Z}$ the defect strength, and $\theta(r)$ interpolates smoothly from 0 at the origin to the heliconical far field angle as $r := \sqrt{x^2+y^2} \to \infty$. In Fig. 5.10 we show these textures for $s = +1, -1$ in panels (a,b) respectively. The phase field ϕ contains a smectic screw disclocation along the z axis such that around any positively oriented loop in the xy-plane encircling the axis ϕ winds by $2\pi s$. This is shown by the winding colour map in Figs. 5.10(a,b)(i), which also show the level set $\phi = 0$ as an orange surface; this surface corresponds to the layers of a smectic screw dislocation. Note the difference in the sense of rotation between panels (a) and (b). Figs. 5.10(a,b)(ii) show the same level set $\phi = 0$ but zoomed out, emphasising that away from the screw dislocation we simply have equally spaced layers, $\phi \approx qz$. In Fig. 5.10(a,b)(iii) we add integral curves of the director, with their intersection with the $\phi = 0$ surface indicated by black points; in the limit $r \to \infty$ the integral curves are exactly helices and the marked points are locations along the integral curves of the same 'helical phase'. The screw dislocation corresponds to a $2\pi s$ 'phase slip', as can be seen in Fig. 5.10(a,b)(iv) in which we show a top down view of the integral curves alongside the phase ϕ on the xy plane.

The bend of (5.13) is

$$\mathbf{b} = (\mathbf{n}\cdot\nabla\theta)\left[\cos\theta\left(\cos\phi\,\mathbf{e}_x + \sin\phi\,\mathbf{e}_y\right) - \sin\theta\,\mathbf{e}_z\right] + (\mathbf{n}\cdot\nabla\phi)\sin\theta\left[-\sin\phi\,\mathbf{e}_x + \cos\phi\,\mathbf{e}_y\right]. \tag{5.14}$$

We first consider its far field behaviour. As $r \to \infty$, $\nabla\theta \to 0$ and (5.14) becomes

$$\mathbf{b} = q\cos\theta_0\sin\theta_0\left[-\sin\phi\,\mathbf{e}_x + \cos\phi\,\mathbf{e}_y\right], \tag{5.15}$$

exactly the heliconical bend but with $qz \to \phi = qz + \arctan(y/x)$. We conclude that the bend winds as ϕ, and so there is a $2\pi s$ winding of the bend vector about the origin. This winding is shown in Fig. 5.10(a,b)(iv). The bend (5.15) also rotates along the pitch axis z with pitch $\frac{2\pi}{q}$, giving a periodic structure to these defects along z, as shown in Figs. 5.10(a,b)(v). For $s = +1$, a radial profile rotates to become azimuthal and then back to radial. For $s = -1$, the axes of the -1 profile rotate along z.

As r decreases and we approach the axis the integral curves are no longer

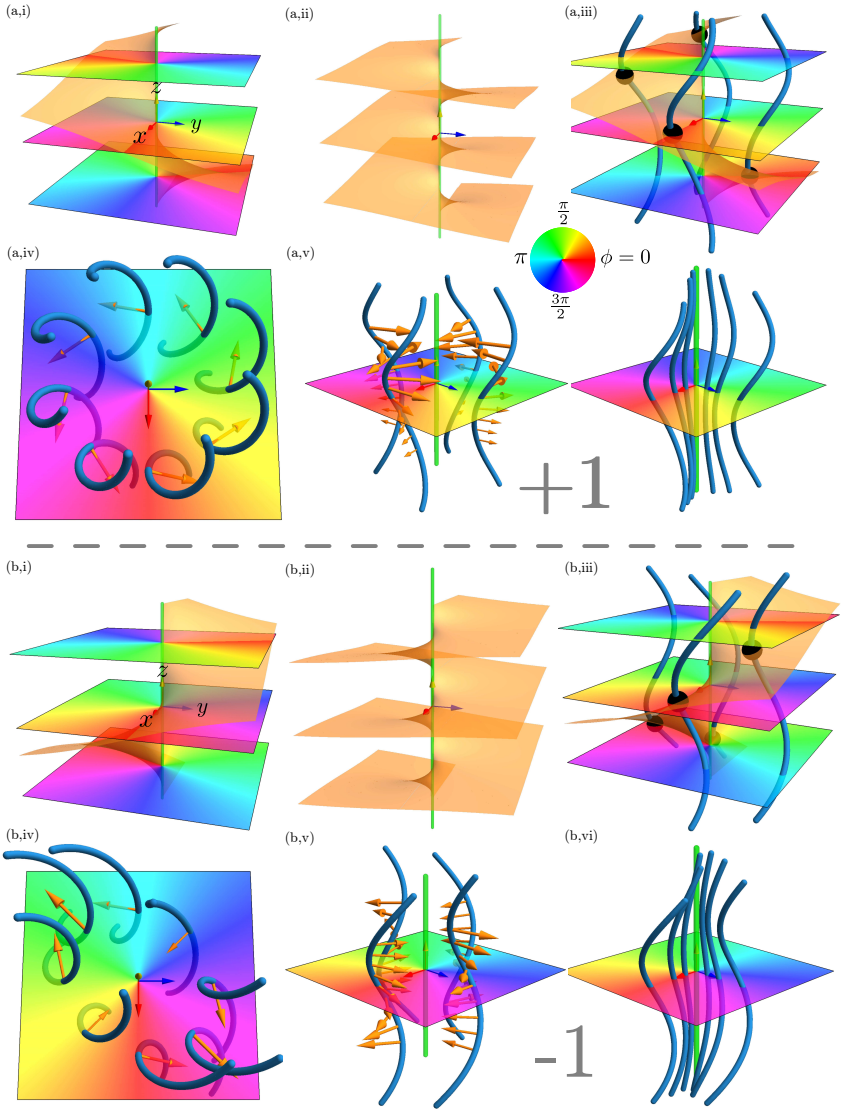

Figure 5.10: Screw dislocations in twist-bend nematics. Panels (a,b) show $+1, -1$ strength screw dislocations respectively. The β line along the z axis is shown in green. (a,b)(i) Helical phase field on three z slices, with $\phi = 0$ level set shown in orange. (a,b)(ii) Zoomed out view of $\phi = 0$ level set, showing equispaced layers away from the screw dislocation. (a,b)(iii) Director integral curves (blue) with their intersection with $\phi = 0$ shown as black dots. (a,b)(iv) Top down view of integral curves, with bend vector (orange) shown on a $z = 0$ slice. (a,b)(v) Perspective view of integral curves and their bend vector, showing periodic variation of the bend along the screw. (a,b)(vi) Degeneration of the integral curves to a straight line, which is also the β line, as we approach the z axis.

exactly helices, however the $2\pi s$ winding of the bend vector is preserved. We can regard the integral curves as approximately helices but with curvature and torsion that vary with r, which is a good approximation provided the tilt angle θ_0 is small. More precisely, consider the magnitudes of the two terms in (5.14),

$$\mathbf{n} \cdot \nabla\theta = \sin\theta\, \theta'(ro) \cos\big(qz + (s-1)\arctan\left(\tfrac{y}{x}\right)\big), \tag{5.16}$$

$$\sin\theta(\mathbf{n} \cdot \nabla\phi) = \sin\theta\left(q\cos\theta + \frac{\sin\theta(r)}{r}\sin\big(qz + (s-1)\arctan\left(\tfrac{y}{x}\right)\big)\right). \tag{5.17}$$

Note that (5.17) shows that we require $\theta(\rho)$ to vanish at least linearly at the origin. The ratio of the two terms is then approximately $\theta'(0)/(q + \theta'(0))$ and taking $\theta'(0)$ to be roughly θ_0 divided by the pitch the ratio is of order $\frac{\theta_0}{2\pi}$ and is small. We can then neglect (5.16), and simplify (5.17) to $|\mathbf{b}| = q\sin\theta(r)\cos\theta(r)$, the curvature of an integral helix. As $r \to 0$ this curvature vanishes, and along the z axis itself the helices degenerate to a straight line, which is also our β line. A schematic of this degeneration is shown in Fig. 5.10(a,b)(vi) and can be compared against numerical relaxation of a screw dislocation shown in Fig. 5.11. We identify the core region of the β line by measuring how the cone angle θ deviates from the preferred value θ_0 of the heliconical state and indicate it by blue shading. On the right, we show the size of the core region for different values of $\frac{K}{\lambda}$, corresponding to the helical pitch, increasing from top to bottom. The value of $\frac{K}{\lambda}$ doubles with each panel, illustrating a roughly linear scaling. The final panel is illustrated in more detail on the left of Fig. 5.11; compare with Fig. 5.10(a)(vi).

5.5.2 Twist Grain Boundary Phases

Twist grain boundaries in smectics are formed by arrays of equally spaced screw dislocations and mediate a rotation of the smectic layer normal. This same structure can be encoded into a director field that locally corresponds to the heliconical state; the grain boundary mediates a rotation of the helical (pitch) axis and each of the screw dislocations becomes a β line. We first review briefly the construction of grain boundaries in smectics.

A single grain boundary in a smectic can be described by the phase field [MKA17]

$$\phi = \operatorname{Im}\ln\left[\mathrm{e}^{-y/\ell}\mathrm{e}^{i\phi_-} + \mathrm{e}^{y/\ell}\mathrm{e}^{i\phi_+}\right], \tag{5.18}$$

where $\phi_\pm = qz\cos(\alpha/2) \pm qx\sin(\alpha/2)$ and we choose $\ell = [q\sin(\alpha/2)]^{-1}$ to make ϕ a harmonic function. The layer structure is the level set $\phi = 0$ and is shown in Fig. 5.12(a). For $y \lesssim -\ell$ we have $\phi \approx \phi_-$ and for $y \gtrsim \ell$ we have $\phi \approx \phi_+$. In the

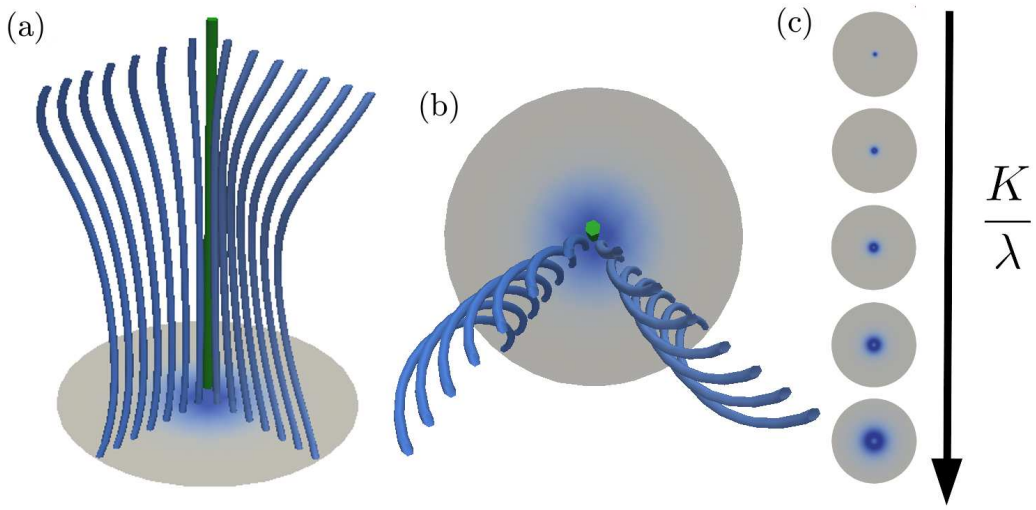

Figure 5.11: Illustration of the core structure of a screw dislocation. The core can be identified with the region where the cone angle θ deviates from the preferred cone angle θ_0. (a,b) We plot the value of $|\theta - \theta_0|$ on a slice orthogonal to the β line in a numerical simulation of a screw dislocation. The region where this is positive is shown in blue. The integral curves deform from helices to a straight line, where $\theta = 0$, along the β line. (c) The size of the core region is shown for several values of K/λ, which doubles with each panel, illustrating a roughly linear scaling.

plane $y = 0$ there are screw dislocations with axes parallel to z at $x = \frac{\pi}{2} + m\pi$, $m \in \mathbb{Z}$. The gradient of the phase field is

$$\nabla\phi = q\cos(\alpha/2)\,\mathbf{e}_z + q\sin(\alpha/2)\,\frac{\sinh(2y/\ell)\,\mathbf{e}_x + \sin(2x/\ell)\,\mathbf{e}_y}{\cosh(2y/\ell) + \cos(2x/\ell)}, \tag{5.19}$$

and its magnitude squared,

$$|\nabla\phi|^2 = q^2\,\frac{\cosh(2y/\ell) + \cos\alpha\cos(2x/\ell)}{\cosh(2y/\ell) + \cos(2x/\ell)}, \tag{5.20}$$

diverges as inverse distance squared along each of the screw dislocations. It is not difficult to extend this construction to create phase fields containing multiple grains and describing full twist-grain boundary phases. See Ref. [MKA17] for details.

We restrict our focus here to describing how the single grain boundary (5.18) can be embedded into a heliconical director field with β lines along each of the screw dislocations, *i.e.* the lines $(\frac{\pi}{2} + m\pi, 0, z)$, $m \in \mathbb{Z}$. We write the director field in the

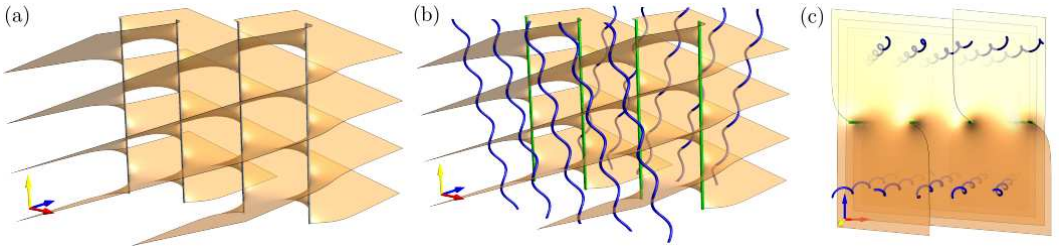

Figure 5.12: (a) Smectic phase field for a single grain boundary. The surface shown is $\phi = 0$, where ϕ is given in (5.18). (b-c) Helical integral curves (blue) of a twist-bend director containing a grain boundary, with β lines shown in green: (b) side view; (c) top view.

form (5.12) and take the basis $\{\mathbf{a}, \mathbf{e}_1, \mathbf{e}_2\}$ to be

$$\mathbf{a} = \cos\sigma\,\mathbf{e}_z + \sin\sigma\,\mathbf{e}_x, \qquad \mathbf{e}_1 = -\sin\sigma\,\mathbf{e}_z + \cos\sigma\,\mathbf{e}_x, \qquad \mathbf{e}_2 = \mathbf{e}_y, \tag{5.21}$$

where σ is a function interpolating between $-\alpha/2$ for $y \lesssim -\ell$ and $+\alpha/2$ for $y \gtrsim +\ell$, for instance $\sigma = \frac{\alpha}{2}\tanh(2y/\ell)$. With this choice $\mathbf{N}$ differs from $\nabla\phi/|\nabla\phi|$ by exponentially small terms away from the cores of the screw dislocations, along each of which it is $\mathbf{e}_z$. To make the cone angle θ vanish linearly along each screw dislocation and approach a preferred value θ_0 outside of the core region we can choose $\theta = q\theta_0/|\nabla\phi|$. A selection of helical integral curves of this director field are shown in Fig. 5.12(b,c).

5.5.3 Edge Dislocations

Returning to (5.13) but taking instead $\phi = qz + s\arctan(z/x)$ yields an edge dislocation in the phase field parallel to the y axis. Tthe case $s = +1$ is shown in Fig. 5.13. As we go from negative to positive x an extra 2π is inserted into ϕ, corresponding to an additional full turn in the integral helices, as can be seen in Fig. 5.13(a). On a positively oriented loop encircling the edge dislocation, the bend therefore acquires a winding of $2\pi s$ as in the case of the screw dislocation. There are, however, several distinct features of the edge dislocation worth emphasising. The first is that the β line (shown in green in Fig. 5.13) is not itself an integral curve of the director—this is the generic situation in an arbitrary director field, the screw dislocation being an exceptional case. The second feature is the location of the β line itself—it is not along the y axis, but slightly displaced from it, as shown in Figs. 5.13(a,b). To understand this feature we recall some details of the phase field ϕ, shown in Fig. 5.13(c) [KM16]. An edge dislocation is composed of two discli-

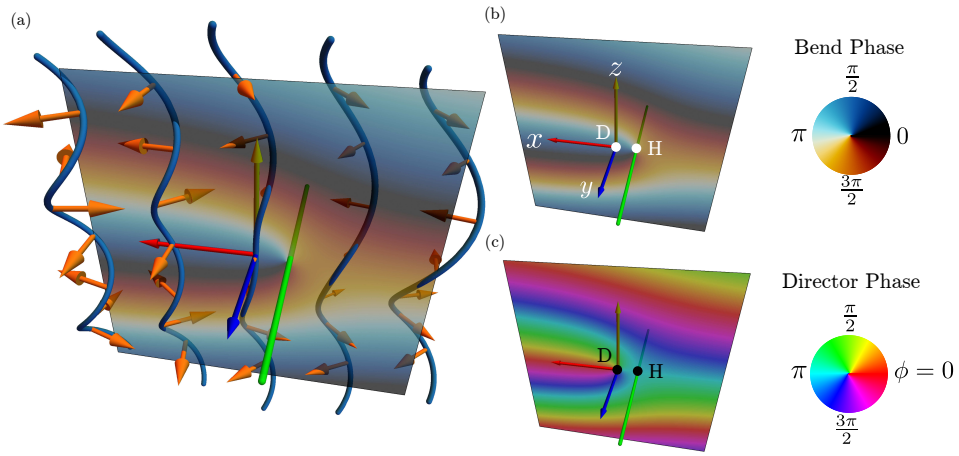

Figure 5.13: Edge dislocations in twist-bend nematics. (a) xz slice through the edge dislocation parallel to the y axis, coloured by the angle the bend vector makes with the x axis, with director integral curves shown in blue, bend vector in orange and the β line shown in green. Across the dislocation the bend acquires a 2π winding. (b, c) The β line does not coincide with the phase singularity **D** along the y axis, but is along the hyperbolic line **H**. We emphasise this difference by showing the angle the bend vector makes with the x axis in (b), and the phase field ϕ in (c). Note the discrepancy in the location of singularities.

nations in $\nabla\phi/|\nabla\phi|$. The first is a $+1$ disclination along the y axis, denoted **D** in Figs. 5.13(b, c), which is a singularity in ϕ. The second is a -1 disclination along $(-\frac{1}{q}, y, 0)$, called the hyperbolic line and denoted **H** in Figs. 5.13(b, c). This second disclination is the unique location where $\nabla\phi = 0$, with ϕ itself nonsingular. We now return to (5.14), derived for the screw dislocation but valid here too. Neglecting $(\mathbf{n}\cdot\nabla\theta)$ as before, we see $\mathbf{b}$ vanishes when $\nabla\phi$ vanishes, and so we have a β line along the hyperbolic line **H**. One might worry about the phase singularity at the origin, but a direct expansion of (5.14) shows that the bend is in fact continuous about the origin, taking value $\mathbf{b} = \theta'(0)\,\mathbf{e}_y$ at the origin itself, and is not (as one might initially suspect) singular—this is reflected in the smooth nature of the bend at the origin shown in Figs. 5.13(a,b).

We briefly remark that the canonical local form of a family of curves which pass through an inflectional configuration (where the bend vanishes) is given in [MR92], where it is shown that on passing through the inflectional configuration the curve normal (equivalently the bend $\mathbf{b}$) picks up a 2π rotation. Locally, this is what happens to our integral curves as we pass through the β line at **H**.

In §3.9, I discussed edge dislocations of cholesterics. One can initialise these in T^3 quite easily, by taking the cholesteric ground state with different values of the

layer number q on two halves of the torus. This can be done just as easily in the twist-bend nematic phase, however the construction (5.12) provides an alternative take that one can use to initialise circular edge dislocations, Fig. 5.14. This texture on T^3 is constructed by taking a tube of radius R around the origin and filling it with heliconical ground state with $q = 2$, and taking the heliconical ground state with $q = 1$ outide the tube, however we can think of this as being constructed using (5.12) starting from the fibration given by a toriodal coordinate system σ, τ, θ on the complement of a flat circle of radius R. The coordinate $\theta = \tan^{-1}(y/x)$ is the usual polar angle, while τ is a variant of the radial coordinate that is tangent to the disks given by the level sets of σ, which define the fibration. One can define adapted Cartesian coordinates by $\bar{x} = \tau\cos(\theta), \bar{y} = \tau\sin(\theta)$, and these coordinate directions given the unit vectors e_1, e_2 in (5.12). The bend zero has winding -1, however the contact structure is overtwisted as can be deduced from looking at the dividing curve on a convex torus. Again, this reiterates that while merons and Skyrmions in chiral materials are always overtwisted disks, not all overtwisted disks are things that would be called a meron or Skyrmion in the physics literature.

This example illustrates several important concepts discussed previously. First, we observe that the profile of the bend around the circular β line changes as we move along it, from a -1 winding to a $+1$ winding. This occurs through a saddle-node bifurcation. Conequently, there are two Legendrian points on the β line, where the tangent vector to the line is tangent to the planes orthogonal to the director. The count of β lines allows us to compute the value of the Euler class on the surface S shown in Fig. 5.14; at the point on the surface where the winding around the β line is $+1$, the β line points out of the surface, and at the point where it has winding -1, it points into the surface, and conequently $e(\xi)[S] = +2$, which also witnesses the fact that this contact structure is overtwisted via the violation of the Bennequin inequalities.

5.5.4 Parabolic Focal Conics

Focal conics are amongst the most celebrated geometric features of any ordered phase. They are the hallmark of smectic order, corresponding to the fundamental singularities of a material composed of equally spaced layers [FG10; Bou72; KL09]. They are also seen in twist-bend nematics [KK18], which serve to emphasise that it is the one-dimensional periodicity that leads to focal conics, rather than a modulation of the mass density.

A director field for a twist-bend phase containing a focal conic defect can be constructed using the general form (5.12), where ϕ is the phase field of a focal

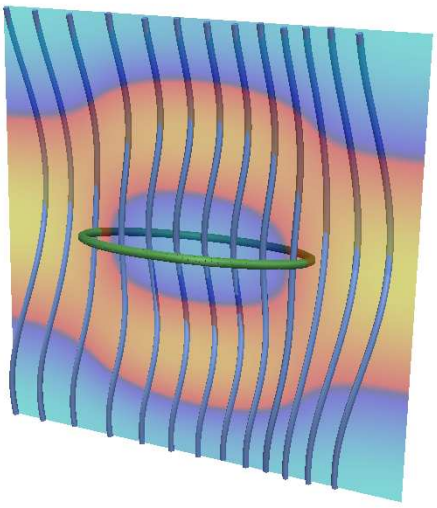

Figure 5.14: Circular edge dislocation in a twist-bend nematic in T^3. The bend zero (green line) has winding -1. The convex torus shown is the $x = 0$ plane, and the colours indicate the dot product of the director with the normal to the surface, with orange being positive and blue negative. The dividing set (black curve) has a nullhomotopic component, showing this contact structure is overtwisted. The blue tubes are integral curves of the director.

conic and $\mathbf{a}$ is the layer normal, away from the conic singularities themselves. The construction and description of the Dupin cyclides and focal conic domains is classical [Max68; Cay73; ACMK10]; here, I simply quote the formulae with a convenient parameterisation.

A focal conic domain consists of a space-filling family of surfaces—level sets of a phase field ϕ—that are singular along a pair of confocal conics and uniformly spaced everywhere else. In the case of a parabolic domain, the confocal parabolae may be taken to be

$$\mathbf{p}_1(u) = \left(\sigma\frac{\cos u}{1+\cos u}, \sqrt{2}\sigma\frac{\sin u}{1+\cos u}, 0\right), \quad \mathbf{p}_2(v) = \left(-\sigma\frac{\cos v}{1+\cos v}, 0, \sqrt{2}\sigma\frac{\sin v}{1+\cos v}\right), \tag{5.22}$$

where σ is a constant parameter corresponding to the distance between the two foci/apices of the parabolae and $-\pi < u, v < \pi$. The domain itself then has the

explicit parameterisation

$$\begin{aligned} x &= \cos u\,\frac{\sigma-\phi(1+\cos v)}{2+\cos u+\cos v} - \cos v\,\frac{\sigma+\phi(1+\cos u)}{2+\cos u+\cos v},\\ y &= \sqrt{2}\,\sin u\,\frac{\sigma-\phi(1+\cos v)}{2+\cos u+\cos v},\\ z &= \sqrt{2}\,\sin v\,\frac{\sigma+\phi(1+\cos u)}{2+\cos u+\cos v}, \end{aligned} \tag{5.23}$$

where each surface of constant ϕ is a parabolic Dupin cyclide. Depending on the value of ϕ the range of u, v should be restricted so as to terminate the surface on the singular parabolae. Specifically, if $\phi < -\sigma/2$ then the range of u should be restricted according to $\cos u < |\sigma/\phi| - 1$; if $\phi > \sigma/2$ then the range of v should be restricted by $\cos v < |\sigma/\phi| - 1$; and if $-\sigma/2 < \phi < \sigma/2$ no restriction is needed. In Fig. 5.15(a) we show the structure of a parabolic focal conic domain, with a selection of individual layers shown in Fig. 5.15(b).

In terms of this parameterisation the frame $\{\mathbf{a}, \mathbf{e}_1, \mathbf{e}_2\}$ is given by

$$\begin{aligned} \mathbf{a} &= \left(-\frac{\cos u+\cos v+2\cos u\cos v}{2+\cos u+\cos v}, -\frac{\sqrt{2}\sin u(1+\cos v)}{2+\cos u+\cos v}, \frac{\sqrt{2}\sin v(1+\cos u)}{2+\cos u+\cos v}\right),\\ \mathbf{e}_1 &= \left(\frac{\sqrt{2}\sin u(1+\cos v)}{2+\cos u+\cos v}, -\frac{1+2\cos u+\cos u\cos v}{2+\cos u+\cos v}, -\frac{\sin u\sin v}{2+\cos u+\cos v}\right),\\ \mathbf{e}_2 &= \left(\frac{\sqrt{2}\sin v(1+\cos u)}{2+\cos u+\cos v}, \frac{\sin u\sin v}{2+\cos u+\cos v}, \frac{1+2\cos v+\cos u\cos v}{2+\cos u+\cos v}\right). \end{aligned} \tag{5.24}$$

Helical integral curves of the director field are then given by

$$\mathbf{h}_{(u,v)}(\phi) = \mathbf{x}_0(u,v) + \frac{\phi}{q}\,\mathbf{a} + \frac{\tan\theta}{q}\big[\sin\phi\,\mathbf{e}_1 + \big(1-\cos\phi\big)\mathbf{e}_2\big], \tag{5.25}$$

where $\mathbf{x}_0(u,v)$ is a point on the cyclide $\phi = 0$. The range of values of ϕ should be limited to $[\frac{-\sigma}{1+\cos u}, \frac{\sigma}{1+\cos v}]$ and the helices then extend from one conic to the other. A selection of such helical integral curves are shown in Fig. 5.15(c-e). In this structure the two focal parabolae are singularities and correspond to β lines. Although there are several possibilities for how the director is resolved along these lines, one natural arrangement places point defects at each focus/apex of the two parabolae; this local structure is especially suggested by Fig. 5.15(e). The two point defects are both chiral [PPČ+19].

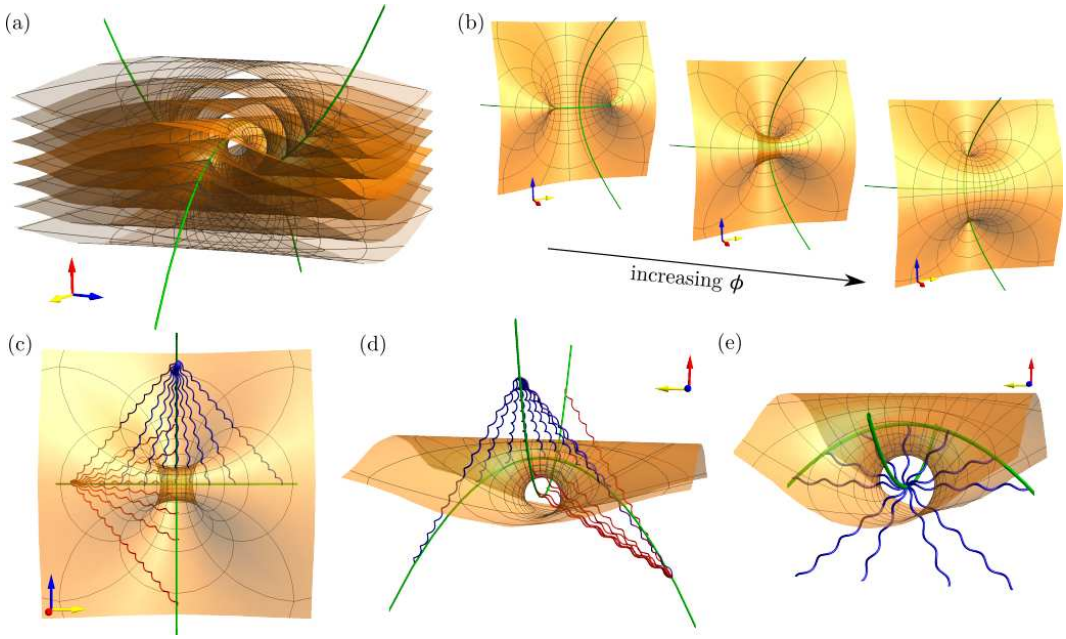

Figure 5.15: (a) Smectic phase field for a parabolic focal conic domain. We show multiple different level sets ϕ = constant. The β lines, singularities in the phase field ϕ, are shown in green. (b) Individual layers in the parabolic focal conic domain are shown for increasing levels of ϕ. (c-e) Helical integral curves of a twist-bend director containing a parabolic focal conic domain: (c) top view; (d) side view; (e) the local structure around each focus / apex is (compatible with) that of a (chiral) point defect. The integral curves connect one focus/ β line to the other. We show two families of integral curves, one in red, one in blue, that converge on the same point on one of the foci.

Chapter 6

Singular Contact Structures: The Local and Global Theory of Point Defects

In this chapter I extend the ideas of contact geometry explained in Chapter 3 to 'singular' contact structures, which allows for a discussion of defects in chiral materials. One of the most interesting parts of this theory is the distinction between defects that may occur in a chiral material, and those that may occur in a Beltrami field. Although the focus is certainly on the former case, I will also comment on Beltrami fields and applications to fluid dynamics. Singular contact structures on so-called b-manifolds have recently been considered and applied to the study of Beltrami fields [MO18; CMPS19]. I was not aware of this previous work while working on the results given in this chapter. The results of Refs. [MO18; CMPS19] overlap slightly with this chapter, but the perspective I adopt is different and the study of the specific types and forms of the singular points given in §6.3 and discussed further in Chapter 7 is novel.

6.1 Singular Contact Structures

The main purpose is to introduce the idea of singular contact structure as a means of applying the methods of contact topology outlined in Chapter 3 to cholesteric directors containing defects. Clearly, away from any defects the ideas of characteristic foliations, convex surfaces, and the general machinery of contact topology can be applied as usual, and consequently the primary questions concern the local structure around the singular points, and also the properties of characteristic foliations

on surfaces that intersect singular points. Not so relevant from the point of view of cholesterics, but very important when considering applications to fluid dynamics, is the singular version of the Etnyre–Ghrist correspondence, which will be addressed below in later sections.

To begin, we define the primary objects of study.

Definition 6.1. A *singular plane field* is a choice, for each $p \in M$, of a subspace $\xi_p \subset T_pM$, such that the choice depends smoothly on $p \in M$ and such that the codimension of ξ_p is 1, except at finitely many points $\Sigma \subset M$, the *singularities*, where the codimension is 0.

This is a particular case of a *Stefan–Sussmann distribution* [Ste74; Sus73], where we have restricted the set of singularities so that it only consists of finitely many points. To deal with disclination lines in cholesterics we need to broaden this definition slightly, but we will hold off on doing this for now and return to the line singularities in Chapter 8.

Clearly, a singular plane field ξ with singularity set Σ corresponds to the kernel of a 1-form η with the property that $\eta_p = 0$ if and only if $p \in \Sigma$.

Definition 6.2. A 1-form η is a *singular contact form* if and only if for all $q \notin \Sigma$, $(\eta \wedge d\eta)_q \neq 0$. The singular plane field defined by a singular contact form is a *singular contact structure*. The singular contact structure is positive (or left-handed) if $\eta \wedge d\eta \geq 0$ with respect to the orientation on M, and negative (right-handed) if $\eta \wedge d\eta \leq 0$. A singular plane field is a *singular foliation* if it is defined by η with $\eta \wedge d\eta = 0$.

To avoid confusion, when I use the term 'plane field' I will always mean in the familiar sense, and when I use the term 'singular plane field' I will always mean that there is at least one singularity. The same applies to the terms 'singular contact structure,' 'singular foliation,' and 'singular Beltrami field.'

Although we do not have a unique Reeb field in the singular case, on the complement of the singular points the kernel of $d\eta$ is still 1-dimensional.

Definition 6.3. A vector field R is *Reeb-like* for a singular contact form η if $\iota_R d\eta = 0$ and $\eta(R) \geq 0$, with equality only at the singular points of η.

Any pair of Reeb-like fields are colinear, and their singular points of Reeb-like fields always agree with the singularities of the contact form.

The Etnyre–Ghrist correspondence follows from the existence of metrics compatible (or weakly compatible) with the contact form, see §3.11. In the singular case

any version of this correspondence will follow from similar considerations. As in the nonsingular case, the Etnyre–Ghrist correspondence for the singular case is essentially equivalent to the existence of a 'compatible metrics.'

Definition 6.4. A Riemannian metric g is *compatible* with a singular contact form η if $\star_g \eta = d\eta$.

Discussions of the properties and existence of these metrics are deferred to §6.2.

The tight/overtwisted dichotomy is central to the study of contact structures. We adapt the definition to the singular case: call a singular contact structure on M with singular set Σ overtwisted if the contact structure on $M - \Sigma$ obtained by removing all singular points is overtwisted. However, this dichotomy is not actually relevant for singular contact structures with point singularities, as the following proposition shows.

Proposition 6.1. *A singular contact structure ξ with a singularity of nonzero index is always overtwisted.*

Proof. Let S be a sphere surrounding a singularity of index $k \neq 0$. Close to S, ξ is contact, and we can consider the value of Euler class $e(\xi)$ on S. Since S contains a singularity we must have $e(\xi)[S] = 2k$. However, the Bennequin inequalities (Theorem 3.12) for contact structures imply that ξ is tight in a neighbourhood of S if and only if $e(\xi)[S] = 0$ [Gei08]. Therefore, ξ must be overtwisted. □

Singularities of index 0 in a singular contact form have tight neighbourhoods. These singularities are removable. A perturbation can remove the singular point and leave a tight neighbourhood, or split the index 0 singular point into multiple singularities of nonzero index, resulting in an overtwisted singular contact form. This suggests an alternative perspective on the Lutz twist, where it occurs through a homotopy through singular contact structures rather than by a surgery—I will come back to this idea in §6.4.3 below.

The final tool we will need is a theory of characteristic foliations induced by singular contact structures. Away from any singular points all the usual results about characteristic foliations and convex surface theory apply: given a generic surface S that does not intersect a singular point of a singular contact structure, Theorem 3.2 provides the only constraint on the singular points of the characteristic foliation induced on S. When S intersects a singular point of ξ we still have a characteristic foliation, defined in the same manner, which will have singularities both in places where ξ is tangent to S and also at places where ξ is singular; only at the latter can novel behaviour occur. Fix a Morse–Smale vector field X on an

orientable surface S with singularities at finitely many points Σ. We can partition $\Sigma = \Sigma^0 \cup \Sigma^1$, where Σ^1 consists of those singular points of X for which the divergence does not vanish (which is independent of the choice of area form) and Σ^0 consists of the points where the divergence vanishes for some area form. If X is to be the characteristic foliation induced on S by a contact structure, then Σ^0 must be empty. In a singular contact structure this is not the case, as the following proposition shows.

Proposition 6.2. *There is a singular contact form η on $S \times [-1, 1]$ inducing a characteristic foliation directed by X on $S \times 0$ and such that the singularities of η occur exactly at the points of Σ^0 on $S \times 0$.*

Proof. We adapt the proof of Theorem 3.2. Let z denote the coordinate on $[-1, 1]$. We can construct an area form Ω on X for which the divergence of X vanishes at each point of Σ^0. Define $\beta = \iota_X \Omega$, so that $d\beta = \mathrm{div}_\Omega X \Omega$. As S is orientable there is a 1-form γ such that $\beta \wedge \gamma \geq 0$, with equality only when $X = 0$. Define Y by $\gamma = \iota_Y \Omega$. As X is Morse–Smale we can choose Y so that its divergence is nonzero on Σ^0.

Define a family of vector fields by $X_z = X - zY$ and a family of functions by $u_z = \mathrm{div}_\Omega X_z$, and then set $\beta_z = \beta + z(du_z - \gamma)$. We claim that $\eta = \beta_z + u_z dz$ is the desired singular contact form. To see this, first observe that the singularities only occur on $S^0 \times 0$, as required. Then we compute that

$$(\eta \wedge d\eta)|_{z=0} = (u_0^2 \Omega + \beta \wedge \gamma) \wedge dz \geq 0, \tag{6.1}$$

with equality at the points where both β and u_0 vanish. It follows that, in a neighbourhood of $S \times 0$, $\eta \wedge d\eta = 0$ only at the points Σ^0. At such points η itself vanishes, so these are the singularties of η. It follows that η is a positive singular contact form. □

Consequently it is possible to distinguish defect points from points where the singular plane field is nonsingular but tangent to the surface. Going back to the classification results of Zhitomirskiĭ, described in §3.7, we see that the same behaviour (vanishing of the divergence in the characteristic foliation) occurs at the points on the boundary between regions of different handedness. It is therefore impossible to tell from the characteristic foliation alone whether we are at a singular point of a singular contact structure, or at a point where the handedness of a singular plane field reverses. This suggests a connection between defects and regions of reversed handedness in cholesterics.

6.2 Generic Singularities

Now I turn to discussion of the types of singularity that can occur in a singular contact form. We will only consider the local structure close to the singular point, and hence reduce to the study of germs. A *germ* of a map at a point p in a manifold M is an equivalence class of maps, where two maps f, h are considered equivalent if there exists an open neighbourhood U of p such that $f|_U = h|_U$. This notion extends to germs of functions, vector fields, differential forms, etc. Thus, when dealing with germs we may assume we are working in a small neighbourhood of the origin in $\mathbb{R}^3$ and that the singular point is at the origin. To simplify matters further, we will assume all germs are analytic, that is, the Taylor series of the germ exists and converges at the singular point.

For germs of analytic functions (vector fields, differenital forms) f we define the k-jet $j^k f$, the germ of a polynomial function (vector field, differential form) obtained by truncating the Taylor series of f at the kth order terms. A generic germ of a 1-form will have linear terms in its Taylor series, and hence a nonvanishing first jet. Cholesteric liquid crystals exhibit singularities that cannot be described by a generic singular point [PČM17; Pos18c], so in order to fully describe the experimentally-realised textures we will have to study nongeneric singularities as well. We will however defer a discussion of the general case to §6.3, and consider only the generic case in this section, developing intuition that we may then apply to the general case.

Let η be a germ at the origin of a singular contact form. The linear part of η can be described purely by a matrix $A = [a_{ij}]$. Write $\omega = \sum_{ij} a_{ij} x_j dx_i$ for $j^1\eta$ in coordinates x_1, x_2, x_3. By making a change of coordinates we can put A into its Jordan normal form, which leaves us with three cases, depending on whether there are one, two, or three Jordan blocks in the Jordan normal form:

$$\begin{aligned}
\omega_1 &= (ax_1 + x_2)dx_1 + (ax_2 + x_3)dx_2 + ax_3dx_3, \\
\omega_2 &= (ax_1 + x_2)dx_1 + ax_2dx_2 + bx_3dx_3, \\
\omega_3 &= ax_1dx_1 + bx_2dx_2 + cx_3dx_3,
\end{aligned} \tag{6.2}$$

where a, b, c are nonzero real numbers. In the third case we can assume, by rescaling the coordinates x_j, that each constant is ± 1. We compute that $\omega_3 \wedge d\omega_3$ vanishes identically, while $\omega_1 \wedge d\omega_1$ and $\omega_2 \wedge d\omega_2$ both change sign over a surface containing the singularity.

We would like to know if the 1-jet $j^1\eta$ determines whether η can be singular contact. We may consider the jets of $\eta \wedge d\eta$. Fixing a volume form $\mu = dx \wedge dy \wedge dz$ in some coordinate system, we can write $\eta \wedge d\eta = f\mu$ for a function f that must be

nonnegative and vanish only at the origin for η to be singular contact. Since η itself vanishes at the origin f does as well, and consequently it cannot have a constant part. If f has nonvanishing 1-jet $j^1 f$, then it necessarily changes sign on some surface that intersects the origin, and hence η would not be singular contact. Notice we have $(j^1 f)\mu = (j^1\eta) \wedge d(j^1\eta)$. This observation then constrains the possible form of the 1-jet of η. Let us make the following definition.

Definition 6.5. A germ of a linear 1-form ω with singularity at the origin is called *chiral* if there exists a germ of a 1-form ν with $j^1\nu = 0$ and $\eta = \omega + t\nu$ is a singular contact structure for every $t > 0$.

The discussion above then proves the following proposition.

Proposition 6.3. *In order for ω to be chiral, it is necessary that $\omega \wedge d\omega = 0$, and indeed there are coordinates so that $\omega = d\phi$ for $\phi = \pm x^2 \pm y^2 \pm z^2$ a Morse function.*

Thus we conclude that the structure around a generic singular point in a singular contact structure is determined entirely by a Morse function ϕ. Such a Morse function ϕ is determined in turn by its Morse index. It is then straightforward to obtain necessary and sufficient conditions on the Morse index for $d\phi$ to be chiral.

Proposition 6.4. *A germ of a singular contact form at a Morse singularity may have Morse index 1 or 2, but not 0 or 3.*

Proof. To illustrate that the Morse index can be either 1 or 2, it suffices to supply an example. The germ of a 1-form

$$\eta = (x + tyz)dx + (y - txz)dy - 2zdz, \tag{6.3}$$

is a positive singular contact form with Morse index 1 for any constant $t > 0$, while $-\eta$ is an example with Morse index 2.

Suppose for a contradiction that η has a singularity of Morse index 0 or 3. Then, close to the singular point, there is a sphere inside a contact structure to which the Reeb field is transverse. But Theorem 3.5 implies this cannot occur. □

The second part of this proposition also follows from a theorem of Eliashberg & Thurston [ET91], which says that one cannot perturb a foliation into a contact structure in the neighbourhood of a spherical leaf.

We can also construct singular contact structures with Morse singularities that have a Beltrami Reeb-like field. For example, for Morse index 1,

$$\alpha = (x\cos y + z\sin y)dx + (y\cos x - z\sin x)dy + (-z(\cos x + \cos y) + x\sin y - y\sin x)dz \tag{6.4}$$

This is constructed using the approach in Theorem 6.4 below, which will be discussed in more detail in the next section. The vector field R dual to α in the Euclidean metric on $\mathbb{R}^3$ is Reeb-like for α and satisfies $\nabla \times R = R$, and is therefore Beltrami. More generally, singular contact forms with only Morse singularities obey an analogue of the Etnyre–Ghrist correspondence theorem.

Theorem 6.1. *(Etnyre–Ghrist Correspondence for Generic Singular Contact Forms) Suppose that η is a singular contact form on a closed 3-manifold M with only Morse singularities. Then there exists a Riemmanian metric g such that $\star_g \eta = d\eta$, and furthermore the vector field R defined by $\eta = \iota_R g$ is Reeb-like and satisfies curl $R = R$ with respect to g.*

Proof. Let p_j, $j = 1, \ldots, n$, be the singular points of η. Any two germs of 1-forms α_1, α_2 with Morse singularities of the same index are related by a germ of a diffeomorphism. Consequently, around each p_j we can find an open ball U_j and a diffeomorphism h_j of U_j that maps p_j to itself, such that the pullback of $\eta|_{U_j}$ along h_j is either equal to the 1-form α of Eq. (6.4), or to $-\alpha$. The Euclidean metric on U_j has the desired properties for α, and its pullback g_j along h_j^{-1} has the desired properties for η.

Let U_j' be a smaller closed ball within U_j, and set $M' = M - \bigcup_j U_j'$. We can choose a set of smooth, nonnegative functions $h_j : M \to \mathbb{R}$ with $h|_{U_j'} = 1$ and $h|_{M-U_j} = 0$. Set $g_j' = h_j g_j$. By Theorem 3.17 there exists a metric g_{n+1} on M' that is compatible with η. Let $h_{n+1} : M \to \mathbb{R}$ be a smooth nonnegative function equal to 1 on M' and 0 on each U_j'.

Choose a partition of unity f_j subordinate to the open cover $U_1, \ldots, U_n, U_{n+1} := M'$ of M. Define a Riemannian metric by

$$g' = \sum_j f_j g_j'. \tag{6.5}$$

Then by construction $\star_{g'} \eta = f d\eta$, where $f > 0$ is some function. To obtain the desired metric, we rescale $g = f^{-2} g'$, which gives the desired $\star_g \eta = d\eta$; this is easily checked, see Lemma 9.21 of Ref. [Far03]. Passing to the dual vector field R defined by $\eta = \iota_R g$ yields the second claim. □

6.3 General Singularities

6.3.1 Singularity Theory

In this section I will recap some ideas from singularity theory, drawing primarily from the work of Arnold [AGZV85; AGLV88]. Consider germs of maps $X : \mathbb{R}^n \to \mathbb{R}^m$ that have an isolated zero at the origin. Two such germs X, Y are considered equivalent, $X \sim Y$, if there exist germs of diffeomorphisms $f : \mathbb{R}^m \to \mathbb{R}^m, h : \mathbb{R}^n \to \mathbb{R}^n$ that map the origin to itself and are such that $X = f \circ Y \circ h^{-1}$. A *singularity* is an equivalence class of germs of maps $X : \mathbb{R}^n \to \mathbb{R}^m$ with isolated zero at the origin. If X is a vector field on an n-manifold M with an isolated zero at a point p, we may take a small open neighbourhood U of p and identify $X|_U$ with some singularity. From now on, we restrict to the case of $n = m = 3$. We can identify these maps $X : \mathbb{R}^3 \to \mathbb{R}^3$ with vector fields, and then use the Euclidean metric to identify vector fields with 1-forms.

We will only consider real analytic singularities. Each component of the map X is then a formal power series in the ring $\mathbb{R}[[x, y, z]]$. Let $\mathfrak{m}$ be the maximum ideal in this ring, generated by all power series without constant part. The components X_1, X_2, X_3 of the map X in some coordinate system generate an ideal I_X in this ring—the ideal is independent of the choice of coordinates. We set $Q_X := \mathbb{R}[[x, y, z]]/I_X$, the *local algebra* of the singularity, which is an algebra over $\mathbb{R}$. Let μ be the dimension of Q_f, i.e., the size of a basis for Q_f. By Tougeron's Theorem [AGZV85] a map germ is *finitely determined*, equivalent to its k-jet for some k, if $\mu < \infty$. The jet $j^k X$ with the smallest k such that X is equivalent to $j^k X$ is called the *sufficient jet*.

In the next theorem I summarise some results from §9 of Ref. [AGZV85].

Theorem 6.2. *The equivalence class of a map germ X is determined by its ideal I_X. If $Y \in I_f$[1], then $X + Y$ is equivalent to X, as they generate the same ideal. If $Q \subset \mathbb{R}[[x_1, \ldots x_n]]$ is a finitely-generated algebra, then it is the local algebra of some map germ X.*

Therefore, adding polynomial maps that belong to I_X does not change the equivalence class of the map germ X. Adding terms from the local algebra Q_X may change the equivalence class of the map. Let f_j be a basis for the local algebra. The map germ $X' = X + \sum_{ij} a_{ij} f_j \mathbf{e}_{x_j}$, for constants a_{ij} is called an *unfolding* of the singularity, and may decompose the singular point into singularities of lower multiplicity.

[1] By which I mean, that each component of the map Y is a polynomial that belongs to the ideal.

We can also apply these ideas to functions $\phi : \mathbb{R}^3 \to \mathbb{R}$. These generate an ideal I_ϕ using the components of the map $\nabla\phi$, which completely classifies the function germ [AGZV85; AGLV88]. There are three invariants of such germs: the multiplicity μ, which is the dimension of the local algebra Q_ϕ, and also determines the maximum number of Morse singularities that the germ breaks apart into under a generic deformation[2]; the modality m, the minimal number of parameters that appear in a normal form for the germ; and the codimension c of the space of germs equivalent to ϕ in the space of all singularity germs. These are related by the formula [AGLV88]

$$\mu = m + c + 1. \tag{6.6}$$

A full tabulation of germs of modality at most 2 is given in Refs. [AGZV85; AGLV88].

6.3.2 Local Structure of Singularities

We wish to understand when a singularity can occur in a singular contact form. We will only consider real analytic singularities of finite multiplicity, which can be reduced via a coordinate transformation to a polynomial 1-form. To determine when a particular germ can occur in a singular contact structure, we will consider the possibily of perturbing a particular form for the germ into a germ of a singular contact form.

Definition 6.6. A germ of a singular polynomial 1-form ω is *chiral* if there exists a germ $\nu \in I_\omega$ such that $\eta = \omega + t\nu$ is a germ of a singular contact form for all t sufficiently small. A chiral ω is additionally called *Beltrami* if there exists a Riemannian metric g such that $\star_g \eta = d\eta$.

The requirement that the perturbation ν belongs to ideal generated by ω ensures, by Theorem 6.2, that η is equivalent to ω, and hence that the type of singularity is preserved by the perturbation.

I have already demonstrated that when ω is linear it can be chiral if and only if it is equivalent after a coordinate reparameterisation to $d\phi$, where ϕ is a Morse function or Morse index 1 or 2. These are additionally Beltrami, so that the phenomenon of 1-forms that are chiral but not Beltrami can occur only for degenerate singularities.

An important part of the classification of the linear chiral 1-forms was the reduction to the case of a closed 1-form. More generally,

[2] μ is the exact number for a complex singularity, but for a real singularity it is possible to perturb the germ in such a way as to produce fewer than μ, as a polynomial of degree d has exactly d complex roots but may have fewer than d real roots.

Proposition 6.5. *If ω is chiral, then $\omega \wedge d\omega \geq 0$.*

Proof. Since ω is chiral, there exists $\nu \in I_\omega$ such that $\eta = \omega + t\nu$ is a singular contact form for $t > 0$. Then we must have

$$\eta \wedge d\eta = \omega \wedge d\omega + t(\omega \wedge d\nu + \nu \wedge d\omega) + t^2 \nu \wedge d\nu. \tag{6.7}$$

Since this must hold for all $t > 0$ we can make the latter two terms as small as we like. Consequently, we see that if $\omega \wedge d\omega$ were to change sign on the some surface containing the origin, η would not be singular contact, and similarly if it were everywhere negative. Therefore, we must have $\omega \wedge d\omega \geq 0$. □

I conjecture that, for any singular contact form η, we must have $\eta \sim \omega$ for $\omega \wedge d\omega = 0$, but have been unable to prove this. For holomorphic 1-forms $\omega \in \Omega^1(\mathbb{C}^3)$, $\omega \wedge d\omega = 0$ implies that ω is equivalent (diffeomorphic) to a 1-form of the form $\psi d\phi$, for functions $\phi, \psi \neq 0$; this is Malgrange's Singular Frobenius Theorem [Mal76]. I conjecture that this is also the case for real analytic forms, but do not have a reference.

I will proceed as if these conjectures were true, and focus only on the case where ω is equivalent to a closed, and therefore exact, germ $d\phi$. I abuse notation slightly and call a function ϕ chiral (resp. Beltrami) if $d\phi$ is. Our problem then is to determine which germs of functions $\phi : \mathbb{R}^3 \to \mathbb{R}$ with an isolated singularity at the origin are chiral.

The topology of the level sets of a singularity ϕ of index k is easily determined. The leaves of the foliation of $\mathbb{R}^3$ defined by $d\phi$ are the level sets of ϕ. Call a leaf singular if it contains the singular point. Take a small $\epsilon > 0$ and consider a closed ball B of radius ϵ centred at the origin in $\mathbb{R}^3$. Let $0 < \delta \ll \epsilon$ be a regular value of ϕ, and let $L^\pm = \phi^{-1}(\pm\delta)$ be two nonsingular leaves of the foliation. Define $F^\pm := L^\pm \cap B$ to be the parts of these leaves that lie in the ball B. The sets $F^\pm$ are compact 2-manifolds, possibly with boundary. The index k of ϕ is related to the Euler characteristic of $F^\pm$ by $\chi(F^\pm) = 1 \pm k$ [Arn78].

Lemma 6.1. *If the level sets $L^\pm$ are compact, then $|k| = 1$, $F^{sgn(k)}$ is diffeomorphic to a sphere, while $F^{-sgn(k)}$ is empty. If they are not compact, then $F^{-sgn(k)}$ is diffeomorphic to the compact manifold obtained by removing $|k| + 1$ disks from S^2, while $F^{sgn(k)}$ consists of $|k| + 1$ disks.*

Proof. First suppose $k > 0$. Let $L_0 := \phi^{-1}(0)$ be the singular level set. It is a closed and connected subset of $\mathbb{R}^3$. If it is compact then all nearby level sets are compact, and vice-versa; thus it suffices to consider both $L^\pm$ compact or both noncompact.

If L_0 is not compact then it must be unbounded. It divides $\mathbb{R}^3$ into pieces. The 'outside' of L_0 consists of the level sets with $\phi < 0$, while the 'inside' consists of the level sets $\phi > 0$. Each level set on the outside of L_0 is also connected. Removing the singular leaf disconnects the set $\phi \leq 0$, and therefore we conclude that the leaf L^+ is not connected. If the singular leaf is compact it must be a single point, so the inside level sets are empty.

Suppose the level sets are compact and that δ is chosen small enough that L^+ does not intersect the boundary of $B(\epsilon)$. Then $F^+ = L^+$ is a compact 2-manifold without boundary, and $\chi(F^+) = 2 - 2g$, where g is the genus of F^+. Since $\chi(F^+) = 1 + k$, it follows that $g = (1 - k)/2$. The genus is always a non-negative integer, so we conclude that $k = 1$ and $g = 0$, so that F^+ is diffeomorphic to a sphere.

Now suppose $L^\pm$ are not compact. No matter which values of δ and ϵ we choose, the sets $L^\pm$ must intersect the sphere. This implies F^- is a connected, compact 2-manifold with boundary, diffeomorphic to a sphere with some number of disks removed, while F^+ is a disconnected, compact 2-manifold with boundary. By the classification of 2-manifolds we conclude that $\chi(F^-) = 2 - b$, where b is the number of boundary components. It follows that $b = k + 1$. F^+ is diffeomorphic to the part of the sphere that remains after removing F^-, consists of $k+1$ pieces, each diffeomorphic to a closed disk.

For $k < 0$, the outside is $\phi > 0$ and the inside $\phi < 0$, and the signs in the above argument change accordingly. We have $\chi(F^\pm) = 1 \mp |k|$. The argument for the compact sets is the same, and we find that we must have $k = -1$ and the level sets are again spheres. When the level sets are not compact, F^+ is a connected, compact 2-manifold with boundary, diffeomorphic to a sphere with some number of disks removed, while F^- is a disconnected, compact 2-manifold with boundary. Otherwise the same conclusions hold. □

Informally, the level sets of a singularity of index k are either spheres, or the singular level set is $|k|+1$ cones adjoined to the singular point, each filled with rounded cones and surrounded by connected surfaces. See Fig. 6.1.

6.3.3 Beltrami Singularities

Chandrasekhar & Kendall proved what is now a classical result about Beltrami fields: a solution to Helmholtz's equation on $\mathbb{R}^3$ can be used to construct a Beltrami field [CK57]. In particular, this applies to solutions to Laplace's equation, so that harmonic vector fields generate Beltrami fields. In this section we will see the

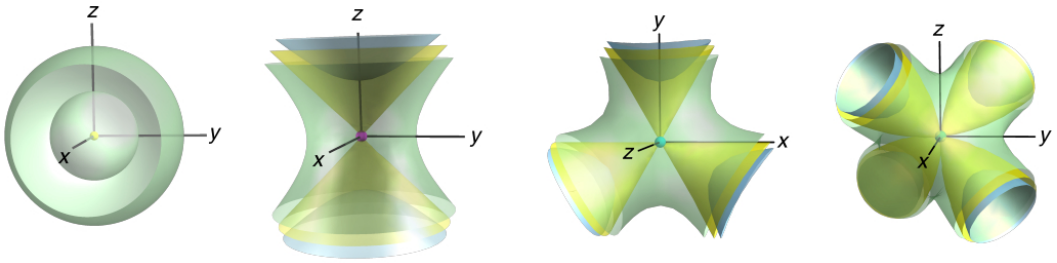

Figure 6.1: Level sets of singularities. From left to right: singularity of Morse index 0 and index +1, singularity of Morse index 1 and index −1, the singularity D_4^- with index −2, and the singularity $T_{4,4,4}$ with index −3 (the names of the singularities are those given in Arnold's classification [AGLV88]). All four of these singularities occur in experiments on cholesteric liquid crystal droplets [PČM17; PPČ+19], see Chapter 7 for more details.

relationship between harmonic functions and Beltrami singularities.

A 1-form α is called *intrinsically harmonic* if there exists a Riemannian metric g for which α is harmonic, $(d\delta + \delta d)\alpha = 0$. We will only consider the case where $\alpha = d\phi$, for which more can be said. In this case the property of being intrinsically harmonic is equivalent to a certain topological property of the leaves of the foliation by the level sets of ϕ.

Theorem 6.3. *(Calabi's Theorem [Cal69; Far03]) Let ω be a closed 1-form with isolated Morse singularities on a closed n-manifold. ω is intrinsically harmonic if and only if for every nonsingular point $p \in M$ there is a closed loop that is transverse to the foliation and passes through p.*

It is clear that being intrinsically harmonic is a property of the foliation and not of the choice of defining 1-form, and therefore is a property of a germ rather than any particular representative of that germ.

Given the result of Chandrasekhar & Kendall, it is natural to expect that intrinsically harmonic singularities are Beltrami—in fact these two statements are equivalent.

Theorem 6.4. *A singularity ϕ is Beltrami if and only if it is intrinsically harmonic. Moreover, if g is a germ of Riemannian metric for which ϕ is harmonic, then there exists a germ of singular contact form η with singularity described by ϕ such that $\star_g \eta = d\eta$, i.e. g is compatible with η.*

Proof. Firstly, suppose g is a germ of a Riemannian metric for which ϕ is harmonic. We may invoke the Hodge decomposition and choose a coclosed ν_1 such that $\star_g d\phi =$

$d\nu_1$. Since ν_1 is coclosed, there exists ν_2 such that $\star_g \nu_1 = d\nu_2$. Iterating this process, we obtain a family of 1-forms ν_j with $\star_g \nu_j = d\nu_{j+1}$. Now define a 1-form via a formal power series in a parameter t,

$$\eta = d\phi + \sum_{j=1}^{\infty} t^j \nu_j. \tag{6.8}$$

On our closed ball we can assume there is a constant bounding the components of the 1-form ν_j for each j; that we can choose a single constant independent of j follows from the relations between the ν_j. Then for t sufficiently small the sum must converge absolutely, and hence it converges, so η is well-defined. Then

$$d\eta = \sum_{j=1}^{\infty} t^j d\nu_j = t \star d\phi + t^2 \star d\nu_1 + t^3 \star d\nu_2 + \cdots = t \star_g \eta. \tag{6.9}$$

Recall that rescaling a Riemannian metric g by a positive constant λ rescales the norm by a factor of λ, the star operator by a factor of $\lambda^{-1/2}$, and the volume form by a factor of $\lambda^{3/2}$. Thus, $\star_{t^2 g}\eta = d\eta$, implying that η is singular contact and that ϕ is Beltrami.

Conversely, suppose that ϕ is Beltrami, so that there exists ν such that $\eta = d\phi + \nu$ is a germ of a singular contact form, and furthermore there exists a Riemannian metric g for which $\star_g \eta = d\eta$, i.e., $\star_g d\phi + t \star_g \nu = d\nu$. We may write $\eta = d\psi + \delta\alpha + \gamma$ via the Hodge decomposition theorem applied to g, where ψ is a function (possibly different from ϕ), α is a 2-form, and γ is a g-harmonic 1-form. Then $\nu = d(\psi - \phi) + \delta_\alpha + \gamma$, from which we conclude that $d \star_g \nu = d \star_g d\psi - d \star_g d\phi$. We also compute that $\star_g d\phi = (d\nu - \star_g \nu)$, from which we conclude that $d \star_g d\psi = 0$, so ψ is harmonic with respect to the Riemannian metric g.

Further, ψ and ϕ are equivalent as germs of functions: we must have $d\psi = d\phi + d\chi$ for $d\chi \in I_{d\phi}$, and then we apply Theorem 6.2. Since being intrinsically harmonic is a property of the germ and not its representatives, we conclude that ϕ is intrinsically harmonic as well. □

Corollary 6.4.1. *Being Beltrami is a property of the equivalence class of germs ϕ, not just a particular representative of that class.*

Applying the construction in Theorem 6.4 to the Morse singularities $\phi = \frac{1}{2}(x^2 + y^2) - z^2$ which are harmonic with respect to the Euclidean metric yields the singular contact forms 6.4. Applying it to a constant 1-form $Adx + Bdy + Cdz$ gives the

Arnold–Beltrami–Childress (ABC) 1-forms

$$\eta_{ABC} = (A\sin z + C\cos y)dx + (B\sin x + A\cos z)dy + (C\sin y + B\cos x)dz, \quad (6.10)$$

The dual (with respect to the Euclidean metric) vector fields, the ABC fields, are important examples of Beltrami fields. We can reparameterise, and assume $A = 1, B, C \in [0, 1]$, and furthermore the vector field is nonsingular if and only if $B^2 + C^2 < 1$ [DFG+86].

Proposition 6.6. *The ABC 1-forms define tight (singular) contact structures when $B^2 + C^2 \leq 1$, and overtwisted singular contact structures when $B^2 + C^2 > 1$.*

Proof. That nonsingular ABC 1-forms, with $B^2 + C^2 < 1$, are tight was shown by Etynre & Ghrist [EG00a]. The argument is simple: every ABC 1-form is clearly homotopic through contact forms to the ABC 1-form with $B = C = 0$, which is the (tight) cholesteric ground state, and since tightness is a homotopy invariant they are tight as well. Proposition 6.1 implies the singular contact forms with singularities of nonzero index are overtwisted. These make up the $B^2 + C^2 > 1$ part of parameter space. The curve $B^2+C^2 = 1$ consists of singular contact forms with only removable singularities, which are also tight. □

Finally, we note that the Etnyre–Ghrist correspondence holds for singular contact structures with Beltrami singularities, almost by definition.

Theorem 6.5. *(Etnyre–Ghrist Correspondence for General Singular Contact Forms) Suppose that η is a singular contact form on a closed 3-manifold M with only Morse singularities. The following are equivalent:*

1. *Every singularity of η is a Beltrami singularity.*
2. *Then there exists a Riemmanian metric g such that $\star_g \eta = d\eta$, and furthermore the vector field R defined by $\eta = \iota_R g$ is Reeb-like and satisfies curl $R = R$ with respect to g.*

Proof. That (2) implies (1) is immediate from the definition of a Beltrami singularity. The prove that (1) implies (2) we can apply essentially the same argument used in Theorem 6.1, using Theorem 6.4 to supply the compatible metrics on open balls around the singular points. □

6.3.4 Chiral Singularities

Finally, we turn to the degenerate types of singularity that are chiral, but are not Beltrami. A simple example shows these exist.

Proposition 6.7. *The singularity D_4^- defined by the function $\phi = x^2y - y^3/3 + z^2/2$ is chiral, but not Beltrami*

Proof. Firstly we construct ν such that the germ $\eta = d\phi + t\nu$ is a germ of a singular contact form, demonstrating that ϕ is chiral. The perturbation is

$$\nu = (z(x^2 - y^2) - yz^3)dx + (xz^3 - 2xyz)dy. \tag{6.11}$$

We can check $\eta \wedge d\eta \leq 0$, so the singularity D_4^- is chiral.[3]

If ϕ were Beltrami, then there would be a Riemannian metric g for which $d \star_g d\phi = 0$. Write $g = g_0 + g'$, where $g_0 := j^0 g$ is the constant part and g' the higher order terms. Since g_0 is flat it is equivalent to the Euclidean metric, and we can find coordinates in which $\star_{g_0}$ is represented by the identity matrix. Then, by linearity

$$d \star_g d\psi = d \star_{g_0} d\phi + d \star_{g'} d\phi. \tag{6.12}$$

The first term on the right-hand side contains a nonzero constant term, as it is equal to the trace of the Hessian matrix of ϕ. The Hessian matrix has corank 2 and therefore has nonzero trace. The second term, $d \star_{g'} d\phi$, vanishes at the origin. Therefore $d \star_g d\psi$ does not vanish at the origin, a contradiction. □

Note that it is enough to check just one form of the singularity, as being Beltrami is property of an equivalence class and not a particular representative.

A singularity of index -2 in a Beltrami field can be produced using spherical harmonics; the simplest example using spherical harmonics yields a singularity equivalent to the germ U_{12} (in Arnold's notation [AGLV88]) which can be defined by a function germ $\phi = x^2y - y^3 + z^4 + axyz^2$, for a parameter $a \in \mathbb{R}$. This implies that the index -2 singularities of lowest multiplicity, *a priori* the most likely to occur, in fact cannot occur in Beltrami fields, and one is forced to have singularities of higher multiplicity and therefore more complicated structure. It also impacts on the possible unfoldings of the singularity.

The classification of chiral singularities follows from similar arguments to those used in Theorem 6.4. To prove this theorem, we need a singular version of Lemma 3.9. Fix a Riemannian metric g on a manifold M with star operator $\star_g$ and volume form μ. Given an orthonormal basis e^j for the space of 1-forms $\Omega^1 M$, we have a basis $\star_g e^j$ for the space of 2-forms $\Omega^2 M$. If we then have a smooth linear map $s : T^*M \to T^*M$, we can express this as a matrix $S = [s_{ij}]$ with respect to the

[3] It can in fact be realised experimentally in a cholesteric droplet, as we will see in the next chapter.

orthonormal basis e^j, and it induces a linear map $\hat{s} : \Omega^1 M \to \Omega^2 M$ by defining the action on basis covectors to be $\hat{s}e^i = \sum_j s_{ij} \star_g e^j$. If the matrix S is nonsingular, symmetric, and positive definite then we can construct a Riemannian metric h such that the $\star$ operator $\star_h$ agrees with $\hat{s}$ when acting on 1-forms. Otherwise, $\hat{s}$ is a generalisation of the Hodge star operator that is, in a sense, 'singular.'

Lemma 6.2. *Let α be a 1-form and β a 2-form on a compact 3-manifold M, with mutual zero set Σ consisting of finitely many isolated points. Suppose that $(\alpha \wedge \beta)_p \geq 0$ for each $p \in M$, vanishing if and only if $p \in \Sigma$. There exists a smooth, symmetric, linear map $\hat{s} : \Omega^1 M \to \Omega^2 M$ that may only vanish on Σ, is positive definite otherwise, and is such that $\hat{s}\alpha = \beta$.*

Proof. As $\beta|_{\ker \alpha} \geq 0$, vanishing only on Σ, the kernel of β is 1-dimensional, spanned by some vector field Y vanishing on Σ and such that $\alpha(Y) \geq 0$, with equality only at the points of Σ. We can find a Riemannian metric h such that α is dual to Y in this metric. Then β defines a skew-symmetric bilinear form on the kernel of α which is positive definite on the complement of Σ. Let A be the matrix defining this form with respect to some local coordinate system on M.

A nonvanishing skew-symmetric matrix can be uniquely polarised, $A = GF$, where G is positive-definite and symmetric and F is orthogonal. When the skew-symmetric matrix is allowed to be singular, we may still define a (not necessarily unique) polar decomposition by a limit. Let A_k be a sequence of nonsingular skew-symmetric matrices tending to A. Their polar decompositions $A_k = G_k F_k$ exist. As $\mathcal{O}(2)$ is compact, there is an $F \in O(2)$ and a subsequence F_{k_j} such that $F_{k_j} \to F$ as $j \to \infty$. Then $A = F\sqrt{A^T A}$.

Take $G = \sqrt{A^T A}$. This defines a smooth linear map on the kernel of α which is symmetric and positive definite away from Σ, where it may vanish. Extend it to all of M by taking it to agree with these matrix for $\star_h$ in the direction Y. This gives a smooth linear map defined by symmetric, positive semi-definite matrix S, which we use to define the linear map $\hat{s}$. By design, $\hat{s}$ is symmetric, positive definite away from Σ, and $\hat{s}\alpha = \beta$. □

Note that we do not know for certain that $\hat{s}$ will fail to be positive definite at the points of Σ, only that this may be the case. For example, if we take $\alpha = cdx+ydy-zdz$ and $\beta = xdy\wedge dz+ydz\wedge dx-zdx\wedge dy$, then we can take $\hat{s}$ to agree with the star operator of the Euclidean metric. If we take $\beta = xdy\wedge dz+y^3 dz\wedge dx-zdx\wedge dy$ instead, then the desired map $\hat{s}$ exists but cannot be positive definite.

Theorem 6.6. *A singularity ϕ is chiral if and only if there is a germ of a symmetric*

map $\hat{s} : \Omega^1\mathbb{R}^3 \to \Omega^2\mathbb{R}^3$ *that is positive definite except at the origin, for which* $d\hat{s}d\phi = 0$.

Proof. Note that we can use $\hat{s}$ to define a 'norm' on germs of 1-forms by $|\alpha|^2 dx \wedge dy \wedge dz = \alpha \wedge \hat{s}\alpha$, and that $|\alpha|$ is nonnegative, and positive away from the origin and any points where $\alpha = 0$.

Suppose first that $d\hat{s}d\phi = 0$. Then $\hat{s}d\phi = d\nu$ for some germ of a 1-form ν. Take $\eta = d\phi + t\nu$. Then

$$\left.\frac{\partial(\eta_t \wedge d\eta_t)}{\partial t}\right|_{t=0} = d\phi \wedge d\nu = |d\phi|^2 dx \wedge dy \wedge dz \geq 0, \tag{6.13}$$

with equality at the origin. Then η is a singular contact form for $t > 0$ sufficiently small, i.e., $d\phi$ is chiral.

For the other direction we note that chirality implies that there exists some ν for which $d\phi \wedge d\nu \geq 0$, and then apply Lemma 6.2 to $\alpha = d\phi, \beta = d\nu$ to obtain the desired map $\hat{s}$. □

In general, singularities of corank 2 may be chiral but not Beltrami. These include the families $D_k^{\pm}$ and E_k of simple singularities. We might reasonably refer to germs satisfying the condition $d\hat{s}d\phi = 0$ as *quasiharmonic* and attempt to classify them in the same way that harmonic germs are classified by Calabi's theorem. However, in this case a topological definition is impossible, as the topology of the leaves of D_4^- is identical to that of the harmonic U_{12}. More work is needed to understand exactly the conditions that make a function germ quasiharmonic, and whether the chiral corank 2 germs are an exhaustive list.

6.4 Global Properties of Singular Contact Structures

Now we turn to global features of singular contact structures, extending those global results already proved in §6.1. The main results are a global existence theorem for singular contact structures on closed manifolds, and also on manifolds with boundary where the Reeb-like fields are constrained by a particular boundary condition. In the latter case, when the boundary condition is tangential there is no obstruction to existence, and when the boundary condition is transversal the only constraint is the one I have highlighted previously, that the boundary cannot have spherical components. Finally, I define a version of the Lutz twist procedure that is effected by a homotopy through singular contact structures rather than a surgery. This homotopy is something that can happen in a real material, and gives some idea how

homotopy invariants of a cholesteric director might be changed during the relaxation of the texture.

6.4.1 Existence Theorems

In this section we demonstrate that every singular plane field with chiral singularities is homotopic to a singular contact structure, showing that singular contact structures exist on every 3-manifold and also that there are no global constraints on the structure of the singular set other than the Poincaré–Hopf theorem. Before turning to this more general result, notice that Theorem 6.4 gives us a global perturbation result for foliations, at least when M has vanishing first homology.

Proposition 6.8. *Let M be a 3-manifold (not assumed to be closed) with $H_1(M) = 0$ and let $\phi : M \to \mathbb{R}$ be a smooth, intrinsically harmonic function such that $d\phi$ has finitely many isolated zeros at the points of a set Σ. Then $d\phi$ can be linearly perturbed into a singular contact form $\eta = d\phi + t\nu$.*

More generally, we have the following.

Theorem 6.7. *(Lutz–Martinet Theorem for Singular Contact Structures) A singular plane field ξ with chiral singularities is homotopic to a singular contact structure via a homotopy that fixes the singular points.*

Proof. Firstly, choose an open neighbourhood U_j of each each singular point p_j. By the fact that the singularities are chiral, we can perturb ξ to a new singular plane field ξ_1 that is contact on U_j. Let $V_j \subset U_j$ be a smaller open neighbourhood and set $M' = M - \cup_j V_j$. Then ξ_1 is a plane field on M' that is contact near the boundary. We need to show it can be homotoped rel. boundary to a contact structure. Let W denote the interior of M'. This is an open manifold with only S^2, and hence the classification of contact structures with some particular behaviour at infinity (as specified by the characteristic foliation induced on $\partial M'$ by ξ_1) is the same as for compact manifolds [Eli93; Tri04]—in particular, there exists at least one contact structure that agrees with ξ_1 at infinity, which gives us a contact structure on M' that agrees with the plane field ξ_1 near the boundary. This may not lie in the same homotopy class as ξ_1, but we can modify the homotopy class using Lutz twists until they agree. Thus ξ_1 is homotopic rel. boundary to a contact structure, which implies that ξ is homotopic to a singular contact structure. □

For applications it would be useful to have a more constructive proof in line with Proposition 6.8. The geometric heat flow method of proving the existence of contact

structures on closed 3-manifolds developed by Altschuler [Alt95] may be useful in this regard. In Altschuler's approach, one begins with a confoliation and regards the contact part as being 'hot'. A heat diffusion equation is then used to diffuse the heat along the leaves of the foliated part. As long as every point in space can be connected to the hot region by a finite length path tangent to the leaves of the foliated part, then the entire manifold will instantaneously become hot: the confoliation will have become a contact structure.

Suppose we have a foliation defined by a closed intricially harmonic 1-form with isolated singularities, which will necessarily be Beltrami singularities by Theorem 6.4. Then, by Calabi's theorem, there exists a finite link L that intersects every leaf of the foliation. We can perturb the foliation into a confoliation in a neighbourhood of L using the method developed in §5 of [Alt95]. As L passes through every leaf of the foliation, this 'hot region' is connected to any 'cold' point by a path tangent to some leaf of the foliated part. Then turning on the heat equation will diffuse the heat and instantly make the plane field contact at every point except for the singularities.

6.4.2 Boundary Conditions

Next we turn to the study of singular contact structures on manifolds with boundary and an appropriate boundary condition. Given a singular contact structure ξ with singular contact form η, there are two boundary conditions that are relevant for experiments on liquid crystals:

1. Normal anchoring: the Reeb-like fields of η are transverse to ∂M,
2. Planar anchoring: the Reeb-like fields of η are tangent to ∂M.

Normal anchoring is the constraint used in the experiments we will study in Chapter 7. Note further that both these conditions are independent of the choice of Reeb-like field, but not of the choice of singular contact form: consequently, in this section we again focus on the particular 1-forms defining the singular contact structure and not the singular contact structure itself.

First we treat the case of normal anchoring, when the Reeb-like fields are transverse to the boundary. Here, we may apply results of Eliashberg & Thurston [ET91].

Theorem 6.8. *Let M be a compact 3-manifold with boundary ∂M. There is a singular contact form η on M whose Reeb-fields are transverse to the boundary if and only if ∂M does not contact a spherical component.*

Proof. Eliashberg & Thurston's Reeb Stability Theorem for Confoliations (Theorem 3.5) establishes that a Reeb-like field cannot be transverse to a sphere, and hence we can immediately deduce that the desired singular contact form cannot exist if M has a spherical boundary component.

To show that the absence of a spherical boundary component is in fact sufficient, we again apply results from *Confoliations*, this time Proposition 1.3.13 [ET91]. This proposition ensures that for a surface S_g of genus $g > 0$ we can find a plane field on $S_g \times (-1, 0]$ that is tangent to the surface $S_g \times 0$ and contact everywhere else. Plainly a small perturbation of such a plane field results in a contact structure with the property that the Reeb field of any contact form defining it is transverse to $S_g \times 0$.

We construct the desired singular contact structure on M in the following manner. Firstly, we construct contact structures in a neighbourhood of each boundary component using the results of Eliashberg & Thurston. We may extend this contact structure as a singular plane field ξ over all of M, ensuring that each singularity of this plane field is of Morse type with Morse index 1 or 2. Finally, we apply Theorem 6.7 to homotope ξ into a singular contact structure, keeping it fixed near to the boundary. □

To understand planar anchoring, we first need to examine the additional properties of the characteristic foliation induced on a surface S that arise when a singular contact form has Reeb-like fields tangent to S.

Lemma 6.3. *Let X_0 be a vector field on an oriented surface S with finitely-many singular points Σ, and suppose that X_0 preserves some area form Ω on X. If a singular contact form η on $S \times [-1, 1]$ induces the characteristic foliation directed by X_0, then its Reeb-like fields are tangent to $S \times 0$. Conversly, if η is a singular contact form with Reeb field tangent to $S \times 0$, then the vector field directing its characteristic foliation preserves an area form.*

Proof. Fix an area form Ω for which $\mathrm{div}_\Omega(X_0) = 0$ and let η be a singular contact form with Reeb-like field R that induces the characteristic foliation directed by X on S. In a neighbourhood of S that is diffeomorphic to $S \times [-1, 1]$ we can write $\eta = \beta_z + u_z dz$, where β_z is a family of 1-forms on S with $\beta_0 = \iota_X \Omega$ and $u_z : S \to \mathbb{R}$ a family of functions. We can similarly write $R = Y_z + v_z \partial_z$, where Y_z is a vector field tangent to $S \times z$ for each z, and $v_z : S \to \mathbb{R}$ is a family of functions.

The condition that the Reeb-like fields be tangent to $S \times 0$ is $v_0 = 0$. To prove the first claim, we must show that $\mathrm{div}_\Omega(X_0) = 0$ implies this condition holds.

We compute that

$$d\eta = \mathrm{div}_\Omega(X_z)\Omega + (du_z - \dot{\beta}_z) \wedge dz, \tag{6.14}$$

where X_z directs the characteristic foliation on $S \times z$. The Reeb-like field satisfies $\iota_R d\eta = 0$, that is

$$0 = \mathrm{div}_\Omega(X_z)\iota_{Y_z}\Omega + v_z(\dot{\beta}_z - du_z) + (du(R) - \dot{\beta}_z(R))dz. \tag{6.15}$$

From this, we conclude that $(du(R) - \dot{\beta}_z(R)) = 0$ and also $\mathrm{div}_\Omega(X_z)\iota_{Y_z}\Omega = v_z(du_z - \dot{\beta}_z)$. Restrict to the surface $z = 0$. Then $\mathrm{div}_\Omega(X_0)$ vanishes by assumption, and hence

$$v_0(du_0 - \dot{\beta}_0) = 0. \tag{6.16}$$

I claim that this implies $v_0 = 0$. At any point where this is not the case, we must have $du_0 - \dot{\beta}_0 = 0$. The singular contact condition is

$$\eta \wedge d\eta|_{z=0} = \beta_0 \wedge (du_0 - \dot{\beta}_0) \geq 0, \tag{6.17}$$

with equality only when $\eta = 0$. This equation implies that we cannot possiblity have $du_0 - \dot{\beta}_0 = 0$ except at isolated points, and hence we conclude that $v_0 = 0$ as required.

For the converse statement, we note that $v_0 = 0$ implies that $\mathrm{div}_\Omega(X_0)\iota_{Y_0}\Omega = 0$. Since Y_0, the Reeb field along the surface $S \times 0$, is nonvanishing except at isolated points, we must have $\mathrm{div}_\Omega(X_0)$, and hence the characteristic foliation induced on $S \times 0$ is directed by a vector field (namely X_0) which preserves an area form. □

It follows that there are no obstructions to having Reeb-like fields tangent to the boundary.

Theorem 6.9. *Let M be any compact 3-manifold with boundary. There exists a singular contact form η whose Reeb-like fields are tangent to the boundary.*

Proof. Fix an area form and choose a divergence-free vector field with isolated singularities on each boundary component. By Lemma 6.3, we can construct a singular contact structure in a neighbourhood of each boundary component that has Reeb-like fields tangent to the boundary. Then we can extend this as a singular plane field over the interior of M, ensuring that there are only chiral Morse singularities in the interior, and homotope it into a singular contact structure using Theorem 6.7, leaving a neighbourhood of the boundary fixed. □

We conclude that topological obstructions to achieving nonvanishing twist in a

cholesteric liquid crystal can arise only in the case when the material domain has a spherical boundary component and sufficiently-strong normal anchoring.

6.4.3 The Singular Lutz Twist

Let Ξ denote the space of all contact structures on a 3-manifold M, and let Ξ_{sing} denote the space of singular contact structures. Let us enlarge Ξ to also include the singular contact structures, producing the space $\Xi' = \Xi \cup \Xi_{\text{sing}}$. By *a homotopy through singular contact structures*, we mean a continuous path in the space Ξ'. In this section we show that any two contact structures $\xi_0, \xi_1 \in \Xi$ are connected by a path in Ξ'. This means that homotopies through singular contact structures can be used to change the usual homotopy invariants of a contact structure.

The consequence for cholesterics is that the usual homotopy invariants can be changed by the creation and annihilation of pairs of defects. This is not altogether surprising, but it is interesting to examine the mechanism by which this occurs.

Recall from §3.8.1 the surgery called the (half) Lutz twist. In a tubular neighbourhood of a transverse curve K in a contact structure ξ, there are coordinates (r, θ, ϕ) such that ξ is defined by $\eta_{\text{std}} = d\phi + r^2 d\theta$. A Lutz twist excises this neighbourhood and glues in the contact structure defined by the 1-form $\eta_{\text{Lutz}} = h_1(r)d\phi + h_2(r)d\theta$, where h_1, h_2 are functions satisfying

1. $h_1(r) = -1$ and $h_2(r) = -r^2$ near $r = 0$,
2. $h_1(r) = 1$ and $h_2(r) = r^2$ near $r = 1$,
3. (h_1, h_2) is never parallel to (h_1', h_2') when $r \neq 0$.

The topological properties of this 1-form are determined by the first two conditions, while the third ensures it is contact. The result of this surgery is to make the contact structure overtwisted and to change the Euler class by $-2\mathcal{PD}[K]$. Since the Euler class can change it is clear that this surgery cannot be effected by a homotopy through plane fields, however we will see that it can be effected via a homotopy in the larger space Ξ'. For this, we simply need to exhibit a homotopy in Ξ' between η_{std} and η_{Lutz} on the solid torus $D^2 \times S^1$ that fixes the boundary.

Our construction is based on the unfolding of the A_2 singularity, also called the fold catastrophe [AGLV88], given by the function germ $\phi_s = x^2 - y^2 + z(z^2 + s)$. This defines a plane field $d\phi = 0$ which has no singularities when $s > 0$ and has two chiral Morse singularities when $s < 0$. To extend this plane field over the solid torus, define $f_s = s - \frac{1}{2}\cos z$ and consider the family of 1-forms

$$\eta_s = f_s dz + x dx - y dy + t(f_s(x dy - y dx) + 2xy dz), \tag{6.18}$$

on the solid torus $D^2 \times S^1$, for $t \neq 0$ a constant and $s \in [-1, 1]$. Depending on the choice of s this 1-form is singular, with singular points at $x = y = 0$ and $\cos(z) = 2s$. There are no singularities when $s = 1$. As s decreases from $s = 1$ to $s = -1$, an A_2 singularity of index zero is born at $z = 0$ when $s = 1/2$, then splits apart into singularities of Morse index 1 and Morse index 2 which move in opposite directions around the circle $x^2 + y^2 = 0$ until they annihilate again at $z = \pi$ when $s = -1/2$. For $s < -1/2$, there are again no singularities. We compute that

$$\eta_s \wedge d\eta_s = 2t \left(f_s^2 + \left(1 - \frac{1}{4}\sin z\right) x^2 + \left(1 + \frac{1}{4}\sin z\right) y^2 \right) dx \wedge dy \wedge dz, \qquad (6.19)$$

so that η_s defines a (singular, depending on the value of s) contact structure on the solid torus for any constant $t \neq 0$. The contact structure is positive or negative depending on the sign of t; in keeping with convention, fix $t > 0$.

Next we wish to show that η_s can be extended to a singular contact form on $D^2 \times S^1$ that agrees with η_{std} close to the boundary. We need Lemma 3.1: two contact structures that define the same characteristic foliation on a surface S are homotopic in a neighbourhood of S.

Take polar coordinates r, θ on D^2 and z on S^1. We can view $D^2 \times S^1$ as a smaller copy of $D^2 \times S^1$ equipped with the singular contact form η_s, and a family of tori $T^2 \times [0, 1]$ glued onto the outside which we need to extend η_s over to that it agrees with η_{std} near $T^2 \times 1$. To construct our desired plane field, we will define a tight contact structure on $T^2 \times [0, 1]$ such that the characteristic foliation induced on the surface $T^2 \times 0$ agrees with that induced on the boundary of the solid torus $D^2 \times S^1$ by η_s, and that is also homotopic to η_{std} near $T^2 \times 1$. We can then glue using Lemma 3.1 to produce a contact structure with the desired properties on $D^2 \times S^1$.

Consider a torus of radius R inside $D^2 \times S^1$. Since the parameter t is arbitrary, we can choose $t = 1/R$. Then the characteristic foliation induced by η_s on this torus is directed by the vector field $(f_s + \sin 2\theta)(\partial_\theta + \partial_z)$. Away from the line $0 \times S^1$ all the contact structures η_s are homotopic, and therefore we may assume that on this torus s is large enough so that $f_s + \sin 2\theta$ is never zero. Thus the characteristic foliation is directed by the vector field $\partial_\theta + \partial_z$. The characteristic foliation induced by η_{std} on a torus of radius R is $\partial_\theta - R^2 \partial_z$. Without loss of generality we can take $R = 1$.

The tight contact structure defined by the 1-form $dz + \sqrt{2} \sin\left(\frac{\pi}{2}(r - \frac{1}{2})\right) d\theta$, where θ, z denote the coordinates on T^2 and r the coordinate on $[0, 1]$, interpolates between the two characteristic foliations. By glueing these pieces together we obtain a singular contact form on $D^2 \times S^1$ that agrees with the standard neighbourhood of

a transverse curve close to the boundary of the solid torus and has the properties of η_s close to the core. Denote this singular contact form by ζ_s.

Finally, we need to check that ζ_1 is homotopic rel. boundary to η_{std}. This follows from the classification of tight contact structures on $D^2 \times S^1$: we can choose a dividing curve on the boundary consisting of two lines of slope -1, and then Theorem 3.16 implies there is a unique tight contact structure with this boundary condition, and consequently $\zeta_1, \eta_{\text{std}}$ are homotopic.

With this procedure it is essentially trivial to prove the main result of this section.

Theorem 6.10. *Any two contact structures ξ_0, ξ_1 are homotopic through singular contact structures.*

Proof. If either of ξ_0, ξ_1 are tight, we first make them overtwisted using the singular Lutz twist. If they now lie in the same homotopy class of plane fields, we are done. Otherwise, we change the homotopy class of ξ_0 to match that of ξ_1 in the same way as in the proof of the Lutz–Martinet theorem, only we use the singular Lutz twist to ensure we are making changes via homotopies. □

The singular Lutz twist can be used to create or remove a meron/Skyrmion tube. However, it first requires us to homotope the centre of the tube so that the winding around the central axis is -1, rather than $+1$. If we try to remove the Skyrmion tube by creating a pair of defects without first doing this, then one of the defects produced will necessarily be a hedgehog. Consequently, there would be a region of reversed handedness between the pair of defects, which would replace the Skyrmion tube. We expect that the conversion into a line with -1 winding will not occur due to the energy cost of the distortions required, and removing a Skyrmion tube requires replacing it with a region of reversed handedness, possibly accounting for their stability in cholesterics. In twist-bend materials there is no energetic preference for a single handedness, so this removal can occur, see §5.4.2.

Chapter 7

Point Defects in Cholesteric Droplets

7.1 Introduction

In this chapter I apply the results of Chapter 6 to the study of point defects in cholesteric droplets, based on recent experimental work. The bulk of this chapter was published as [PPČ+19].

The character of point defects in cholesteric liquid crystals (or magnetic Skyrmion textures) appears not to have been considered previously, apart from recent experimental work realising them [PČM16; PČM17; Pos18c]. This contrasts with the situation in nematics where point defects, known colloquially as hedgehogs, have been extensively studied over several decades [PSLW97; ŠRŽ+07; MŠT+06; Nab72; KL82; VL83; PTY91; KL06; LK01]. They can be generated deliberately as satellite defects to colloidal inclusions, or in droplets, with normal anchoring. For spherical colloids, point defects form elastic dipoles and facilitate self-assembly of colloidal chains and lattices [Muš17], while in droplets transitions between defect states produced by changes in boundary conditions [VL83] can provide highly sensitive sensors [LMB+11; LMP16]. Point defects in nematics are classified by an integer known as the topological charge, or degree [ACMK12]. Normal anchoring boundary conditions on a surface of genus g correspond to a topological charge $1 - g$ and induce compensating point defects of the same total topological charge in liquid crystal surrounding colloidal inclusions [SLH+13] or inside toroidal droplets [PVK+13]. In addition to their own phenomenology the topological character of point defects has also provided fundamental insight into disclination loops and their classification [ACMK12; ČŽ11b; ČŽ11a]. The lack of a similar body of work for point defects

in cholesterics represents a gap in our understanding of chiral materials; closing it provides considerable insight into cholesterics and also Skyrmion textures of chiral ferromagnets.

In recent experiments [PČM16; PČM17; Pos18c] point defects were created in spherical droplets of cholesteric liquid crystal with normal surface anchoring and shown to have markedly different properties from their nematic counterparts. These included point defects of topological charge $+1, -1, -2$ and -3, the higher charge defects observed for the first time, as well as arrangements of multiple defects into 'topological molecules'. Defects were located both in the centre of the droplet and in close proximity to its surface. The latter are not the surface defects associated to planar anchoring [VL83] but a feature of the cholesteric order.

7.2 The Experiments

Before turning to the theory I will give a brief description of the experiments; for more detail, consult the original sources [PČM16; PČM17; Pos18c]. The experiments involve creating droplets of cholesteric liquid crystal. The experimental samples were prepared by mixing small amounts of a chiral nematic liquid crystal mixture (1 : 1 weight ratio of CCN-47 and CCN-55 with 1.7% S-811 chiral dopant) into glycerol with 4% L-α-phospathidylcholine (egg yolk lecithin) to ensure homeotropic (normal) anchoring on the droplets of liquid crystal. The samples were then heated to isotropic phase above 65°C and quickly cooled back to the chiral nematic phase. This procedure enables the formation of a diverse range of stable and metastable director structures [PČM17; Pos18c], some of which include the charge -2 and -3 defects.

The director structures were examined by Fluorescent Confocal Polarizing Microscopy (FCPM) [SL01; Pos18a] where a small amount of a fluorescent dye *N,N′*-bis(2,5-di-*tert*-butylphenyl)-3,4,9,10-perylenedicarboximide (BTBP) which aligns with the director was added to the LC mixture. The dye can be excited with linearly polarized light (wavelength 488 nm, linear polarisations at 0°, 45°, 90° and 135° in the plane of the image) and the resulting fluorescence is detected through a polarizer with the same orientation as excitation light in the band 515 - 575 nm, so that the fluorescence intensity depends on the orientation of the LC.

The director fields were reconstructed from the experimental data with the help of a simulated annealing algorithm [PČM16; Pos18b]. In experimental images the director is shown with streamlines which point along the in-plane projection of the director, and are not shown where the director is mostly perpendicular to

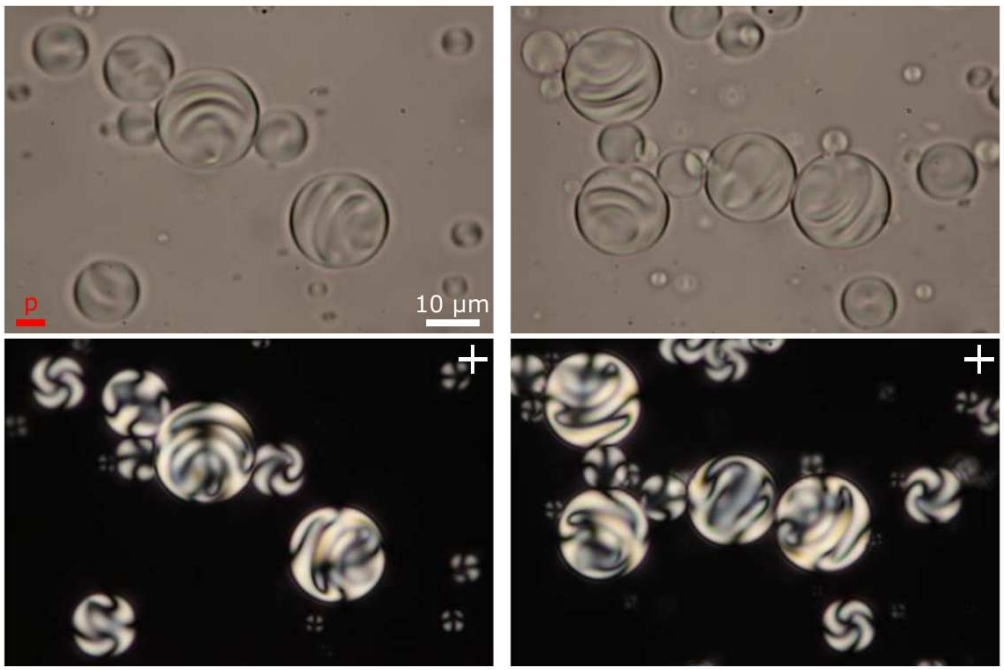

Figure 7.1: Typical experimental images of droplets. The upper row shows the droplets through unpolarised light, while in the bottom row crossed polarisers have been applied. The pitch length is indicated by the red bar. Reproduced from Ref. [Pos18c].

the plane. Positions of point defects are identified from the experimental data and marked with colour-coded spheres indicating their degree. Grey rods have been added between the defects to aide the visualisation of their 3D arrangement.

7.3 Morse Defects

We can break down the description of point defects in directors into those that possess a Morse singularity, and those that exhibit a degenerate singularity. In this section I describe the former.

In a nematic, the ground state director in a droplet is realised by the hedgehog director (Morse index 0) $\mathbf{n} = \mathbf{e}_r$, where r is the radial coordinate in a spherical coordinate system. By Proposition 6.4, such defects cannot be chiral and must sit on a surface dividing regions of opposite handedness, or else convert into a Morse index 2 singularity. In the former case, the size of the region of 'wrong' handedness will depend on the strength of the chirality.

A natural dimensionless measure of the strength of the chirality in the droplet

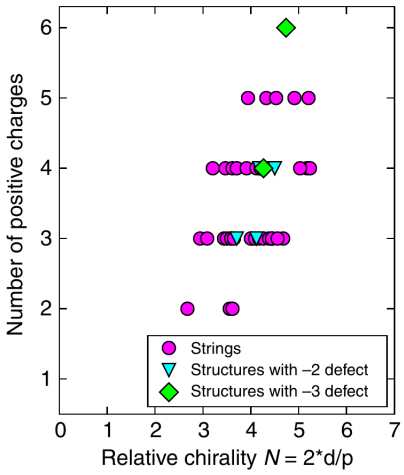

Figure 7.2: Types of defects found as a function of the dimensionless chirality N. Reproduced from Ref. [PČM17].

is the ratio of the droplet diameter $2R$ to the cholesteric half-pitch, $N = 2R/p$. In the experiments of Refs. [PČM17; Pos18c], typical values were $2 \lesssim N \lesssim 6$; in the simulations shown in this chapter I use values between 2 and 4. The distribution of structures found in the experiment is shown in Fig. 7.2. Numerical minimisation of Eq. 1.2 is done using a finite difference relaxation algorithm on a cubic grid; for simplicity I adopt a one elastic constant approximation ($K_1 = K_2 = K_3$) and the only relevant parameter is then the dimensionless ratio N. Typical simulations are run on a spherical droplet inside a 100^3 grid with Dirichlet boundary conditions and initial conditions provided by the local forms that arise from Theorem 6.4. It is sufficient to specifically initialise only the interior point defect(s), allowing those on the 'surface' to emerge naturally through matching to the radial boundary conditions. The use of a vector field for the simulation of the liquid crystal ensures that only point defects arise; in simulations using a Q-tensor such points typically expand into small disclination loops [RŽ09]. This approach captures all the phenomenology and major experimental observations; more quantitative comparison can come from including defect core structure, elastic anisotropy and surface anchoring energy in place of Dirichlet boundary conditions.

For $N = 0$, we have a radial hedgehog structure, as shown in Fig. 2.2. For small N, the central defect is displaced towards the boundary, Fig. 7.3(a). In simulations, increasing the value of N, but still keeping it small, continues this trend; the defect moves further towards the surface to reduce the size of the region with the wrong handedness and the axis it defines becomes increasingly recognisable as a double twist cylinder. However, this behaviour does not continue for larger values

of N and for values of $N \gtrsim 2$ the defect starts to move away from the surface again as the director field restructures continuously to the form shown in Fig. 7.3(c), (d); the Morse index changes from 0 to 2. These simulation results may be compared with the experimental images of Fig. 7.3(e) and (f), showing a cholesteric droplet containing a single, off-centre located, point defect. By eye, the comparison is excellent. From simulations we find that the twist is uniformly right-handed around the point defect, meaning that it is chiral and fundamentally different from its initial radial structure.

The transition observed here between the states shown in Fig. 7.3(a) and (c) is reminiscent of a transition between radial and hyperbolic point defects observed in nematic droplets with unequal elastic constants [LT86]. There the transition is precipitated by a change in the elastic constants with temperature that sees the radial hedgehog become energetically unfavourable relative to the hyperbolic one when the splay elastic constant is sufficiently large compared to twist and bend [RS99]. In this case the 'twist instability' is driven by the explicit chiral coupling, even without elastic anisotropy. This different energetic drive also leads to different phenomenology where the achiral 'radial' defect is expelled from the droplet interior until it sits near the surface.

We can use tomography to examine the Morse index 2 defect. A sphere of radius $r > 0$ is convex provided that it lies in the contact part of the director. The dividing curve contains two components, witnessing the fact that the singular contact structure must be overtwisted, as described in §3.8.1. In fact, is the same as the dividing curve induced on an appropriately-sized sphere around the standard overtwisted disk.

7.4 Droplet Surface and Boundary Layer

The Reeb stability theorem for confoliations of Eliashberg & Thurston (Theorem 3.5) applies to a boundary layer at the droplet surface where the director becomes radial to match the boundary conditions: the twist cannot be uniformly right-handed and by necessity there is some region of reversed twist close to the surface. Furthermore, it provides a topological demarcation of the surface boundary layer in a chiral droplet; namely, the region near the surface in which the director remains transverse to the family of concentric spheres extending in from the boundary itself. The beginning of boundary layer can also be defined using tomography: it starts at the radius r where the dot product between the director and the normal to the sphere of radius r is nowhere zero.

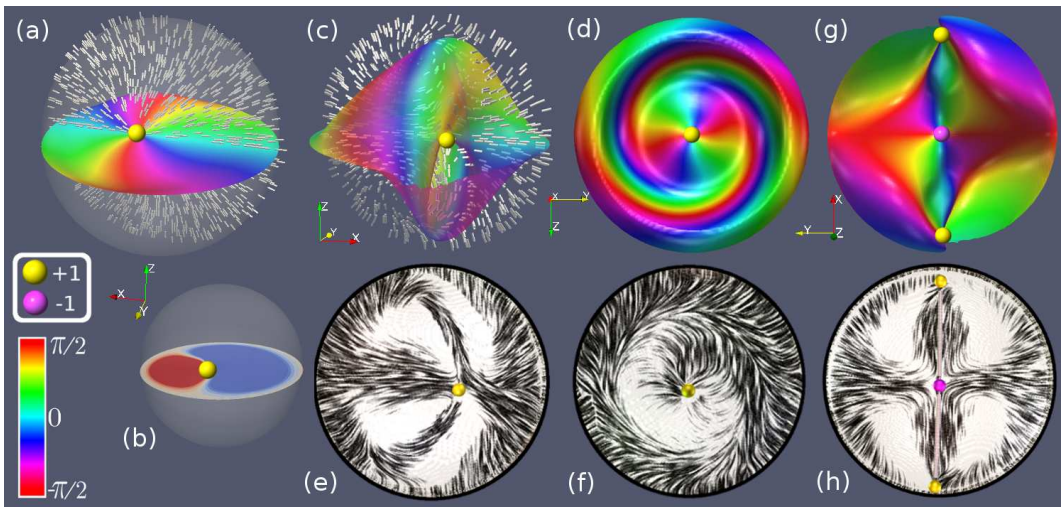

Figure 7.3: (a) Generic, achiral defect with topological charge +1, obtained for small values of N. The surface is the locus $n_z = 0$ (Pontryagin-Thom surface), with colour indicating the angle between the x and y components of the director. (b) The twist on a midplane xy-slice showing the reversal of twist at the location of the defect; the left-handed region is shown in red and the right-handed region in blue. (c) $n_z = 0$ and (d) $n_x = 0$ surfaces for a chiral defect with Morse index 2. In (c) the director has also been shown on a midplane xz-slice for added clarity. In (d) the viewing direction is along x. Corresponding experimental observations of this defect are shown in (e) and (f). (g) Chiral defect with Morse index 1 and topological charge -1 (central defect); viewing direction along z. Two achiral charge +1 defects reside close to the droplet surface. (h) An experimental observation of the same defect. In all panels, defects have been highlighted and colour-coded according to their charge (legend). Panels (e) and (f) reproduced from Ref. [Pos18c]. Panel (h) reproduced from Ref. [PČM17].

These general considerations assert that there must be some region of reversed twist close to the spherical droplet surface, but do not say anything about its actual form. We find from our numerical simulations that two situations arise, exemplified by the chiral Morse index 1 and 2 defects. In the case of the Morse index 2 defect (Fig. 7.3(c)) this takes the form of a non-singular ring, as shown in Fig. 7.4(a). The twist is right-handed throughout the interior of the droplet but becomes left-handed in a ring localised near the droplet surface. The ring lies in a vertical yz-plane, at the x location of the defect (slightly displaced from the centre). This region of reversed twist is a novel, non-singular topological soliton. Its existence is protected by topology and the energetic cost of having the wrong handedness leads to it being strongly spatially localised. The structure of the director field across the soliton is shown in Fig. 7.4(b) and (c).

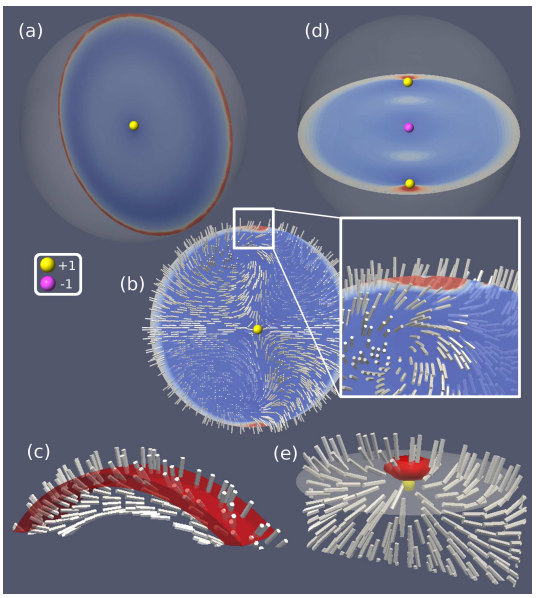

Figure 7.4: Boundary layer and reversal of twist. (a) Chiral structure of a droplet containing a Morse index 2 defect showing the twist on a vertical yz-plane passing through the defect. The twist is uniformly right-handed (blue) around the central defect but there is a localised ring of twist reversal (red) near the surface. (b) Structure of the director field on a vertical xz plane, with a inset showing the director close to the ring of reversed twist. (c) Structure of the director close to the ring of reversed twist, which is shown in red, (d) The twist on a midplane (z slice) through a droplet containing a Morse index 1 chiral defect (Fig. 7.3(g)). The blue region is right-handed; the red regions between the 'surface' point defects and the surface itself are left-handed. This structure is common to all 'surface' point defects. Note that the twist is uniformly right-handed around the central charge -1 defect. (e) Structure of the director in a region around an achiral defect anchored to the surface of the droplet (white surface). The region of reversed handedness is shown in red.

In all other cases, the chiral point defects in the droplet interior are encaged by an arrangement of charge +1 defects localised close to the droplet surface. These 'surface' defects are achiral and demarcate a localised region between themselves and the droplet surface in which the sense of twist reverses. An example, for the Morse index 1 defect is shown in Fig. 7.4(d), with the structure of the director close to the achiral defect given in Fig. 7.4(e). The topological argument for twist reversal near the boundary provides an explanation for the presence of such defects localised close to the surface, although we should emphasise that they are not topologically bound to the surface and so only held there by an energetic barrier.

Regions of opposite twist localised near point defects close to surfaces with

normal anchoring have recently been observed in experiments and numerical simulations [AS16]. In those, the surface is the flat plane of a glass slide, as opposed to being spherical. It is only spherical surfaces that have a topological requirement for regions of reversed twist. The appearance of regions of opposite twist in situations where it is not topologically required is then an energetic phenomenon.

The structure of the director in a neighbourhood of the surface over which the handedness reverses is determined by the characteristic foliation induced on that surface, as described in Chapter 3, and in particular §3.7.

7.5 Singularity Theory and Defects of Higher Charge

Morse critical points have topological charge ± 1 and so cannot describe the defects with higher charge $(-2, -3)$ observed experimentally [PČM17]. The latter are still described by a gradient field but with a degenerate critical point in the function ϕ. The classification of degenerate critical points is significantly more involved than that of Morse critical points; here, we follow Arnold's classification [AK98]. Although it is natural to expect that the simplest degenerate critical points will appear first, this is not the case, essentially because the topological charge of the gradient field is not central to the classification of degenerate critical points. As we will show, the experimentally observed higher charge defects are captured by the elliptic umbilic, or D_4^-, singularity (charge -2) and the $T_{4,4,4}$ singularity (charge -3). Moreover, we shall show that the 'topological molecules' that have been observed are consistent with the unfoldings of these, and higher charge, singularities.

I gave a description of the basics of singularity theory in §6.3.1, but I will give an informal overview here as well. A systematic study of degenerate critical points can be developed from their local algebra; loosely, the linearly independent polynomials of lower order than anything appearing in the gradient field; more formally, the quotient of the ring of Taylor series $\mathbb{R}[[x, y, z]]$ by the gradient ideal $\langle \partial_x\phi, \partial_y\phi, \partial_z\phi \rangle$. The dimension of this local algebra is called the multiplicity of the singularity—it is the number of non-degenerate critical points that it splits into (as a complex polynomial) under a generic perturbation. Said differently, the multiplicity is the number of non-degenerate critical points that simultaneously coalesce in forming the singularity. It is typical to represent a singularity by a standard polynomial, called its normal form. The simplest degenerate critical points have unique normal forms, however, the more degenerate ones have moduli, or free continuous parameters. The number of moduli appearing in the normal form is called the modality of the singularity. The singularities without moduli, known as the simple singularities,

were completely listed by Arnold in his celebrated ADE classification [Arn72]; there are two infinite families and three exceptional cases:

$$\begin{aligned} &A_k^{\pm} : \pm x^{k+1} \ \ (k \geq 1), \quad D_k^{\pm} : x^2 y \pm y^{k-1} \ \ (k \geq 4), \\ &E_6 : x^3 \pm y^4, \qquad E_7 : x^3 + xy^3, \qquad E_8 : x^3 + y^5. \end{aligned} \tag{7.1}$$

In three dimensions, these minimal models should be supplemented by quadratic terms in the remaining variables, *i.e.* y and z for the $A_k^{\pm}$ singularities, and only z for the others. For instance, for the A_2 singularity we might write $\pm x^3 + y^2 + z^2$. The subscript indicates the multiplicity of the singularity.

The addition of less degenerate terms to the normal form of any singularity results in a simplification of the singularity, known as an unfolding and usually breaking it into multiple critical points of lower multiplicity. The number of independent terms in a complete unfolding is called the codimension and can be thought of as the number of parameters that need to be tuned in order to create the degenerate critical point. For example, for the A_k singularity, a complete unfolding consists of the monomials x^n for $n = 1, \dots, k-1$ and the codimension is $k-1$. In general, the multiplicity μ, codimension c and modality m are related by $\mu = c + m + 1$.

Among the simple singularities (7.1), the only models for defects with topological charge -2 are furnished by the classes D_{2k}^-; all the other simple singularities have charge 0 or ± 1. Therefore, the simplest model for a point defect of topological charge -2 comes from the simple singularity D_4^-, which we write as

$$\phi = \kappa\left(x^2 y - \frac{1}{3}y^3\right) + \frac{1}{2}z^2, \tag{7.2}$$

where κ is a constant with dimensions of an inverse length. Its gradient vector field can be made chiral in a neighbourhood of the origin by adding the higher order term

$$\mathbf{m}_c = q\big[-\kappa z\big(x^2 - y^2\big)\mathbf{e}_x + 2\kappa xyz\,\mathbf{e}_y\big] - q^2 z^3\big[-y\,\mathbf{e}_x + x\,\mathbf{e}_y\big]. \tag{7.3}$$

The correspondence between this local model and experimental observations [PČM17; Pos18c] is striking (Fig. 7.5(a), (b)), although we find in our simplified director-based simulations that the defect is unstable and breaks apart into two charge -1 defects, each with the Morse-type local structure described above. This points to the importance of defect core structure, or elastic anisotropy, for stability in physical systems. It is interesting that the D_4^- singularity is chiral but not Beltrami (Proposition 6.7). I am not aware if this has any impact on the stability. There is a Beltrami singularity of index -2, which is obtained by taking ϕ to be the appropriate spherical

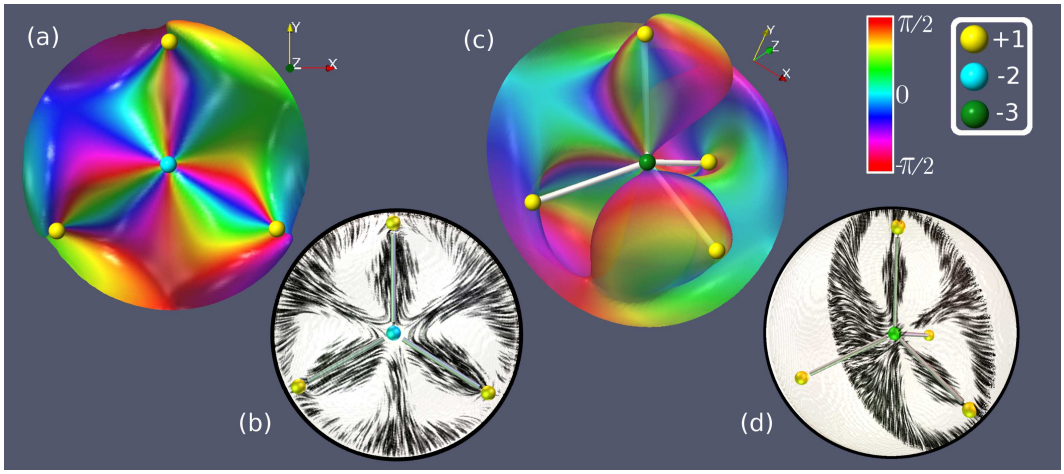

Figure 7.5: (a) Point defect with topological charge -2 associated to the D_4^- singularity. The surface is the locus $n_z = 0$ (Pontryagin-Thom surface), with colour indicating the angle between the x and y components of the director. (b) Experimental realisation of the charge -2 defect with superimposed director field in the $z = 0$ droplet midplane. (c) Point defect with topological charge -3 associated to the $T_{4,4,4}$ singularity ('bonds' between defects added for visual clarity). (d) Corresponding experimental image of a droplet containing a charge -3 defect. In all panels, defects have been highlighted and colour-coded according to their degree. Panel (b) reproduced from Ref. [PČM17].

harmonic; in Arnold's classification it is U_{12}, and it is also not stable numerically.

The experimentally observed defect with topological charge -3 [PČM17; Pos18c] (Fig. 7.5(d)) is reproduced by the unimodal singularity $T_{4,4,4}$, which we write

$$\phi = axyz + \frac{1}{4}\left(x^4 + y^4 + z^4\right), \tag{7.4}$$

where the modulus a has dimensions of length. $T_{4,4,4}$ is a codimension 9 singularity with multiplicity 11, characteristics which convey its high complexity. In addition to the origin, where there is an isolated zero of topological charge -3, the gradient vector field has isolated zeros of charge $+1$ (and Morse index 0) at the four points $a(1,-1,1), a(-1,1,1), a(1,1,-1), a(-1,-1,-1)$, corresponding to the vertices of a tetrahedron. This suggests that the modulus a should take a value of $R/\sqrt{3}$, up to an $O(1)$ factor, so that these defects sit near the surface of the droplet, as observed experimentally. The gradient field of (7.4) can be perturbed into a chiral point defect via a generic method that we describe in the following section. Simulations initialised with the $T_{4,4,4}$ singularity produce a numerically stable charge -3 point defect surrounded by four tetrahedrally-arranged surface defects in excellent agreement with the experiment (Fig. 7.5(c)).

The appearance of D_4^- and $T_{4,4,4}$ is not due to topological effects, but a combination of geometric and energetic considerations that influence the positioning of the boundary defects, which in turn impose a particular symmetry of the droplet. For instance, $T_{4,4,4}$ is topologically equivalent to X_9, another charge -3 singularity. X_9 would naturally arise if the four boundary defects were to sit in a square on an equator of the droplet, rather than arrange themselves into a tetrahedron, which imposes the $T_{4,4,4}$ symmetry—this configuration of boundary defects does not arise in the experiments and appears to be energetically disfavoured. However, changes in the boundary anchoring conditions and in the elastic constants will change the preferred configuration of the boundary defects. A similar effect occurs for a two-dimensional nematic confined on a sphere: generally there are four $+1/2$ defects that sit at the points of a tetrahedron, but changes in the elastic constants can result in the defects forming the points of a square instead.

7.6 Unfoldings and Topological Molecules

In addition to droplets containing individual chiral point defects, experiments also reveal a variety of multiple-defect structures [PČM17]. Unlike nematic droplets, these multi-defect cholesteric textures are metastable and the defects do not annihilate pairwise to obtain a minimal number. Moreover, the arrangements appear far from random, exhibiting definite structure and symmetry, leading to them being dubbed as 'constellations' and 'topological molecules'. As we will show in this section, the unfoldings of singularities provide a natural framework for these topological molecules, with excellent agreement with experiment. Subsequently, in § 7.7 we will show that the geometric structure of cholesterics, and in particular their degeneracies, known as λ lines or umbilics, serve to furnish the 'chemical bonds' of these topological molecules.

The unfoldings of singularities provide systematic descriptions of how degenerate critical points can break apart into simpler pieces, or how generic critical points coalesce to form degenerate ones. In the present context, these unfoldings provide models for the combination and splitting of chiral point defects.

For instance, the simplest description of the annihilation of two chiral defects with opposite topological charge is given by the unfolding of the A_2 singularity

$$\phi = \frac{\kappa}{3}x^3 + \frac{1}{2}y^2 - \frac{1}{2}z^2 + c_1 x, \tag{7.5}$$

where κ is a constant with dimensions of an inverse length and c_1 is a parameter

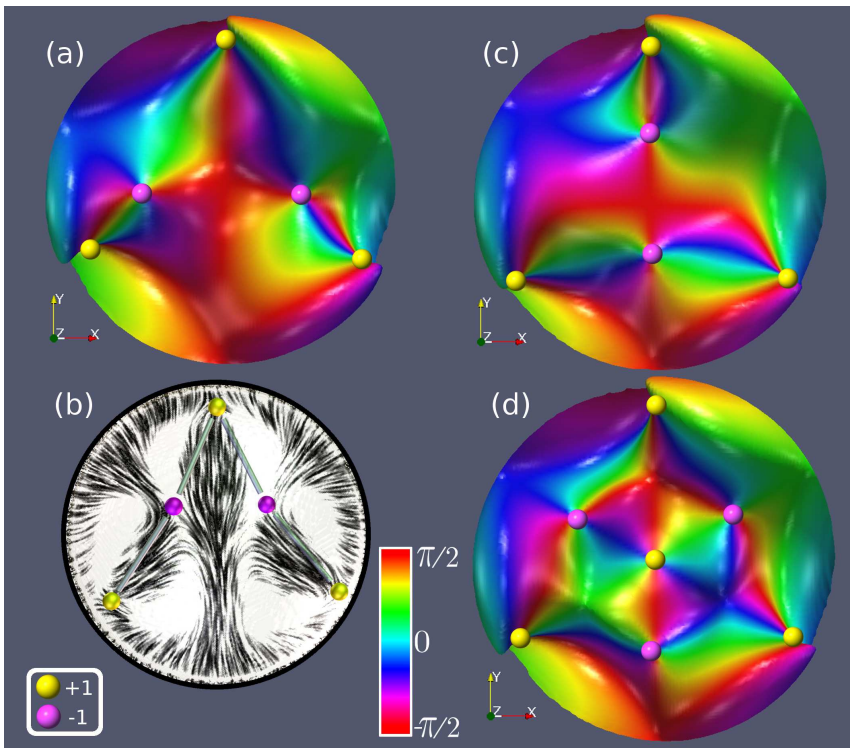

Figure 7.6: Unfoldings of the D_4^- singularity. (a) A splitting of the charge -2 defect into two Morse index 1 defects producing a 'V'-shaped constellation closely similar to textures observed experimentally. (b) An example of such an experimental configuration with the director field in the $z = 0$ droplet midplane superimposed. (c) By tuning the unfolding the splitting can also produce a 'T'-shaped constellation, which remains stable numerically but has not been observed in experiments. (d) The isotropic term in the unfolding splits the D_4^- singularity into four Morse critical points without breaking the symmetry of the droplet. Again, this is stable numerically but has not been observed in experiments. Panel (b) reproduced from Ref. [PČM17].

of the unfolding with dimensions of length. When c_1/κ is positive there are no critical points, while when it is negative there are isolated Morse critical points at $(\pm|c_1/\kappa|^{1/2}, 0, 0)$ with Morse indices 1 (+) and 2 (−). Note that in the way that we have written the A_2 singularity (7.5) the Morse terms appear with opposite signs, *i.e.* $y^2 - z^2$. This ensures that after unfolding the two Morse-type defects are both chiral; if these Morse terms had both been given the same sign—$\pm(y^2 + z^2)$—then one of the two critical points the singularity splits into would have had Morse index 0 (+) or 3 (−) and hence would not be chiral.

The unfolding of the D_4^- singularity provides a description of the splitting of a charge -2 chiral defect, or merging of two point defects with the same charge

(-1)

$$\phi = \kappa\left(x^2 y - \frac{1}{3}y^3\right) + \frac{1}{2}z^2 + c_1 x + c_2 y + \frac{c_3}{2}\big(x^2 + y^2\big). \tag{7.6}$$

The c_3 term is isotropic and does not alter the symmetry of the defect; it is therefore natural to consider it separately and we start with the case $c_3 = 0$. Critical points of ϕ are given by $z = 0$ and (using a compact complex notation)

$$\partial_y \phi + i\partial_x \phi = \kappa\big(x + iy\big)^2 + c_2 + ic_1 = 0. \tag{7.7}$$

There are two Morse critical points (both of Morse index 1) with locations (assuming $\kappa > 0$)

$$x + iy = \pm\frac{(c_1^2 + c_2^2)^{1/4}}{\sqrt{\kappa}}\, \mathrm{e}^{i(\alpha+\pi)/2}, \tag{7.8}$$

where $\alpha = \arctan c_1/c_2$. The splitting is along the x-axis when $c_1 = 0$ and c_2 is negative. This produces a 'V-shaped' arrangement of defects within the cholesteric droplet and is strongly reminiscent of the 'constellations' observed experimentally (Fig. 7.6(a), (b)) [PČM17; Pos18c]. The 'T' splitting produced when c_2 is positive (c_1 still zero) has not been observed in experiments, but is readily produced numerically (Fig. 7.6(c)).

Returning to the c_3 term, consider now the case where only it is non-zero. Then the D_4^- singularity splits into four critical points, again all lying in the $z = 0$ plane: one at the origin of Morse index 2 and three of Morse index 1 at the points

$$(x, y) = \left(0, \frac{c_3}{\kappa}\right),\ \left(\pm\frac{\sqrt{3}\, c_3}{2\kappa}, \frac{c_3}{2\kappa}\right). \tag{7.9}$$

This is shown in Fig. 7.6(d).

The unfoldings of the $T_{4,4,4}$ singularity, and the resultant topological molecules, are significantly more involved mathematically, due to the high codimension and multiplicity. For this reason we restrict our presentation to consideration of particular unfoldings most directly pertinent to the observed topological molecules. A basis for the local algebra of the $T_{4,4,4}$ singularity can be taken to be the 11 monomials

$$1,\ x,\ y,\ z,\ x^2,\ y^2,\ z^2,\ x^3,\ y^3,\ z^3,\ xyz. \tag{7.10}$$

Note that, *e.g.*, $x^3 \sim -ayz$ as elements of the local algebra so that we could replace x^3, y^3 and z^3 by yz, zx and xy if desired. The constant obviously does not change the nature of the critical point, while the term xyz acts only to change the value of the modulus. The remaining nine terms are associated to the unfoldings, of which

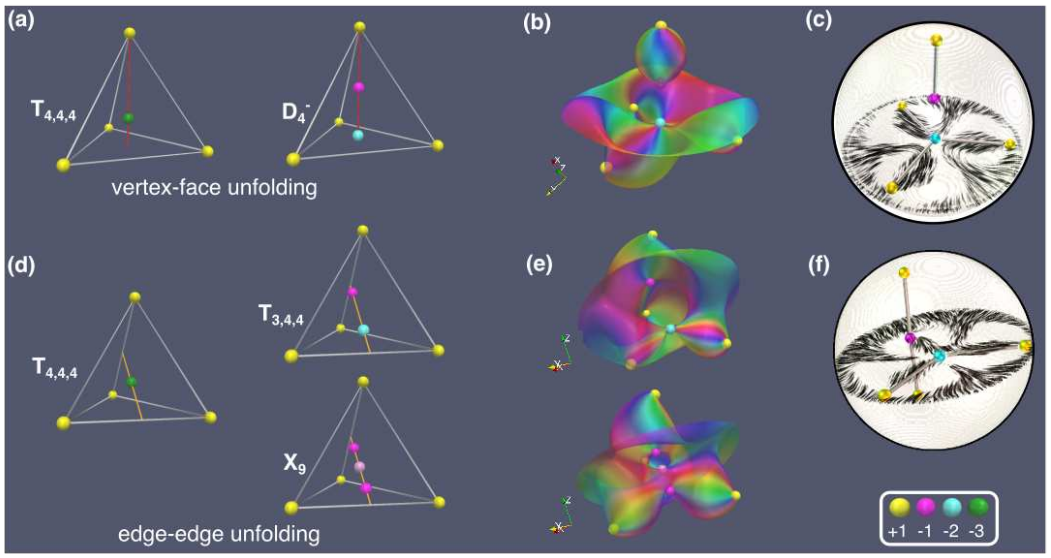

Figure 7.7: Unfoldings of the $T_{4,4,4}$ singularity and topological molecules. (a) Schematic of the vertex-face unfolding, splitting $T_{4,4,4}$ into a Morse index 1 and a D_4^- singularities. (b) Numerical simulation of the unfolding: the charge -2 defect remains stable for long times. (c) Topological molecule observed experimentally corresponding to the vertex-face unfolding. (d) Schematic of the edge-edge unfolding, with splittings of $T_{4,4,4}$ into two Morse index 1 critical points and a X_9 singularity, with topological charge -1, or into a single Morse critical point and a $T_{3,4,4}$ singularity, with topological charge -2. (e) Numerical simulation of the unfolding: the charge -2 defect is unstable numerically and is shown here artificially stabilised. (f) Topological molecule observed experimentally corresponding to the edge-edge unfolding. Panel (c) reproduced from [Pos18c]

we consider two particular cases pointed to by symmetry. We describe these in terms of the tetrahedral environment of the $T_{4,4,4}$ singularity. In the first, the three-fold symmetry about an axis connecting a vertex and face-centre of the tetrahedron is preserved: we refer to this as the vertex-face unfolding. In the second, we preserve the two-fold rotational symmetry about the z-axis: as this connects two edges of the tetrahedron we refer to it as the edge-edge unfolding. These are shown schematically in Fig. 7.7(a) and (d).

The analysis of the vertex-face unfolding is naturally given in terms of the

adapted coordinates

$$\begin{aligned} u &= \frac{1}{\sqrt{2}}\big(x-y\big), \\ v &= \frac{1}{\sqrt{6}}\big(x+y-2z\big), \\ w &= \frac{1}{\sqrt{3}}\big(x+y+z\big), \end{aligned} \tag{7.11}$$

in which the $T_{4,4,4}$ singularity takes the form

$$\begin{aligned} \phi = {} & \frac{a}{\sqrt{6}}\left(u^2v-\frac{1}{3}v^3\right) - \frac{a}{2\sqrt{3}}\big(u^2+v^2\big)w + \frac{a}{3\sqrt{3}}w^3 \\ & + \frac{1}{8}\big(u^2+v^2\big)^2 + \frac{1}{12}w^4 + \frac{1}{2}\big(u^2+v^2\big)w^2 \\ & + \frac{1}{\sqrt{2}}\left(u^2v-\frac{1}{3}v^3\right)w. \end{aligned} \tag{7.12}$$

We consider an unfolding that preserves the three-fold symmetry about the w-axis, given by the addition of the terms (terms in w^2 and w^3 are omitted for simplicity)

$$c_1w + \frac{c_2}{2}\big(u^2+v^2\big). \tag{7.13}$$

There are critical points with $u=v=0$ and w given by the roots of the cubic

$$c_1 + \frac{a}{\sqrt{3}}w^2 + \frac{1}{3}w^3. \tag{7.14}$$

When $c_1=0$ these reduce to $w=0$ (double root) and $w=-\sqrt{3}\,a$; when $c_1>0$ the former disappear and only the latter remains; and when $c_1<0$ the double root resolves to two simple roots at $w\approx\pm(-\sqrt{3}\,c_1/a)^{1/2}$. We consider only this last case. Expanding about one of the new critical points, which we denote $w=r$, gives

$$\begin{aligned} \phi \sim {} & \frac{c_2-ar/\sqrt{3}}{2}\big(u^2+v^2\big) + \frac{ar}{\sqrt{3}}\big(w-r\big)^2 \\ & + \frac{a}{\sqrt{6}}\left(u^2v-\frac{1}{3}v^3\right), \end{aligned} \tag{7.15}$$

corresponding to a Morse critical point. Neglecting c_2, the Morse index is 1 if r is negative and 2 if r is positive. The latter we may view as an unfolding of the D_4^- singularity that we recover by setting $c_2=ar/\sqrt{3}$. In this case, the initial $T_{4,4,4}$ singularity splits into a Morse index 1 critical point in the direction of the vertex

and a D_4^- singularity in the direction of the face-centre of the tetrahedron formed by the accompanying charge +1 surface defects.

This picture is confirmed by simulations of the unfolding, which produce a charge −2 chiral defect corresponding to the D_4^- singularity that is numerically stable for orders of magnitude longer than the directly initialised defect. An example of such a simulation, showing the Pontryagin-Thom surface $n_w = 0$, is shown in Fig. 7.7(b). This can be compared with the topological molecule observed experimentally and shown in Fig. 7.7(c); the agreement is striking.

Turning now to the edge-edge unfolding, we consider the function

$$\phi = axyz + \frac{1}{4}\big(x^4 + y^4 + z^4\big) + c_1 z + \frac{c_2}{2}z^2 + \frac{c_3}{3}z^3 + dxy, \tag{7.16}$$

where the parameters c_k have dimensions of (length)$^{4-k}$ and d has dimension (length)^2. There are critical points with $x = y = 0$ and z given by the roots of the cubic $z^3 + c_3 z^2 + c_2 z + c_1$. The number of roots depends on the value of the discriminant

$$27c_1^2 - 18c_1c_2c_3 + 4c_1c_3^3 + 4c_2^3 - c_2^2c_3^2. \tag{7.17}$$

When this is positive there is only one root; when it is negative there are three; and when it vanishes there are two. Expanding about one of the roots (at $z = r$) gives the form $\sim (ar + d)xy \pm (z - r)^2$, which is of Morse type and Morse index 1 (+) or 2 (−), the latter occuring only for the 'middle' root when there are three roots. There are additional critical points off-axis ($x, y \neq 0$) unless the parameter d takes the value $d = -ar$, with r corresponding to the 'middle' critical point. It is then of type $X_9 = T_{2,4,4}$ and has topological charge −1. We emphasise that this unfolding produces a linear string of three chiral point defects each with topological charge −1 but which are not all equivalent; the two outer defects have a local structure corresponding to the gradient field of a Morse critical point with Morse index 1, whereas the middle defect has the local structure of the gradient field of an X_9 singularity. A numerical simulation of this unfolding is shown in Fig. 7.7(e).

When there is a double root (at $z = r$) the function has the form $(ar + d)xy + r(z-r)^3$ corresponding to an A_2 singularity with topological charge 0, unless $d = -ar$ when it is instead a $T_{3,4,4}$ singularity with charge −2. Thus, the function

$$\phi = axy(z - r) + \frac{1}{4}\big(x^4 + y^4 + z^4\big) - \frac{3r^2}{2}z^2 + 2r^3 z, \tag{7.18}$$

describes, for $r \neq 0$, a splitting of the $T_{4,4,4}$ singularity into a Morse index 1 critical point at $z = -2r$ and a $T_{3,4,4}$ singularity at $z = r$. A numerical simulation of this

unfolding is shown in Fig. 7.7(e), however, in this case the charge -2 defect is not stable numerically and splits (transverse to the edge-edge axis) into two Morse index 1 defects. Nonetheless, this configuration of point defects is observed experimentally (Fig. 7.7(f)), with a stable charge -2 defect, and its structual similarity to the edge-edge unfolding is strongly suggestive. The main implication of this is that the two charge -2 defects in the observed topological molecules—Fig. 7.7(c) and (f)—correspond to topologically distinct chiral defects, one having the structure of the D_4^- singularity and the other the structure of the $T_{3,4,4}$ singularity.

7.7 λ Lines and Umbilics: Defects in the Cholesteric Pitch

Point defects in the director are associated with a confluence of λ lines, whose number and type are related on topological grounds to the type of point defect; for a defect of topological charge k there are a total of $4|k|$ lines, counted with multiplicity [MA16b]. For chiral point defects, however, a much more detailed description can be given. As the structure of chiral point defects is determined by the gradient field of an isolated singularity, the location and type of the defects in the pitch axis coincides with the structure of umbilic lines of the local level manifolds of the function describing the critical point. Passing through the critical value the level sets change between $1 + |k|$ disconnected discs and a connected surface of Euler characteristic $1 - |k|$ (see Lemma 6.1). Each disc is pierced by the axis of a double twist cylinder (λ/umbilic line of multiplicity 2), while a further $2|k| - 2$ elementary lines pierce the connected surface along directions of high symmetry. The pattern of lines for the Morse index 2, D_4^- and $T_{4,4,4}$ singularities is shown in Fig. 7.8, with the umbilic lines indicated by white tubes, obtained numerically as isosurfaces where the norm of Δ drops below some threshold value.

Taking D_4^- as an example, the topological charge is -2 so that the topology requires there to be 8 umbilic lines, counted with multiplicity. There are three degenerate umbilic lines (double twist cylinders—Fig. 7.8(d)), connecting the central defect to the $+1$ surface defects, which should be counted with multiplicty 2 [MA16b] for a total of 6 umbilic lines. Symmetry considerations tell us that the remaining two umbilic lines (with $\lambda^{-1/2}$ profile—Fig. 7.8(e)) extend along the z-axis. The structure is shown in Fig. 7.9(a). A similar description can be given in all cases.

It is interesting to consider the behaviour of umbilic lines under an unfolding of the singularity. Consider the unfoldings of D_4^- into a pair of charge -1 defects. Each defect produced must have 4 umbilic lines, counted with multiplicity. With

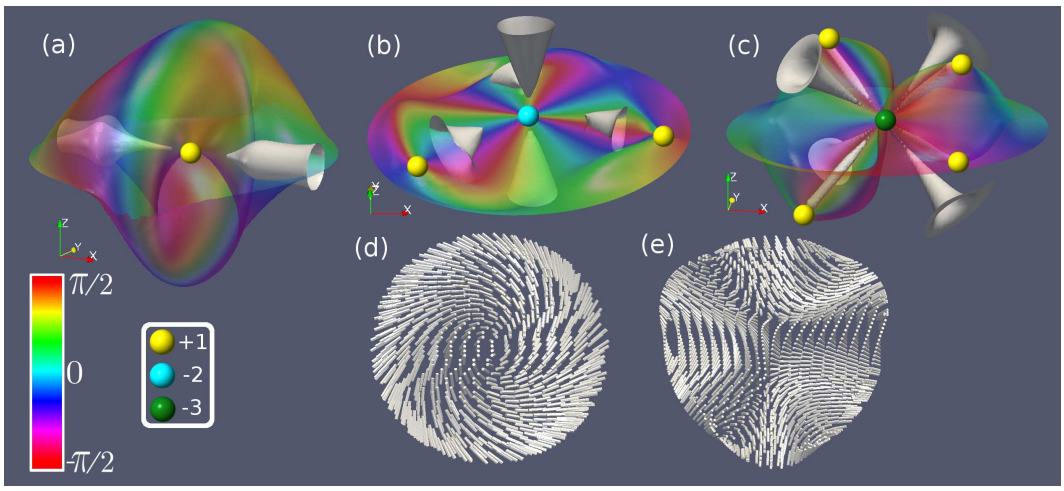

Figure 7.8: Umbilic lines for the (a) Morse index 2, (b) D_4^- and (c) $T_{4,4,4}$ singularities, indicated by white isosurfaces. Each defect has double twist cylinders connecting it to the charge +1 'surface defects'. The remaining umbilics are $\lambda^{-1/2}$-lines that terminate on the droplet surface. Typical cross-sectional profiles for the umbilics are shown in (d) double twist cylinders and (e) $\lambda^{-1/2}$-lines. In all panels, defects have been highlighted and colour-coded according to topological charge.

this constraint, there are two possible configurations. In one case, Fig. 7.9(b), one of the degenerate umbilic lines splits into a pair of $\lambda^{1/2}$-lines. The pair of defects produced by the unfolding each take charge of one of these $\lambda^{1/2}$-lines, along with one each of the two $\lambda^{-1/2}$ lines and two remaining degenerate umbilic lines that were connected to the original charge -2 defect, so that each defect has a total of 4 umbilic lines when counted with multiplicity. The other case, shown in Fig. 7.9(c), has one defect connected to a pair of degenerate umbilic lines, while the other defect has a single degenerate umbilic line and both of the $\lambda^{-1/2}$ lines.

Both cases can be realised in numerical simulations by initialising the simulation with the model given by Eq. (7.6) with unfolding parameters $c_1, c_3 = 0$, and $c_2 \neq 0$. When $c_2 > 0$ this gives a V unfolding, and the configuration of umbilic lines is as in Fig. 7.9(b). When $c_2 < 0$ this gives a T unfolding, and the configuration of umbilic lines produced is Fig. 7.9(c). A similar description can be given for the unfoldings of $T_{4,4,4}$.

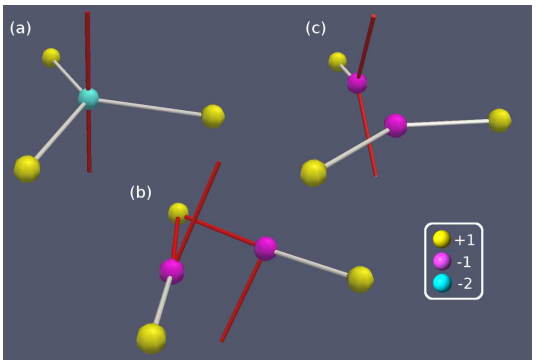

Figure 7.9: (a) Position of the umbilic lines for the D_4^- singularity. (b), (c) Possible configurations of umbilic lines after an unfolding into a pair of charge -1 defects. In each case the white tubes indicate degenerate umbilic lines with multiplicty 2 (the axes of double twist cylinders), while the red tubes indicate generic umbilic lines ($\lambda^{-1/2}$-lines).

Chapter 8

Singular Contact Structures: The Local and Global Theory of Line Defects

8.1 Disclination Lines in Cholesterics

Liquid crystal materials do not only exhibit point defects, but also line defects known as disclination lines. The fundamental group of the nematic order parameter space is $\mathbb{Z}_2$, meaning that, to a first approximation, a line singularity is determined by whether or not the director is orientable on a closed curve encircling it. Orientable singular lines are unstable in a nematic material, and can be removed by a perturbation. Nonorientable disclination lines are stable as they cannot be removed by a local perturbation. They also carry a topological charge: if a link L of disclination lines can be surrounded by a sphere S such that the director $\mathbf{n}$ is nonsingular and orientable in a region of S, then we may define the absolute value of the charge carried by L to be $|e(\xi)[S]|$, where ξ is the plane field orthogonal to $\mathbf{n}$.

I now give a brief overview of previous work on disclination lines, the topological arguments present in early work [PT77; VM77; BDP$^+$78b; Jän87] as well as the more recent geometric descriptions of disclinations [ČŽ11b; ČŽ13; ČDKŽ13].

To completely understand the homotopy classes of disclination loops, it is not sufficient to consider just the maps $S^1 \to \mathbb{RP}^2$ obtained from looking at the director around a meridian, but the maps $T^2 \to \mathbb{RP}^2$ that are obtained by looking at the director on a torus around the singular line. Jänich [Jän87] studied the homotopy classes of maps $T^2 \to \mathbb{RP}^2$ which are not orientable around the meridian and hence correspond to disclination lines in the director, and obtained a complete

classification. Broadly speaking, there are two invariants of such maps. Firstly, one can ask whether the map is orientable or not along a longitude. If such a disclination line is nonorientable along a longitude, then it must link with with an odd number of other lines, although we cannot determine the exact count just from the structure around this one line. Thus there is a $\mathbb{Z}_2$ invariant associated to a disclination that counts, mod 2, the number of other disclination lines linking it. Further, one can surround the disclination line with a sphere and look at the map $S^2 \to S^2$ that is induced on this sphere (note that the codomain of the map is S^2 because this map can always be orientated). This map has a degree $q \in \mathbb{Z}$ that counts the defect charge inside this sphere. Now, one can homotope the map $T^2 \to \mathbb{RP}^2$ in a nonsingular way that changes the charge on the surface of this measuring sphere by ± 2; essentially, this involves moving a point defect once around a loop that links the disclination line in question. Thus there is an additional $\mathbb{Z}_2$ invariant that counts the charge mod 2.

Thus this space of maps has at least a $\mathbb{Z}_4$ invariant, and each disclination line can be associated with an integer $\nu_j \in \{0, 1, 2, 3\}$, the *Jänich index*. Jänich then demonstrates that this $\mathbb{Z}_4$ invariant characters the space of maps $T^2 \to \mathbb{RP}^2$ that a nonorientable around a meridian [Jän87]. These four homotopy classes correspond to the vector fields

$$\mathbf{n}_\nu = \cos\left(\frac{\theta + \nu z}{2}\right)\mathbf{e}_r - \sin\left(\frac{\theta + \nu z}{2}\right)\mathbf{e}_\theta, \tag{8.1}$$

on $D^2 \times S^1$. That $\mathbf{n}_\nu$ is homotopic to $\mathbf{n}_{\nu+4}$ can be proved using the belt trick, the Pontryagin–Thom construction, or equivariant homotopies in the double cover [Mac16].

The Jänich index also contains global information. Because one part of the index corresponds to the linking number of disclination with other disclination lines, we have,

$$\nu_j \bmod 2 = \sum_{i \neq j} \mathrm{Lk}(K_i, K_j) \bmod 2, \tag{8.2}$$

where the sum is over all other disclination lines in the system. The *parity* of disclination K_j is

$$s_j := \frac{1}{2}\left(\nu_j - \sum_{i \neq j} \mathrm{Lk}(K_i, K_j)\right) \bmod 2 \in \mathbb{Z}_2. \tag{8.3}$$

The sum $\sum_j s_j$ of all parities is invariant under crossings and reconnections of disclination lines.

When a disclination line has additional geometric structure we can say more. Associated to each line K_j with winding (or profile) $-\frac{1}{2}$ is a self-linking number q_j, which counts the number of times the director profile rotates as we move along the disclination line. This self-linking number is not an integer, rather it is of the form $\frac{m}{3}$ for $m \in \mathbb{Z}$, where m is odd if K_j is linked by an odd number of other disclination lines, and even otherwise—the fact that it is quantised into thirds follows from the symmetry of the $-\frac{1}{2}$ singularity. In an ordinary nematic, this number is evidently not preserved by an arbitrary homotopy, and thus cannot be said to be a topological invariant of the line. Given a link L comprised of disclination lines K_j, the linking numbers $\mathrm{Lk}(K_i, K_j)$ and self linking numbers q_j obey the relation [ČŽ13; ČDKŽ13],

$$\frac{3}{2}\left(\sum_j q_j + \sum_{i\neq j} \mathrm{Lk}(K_i, K_j)\right) + n = Q \bmod 2, \tag{8.4}$$

where n is the number of disclination lines and Q denotes the topological charge carried by the link L.

The above describes the theory of line defects in nematics. The existence and basic homotopy classification of disclinations in cholesterics comes from the theory described in §1.1. In a cholesteric, the fundamental group of the order parameter space is the quaternion group, the group $\mathcal{Q}$ with generators $1, -1, i, -i, j, -j, k, -k$ and the relations $(-1)^2 = 1, i^2 = j^2 = k^2 = ijk = -1, ij = -ji = k$, such that 1 is the identity [PT77; BDP$^+$78b]. These four group elements label the types of line defects that can occur in a cholesteric. The identity element corresponds to no singularity or to a removable singular line (a χ^s line with s an integer), in the same way that $0 \in \mathbb{Z}$ corresponds to either no defect or a removable defect when discussing point defects in nematics and cholesterics. A λ line with integer winding has type -1, and a disclination line around which the director is nonorientable has type i, and a λ line around which the pitch is nonorientable has type j. An important consequence of the noncommutativity of this group is that passing one defect line through another may result in a 'tether' connecting the two. The type of the tether is identified by computing the product of the group elements corresponding to the two lines; in particular, obstructions to passing defect lines through one another can be identified with elements of the commutator subgroup $[\mathcal{Q}, \mathcal{Q}]$. For example, if one crosses a pair of disclination lines, the resulting tether is of type $i^2 = -1$, a λ line. This observation is of central importance, and admits an interpretation in terms of contact topology that will be discussed below.

In this chapter I will discuss the local and global classification of both removable and nonremovable disclination lines in cholesterics, and hence complete the

description of director defects in a cholesteric that was begun in Chapter 6. The primary object of study is as follows.

Definition 8.1. A germ along $0 \times S^1$ of a singular plane field ξ on $D^2 \times S^1$, not assumed orientable, which is singular only along $0 \times S^1$ is called a *line singularity*. A line singularity ξ is called a *chiral line singularity* if it is (locally, if ξ is nonorientable) defined by a 1-form η with $\eta \wedge d\eta \geq 0$, with equality only on $0 \times S^1$. A chiral line singularity ξ is *overtwisted* if there exists some $\epsilon > 0$ such that, for every $0 < R < \epsilon$, the contact structure in a neighbourhood of the torus of radius R is *overtwisted*; otherwise, ξ is called *tight*.

When dealing with orientable chiral line singularities ξ, I abuse notation and also refer to a 1-form η defining ξ as a chiral line singularity.

An unknotted disclination line threaded by a single λ^{+1} line results in a overtwisted texture, however we shall see that the director can be tight in a neighbourhood of the disclination even though it is globally overtwisted, in contrast to point singularities. The essential overtwistedness of a neighbourhood of a disclination line is associated with λ line tethers being attached to the disclination line itself.

Here is a brief outline of the classification results given below. For overtwisted chiral line singularities there is an h-principle, §8.6, and therefore the homotopy classes of overtwisted chiral line singularities correspond to homotopy classes of germs of singular plane fields with line singularities, which are classified by the Jänich index. We show that there is an overtwisted chiral line singularity in each homotopy class. For tight chiral line singularites structures, there are multiple different homotopy classes for each Jänich index, and their classification proceeds using very similar ideas to those used for studying tight contact structures explained in Chapter 3. Breifly, the approach is as follows:

1. I first examine the characteristic foliations on disks transverse to the singular line, and prove convex surface theory type results about extending profiles to singular contact structures on $D^2 \times [-1, 1]$.

2. I exhibit a family of tight chiral line singularities $\eta_{k,q}$ and prove, using the same ideas used in the classification of tight contact structures on T^3, that they each represent different homotopy classes.

3. I prove a uniqueness result for tight singular contact structures on $D^2 \times [-1, 1]$ with a line singularity along $0 \times [-1, 1]$ and a fixed boundary, analagous to the unqiueness result for tight contact structures on the 3-ball.

4. Using these results, I show that every tight chiral line singularity is homotopic to one of the models, completing the homotopy classification.

I explain the classification of the orientable chiral line singularities in detail in §8.4 after some setup in §8.2 and §8.3. The arguments carry through to the nonorientable case, for which the classification is explained in §8.5. Although removing an orientable line singularity is trivial in a nematic, in a cholesteric the process of removing defects of type 1 and replacing them with defects of type -1 is more subtle. I discuss this in §8.7. The global classification of singular contact structures with both point and line singularities is completed in §8.8.

8.2 Profiles of Singular Lines

As the first part of the classification, we examine which characteristic foliations can be induced on disks transverse to the singular line. We focus on the orientable case, as the nonorientable case is completely analagous. Let z denote the coordinate on the S^1 factor of $D^2 \times S^1$. On this neighbourhood we write the singular contact form as $\eta = \beta_z + u_z dz$, for β_z a family of 1-forms on the disk and u_z a family of functions on the disk depending on the coordinate $z \in S^1$, such that η vanishes only at the origin of the disk, i.e we have $\beta_z = u_z = 0$ exactly along the line $0 \times S^1$. The characteristic foliation induced on $D_z := D^2 \times z$ is directed by a vector field X_z defined by $\iota_{X_z}\Omega = \beta_z$, for some fixed area form Ω. We will use the Euclidean area form $\Omega = dx \wedge dy = r dr \wedge d\theta$, but the choice is not important.

Definition 8.2. We call either β_z or X_z the *profile* of the singularity.

The condition that η be (positive) singular contact is

$$\eta \wedge d\eta = (\beta_z \wedge du_z + u_z d\beta_z - \beta_z \wedge \dot{\beta}_z) \wedge dz \geq 0, \tag{8.5}$$

where the overdot denotes differentiation with respect to z, and equality holds only along the line $0 \times S^1$ where η vanishes.

Definition 8.3. A chiral line singularity $\eta = \beta_z + u_z$ has a *uniform profile* if there exists an integer k such that, for each z, the 1-form β_z has a singularity of winding k.

Note that this is not the same as requiring each β_z is the same. This condition can also be defined for nonorientable lines, and precludes the phenomenon of changing from a $-\frac{1}{2}$ to a $+\frac{1}{2}$ winding around the line, which is common in nematics. For example, the disclination lines in the experiments described in Refs. [ČŽ13; ČDKŽ13],

which have a constant $-\frac{1}{2}$ profile, would be said to have a uniform profile in the language we employ here.

Simple examples can be generated by following the approach used in Chapter 6. Suppose we are given a smooth 1-parameter family of germs of 1-forms β_z, $z \in S^1$, on the disk. When does there exist a smooth family of germs of functions $u_z : D^2 \to \mathbb{R}$ such that $\eta = \beta_z + u_z dz$ is a chiral line singularity? First we will treat the case where β_z is closed. Since the disk is simply connected, there exists a smooth family of functions ϕ_z such that $\beta_z = d\phi_z$. We say such a family is *chiral* if there exist functions u_z such that $\eta = d\phi_z + u_z dz$. Then we have an analogy with Theorem 6.4 of Chapter 6.

Proposition 8.1. *A smooth family of germs of closed 1-forms $\beta_z = d\phi_z$, $z \in S^1$, is chiral if there exists a smooth family of Riemannian metrics g_z such that ϕ_z is harmonic with respect to g_z for each z.*

Proof. Suppose there exists a smooth family of Riemannian metrics g_z such that ϕ_z is harmonic with respect to g_z for each z. Then $d \star_z d\phi_z = 0$, where $\star_z$ is the Hodge star of g_z. Since the disk is simply connected, $\star_z d\phi_z = du_z$, for some functions $u_z : D^2 \to \mathbb{R}$. We can choose the family u_z so that it depends smoothly on z and such that $u_z + \dot{\phi}_z = 0$ at the origin of the disk. Let $\eta = d\phi_z + (u + \dot{\phi}_z)dz$. Then

$$\begin{aligned} \eta \wedge d\eta &= -d\phi_z \wedge d\dot{\phi}_z + d\phi_z \wedge (du + d\dot{\phi}_z), \\ &= d\phi_z \wedge \star_z d\phi_z, \\ &= \|d\phi_z\|^2_{g_z} \geq 0, \end{aligned} \tag{8.6}$$

with equality only on $0 \times S^1$. □

For example, consider $\phi = x^2 - y^2$. This is evidently harmonic with respect to the Euclidean metric on this disk, and we obtain chiral forms $\eta_\pm = xdx - ydy \pm xydz$ for both positive and negative singular contact structures.

Note that in general Proposition 8.1 does not 'perturb' the family of 1-forms $d\phi_z$ into a singular contact form as with point singularities, since there is no free parameter t that allows us to connect the chiral form to the achiral form via a homotopy. It is possible to realise the construction as a perturbation when the family of functions $\phi_z = \phi$ does not depend on z, i.e., the profile does not change along the line. In this case we may set $\eta = d\phi + tudz$ for a parameter t.

Observe that the chiral line singularities constructed in Proposition 8.1 are tight. The existence of tight chiral line singularities suggests the existence of a local invariant that does not exist for point singularities or achiral line singularities, by

analogy with layer numbers and the Thurston–Bennequin number. At first this may seem a little artificial, as the removable point singularities can also have tight neighbourhoods, but we will see that this still holds for actual disclinations.

Proposition 8.1 also implies the following, which does not follow the local description we are using in this section but is nonetheless worth mentioning.

Corollary 8.0.1. *Let $d\phi$ be an exact intrinsically harmonic 1-form on a contractible space, such that $d\phi$ that vanishes along a link L and at some points Σ. Then there exists a 1-form ν such that for $t > 0$ sufficiently small $\eta = d\phi + t\nu$ is singular contact with singularity set $L \cup \Sigma$.*

The winding around the singularities in this proposition can be any negative integer, but not a positive integer as then the function could not be harmonic.

For general 1-forms on the disk we have the following simple result, showing that any 1-form β on D^2 with a point singularity at the origin can be included into a chiral family β_z such that $\beta_0 = \beta$.

Proposition 8.2. *Let β be any 1-form on the disk with an isolated singularity at the origin. There exists a family of 1-forms β_z on the disk, $z \in S^1$, such that $\beta_0 = \beta$ and β_z, when regarded as a 1-form on $D^2 \times S^1$, defines a singular contact structure. This singular contact structure can be either positive or negative.*

Proof. Let γ be any 1-form such that $\beta \wedge \gamma \geq 0$, with equality only at the origin; to obtain γ, we may fix a metric g on the disk with area form Ω and let $\gamma = \iota_Y \Omega$, for Y the vector field orthogonal to the vector field X defined by $\beta = \iota_X \Omega$. Then for any integer $q > 0$ the family of 1-forms $\beta_z = \cos(qz)\beta - \sin(qz)\gamma$ is a positive singular contact form with the desired properties, while $\beta'_z = \cos(qz)\beta + \sin(qz)\gamma$ is a negative singular contact form. □

In the above proof, the integer q keeps track of how many times the profile rotates as we move along the line. For example, let $\beta_z = \cos(qz)(xdx+ydy)-\sin(qz)(xdy-ydx)$ for any integer $q > 0$. Then $-\beta_z \wedge \dot{\beta}_z = q(x^2+y^2)dx \wedge dy \wedge dz \geq 0$, and hence $\eta = \beta_z$ is a chiral line singularity. The profile has winding $+1$, and rotates q times as we track along the singular line. We can also have 1-forms $\eta_t = \beta + tudz$ that are singular contact and independent of z without β being closed; for example, $\beta = xdy - ydx$ and $u = x^2 + y^2$ gives a chiral line singularity of winding $+1$ with a fixed profile along the line.

Proposition 8.3. *We can realise any integer k as the winding around a singular line in a tight chiral line singularity.*

Proof. For $k \neq 0$, let $\beta = r\cos(k\theta)dx + r\sin(k\theta)dy$ and $\gamma = -r\sin(k\theta)dx + r\cos(k\theta)dy$, where x, y are Cartesian coordinates on the disk and r, θ are the associated polar coordinates. For $k = 0$, one may take $\beta = x^2dx - ydy$ and $\gamma = -x^2dy - ydx$. All chiral line singularities constructed this way are tight, as can be seen by, for example, looking at the dividing curve induced on any convex torus surrounding the line (see §8.3 below). □

Using the results of Chapter 6 we can also conclude that

Corollary 8.0.2. *If β is a closed 1-form on the disk and there exists a closed γ such that $\beta \wedge \gamma \geq 0$, vanishing only at the singular point, then $\beta_z = \cos(qz)\beta - \sin(qz)\gamma$ is a singular contact form whose Reeb field is tangent to the disks $D^2 \times z$.*

8.3 Convex Surfaces and Tight Chiral Line Singularities

To classify tight chiral line singularities, we need to understand the local structure on a torus T^2 surrounding the line, and also the local structure along a meridional disk. In the tight case, this information will be sufficient to completely determine the contact structure. The enclosing torus is embedded in a genuine contact structure, since we can obviously arrange for it not to intersect any singularities. Thus the usual convex surface theory for contact structures, §3.9, is sufficient to understand the behaviour of the singular contact structure near this surface. The actual structure of the characteristic foliations on the meridional disks was discussed in the previous section. We shall see however that the geometry of the characteristic foliation is irrelevent, an unsurprising assertion given the ideas of convex surface theory, and that one can introduce an analogue of convex surface theory for these disks.

Firstly, let us make an important observation that connects tightness to concrete physical properties of the director field. This also holds for the nonorientable case.

Proposition 8.4. *A chiral line singularity is tight if and only if it has uniform profile.*

Proof. Let ξ be a chiral line singularity defined by $\eta = \beta_z + u_z dz$, and suppose it is tight. Then, by Giroux's criterion, there exists a torus T surrounding the line singularity on which the dividing curve consists of some number of homotopically essential components. Via the relationship between the dividing curve and lines of singularities in the characteristic foliation described in §3.9, we may homotope the contact structure close to this boundary torus so that the dividing curve becomes

a curve of singular points. These are points where ξ is tangent to the boundary torus. Moreover, we can assume these lines are straight lines of some fixed slope. Now consider a meridional disk $D_z = D^2 \times z$. The boundary of this disk lies in T, and thus intersects the dividing curve some finite number, say k_z, times. Since the components of the dividing curve are straight lines of fixed slope, then the number k_z is actually independent of z. But this number determines the winding around the (unique, by the assumption we have close to the singular line) singular point of the 1-form β_z, and consequently each of these 1-forms has a singularity of the same winding, the definition of a uniform profile.

Conversely, suppose that ξ has a uniform profile. We can cut $D^2 \times S^1$ along a disk, say $D^2 \times 0$, to obtain a singular contact structure on $D^2 \times [0,1]$, which we also call ξ. Let $\eta = \beta_z + u_z dz$ define ξ. The condition that ξ has a uniform profile implies that there exists a constant k, such that on each disk D_z there are exactly k points where ξ is tangent to the boundary. Thus the lines of points on the boundary torus where ξ is tangent form some number of closed, homotopically essential, curves. Perturbing the surface, we make it convex with a dividing curve without nullhomotopic components, implying ξ is tight in a neighbourhood of that surface. Since this observation holds for any sufficiently small neighbourhood, we conclude that ξ is indeed tight. □

Let us move away from the setting of chiral line singularities for a moment, and turn to study the germs of singular contact structures with line singularities in the neighbourhood of a surface that intersects these singularities transversally, and establish some results analagous to those from convex surface theory. These results can of course be applied to the disks $D^2 \times z$ in our local trivialisation for chiral line singularities. The following lemma gives a singular version of a well-known fact about contact structures near surfaces.

Lemma 8.1. *Let S be a surface and X_0, X_1 a pair of vector fields on the disk with singularities at the points of a finite set Σ.*

1. *Let η_0, η_1 be two germs along S of singular contact structures with line singularities passing through all points of Σ, which induce the same characteristic foliation directed by X_0. Then η_0, η_1 are homotopic via a homotopy that fixes the singular lines.*

2. *If there is a homotopy X_t between X_0, X_1 through vector fields that vanish exactly at the points of Σ, and η_0, η_1 are germs along S of singular contact structures with line singularites that induce characteristic foliations directed by*

X_0, X_1 on S, then η_0 and η_1 are homotopic through singular contact structures via a homotopy that fixes Σ.

Proof. Statement (1) is proved the same way as for contact structures. Let η be a singular contact form on $S \times [-1, 1]$ and write $\eta = \beta_z + u_z dz$. The singular contact condition is

$$\beta_z \wedge du_z + u_z d\beta_z - \beta_z \wedge \dot{\beta}_z \geq 0. \tag{8.7}$$

This equation is linear in $\dot{\beta}_z$ and u_z. Therefore, convex combinations of solutions β_z, u_z that have the same β_0 are also solutions for sufficiently small z. Moreover, if the pair of solutions both vanish at Σ, then convex combinations of them will also. Consequently any pair of singular contact forms inducing the same characteristic foliation on $S \times 0$, i.e., the same β_0, will be homotopic through singular contact forms.

To prove statement (2), fix an area form Ω on the disk. We can write $\eta_j = \beta_j + u_j dz$, where $\beta_j = \iota_{X_j}\Omega$, $j = 1, 2$. We can find γ_i such that $\beta_j \wedge \gamma_j \geq 0$ except at the singular points, and by statement (1), we can homotope η_j into the singular contact form $\eta_j' = \cos(z)\beta_j + \sin(z)\gamma_j$, since these contact forms induce the same characteristic foliation on $S \times 0$. Let $\beta_t = \iota_{X_t}\Omega$, where X_t is the homotopy between X_0 and X_1. We can find a path γ_t such that $\beta_t \wedge \gamma_t \geq 0$. Then $\eta_t' = \cos(z)\beta_t + \sin(z)\gamma_t$ is the desired homotopy. □

As all singularities of winding k are homotopic to one another via homotopies that leave the singular point fixed—Arnold's classification [AGLV88] shows that they need not be diffeomorphic, but they are 'topologically equivalent' in the sense that the integral curves of one can be carried into the integral curves of another via a continuous map—it follows that there are no local (i.e., in a neighbourhood of a point) invariants of chiral line singularities except for the winding. Any further invariants must be defined in a neighbourhood of the entire line.

Now consider *vertically-invariant chiral line singularities*, those that can be defined by contact forms that are independent of the coordinate on S^1. These mimic the vertically-invariant contact forms that exist in a neighbourhood of a convex surface, Proposition 3.2.

Proposition 8.5. *For each integer k, there exists a germ of vertically-invariant singular contact form $\eta = \beta + u dz$ on the disk with line singularity passing through the origin, and such that β is a 1-form with a singularity of winding k.*

Proof. For $k < 0$, there exists a harmonic function ϕ_k, independent of z, such that $\beta = d\phi_k$ has a singularity of winding k, and the desired function u is obtained as in

Proposition 8.1.

For $k = 1$, we use $\eta = xdy - ydx - (x^2 + y^2)dz$. For $k > 1$, let $\beta = r\cos(k\theta)dx + r\sin(k\theta)dy$, where r, θ are polar coordinates on the disk. Define u by $d\beta = udx \wedge dy$; that is, u is the divergence of the vector field X directing the characteristic foliation with respect to the area form $\Omega = dx \wedge dy$. We compute that $u = (kr + 1)\sin((k-1)\theta)$ and

$$(ru)d\beta + \beta \wedge d(ru) = r((1-kr)\sin^2((k-1)\theta) + (k-1)(kr+1)\cos^2((k-1)\theta))\Omega \geq 0, \tag{8.8}$$

for r sufficiently small, with equality only at the origin. Then $\eta = \beta + rudz$ is the desired singular contact form. □

This proposition generalises somewhat, giving us an analogue of results from convex surface theory.

Theorem 8.1. *Let β be a germ of a 1-form on the disk with singularity of winding $k \neq 1$ such that the set $\Gamma = \{d\beta = 0\}$ consists of finitely many lines that meet at the origin and are transverse to the foliation defined by β. There exists a function u such that $\eta = \beta + udz$ is a germ of a vertically-invariant singular contact form, and u vanishes only on Γ.*

Proof. Fix an area form Ω, define X by $\iota_X\Omega = \beta$, and let u be defined by $d\beta = u\Omega$. By orientability we can choose γ such that $\beta \wedge \gamma \geq 0$, with equality only at the origin. Now consider $\eta = \beta + udz$. This is the desired singular contact form if

$$\eta \wedge d\eta = (u^2 - Y(u))\Omega \wedge dz \geq 0, \tag{8.9}$$

where Y is the vector field defined by $\iota_Y\Omega = \gamma$. By rescaling γ, we can assume this is positive everywhere except in a small neighbourhood of the collection of curves Γ where $u = 0$. Here, we need that $Y(u) \leq 0$, with equality only at the origin. These lines are the points where the divergence of X vanises, and Γ is transversal to the flow of X by assumption. Consequently, by modifying the vector field Y slightly in a neighbourhood of Γ if necessary, we may assume it points transversally through Γ as well, and is such that u is decreasing along the flow of Y, i.e. $Y(u)$ is non-positive. □

Note that all vertically-invariant singular contact structures can be realised as perturbations of an underlying foliation, simply by replacing the function u with tu, where $t \geq 0$ is a small parameter. For example, take $\beta = 2xydx + (y^2 - x^2)dy$ and $u = -x$. Then $ud\beta + \beta \wedge du = 4x^2dxdy - (x^2 - y^2)dxdy = (3x^2 + y^2)dxdy \geq 0$,

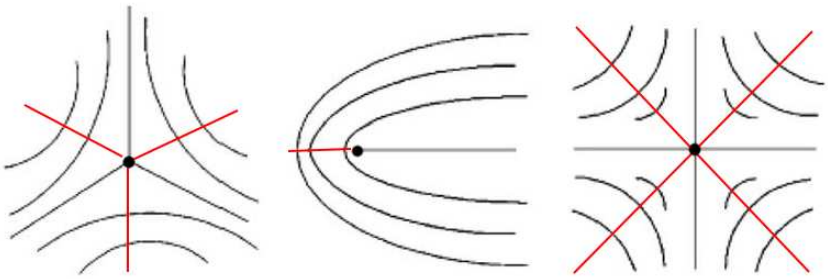

Figure 8.1: Examples of a dividing curve (red) for certain singularities on the disk. From left to right we have $k = -\frac{1}{2}, k = \frac{1}{2}, k = -1$. In each case, we see the dividing curve has $2|k-1|$ components.

so $\eta \wedge d\eta$ is a vertically invariant singular contact structure on $D^2 \times [-1,1]$ with a line singularity of winding $+2$ along $0 \times [-1,1]$. Since it does not depend on z, it evidently descends to a 1-form on the solid torus $D^2 \times S^1$, which is independent of the coordinate $z \in S^1$

We can use the ideas in the proof of Theorem 8.1 to adapt the notion of a dividing curve from convex surface theory to the singular case. Let $\mathcal{F}$ be a characteristic foliation on the closed disk with a singularity of winding $k \neq +1$ at the origin. A *dividing curve* for $\mathcal{F}$ is a collection of arcs Γ such that

1. Each curve in Γ begins on the boundary of the disk and terminates at the origin, and is transverse to $\mathcal{F}$ everywhere except at the origin.

2. There exists a vector field X directing $\mathcal{F}$ and a volume form Ω such that the function u defined by $u\Omega = d\iota_X\Omega$ vanishes only on Γ and changes sign as we cross Γ, and X flows from regions where $u > 0$ into regions where $u < 0$.

See Fig. 8.1 for examples of the dividing curve in the case of both orientable and nonorientable singularities.

Every foliation with a singularity of index $k \neq +1$ admits a dividing curve.

Lemma 8.2. *Let $\mathcal{F}$ be a germ of a foliation on the disk with a singularity of winding $k \neq +1$ at the origin. Let Γ be any set of curves on D^2 with the following properties:*

1. *Γ is transverse to $\mathcal{F}$,*

2. *Γ intersects every leaf except for $2|k-1|$ leaves $L_1, \dots L_{2|k-1|}$ which connect the origin to the boundary of the disk and divide the disk up into regions $S_1, \dots S_{2|k-1|}$,*

3. *There is exactly one component of* Γ *in each region* S_i.

Then Γ *divides* $\mathcal{F}$.

Proof. Condition (1) in the definition of the dividing curve is clearly satisfied by such a set of curves, so we only need to show we can choose a vector field X directing $\mathcal{F}$ so that it satisfies condition (2). Fix an area form Ω. For a generic choice of vector field directing $\mathcal{F}$, $u' = \operatorname{div}(X')$ vanishes on a set of curves Γ' that also satisfy the three conditions given in the statement of the lemma, for the same set of regions S_i. Consequently Γ' is isotopic to Γ via an isotopy ϕ_t that fixes the foliation $\mathcal{F}$ – we are just pushing Γ' along directions tangent to the leaves, and there is a single component of both Γ and Γ' in each S_j. Pushing X' along this isotopy results in another vector field X directing $\mathcal{F}$ such that $u = \operatorname{div}(X)$ vanishes on Γ. □

According to Theorem 8.1 we can use the dividing curve to define a vertically-invariant singular contact structure inducing $\mathcal{F}$. Continuing the strategy of generalising standard results about convex surface theory we have following result, similar in spirit to a result of Eliashberg: a tight contact structure on the 3-ball B is determined completely by the characteristic foliation on the boundary of the ball [Eli92].

Lemma 8.3. *Let* ξ_0, ξ_1 *be two tight singular contact structures on* $D^2 \times [-1, 1]$ *with the following properties:*

1. *Both* ξ_0 *and* ξ_1 *have a single line singularity of winding* $k \neq +1$ *along* $0 \times [-1, 1]$,
2. *The characteristic foliations induced by* ξ_0, ξ_1 *on each* D_z *have no singularities except at the origin,*
3. ξ_0 *and* ξ_1 *induce the same characteristic foliation on* D_{-1} *and* D_1 *and on* $\partial D^2 \times [-1, 1]$.

Then ξ_0 *and* ξ_1 *are homotopic relative to the boundary* $\partial D^2 \times [-1, 1]$.

Proof. Let us find a family of curves Γ_z that divide the characteristic foliations induced on D_z by both ξ_0 and ξ_1. By Lemma 8.2, it suffices for the family Γ_z to be transverse to both characteristic foliations and intersect all but $2|k - 1|$ leaves. Clearly we can arrange for this to be the case while also ensuring Γ_z depends smoothly on z. Once we have this family of curves, the proof works the same as Lemma 3.6, using Theorem 8.1 to provide the necessary vertically-invariant singular contact forms. □

8.4 Tight Chiral Line Singularities that are Orientable

In this section and the next section I describe the classification of tight chiral line singularities up to a homotopy through chiral line singularities. Here we will only treat the singularities that are orientable around a meridian, those that correspond to the element $1 \in \mathcal{Q}$ in the fundamental group of the order parameter space. Tight contact structures have invariants beyond the homotopy invariants, so it is reasonable to expect that the same is true for tight singular contact structures. It is sufficient to fix a dividing curve on the boundary rather than the exact characteristic foliation, Proposition 3.5. The dividing curve will consist of an even number of homotopically essential components, which we can regard as parallel lines of some fixed slope. The slope depends on a trivialisation of the torus, but as with the classification of tight contact structures on $T^2 \times [0,1]$ and $D^2 \times S^1$, the classification itself is independent of the trivialisation.

In order to see what slopes are possible I introduce a two-parameter family of tight chiral line singularities. Let $\beta_k = r\cos(k\theta)dx + r\sin(k\theta)dy$ and $\gamma_k = r\sin(k\theta)dx - r\cos(k\theta)dy$. These are 1-forms with a singularity of index $k \neq 0$. For each pair of integers $k \neq 0, q > 0$, define

$$\eta_{k,q} = \cos(qz)\beta_k + \sin(qz)\gamma_k, \tag{8.10}$$

For each k, define a singular contact form $\eta_{k,0}$ as in Proposition 8.5. Let $\xi_{k,q}$ be the singular contact structure on $D^2 \times S^1$ defined by $\eta_{k,q}$. The integer k is the *winding* and q the *twisting number* of $\xi_{k,q}$. The winding number is not a homotopy invariant of singular plane fields, as it can e possible to homotope between a winding of k and a winding of $-k$ depending on the value of q, as we shall demonstrate below. The twisting number is also not a homotopy invariant of singular plane fields, however we will show that it is a homotopy invariant of tight chiral line singularities. First note that we can rewrite $\eta_{k,q}$ in polar coordinates as

$$\eta_{k,q} = r\cos((k-1)\theta - qz)dr + r\sin((k-1)\theta - qz)d\theta, \tag{8.11}$$

when $q > 0$. This form makes it clear that $\eta_{k,q} \wedge d\eta_{k,q} = qr^2 dr\theta dz$. The characteristic foliation on the boundary of the tube is determined by the kernel of the 1-form

$$\alpha = \sin((k-1)\theta - qz)d\theta. \tag{8.12}$$

Consequently, the characteristic foliation has some number of lines of singularities that we call *Legendrian divides*. We refer to the nonsingular leaves as *Legendrian*

rulings. The Legendrian divides have a *slope* s that comes from them being isotopic to a linear curve $x + sy = 0$. The boundary is convex, and the dividing curve will be isotopic to the Legendrian divides, and therefore also consist of curves of slope s. After acting on the boundary by an element of $\mathrm{SL}(2, \mathbb{Z})$, we can assume that the Legendrian divides and the dividing curve have slope 0, i.e. are meridians, while the Legendrian rulings have slope $-s$. A foliation of the torus that has been put into this normal form is said to be in *standard form*. All these terms are in analogy with the terms used in classification of tight contact structures on the toric annulus and the solid torus, see §3.10.2—after a perturbation, the Legendrian divides become the dividing curve.

It remains to determine the number of divides and the slope. When $q \neq 0$, the slope of the divides will always be $s = \frac{1-k}{q}$. When $k = +1$, there are $2q$. Otherwise, for $k \neq 1, q > 0$, we may consider the number of components of the zero set that appear in a fundamental square $[0, 2\pi]^2$. There are $2q$ endpoints of zero lines on the line $E_1 = [0, 2\pi] \times 2\pi$ and $2|k-1|$ on $E_2 = 2\pi \times [0, 2\pi]$. A single line of slope $0 < \frac{p}{r} < 1$ beginning at $(0, 0)$ will pass through the line E_1 exactly r times as it wraps around the torus, while a line of slope $\frac{p}{r} > 1$ will pass through E_2 p times as it wraps around the torus. Therefore, when the slope is $s \neq 1$, the set of Legendrian divides has 2 components. Only when the slope is equal to 1, when we must have $|1 - k| = q$, do we have more than two components; in fact, we will have $2q$ components. See Fig. 8.2 for an example with $k = +2, q = 3$. When $q = 0$, there are $2|k-1|$ Legendrian divides with infinite slope, i.e. longitudes on the torus.

Notice that when $k = 0$ the divides have slope $1/q$. The $k = 0$ line case really corresponds, after a small perturbation, to a Legendrian curve with Thurston–Bennequin number q, and hence has the same slope as the local model for such a curve, see Ref. [Gei08].

Now that we have understood the slopes for our local models, we will show that, close to the boundary torus, these are the only possible models. Consider a general singular contact structure ξ, and a line singularity K in that contact structure. Suppose there is a neighbourhood of K in which ξ is tight. This implies there is a uniform profile along K, with some winding k.

Lemma 8.4. *In this situation, there is a torus T^2 surrounding K and an integer q such that the dividing curve such that the dividng curve induced on T^2 is the same as $\xi_{k,q}$.*

Proof. Begin by putting the boundary in standard form. Then we may choose a meridional disk D_0 whose boundary is a Legendrian ruling, which without loss of

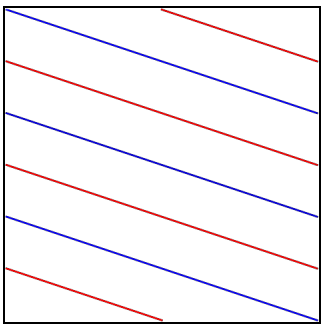

Figure 8.2: The dividing curve induced on a boundary torus by the contact structure $\xi_{+2,3}$. In the image the left and right sides should be identified, as should the top and bottom. The dividing curve has two components, shown in red and blue, and they have slope 1/3.

generality we will take to be the disk $D^2 \times 0$. The Legendrian divides on the boundary of the torus intersect ∂D_0 exactly at the places where the characteristic foliation on D_0 is tangent to ∂D_0. We can assume without loss of generality that the characterisic foliation has a single singularity of winding k at the origin where the disk intersects the singular line, and hence there are $2|k-1|$ such points, unless $k = +1$ and we have been unlucky enough to choose a disk on which the characteristic foliation contains a centre; this situation is non-generic, and hence we may replace D with a nearby disk. If we cannot find any disk where the singularity is not a centre, then we must be in the degenerate case where the characteristic foliation on the boundary torus is the same as for $\xi_{1,0}$. Otherwise, label the angles of these points θ_j, $j = 1, \ldots, 2|k-1|$. We may assume, via a homotopy near the boundary, that these are equally spaced.

Consider the family of disks $D_z = D^2 \times z$. Provided that $k \neq +1$, there are $2|k-1|$ points on the boundary where the characteristic foliation is tangent to the boundary, which we may label $\theta_j(z)$ in such a way that $\theta_j(0) = \theta_j$ for each j. There must be some number of points z_l, with $z_1 = 0$, such that $\theta_j(z_l) = \theta_j(0)$ for each l. If there are finitely many, say there are q such points. Otherwise, it must be the case that, for each j, $\theta_j(z) = \theta_j(0)$ for every z, and the slope of the Legendrian divides is infinite; we may take $q = 0$, and the lemma is true in this case.

Suppose we are not in this situation, so that the slope s of the dividing curves is rational, $s = \frac{p}{r}$ for some integers p, r. Then we claim that the Legendrian divides must have slope $\frac{1-k}{q}$. The follows from the observation that the spacing between the θ_j on a particular z level is (after a homotopy near the boundary) $2\pi/|1-k|$, and the fact that they make q full rotations. The number of components of the dividing curve follows from the argument we used for $\xi_{k,q}$.

Finally, we return to the case where $k = +1$. Generically there are no points $\theta_j(z)$ on the disk D_z where the characteristic foliation is tangent to the boundary, so that this can be assumed to hold on all but finitely many levels $z_1, \ldots, z_{2q}$, for some $q > 0$; it is clear that there are an even number of levels where this happens, as the direction of the characteristic foliation induced on the boundary torus reverses as we cross them. Then there will be $2q$ Legendrian divides of slope 0 on the boundary torus, the same as for $\xi_{1,q}$. □

Now we are in good shape to prove that the $\xi_{k,q}$ are an exhaustive list of the tight chiral line singularities. Suppose we fix an integer k to give the winding around a tight chiral line singularity. We also see that when $q > 0$, it serves as a genuine homotopy invariant of a tight chiral line singularity.

Theorem 8.2. *Let ξ be a singular contact structure containing a line singularity K with a tight neighbourhood, which has a winding k. Then there exists a neighbourhood $N \cong D^2 \times S^1$ of K and a nonnegative integer q such that ξ is homotopic to $\xi_{k,q}$ on N. Furthermore for any nonzero integers k, k' and nonnegative integers $q \neq q'$, the tight chiral line singularities $\xi_{k,q}$, $\xi_{k',q'}$ are not homotopic through any homotopy that leaves the singular line fixed, even if we do not require the boundary dividing curve to be fixed.*

Proof. First assume $k \neq +1$. By Lemma 8.4, there exists an integer q such that ξ induces a dividing curve of the same slope and number of components as $\xi_{k,q}$ on the boundary of a neighbourhood $N \cong D^2 \times S^1$. Since $\xi, \xi_{k,q}$ are both nonsingular in a neighbourhood of the boundary, by standard results of convex surface theory for contact structures we can make ξ and $\xi_{k,q}$ agree in a neighbourhood of the boundary. Let D be a meridional disk. By Lemma 8.1(2) and the fact that all singularities of winding k are homotoptic, we can arrange for ξ and $\xi_{k,q}$ to agree in a neighbourhood of this disk.

The part of the tube over which we have not yet constructed a homotopy between ξ and $\xi_{k,q}$ is a manifold diffeomorphic to $D^2 \times [-1, 1]$, and $\xi, \xi_{k,q}$ can be made to induce the same characteristic foliation on both D_{-1}, D_1, and $\partial D^2 \times [-1, 1]$. If $k \neq +1$, then we can apply Lemma 8.3.

Now we turn to the remaining case $k = +1$. From our observations so far, we know we can find at most finitely many z levels $z_1, \ldots z_q$ for which the characteristic foliation is purely radial, while on the other levels the characteristic foliation is either a centre, or a spiral. By reparameterising z if necessary, we can assume $z_1 = 0$ and the distance between z_j and z_{j+1} is $2\pi/q$. On each cylinder $C_j = D^2 \times [z_j, z_j + 1]$,

we can use Lemma 8.3 to deduce that $\xi|_{C_j}$ is homotopic to $\xi_{+1,1}|_{C_j}$ relative to the boundary. Consequently, ξ is homotopic to $\xi_{+1,q}$.

Now we turn to the second claim. A curve $\gamma : S^1 \to D^2 \times S^1$, $\gamma(t) = (0, 0, nt)$ for a positive integer n is Legendrian for the singular contact structure $\xi_{k,q}$ and has Thurston–Bennequin number nq (or $-nq$, depending on the sign of the singular contact structure). Moreover, if we are close enough to the line we can assume all closed, homotopically-essential Legendrian curves in these structures are homotopic through Legendrian curves to one of this type. Consequently, the smallest Thurston–Bennequin number a homotopically-essential Legendrian curve close to the line can attain is q. If $\xi_{k,q}$, $\xi_{k',q'}$ were homotopic, we would have a homotopy of the curve $\gamma(t) = (0, 0, 1)$ through Legendrian curves, where at one of the homotopy the Thurston–Bennequin number of the Legendrian curve would be q, and at the other end q', a contradiction. □

The statement that q is a homotopy invariant implies that one cannot identify distinct $\xi_{k,q}$ that induce the same dividing curve on the boundary, for instance $\xi_{-1,1}$ and $\xi_{-3,2}$ are not homotopic even though these two chiral line singularities induce the same dividing curve on a boundary torus and hence can be made to agree in the neighbourhood of that torus.

Generally k is not a homotopy invariant of the chiral line singularity, as the following proposition illustrates.

Proposition 8.6. *The negative chiral line singularities $\eta_{+1,0} = xdy - ydx - (x^2 - y^2)dz$ and $\eta_{-1,0} = xdx - ydy - 4xydz$ are homotopic. This also holds for the positive twist case.*

Proof. Let $\eta_t = \cos(t)\eta_{+1,0} + \sin(t)\eta_{-1,0}$, for $t \in [0, \pi/2]$. We easily compute that

$$\eta_t \wedge d\eta_t = -(4x^2 + 4y^2 + 2xy\sin(2t))dxdydz \tag{8.13}$$

I claim that the expression in brackets is strictly nonnegative. To see this, regard it as a quadratic equation in x. The zeros are readily computed using the quadratic formula, and occur at points for which

$$x = \frac{y}{4}(-\sin(2t) \pm \sqrt{\sin(2t) - 16}). \tag{8.14}$$

However, the expression under the square root is always negative, meaning the only roots of the quadratic are complex unless $x = y = 0$. It follows that η_t is a negative chiral line singularity for every t, and gives a homotopy between $\eta_{+1,0}$ and $\eta_{-1,0}$. □

This takes care of the situation where the singular line is orientable about both the meridian and the longitude. To complete the classification of defect lines of type $1 \in \mathcal{Q}$, it remains to consider the case when the chiral line singularity is not orientable along a longitude. Any nonorientable plane field on $D^2 \times S^1$ that falls into this class can be defined by taking a 1-form η on the cylinder $D^2 \times [0,1]$ such the kernels of $\eta|_{D^2 \times 0}$ and $\eta|_{D^2 \times 1}$ agree as nonoriented plane fields, and then identifying $D^2 \times 0$ with $D^2 \times 1$. In fact, it obviously suffices that the characteristic foliations on $D^2 \times 0$ and $D^2 \times 1$ agree as nonoriented line fields. We can again use the models $\eta_{k,q}$ for k an integer and q a fraction. The allowed fractions are dependent on the winding k.

Firstly, assume $k < 0$. Without loss of generality, we consider the maximally symmetric form of an index k singularity, so the characteristic foliation has $2|k|$ 'spokes' coming out of the singularity, as discussed previous. Thus it is invariant under a rotation by $\frac{2\pi}{2|k|}$. It follows that we can take $q \in \frac{1}{2|k|}\mathbb{N}$. When $k > +1$, the situation is similar: we can take $q \in \frac{1}{2(k-1)}\mathbb{N}$. For $k = 1$, we need $q \in \frac{1}{2}\mathbb{N}$. To prove Theorem 8.2 for these singularities, it suffices to pull back the nonorientable contact structure to an appropriate cover so that it becomes nonorientable, e.g. when $k < 0$ we can pullback to a $2|k|$ cover with covering map $(x, y, 2|k|z) \mapsto (x, y, z)$.

8.5 The Homotopy Classification of Tight Disclination Lines

Now we consider the homotopy classification of tight chiral line singularities that are not orientable around the meridian, corresponding to disclination lines of type $i \in \mathcal{Q}$ in a cholesteric. The ideas of §8.3 are still true for nonorientable singularities, and Proposition 8.4 also holds. As with the orientable case, we can have any kind of profile.

Lemma 8.5. *Let $\mathcal{F}$ be a germ of a nonorientable singular foliation on the disk divided by a curve Γ. Then there exists a germ of a singular contact structure in a neighbourhood of the disk with a line singularity through the origin inducing that characteristic foliation.*

Proof. We can cover the disk with open sets U_i and choose local vector fields X_i directing $\mathcal{F}$, with transition functions given by a sign flip. We can choose this cover so that each component of Γ lies in exactly one U_i. Fix an area form Ω and let $u_i = \operatorname{div} X_i$. Applying Theorem 8.1 to each U_i yields a contact form $\eta_i = \beta_i + u_i dz$, where $\beta_i = \iota_{X_i}\Omega$. The vector field $u_i X_i$ agrees with $u_j X_j$ on the intersection U_{ij} up

to a sign flip, and hence we can glue the singular contact structures defined by the η_i to form a singular contact structure in the neighbourhood of the disk. □

First consider the case where the disclination is orientable along the longitude. We have models defined locally by 1-forms[1] $\eta_{k,q} = \cos(qz)\beta_k + \sin(qz)\gamma_k$ with $k \in \mathbb{Z} + \frac{1}{2}$ and a nonzero integer q. Convex surfaces are defined for nonorientable contact structures as well, except the number of components of the dividing curve does not have to be even, because it no longer separates regions where the divergence of the (nonorientable) characteristic foliation takes opposite signs. The pattern of slopes and number of dividing curves induced by $\eta_{k,q}$ are computed as in the orientable case. In particular, the situation for $\xi_{1/2,q}$ and $\xi_{-1/2,q}$ is as follows.

1. For $k = +\frac{1}{2}$, there is a single Legendrian divide with slope $\frac{1}{2q}$, which we regard as infinite slope when $q = 0$.

2. For $k = -\frac{1}{2}$, the Legendrian divides have slope $\frac{3}{2q}$, which is again infinite when $q = 0$. There is a single Legendrian divide, except when $q = 3$ when there are 3 Legendrian divides.

The existence of a dividing curve for the nonorientable characteristic foliation on disks D_z is evident, see Fig. 8.1. To prove Theorem 8.2 in the nonorientable case we follow the same arguments as in the orientable case, as it only requires the existence and uniqueness of vertically-invariant contact forms in a neighbourhood of the surface.

There is one final remark to make concerning the $q = 0$ case for $k = \pm\frac{1}{2}$. Here, the Legendrian divides are the same. Consequently, $\eta_{+1/2,0}$ and $\eta_{-1/2,0}$ are homotopic in a neighoburhood of the boundary torus. In fact, we can check that $\eta_t = \cos(t)\eta_{+1/2,0} + \sin(t)\eta_{-1/2,0}$, $t \in \left[0, \frac{\pi}{2}\right]$ is a homotopy through singular contact forms that leaves the dividing curve on the boundary fixed. To see this, note that by Proposition 8.5 we may take $\eta_{k,0} = \cos(k\theta)dx + \sin(k\theta)dy - k\sin((k-1)\theta)dz$, for $k = \pm\frac{1}{2}$. Then we compute that

$$\begin{aligned}\eta_t \wedge d\eta_t = \frac{1}{2}\left(\sin^2(\theta/2) + r(r+1)\cos^2(\theta/2)\right) + \frac{3}{2}\left(\sin^2(3\theta/2) + r(r+1)\cos^2(3\theta/2)\right) \\ + \frac{1}{4}\sin(2t)\sin(\theta/2)\sin(3\theta/2),\end{aligned} \tag{8.15}$$

which is nonnegative. Thus η_t defines a homotopy between $\xi_{+1/2,0}$ and $\xi_{-1/2,0}$ such that, one any boundary torus, the characteristic foliation is divided by the same

[1] Of course these are not 1-forms in the usual sense, however we can regard them as sections of the projectivised cotangent bundle $\mathbb{P}T^*D^2 \times S^1$.

curve for each t. We can regard this is a local homotopy that may be used to change the winding around a disclination line from $+\frac{1}{2}$ to $-\frac{1}{2}$ via purely local modifications, whislt keeping the neighbourhood of the line chiral. Such transitions

Now we treat the case where the disclination is not orientable along a longitude. Any nonorientable plane field on $D^2 \times S^1$ that falls into this class can be defined by taking a 1-form (again, a section of the projectiveised cotangent bundle) η on the cylinder $D^2 \times [0,1]$ such the kernels of $\eta|_{D^2 \times 0}$ and $\eta|_{D^2 \times 1}$ agree as nonoriented plane fields, and then identifying $D^2 \times 0$ with $D^2 \times 1$. In fact, it obviously suffices that the characteristic foliations on $D^2 \times 0$ and $D^2 \times 1$ agree as line fields. We can again use the models $\eta_{k,q}$ with q a fraction. The allowed fractions are dependent on the winding k: for $k = -\frac{2m+1}{2}$ and m non-negative, there are $2m+3$ 'spokes', and hence we can take $q \in \frac{1}{2m+3}\mathbb{Z}$. When $k > 0$, then the structure of the singularities means that only integer rotations bring the profile back to itself, and hence there are no additional examples.

It is worth making a few remarks on the actual geometry of disclination lines. The invariant q can readily be interpreted as a self-linking number, and we can choose a framing of the line that corresponds to this self-linking number, turning it into a ribbon which has both writhe and twist, related by the Călugăreanu theorem [Cě61; ČŽ11a; ČŽ11b],

$$q = \mathrm{Tw}(K) + \mathrm{Wr}(K). \tag{8.16}$$

The geometric twist of the ribbon is coupled to the twist elastic distortion, and consequently we expect it to be be largely determined by q_0. Since the twisting number q of the line is essentially fixed, requiring the director to overcome a large energy barrier (of order $K_2 q_0^2$) to change, this means that any disparity will have to be met by introducing writhe.

This restriction leads to an instability of $+\frac{1}{2}$ disclinations that is similar in spirit to the buckling of an elastic column. Consider a cell of cholesteric material whose height h is equal to the cholesteric pitch, and suppose that there is a straight disclination line of self-linking number $q > 1$ stretching between the top and bottom surfaces of the cell, where the director is fixed. The self-linking number sets a preferred length qh for the disclination. Since the self-linking number is fixed, the director can only alleviate this geometric frustration while preserving the condition $\mathbf{n} \cdot \nabla \times \mathbf{n} \neq 0$ is for the line to convert twist into writhe by coiling up into a helix, thereby extending its length, which is shown for an $\mathbf{n}_{+1/2,2}$ disclination in Fig. 8.3(b). Interestingly, we do not observe this for the $\mathbf{n}_{-1/2,2}$ disclination, which

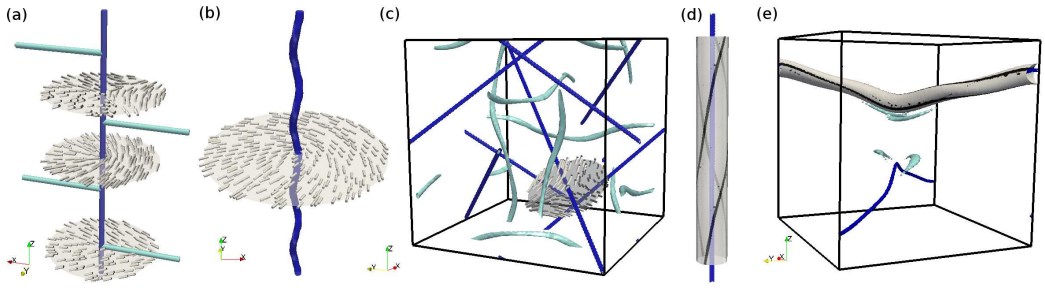

Figure 8.3: Examples of disclinations in cholesterics. (a) Overtwisted disclination line (dark blue) attached to four λ lines (light blue tubes) The director is shown on several transverse slices. (b) Tight disclination line $\mathbf{n}_{1/2,2}$ in a cell with fixed boundary conditions. The cell height is chosen to be equal to one cholesteric pitch p, while the self-linking number of 2 for the line gives an energetic preference for a length of $2p$. This geometric frustration is relieved by converting twist into writhe, and the line coils up into a helix, increasing its length. (c) Disclinations and λ lines in the O8$^-$ blue phase. We show the director on a cross section of a disclination. (d) Each disclination is tight and of type $\mathbf{n}_{-1/2,2/3}$, as seen from the the dividing curve (black) on a convex torus around the line. (e) Blue phase O2 with broken symmetry. There are four $\lambda^{-1/2}$ lines attached to the dislinations. The dividing curve is shown on a neighbourhood of a disclination, which illustrates that it is tight. It is equivalent to the model $\mathbf{n}_{-1/2,2/3}$.

remains straight.

The classification scheme can be applied to the disclination lines in the blue phases. Examination of the O8$^-$ blue phase, Fig. 8.3(c), shows that none of the disclination lines are tethered to λ lines, and are therefore tight. This is also seen by an examination of the dividing curve on a convex torus around the disclination, Fig. 8.3(d). By inspection, we find that both disclinations are of the type $\mathbf{n}_{-1/2,2/3}$. The O8$^+$ and BPX structures also contain only tight disclination lines of type $\mathbf{n}_{-1/2,2/3}$. Most interesting is the O2 blue phase, which has cubic symmetry. There are four segments of disclination line meeting at centre of the box, each with a profile $-\frac{1}{2}$, and additionally four λ lines also meeting at the centre of the structure. This highly-degenerate situation falls outside of our classification results, which assume that a disclination has a tubular neighbourhood free of defects. By breaking the symmetry of the phase, for instance by applying an electric field, we split the structure into a pair of disclinations. The director is then chiral throughout, the disclination lines are tight and of type $\mathbf{n}_{-1/2,2/3}$, Fig. 8.3(e). Note that the λ lines do terminate on the disclination lines, but they are $\lambda^{-1/2}$ lines and therefore do not violate the tightness constraint, as seen from an examination of the dividing curve.

8.5.1 Summary of the Classification of Tight Chiral Line Singularities

To summarise, we have a collection of models $\eta_{k,q}$ for chiral line singularities with k, q as below:

1. $k \in \mathbb{Z}$ and $q \in \mathbb{Z}, q \geq 0$.
2. $k = \frac{2m+1}{2}, m \in \mathbb{Z}$ and $q \in \mathbb{Z}, q \geq 0$.
3. $k \in \mathbb{Z}$ and $q \notin \mathbb{Z}$, $q \in \frac{1}{2(k-1)}\mathbb{N}$ for $k > +1$, $q \in \frac{1}{2|k|}\mathbb{N}$ for $k < 0$, $q \in \frac{1}{2}\mathbb{Z}$ for $k = 0, 1$.
4. $k = -\frac{2m+1}{2}, m \in \mathbb{N}$ and $q \notin \mathbb{Z}$, $q \in \frac{1}{2m+3}\mathbb{Z}$.

The general classification theorem is as follows.

Theorem 8.3. *Every chiral line singularity is homotopic to $\xi_{k,q}$, with k, q, with the permissable values of k, q as given above. In each case, the value of q is a homotopy invariant.*

Finally, let us note which Jänich index ν each nonorientable chiral line singularity corresponds to. To do this, we write

$$\eta_{k,q} = \cos\left(\left(m - \frac{1}{2}\right)\theta - qz\right) dr + \sin\left(\left(m - \frac{1}{2}\right)\theta - qz\right) d\theta, \tag{8.17}$$

to see the correspondence with Jänich's model, where m is defined by $k = (2m+1)/2$. Let us take $m = 0$, for a $+\frac{1}{2}$ disclination. Then

$$\eta_{k,q} = \cos\left(\frac{\theta}{2} + \frac{2qz}{2}\right) dr - \sin\left(\frac{\theta}{2} + \frac{2qz}{2}\right) d\theta, \tag{8.18}$$

If q is an even multiple of its smallest nonzero value then the line is orientable along a longitude, and if it is an odd multiple then it is not. For example, for a $k = -\frac{1}{2}$ disclination, odd multiples of $\frac{1}{3}$ give lines that are not orienatable along a longitude, while even multiples of $\frac{1}{3}$, including $q = 0$, give lines orientable around a longitude. This gives one $\mathbb{Z}_2$ part of the Jänich index. The other $\mathbb{Z}_2$ part, whether or not the line carries a charge, is determined by $2\lfloor q \rfloor \mod 4$, which is the same as $\lfloor q \rfloor \mod 2$. Thus it is possible to have tight disclinations in each of the different homotopy classes of disclinations, in contrast to the situation for nonsingular contact structures, where tight structures only appear in the zero homotopy class of plane fields on S^3 and T^3.

8.6 Edge Disclocations, λ Lines, and Overtwistedness

8.6.1 The Classification of Overtwisted Chiral Line Singularities

So far, I have only given examples of tight chiral line singularities. Proposition 8.4 implies that any overtwisted chiral line singularity $\eta = \beta_z + u_z$ must have changes in the profile. Let us take a look at a simple example of a change in profile from $+1$ to -1. Consider the following pair of 1-forms,

$$\begin{aligned} \beta &= xdy - ydx - (x^2 - y^2)dz, \\ \gamma &= xdx - ydy - 4xydz. \end{aligned} \tag{8.19}$$

These are, up to homotopy, just $\eta_{+1,0}$ and $\eta_{-1,0}$ from the classification of (negative) tight chiral line singularities. Define $\omega = \cos(z)\beta + \sin(z)\gamma$. We compute that

$$\omega\wedge d\omega = \cos^2(z)\beta\wedge d\beta+\sin^2(z)\gamma\wedge d\gamma+\cos(z)\sin(z)(\beta\wedge d\gamma+\gamma\wedge d\beta)+\beta\wedge\gamma\wedge dz. \tag{8.20}$$

The terms are easily computed. Firstly, $\beta\wedge d\beta+\gamma\wedge d\gamma = -4(x^2+y^2)dxdydz$. Then, we compute that

$$\begin{aligned} \beta \wedge d\gamma + \gamma \wedge d\beta &= -4xydxdydz, \\ \beta \wedge \gamma \wedge dz &= (y^2 - x^2)dxdydz. \end{aligned} \tag{8.21}$$

Then we conclude that

$$\omega \wedge d\omega = (-5x^2 - 3y^2 - 2\sin(2z)xy)dxdydz. \tag{8.22}$$

To see that ω is a chiral line singularity, argue as in Proposition 8.6 and regard the expression in brackets as a quadratic equation in x. The zeros occur at points for which

$$x = \frac{y}{5}(-\sin(2z) \pm \sqrt{\sin^2(2z) - 15}). \tag{8.23}$$

As before, the expression under the square root is always negative, meaning the only roots of the quadratic are complex unless $x = y = 0$. It follows that ω is a chiral line singularity.

The characteristic foliation induced on a torus of radius R around the line is directed by the vector field

$$X = R(\cos(z) + 2\sin(z)\sin(2\theta))e_\theta + (\cos(z) - \sin(z)\sin(2\theta))e_z \tag{8.24}$$

There are multiple singularities, implying that the contact structure in a neighbourhood of this torus is overtwisted, exactly as we expect from Proposition 8.4. These

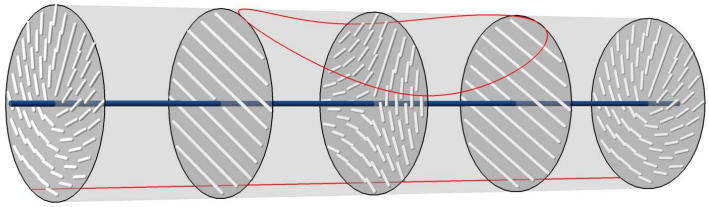

Figure 8.4: Dividing curve (red on a convex torus surrounding an overtwisted chiral line singularity (blue). The projection of the director into the surface changes from a $\frac{1}{2}$ singularity to a $-\frac{1}{2}$ singularity and back again, leading to a closed component of the dividing curve. In between these two different windings there must be a disk where the projection of the director into the disk has a singularity of winding 0.

singularities occur on z-levels where $\cos(z) = 0$,at the points $\theta = 0, \pi$. One can send $z \mapsto qz$ to get an examples with additional λ lines.

We can do the same thing with $\eta_{\pm 1/2,q}$ to produce overtwisted disclination lines, see Fig. 8.3(a) for a simulation and Fig. 8.4 for a schematic of the dividing curve.

There is an h-principle for the overtwisted singular contact structures, i.e. that the homotopy classification of overtwisted chiral line singularities reduces to the homotopy classification of germs of singular plane fields. I prove this for both point and line singularities. A germ at a point (resp. a line) of an overtwisted singular contact structure ξ is a plane field on the 3-ball B (resp. the solid torus $D^2 \times S^1$).

Theorem 8.4. *(Local h-principle for overtwisted singular contact structures) A germ of an overtwisted chiral point (resp. line) singularity ξ is determined up to homotopy through germs of chiral point (resp. line) singularities by its homotopy class as a germ of a singular plane field. In the line singularity case, there is a unique up to homotopy overtwisted chiral line singularity for each Jänich index.*

Proof. Removing the singularity itself, we can view ξ as a nonsingular plane field on $S \times [\epsilon, 1]$, where S is the 2-sphere for a point singularity and the 2-torus for a line singularity, and $\epsilon > 0$. The contact structure is determined by the dividing curves Γ_z induced on the levels $S \times z$, where z is the coordinate on $[\epsilon, 1]$, which we can assume to be convex. Moreover, since we dealing with germs, we can also assume that the dividing curves Γ_z form a smooth 1-parameter family, as is described in the uniqueness result, Lemma 3.6. For S the sphere, the homotopy class of the plane field is determined by the index of the singularity, equivalently the number of components of the dividing curve and the assigment of signs to the different regions (to

distinguish index $+1$ from -1, etc). We can apply the usual h-principle of Eliashberg to conclude that for any ϵ, ξ is homotopic through overtwisted contact structures to some model overtwisted contact stucture ξ_k that would have a singularity of index k at the origin, say the one produced by taking the appropriate harmonic function as the local structure. Moreover, we still have this homotopy when we take the limit $\epsilon \to 0$, as there is a unique way to extend the homotopy over the origin, by having it be fixed there.

For line singularities, the homotopy class of a line singularity is determined by the Jänich index ν. To produce an example in each class, observe that we can produce a $\nu = 0$ examples by taking $\omega_0 = \cos(z)\eta_{+1/2,0} + \sin(z)\eta_{-1/2,0}$. Then we produce examples ω_ν for each ν by cutting the line somewhere in the segement where the profile is $-1/2$ and inserting a segment of the form $\eta_{-1/2,q}$ for some $q \in \frac{1}{3}\mathbb{Z}$. Taking q so that it is not an integer will lead us to the class $\nu = 1$, and taking $1 < q \leq 2$ will allow us to reach the classes $\nu = 2$ and $\nu = 3$ depending on whether we take it to be an integer or not. This illustrates that there is an overtwisted chiral line singularity in each class. To show it is unique, we run the same argument just given for the point defect case. □

8.6.2 Creating Edge Dislocations

Let us briefly examine how to about changing the invariants k, q in either an orientable or nonorientable tight chiral line singularity $\eta_{k,q}$. Proposition 8.4 implies that this must involve changing the profile on some meridional disk. In the case of nonorientable singularities, we rotate the director out of the plane of a disk to change the winding of the singularity in the characteristic foliation from $+\frac{1}{2}$ to $-\frac{1}{2}$, or vice-versa. Consider the impact on a neighbourhood of a meridional disk $D_z := D^2 \times z$ on which we make this change. A $+\frac{1}{2}$ singularity has a dividing curve with one component. Rotating the director out of plane so that the singularity has $-1/2$ produces two new components of the dividing curve. This also impacts the dividing curve on a convex boundary torus T^2. In a neighbourhood of the disk where we have modified the director, the dividing curve has picked up two new components. Since we only modifed the director near a disk, these must close up into a circle.

This implies (via Giroux's criterion) that the resulting singular plane field, if it were contact, would be overtwisted. Consequently, we see that this modifcation must introduce regions of reversed handedness, else we would have produced a homotopy between a tight and an overtwisted contact structure. Moreover, the fact that the value of the Euler class of the plane field on T^2 is now nonzero implies that there must be λ lines. Generically, this homotopy will produce a pair of λ lines, one

with winding $+\frac{1}{2}$ and another with winding $-\frac{1}{2}$. The structure of this pair is exactly the structure of an edge dislocation, as described previously in §3.9 and §5.5.3.

In the cholesteric ground state in T^3, the creation of edge dislocations allows us to change the layer number at the cost of introducing regions of reversed handedness. This is done by creating the pair of λ lines, moving them in opposite directions around a homotopically essential cycle, and finally annihilating them again on the other side. For the contact structures $\xi_{k,q}$, we can condier the effect of creating an edge dislocation and moving the resulting pair of λ lines around either the meridional or longitudinal cycles on a boundary torus. In the latter case, creating the edge dislocation changing the winding number around the line to be $-k$ in a neighbourhood of some disk, and the effect of moving the λ lines around the longitudinal cycle is to increase the size of this neighbourhood. Once they annihilate again, the winding will have changed along the entire line. The result of moving these lines around a meridional cycle is to change the twisting number q by 1.

I emphasise that it is not *a priori* clear if the singular plane fields that result from these processes are actually singular contact, or if there are regions of reversed handedness, nor is it clear whether, in the latter situation, the regions of reversed handedness can be removed via some local operation. Moreover, the process of creating the edge dislocation is evidently not local, so something must happen away from the disclination line. The homotopy theory suggests one possible way in which this operation can be performed is to pass a second disclination line through the one we are considering, which must result in at least one λ line of positive winding and hence a change of profile, and then we would not worry about global constraints: the new λ line simply terminates on the second disclination.

These fundamental questions are part of a larger problem, the problem of understanding how topological invariants change in liquid crystal materials and the interaction this has with geometry and with chirality. Answering this question in totallity is beyond the scope of this thesis and will be addressed in future work.

8.7 Removing Orientable Chiral Line Singularities

In a nematic, an orientable singular line with $\nu = 0$ is removed by 'escape into the third dimension'; we homotope the local structure of the line in a neighbourhood diffeomorphic to $D^2 \times S^1$ so the the director is tangent to the surfaces $D^2 \times z$, and then add a small component along the S^1 factor, which removes the singulaity. In this section I investigate the possiblity of doing this to a tight chiral line singularity when one also requires that the resulting plane field be contact. In some cases

tightness will be preserved, in other cases, notably if the winding around the line is $+1$, chirality can be preserved but tightness will not be.

Let $\eta_{k,q}$ be the germ of a singular contact form along an orientable line singularity, according to the classification result of Theorem 8.2. Conveniently this director is already 2-dimensional, at least when $q > 0$. We capture the notion of escape into the third dimension in the following definition.

Definition 8.4. An *escape* of $\eta_{k,q}$ is a 1-form $\bar{\eta}_{k,q} = \tilde{\eta}_{k,q} + t\omega$ on $D^2 \times S^1$ such that

1. $\tilde{\eta}_{k,q}$ is homotopic to $\eta_{k,q}$ through chiral line singularities,
2. $\bar{\eta}_{k,q}$ is a nonsingular contact form for all $t > 0$ sufficiently small,
3. $\omega|_{\partial D^2 \times S^1} = 0$,
4. The singular line $0 \times S^1$ is a transverse curve of the contact structure defined by $\bar{\eta}_{k,q}$ for $t > 0$ sufficiently small.

Observe that, for t sufficiently large, we could take any contact form $\omega = \alpha + udz$ with $u(0, z) \neq 0$ and this would satisfy the above conditions; the challenge is to find a 1-form so that $\bar{\eta}_{k,q}$ becomes nonsingular and contact for all $t > 0$.

Firstly, consider the case where $k = +1$. The simplest situation is where the twisting number q vanishes, and along the singular line the singular contact form is homotopic to the 1-form $\eta_{1,0} = rd\theta - r^2dz$ in cylindrical coordinates on $D^2 \times S^1$. We can escape this by taking $\omega = (1 - r^2)dz$. Furthermore, escape is possible for $k = -1, q = 0$ as well: $\eta_{-1,0}$ is homotopic to $\tilde{\eta}_{-1,0} = xdx + (x - y)dy + \frac{r^2}{4}dz$, which we can also escape by taking $\omega = (1 - r^2)dz$, and the resulting Reeb field also has the line $r = 0$ as a periodic orbit.

Now, we see that escape is impossible for $k = +1, q > 0$.

Proposition 8.7. *There is no escape of $\eta_{+1,q}$, for any $q > 0$.*

Proof. Since an escape of $\eta_{1,q}$ does not change the characteristic foliation on $D^2 \times z$ near the boundary, we cannot remove the singularity from the characteristic foliation on any disk $D^2 \times z$ by this process. For $q > 0$, the characteristic foliation on some of these disks $D^2 \times z$ contains a radial singularity such that the divergence of the vector field directing the characteristic foliation vanishes there. After any small perturbation of $\eta_{1,q}$ there will still be some nearby disks with this property. Theorem 3.2 implies this cannot happen in a contact structure. □

Consequently, we cannot escape a singular line with $+1$ winding without introducing regions of reversed handedness that prevent the resulting plane field from being

contact; the consequences of this will be discussed further in Chapter 9. This gives a contact topological interpretation of a well-known fact: one cannot convert a χ line into a λ line [BMČ$^+$14]. Alternatively, instead of escaping in a fixed direction one can alternately escape up and down, replacing the singular line with a series of chiral point singularities of alternating index on the surfaces where the characteristic foliation has a centre singular point, creating a singular contact structure with singularities of a higher codimension.

The proof of Proposition 8.7 extends to the general case of winding k. Theorem 3.2 implies that no characteristic foliation on a surface in a contact manifold ever has a singularity at which the divergence vanishes. Except in certain cases, the 1-forms $\eta_{k,q}$ induce such 'bad' singularities on transverse disks, and this property cannot be destroyed by a small perturbation because, while it the nonvanishing of the divergence at critical points is generic for a single vector field, it is not generic in one parameter families.

Theorem 8.5. *The is no escape of $\eta_{k,q}$ except in the cases $k = +1, q = 0$, $k = -1$, and $k = 0$.*

The natural question then is to ask whether it is possible to break apart the degenerate line singularities and escape at the same time, in such a way that we end up removing the singular line, a process that yields a contact structure with some number of transverse curves, of winding equal to ± 1.

Proposition 8.8. *For each $k \neq 1, q \geq 0$ there exists a perturbation of $\eta_{k,q}$ such that the resulting 1-form is nonsingular and induces a characteristic foliation on each $D^2 \times z$ where the divergence is nonzero at the singularities.*

Proof. This follows from the fact that singularities can be decomposed into a set of Morse singularities. We can do this splitting for each z. Since the characteristic foliation depends smoothly and periodically on z, we can obviously arrange for the splitting to depend smoothly and periodically on z as well. □

Note that we have not asked that the perturbed 1-form be contact in this proposition, only that it induce the same kinds of characteristic foliations that a contact structure would. To show we can do this splitting so that the resuling structure is contact, we modify the argument in Lemma 3.6. Fix a surface S.

Proposition 8.9. *Let ξ be a (possibly singular) plane field on $S \times [0, 1]$ or $S \times S^1$ such that there is a smooth family of curves Γ_z that divide the characteristic foliation induced by ξ on each $S \times z$. Moreover, suppose that ξ is defined by a 1-form $\omega =$*

$\beta_z + v_z dz$ *with* $\beta_z \wedge \dot{\beta}_z \leq 0$. *Then* ξ *is homotopic to a (nonsingular) contact structure that induces the same characteristic foliation on each* $S \times z$.

Proof. Let β_z be a smooth family of 1-forms defining the characteristic foliations induced by ξ on $S \times z$. By Proposition 8.5, there is a smooth family of functions u_z such that

$$A_z := u_z d\beta_z + \beta_z \wedge du_z > 0. \tag{8.25}$$

Let $\eta = \beta_z + tu_z dz$. Then, by the assumption $\beta_z \wedge \dot{\beta}_z < 0$, we have $\eta \wedge d\eta = (tA_z - \beta_z \wedge \dot{\beta}_z) \wedge dz > 0$. That ξ is homotopic to the contact structure defined by η follows from the same argument used in Lemma 3.6. □

Therefore, to remove the degenerate singular lines we need only unfold them so that the resulting family of characteristic foliations are z-periodic and otherwise satisfy the conditions of Proposition 8.9. Before turning to the general discussion, consider the $+2$ disclination line $\eta_{2,q}$, $q > 0$, as an example. The desired unfolding of the $+2$ singularity is given by $\bar{\beta} = \beta + R^2 \sin(2qz)dx + R^2 \cos(2qz)dy$ and $\bar{\gamma} = \star\bar{\beta}$ for $R \geq 0$ small and $\star$ the Hodge star operator of the Euclidean metric on $D^2 \times S^1$. Then set

$$\alpha_z = \cos(qz)\bar{\beta} - \sin(qz)\bar{\gamma}. \tag{8.26}$$

Note that $\alpha_z \wedge \dot{\alpha}_z = -q\bar{\beta} \wedge \bar{\gamma} = -q \left\|\bar{\beta}\right\|^2 \leq 0$. The singularities of α are at $(R\cos(qz), -R\sin(qz), 0)$ and $(-R\cos(qz), R\sin(qz), 0)$, and the characteristic foliation has a singularity there of radial type. There exists a dividing curve for such as foliation, and since the characteristic foliation depends smoothly on z we can take the dividing curve so that it too depends smoothly on z. Thus we can apply Proposition 8.9 in this case.

Concretely, we take $u_z = 4(-\cos(qz)x + \sin(qz)y)$. This function is defined by $d\alpha_z = u_z dx \wedge dy$, where α_z is regarded as a 1-form on the disk $D^2 \times z$, and it is positive at one singularity of α_z and negative at the other, and it vanishes along the straight line $x = \tan(qz)y$, which divides the characteristic foliation on each z level. Let $\eta = \alpha_z + tu_z dz$, for $t \geq 0$. This is a non-vanishing 1-form. We see that

$$u_z d\alpha_z + \alpha_z \wedge du = u_z^2(\bar{\beta}_x^2 + \bar{\beta}_y^2) + \bar{\beta}_y, \tag{8.27}$$

where $\bar{\beta}_x, \bar{\beta}_y$ are the dx, dy components of $\bar{\beta}$. This is strictly positive close to the zeros of α_z, and consequently for t small enough η is a contact form. Treating η as being parameterised by R, t, we have a homotopy that unfolds and escapes the $+2$ disclination line, keeping it chiral all the time.

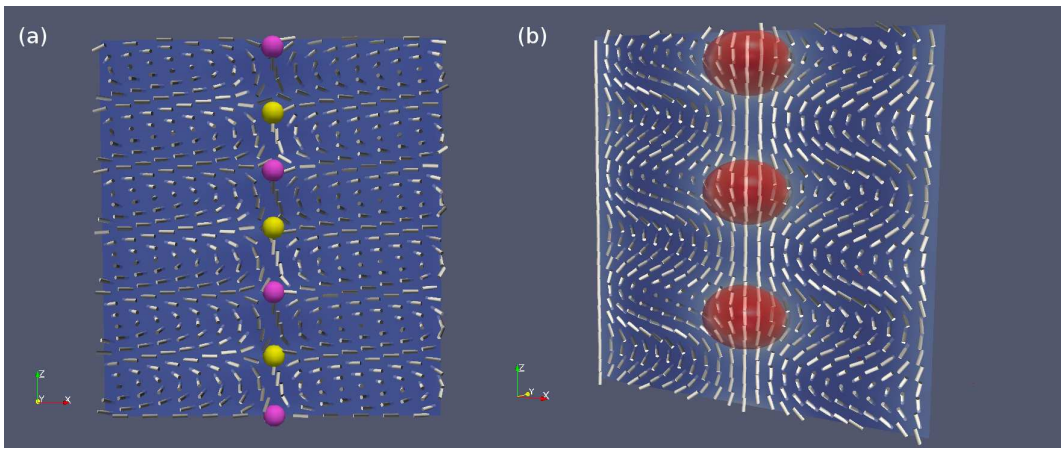

Figure 8.5: Trying to remove the $\eta_{+1,q}$, $q > 0$, singular line results in either (a) a string of chiral point defects of alternating charge, or (b) a string of regions of reversed handedness (red).

The impossiblity of escaping $\eta_{+1,q}$ for $q > 0$ leads to a novel type of structure in a cholesteric, which we are justified in regarding as a type of defect. Define a *twist soliton* in a right-handed material to be a region U of space, diffeomorphic to a ball, where the twist of the director has the wrong sign. We will call the twist soliton *unstable* if there exists a ball B containing U and a homotopy of the director $\mathbf{n}_t$ that is fixed outside B and such that $\mathbf{n}_1$ is right-handed throughout all of B. We call the twist soliton *locally stable* otherwise.

The plane field $\eta_{+1,q} + \epsilon\mathbf{e}_z$, $q, \epsilon > 0$, contains locally stable twist solitons, Fig 8.5. These appear close to each surface where the characteristic foliation induced by $\eta_{+1,q}$ violates the condition of Theorem 3.2, i.e., where the director is purely radial. As we have observed, these twist solitons are locally stable because this property, of the director being purely radial, cannot be removed from the family of characteristic foliations by modifications near a point.

These locally stable twist solitons behave in a similar fashion to point defects. They cannot be removed by local modifications, only modifications along a line. One can create a field of them, and then they self organise into a lattice, Fig. 8.6. They could be created in an experiment by first constructing a lattice of singular lines of winding ± 1, and then using an applied field to encourage the director to escape up everywhere. The -1 winding lines will be chiral after the escape, while the $+1$ winding lines will be converted into strings of twist solitons. This lattice of twist solitons gives an idea of what such objects might look like in a bulk sample.

We can try to estimate the size of a twist-soliton. Changes in the handedness occur as one crosses a surface where the director is purely radial. Thus a spherical

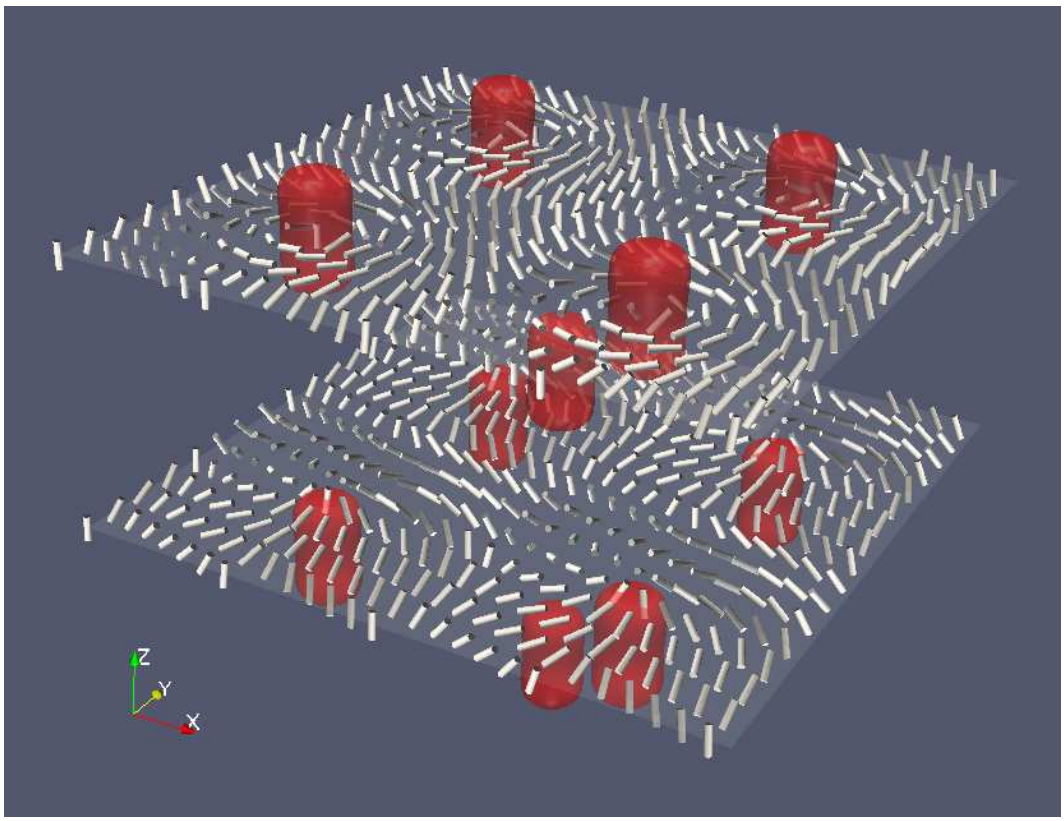

Figure 8.6: A lattice of locally stable twist solitons. The red surfaces indicate the boundary of the twist solitons; the solitons themselves are the interior of the surfaces. The director is shwon on two slices. The lower slice touches the boundary of one of the solitions at a point. Here, the director itself is purely radial, and the characteristic foliation has a centre. The upper slice intersects a twist soliton in the interior, where the director field has a more 'spiral-like' quality to it.

twist solition should be 'pinned' to such a surface at both ends, i.e. the director is $\mathbf{e}_r$ at one pole of the twist soliton, and $-\mathbf{e}_r$ at the other pole. The lengthscale ℓ over which this happens is of the order of half the cholesteric pitch. To describe a single locally stable twist soliton, one can take the plane field defined by

$$\eta = \eta_{+1,1} + (1 + \ell r \sin(z)/2)dz \tag{8.28}$$

On $\mathbb{R}^2 \times [-\pi/2, \pi/2]$, where the length of the interval has beeen rescaled so that $\ell \sim \pi$. Normalising gives a unit director. This argument suggests that the radius of the twist soliton scales like $1/4$ of the cholesteric pitch.

Twist solitons are an interesting type of defect that can occur in a cholesteric. I have already described some properties of twist solitons in Chapter 7, where they

occur close to the droplet boundary, and further examples appear below in Chapter 9. The examples given in this section are of a different character, in that they lie in the interior of the droplet and can be removed via a homotopy, although not a local one. Further investigation of the properties of these defects will be the subject of future work.

8.8 Global Homotopy Classification of Singular Contact Structures

Let $\Xi(\Sigma, L)$ denote the space of orientable singular plane fields on M that have singularities (of nonzero charge) at the points of $\Sigma = \{p_1, \dots, p_m\}$ and line singularities (of nonzero winding) along the components of the finite link L. Let $\Xi_c(\Sigma, L)$ denote the subspace of these that are singular contact and $\Xi_O(\Sigma, L), \Xi_T(\Sigma, L)$ the subspaces which are respectively overtwisted and tight singular contact; the latter is empty whenever Σ is nonempty, according to Proposition 6.1. When Σ is empty, we denote these spaces $\Xi(L)$, etc, and when L is empty we denote the spaces $\Xi(\Sigma)$, etc.

Our aim is to compute π_0 of these various spaces. This was described in §2.5 for standard singular plane fields, following the description in [MA16a]. We wish to do the same for the contact structures. Firstly, we observe the following simple

Proposition 8.10. *Let Σ, Σ' be sets with the same finite number of points, and let L, L' be isotopic links. Then $\pi_0(\Xi_c(\Sigma, L)) \cong \pi_0(\Xi_c(\Sigma', L'))$*

When there only point defects, we have an extension of Eliashberg's h-principle for overtwisted contact structures.

Theorem 8.6. *$\pi_0(\Xi_c(\Sigma)) \cong \pi_0(\Xi(\Sigma))$, for any nonemtpy set Σ.*

Proof. Any contact structure belonging to $\Xi_c(\Sigma)$ is overtwisted by Proposition 6.1. Let ξ_0, ξ_1 be two such structures, and suppose that they are homotopic through singular plane fields leaving the singularities fixed; in particular, they have singularities of the same charges. Let N be a set consising of small open balls around each singular point. Suppose we know that ξ_0, ξ_1 are homotopic through singular contact structures on N, by Theorem 8.4. Then, by choosing a smaller open $N' \subset N$, we can extend this homotopy through contact structures as a homotopy through contact structures on $M - N'$; the h-principle of Eliashberg implies there is a homotopy ξ'_t through contact structures with $\xi'_0 = \xi_0|_{M-N'}$ and $\xi'_1 = \xi_1|_{M-N}$ leaving the boundary $\partial M - N'$ fixed [Eli89; Eli92].

That ξ_0, ξ_1 must be homotopic rel. boundary through contact structures on N follows from the description of the local structure of chiral singularities given in Chapter 6. □

In contrast to nonsingular contact structures, Theorem 8.2 implies that the h-principle now fails to hold whenever there are any line singularities with tight neighbourhoods, even if the contact structure is overtwisted on the complement of the line singularities. However, we can show that the invariants associated to the tight neighbourhoods of the line singularities are the only additional topological invariants in this case.

Let L be a fixed link in M with components $K_1, \dots K_l$. A *marking* of a link L' is an assigment of a pair of integers k, q to each component of the link, so that the local structure is given by $\eta_{k,q}$.

Theorem 8.7. *Fix $\xi \in \Xi_C(\Sigma, L)$ or $\xi \in \Xi_O(L)$. Let $L' \subset L$ consist of the components of the singular link L that have tight neighbourhoods, and let N be a small open neighbourhood of L'. Suppose a marking is specified on L'. The homotopy classes of overtwisted singular contact structures on M with this assignment are in a 1-1 correspondence with homotopy classes of singular plane fields on $M - N$ relative to the boundary condition implied by the choice of assignment.*

Proof. Once an assignment is specified, the homotopy classification of singular contacts structures on the complement of N follows from the classification of singular plane fields by Theorem 8.4 and Eliashberg's h-principle. It remains to show that contact structures with different assignments cannot be homotopic through singular contact structures; this follows from Theorem 8.2. □

This theorem takes of the cases $\Xi_C(\Sigma, L)$ and $\Xi_O(L)$—we again have an h-principle, up to the specification of the local structure of the tight line singularities. The only really interesting space is $\Xi_T(L)$.

Finally, the tight case.

Theorem 8.8. *Let L be a link, and N a small open neighbourhood of L. For each boundary component ∂N_j, specify a slope $(k_j - 1)/q_j$. The tight singular contact structures $\Xi_T(L)$ on M with this set of slopes are in a 1-1 correspondence with tight contact structures on the manifold $M - N$ with the appropriate boundary condition on $\partial_M = \cup_j \partial N_j$.*

Theorems 8.6, 8.7, and 8.8 complete the homotopy classification of singular contact structures in the overtwisted case and reduce the tight case to understanding tight

contact structures on knot and link complements. The classification of tight contact structures on the complement of an arbitrary link L in S^3 is difficult, and to my knowledge there are only two known cases. The manifold that is the complement of an m-component link L in S^3 will always be a compact manifold whose boundary consists of m torii. When $m = 1$, the complement is always diffeomorphic to $D^2 \times S^1$ and we may apply the classification theorem of Honda, described in §3.10. When $m = 2$ and L is the Hopf link,the complement is $T^2 \times [0, 1]$ and we may again apply the results of Honda.

Chapter 9

Layered Stuctures, Hopfions, and Disclination Lines in Cholesteric Droplets

9.1 Introduction

In Chapter 7 I studied defect strutures in cholesteric droplets using the tools of singular contact topology. Primarily this is a local theory that happens to extend globally: by prescribing a symmetry group for the droplet, which is done by, for example, placing a set of achiral defects near to the boundary, the entire structure is determined, with 'degenerate' variants of the structures being produced by unfoldings of the central singularity. In this chapter I focus on other kinds of structures in cholesteric droplets found in the experiments of Ref. [Pos18c] which are not determined by the placement of singularities, but rather the geometry of the cholesteric layers. These include textures with linked λ lines and nonzero Hopf invariant. Many of these textures also occur in droplets with planar anchoring, both in experiment and simulation, to which they can be compared [SPRŽ12]. I demonstrate that structures in droplets with planar and normal anchoring are the same up to the addition of a boundary layer that interpolates between the two kinds of anchoring.

9.2 The Boundary Layer of a Droplet with Normal Anchoring

A droplet with normal anchoring can be see as a droplet with planar anchoring plus an additional 'boundary layer' that interpolates between planar and normal

anchoring. This perspective is useful in adapting the textures constructed by Seč *et. al.* [SPRŽ12] to textures in droplets with normal anchoring. In this section we will construct this boundary layer.

Let B be a droplet of radius R_0 with planar anchoring, equipped with a singular contact structure that agrees with the standard planar boundary. We will add a boundary layer $S^2 \times [0,1]$ to the outside of B, along with a singular plane field that is tangent to $S^2 \times 1$. We will assume (1) that the interior of the boundary layer contains no defects, (2) any defects sit on the inner boundary ($S^2 \times 0$, glued to ∂B) of the boundary layer, and (3) that the region of reversed handedness whose presence is implied by Theorem 3.5 begins at the inner boundary of the boundary layer; recall that this third condition was essentially the definition of the boundary layer given in Chapter 6.

I assume the characteristic foliation on the inner surface of the boundary layer is as simple as possible, with the leaves being great circles. Note however that the construction below works no matter the choice of characteristic foliation. Further, assume that the interior of the droplet contains no defect. Then there are two possibilities for the structure of the single defect in the boundary layer: either it is chiral, with Morse index 2, and there is a region of reversed handedness at the opposite pole, or it is achiral, with Morse index 0, and pinned to a region of reversed handedness.

Denote by r the coordinate on $[0,1]$. The coordinate system on the sphere $S^2 \times 0$ is $\theta = \arccos(z/r)$, and $\phi = \arctan(y/x)$, with $0 \leq \theta \leq \pi, 0 \leq \phi \leq 2\pi$, with area form $\sin(\theta) d\theta d\phi$. The characteristic foliation on $S^2 \times 0$ must therefore be directed by $X_0 = e_\phi$. Consider the family of foliations directed by $X_r = (1-r)e_\phi + r(1-r)e_\theta$. If we set $\eta = \beta_r + r dr$, where $\beta_r = \iota_{X_r}\Omega$, then

$$\eta \wedge d\eta = r^2((1-r)\cot(\theta) - (2 - 3r + 2r^2)\sin(\theta))dr \wedge \Omega. \tag{9.1}$$

This is negative everywhere except for a region around $\theta = 0$, and evidently $\eta|_{r=1}$ is defines a plane field tangent to the boundary sphere. Thus we have interpolated between planar and normal anchoring. One can tweak the size and shape of the region of positive twist by adding parameters to X_r and putting a function in front of the dr term in η, but I refrain from doing so, as the primary aspect of interest here is understanding the topology of the boundary region rather than getting the exact director; this is best left to the numerical simulations. It is however helpful to have a version of the boundary director that is parametered by h, the thickness of the boundary region, which is set to 1 in the discussion above. Concretely, we

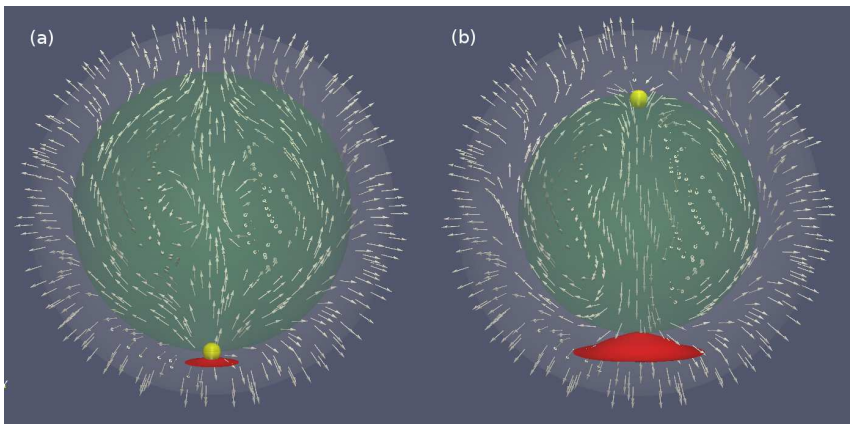

Figure 9.1: Examples of how the orientation of a director close to a spherical surface with planar anchoring influences the presence of chiral/achiral defects when a radial boundary layer is added. (a) The director is oriented from the south pole to the north pole. When the boundary layer is added, this produces an achiral Morse defect (Hedgehog) at the south pole. (b) When the director is oriented from the north to the south pole, the defect appears at the north pole and is chiral, while a region of reversed handedness appears near the south pole. In each case the red surface is where the twist vanishes, and the green sphere indicates the interior part of the droplet where the twist has a single sign—the director is approximately tangent to the boundary of this sphere. The white arrows indicate the oriented director.

obtain this director by normalising

$$\mathbf{m} = \sin\theta(R+h-r)\mathbf{e}_\theta - \sin\theta(R-r)(R+h-r)\mathbf{e}_\phi + (r-R)\mathbf{e}_r. \tag{9.2}$$

While the twist soliton always appears at the south pole, where $\theta = 0$, the positioning of the point defect depends on the director in the interior. Let S^{in} be a surface inside but close to ∂B, i.e. a sphere with radius slightly smaller than R_0. Where the defect appears will depend on the sign of the e_r component of the director on the inside of the sphere, as shown in Fig. 9.1. If the director is pointing into S^{in} at the south pole and out at the north pole, then the result of glueing the boundary director onto the droplet with planar anchoring is to produce an achiral defect at the south pole, and a corresponding bubble of wrong handedness. However, if the orientation of the director is reversed, so that it points out of south pole and into the north pole, then glueing on the boundary director produces a chiral Morse index 2 defect at the north pole, and a corresponding twist soliton at the south pole that is not attached to any defect.

The boundary condition given here is appropriate for almost all of the structures in planar droplets that are described in Ref. [SPRŽ12]. To interpolate be-

tween a more complex boundary director on $S^2 \times 0$ and normal anchoring, then it is relatively straightforward to adapt the construction given above. For example, to model the boundary conditions of the droplets with high-charge defects and multiple achiral boundary singularities examined in Chapter 7, one would choose a characteristic foliation with k centres equally spaced on the sphere, which become the defect points, and fill in the remainder of the foliation with maximum symmetry. Of course there will be other singularities in this characteristic foliation, some of which will demarcate the positions where λ lines pierce the boundary layer—the position and structure of these is especially evident for the tetrahedral T_{444} defect. Let X be a vector field directing this foliation, and Y the orthogonal vector field. Then $X_r = (1-r)X + r(1-r)Y$ defines a series of characteristic foliations on $S^2 \times [0,1]$, and taking $\eta = \iota_{X_r}\Omega + rdr$ gives an appropriate model for boundary of these droplets.

9.3 Droplets With Layered Structures

In this section I describe various layered structures that arise in cholesteric droplets. I define a 'layer' only loosely, to be a surface to which the director is 'approximately' tangent. By Proposition 3.6, the dividing curve on a convex surface will give us a good idea of the layer structure. In each of the figures in this section I show $\mathbf{n} \cdot N$ on a slice S through the droplet, where N is the unit normal to S, the zero set of which is the dividing curve by Proposition 3.3. This visualisation also allows for easy comparison with experimental images, which show streamlines of the director. The places where the director is visible in these images are the places where is roughly in the plane of the slice, which corresponds to neighbourhoods of the dividing curve in the numerical images. The places where the director is not visible in the experimental images are the places where it is highly out of the plane of slice, the bright regions in the numerical images.

9.3.1 Flat Layers

The simplest way to realise a structure with flat layers is initialise a simulation with the director given by the usual cholesteric ground state in a flat geometry, $\mathbf{n} = \cos(\pi qz/R)\mathbf{e}_x + \sin(\pi qz/R)\mathbf{e}_y$. In a droplet with normal anchoring, this initialisation will produce aan achiral boundary defect. A simulation of this texture with $q/R = 3$ is shown in Fig. 9.2(a-b), to be compared with experimental realisations of flat layers, Fig. 9.2(c). There are two λ^{+1} lines which emanate from the point defect and move in a spiral around the boundary layer of the droplet, terminating at the north and south

poles. These are indicated by an isosurface of Δ in Fig. 9.2(b). Similar structures have been observed previously in cholesteric droplets, but with a disclination line instead of the λ lines [SPRŽ12]. The twist soliton attached to the achiral boundary defect extends over a large part of the boundary region, following the λ lines. The surface over which the twist changes sign is shown in red in Fig. 9.2(b). In planar droplets this texture is called the planar bipolar structure (PBS) [SPRŽ12].

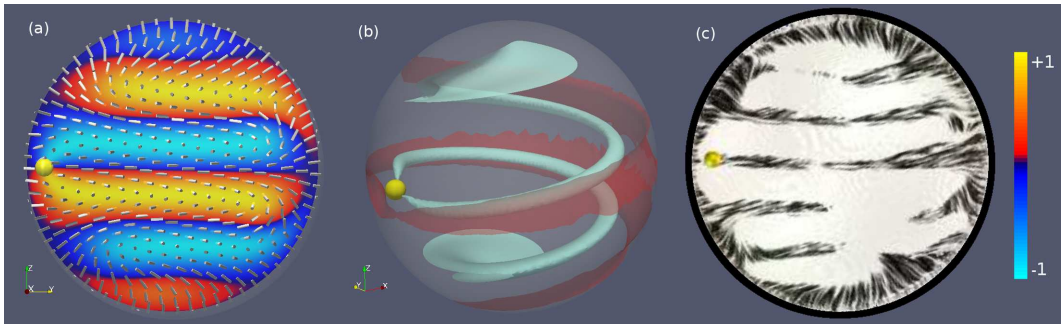

Figure 9.2: (a) A droplet with flat layers. The colours indicate the dot product between the normal to the slice and the director, with blue being negative and orange positive. The black lines are the places where the director is tangent to the slice. There is a single achiral boundary defect (yellow sphere). (b) Two λ lines (light blue) emanate from the point defect and spiral towards opposite poles of the droplet The twist soliton (red) pinned to the point defect extends over a large part of the boundary region, tracking the λ lines. In both panels, the director is shown as white sticks. (c) Experimental image, repoduced from Ref. [Pos18a]. The bright blue/yellow regions shown in panel (a) correspond to points where the director is strongly out of the plane of the slice, the white regions in panel (c).

One can construct alternative textures with flat layers from a χ^{+1} line using the director $\mathbf{n}_{+1,q}$ from Chapter 8. We may either escape in one direction along the singular line, which produces no defects but must produce twist solitons, or we can escape in alternating directions and have a string of point defects that is structurally distinct from the strings described in Chapter 7. The former is shown in Fig. 9.3(a,b). There are no defects in the interior, only an achiral boundary defect. The regions of reversed handedness in this simulated texture are shown in Fig. 9.3(b), and illustrate all types of twist solition we have observed in chiral droplets: there is an achiral boundary defect with associated region of reversed handedness at the south pole; at this north pole, there is an additional spherical region of reversed handedness pinned to the boundary but without a defect; two toroidal twist solitions appear in between them; and finally, there are two roughly spherical twist solitons in the interior of the droplet, whose poles corresponds to surfaces where the characteristic foliation has vanishing divergence at the singularities.

For sufficiently strong chirality this escaped director is not the energetically-favoured way of removing the χ^{+1} line. Instead the director escapes alternately up and down, producing chiral point defects on the surfaces where the director is purely radial instead of regions of reversed handedness, Fig. 9.3(c,d). This structure is similar to the diametric spherical structure (DSS) observed in chiral droplets with planar anchoring [SPRŽ12], except with the spherical layers unfolded into flat layers and with an additional point defect of degree +1 that sits on the boundary layer in a droplet with normal anchoring. In Fig. 9.3 the boundary defect is chiral, and there is a twist soliton at the opposite pole of the droplet. I suggest referring to the texture shown in Fig. 9.3(c,d) as the chiral escape structure (CES), and the texture shown in Fig. 9.3(a,b) as the achiral escape structure (AES), in keeping with the naming scheme used in Ref. [SPRŽ12].

In both the CES and AES, the director is largely tangent to the level sets of z, but deviates from these layers close to the z-axis, which becomes a single λ^{+1} line in the achiral string, and a series of λ^{+1} lines connecting the point defects in the CES. On the level of defects and λ lines, the difference between the AES and PBS directors—neither of which have defects in the interior part of the droplet—is that the λ line is orthogonal to the layers in the former and tangent to them in the latter; the price of changing the relative orientation of the λ line and the layers is to produce regions of reversed handedness, or else nucleate a series of point defects to produce the CES. Although I am focussing on structures in spherical droplets here, I remark that these two escape structures can also occur in cholesteric cells, cholesteric material in cylindrical capillaries with normal anchoring, and in toroidal droplets of cholesteric material. The reasoning we have given to conclude the existence of twist solitons in the achiral string is completely general, and implies that bulk twist solitons can be stablised in these geometries as well. Numerical experiments in cylindrical capillaries suggest it is also possible to stablise twist solitons in the form of rings pinned to the capillary boundary in this geometry, analagous to the rings shown in Fig. 9.3(b).

Neither the CES or the AES were observed in the experiments of Ref. [Pos18c] or the numerical simulations of Ref. [SPRŽ12]. Both textures are numerically (meta)stable, so the failure to observe them experimentally is likely due to them requiring very specific initial conditions that do not arise naturally in the experiment. Instead we observe the DSS structure, where the flat layers of the CES are folded up into spheres, which I will describe in §9.3.3 below.

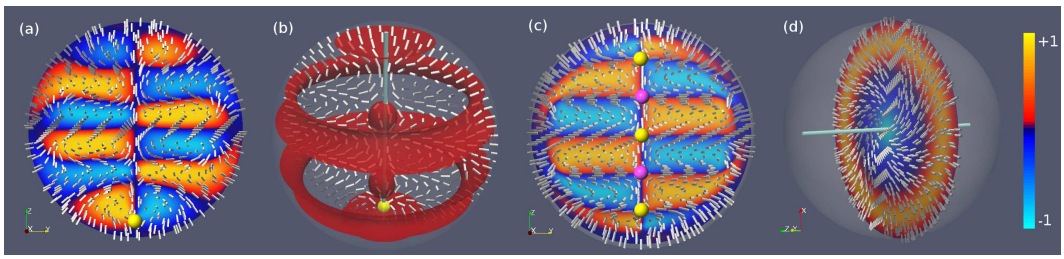

Figure 9.3: Layered structures produced from the escape of χ^{+1} line. (a) Escaping up everywhere along the line produces a texture without defects in the interior, the AES structure. (b) Instead of point defects there are stable regions of reversed handedness, twist solitons, in the interior of the droplet, which are shown in red. There are also twist solitons close to the boundary, in the form of both rings and spheres. There is a λ^{+1} line running between poles of the droplet. (c) Escaping alternately up and down produces a texture with a string of chiral point defects of alternating charge, connected by λ lines, the CES structure. (d) A view of the CES structure on a slice transverse to the λ line (light blue). In each panel the director is shown as white sticks.

9.3.2 Cylindrical Layers

The simplest structure with cylindrical layers is defined by the director,

$$\mathbf{n} = \cos(2\pi qr/R)\mathbf{e}_z - \sin(2\pi qr/R)\mathbf{e}_\phi, \tag{9.3}$$

for some $q > 0$ that sets the number of layers. This particular initialisation will produce an achiral boundary defect. In [SPRŽ12] this is called the bipolar structure (BS). This is shown for $q/R = 2$ in Fig. 9.4(a,c), to be compared with experimental images, Fig. 9.4(b,d). The BS director also has similarities with the CES and AES textures: the central λ^{+1} line is the axis of a double-twist cylinder in all three cases, as can be seen by looking at the director on slices orthogonal to the λ line, Fig. 9.3(c) and Fig. 9.4(c); the change in colours from blue to orange on the orthogonal slices indicates that the director undergoes a rotation by π as we move out from the λ line.

Simulations show that there are two additional $\lambda^{+1/2}$ lines where the central structure matches on to the boundary layer. There are twist solitons at both the south pole, where there is an achiral defect, and the north pole. There are also two ring-shaped twist solitons shadowing the boundary λ lines, as in the flat layers, Fig. 9.2. The structure of this ring is the same as that shown in Fig. 9.3(b), and also that which occurs in the droplet with a single Morse index 2 defect, Fig. 7.4

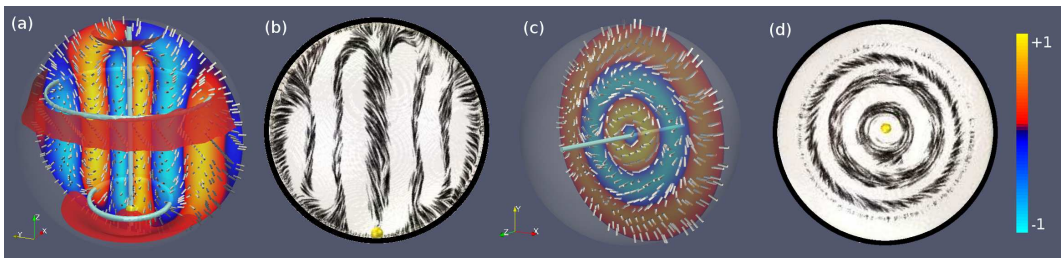

Figure 9.4: Cylinderical layers in a droplet with normal anchoring, with $q = 2$. The numerically simulated director (9.3) and dividing curve is shown on (a) the xz-plane, and (c) the xy-plane. In the latter the λ line is indicated by a blue tube. Panels (b,d) show an experimental realisation of the same director; reproduced from [Pos18c]. In the simulation, the boundary defect is achiral.

9.3.3 Spherical Layers

We can produce a director with a series of spherical layers using the χ^{+1} director, but wrapping up the z planes into spheres. The χ^{+1} line is removed as before, by escaping alternately up and down to produce a string of chiral point defects. Concretely, this director is given in spherical coodinates by taking

$$\mathbf{m} = -\cos(2\pi qr/R)\mathbf{e}_\phi + z\cos(2\pi qr/R)\mathbf{e}_r + \sin(2\pi qr/R)\mathbf{e}_\theta, \tag{9.4}$$

and then normalising, $\mathbf{n} = \mathbf{m}/|\mathbf{m}|$. This produces a director tangent to a series of concentric spheres at values of r where $\cos(2\pi qr/R) = 0$, with point defects at the poles of those spheres. The ball interior to each values of r with $\cos(2\pi qr/R) = 0$ can be thought of as a droplet with planar anchoring. The interior of the innermost spherical layer is a toron [PČM16].

As with the CES of Fig 9.3(b), a structure with multiple spherical layers can be seen as a χ^{+1} running through an axis of the droplet that escaped in alternating directions to produce a string of chiral point defects. When the CES has spherical layers in this manner, the texture is called the diametric spherical structure (DSS) [SPRŽ12]. Each interior defect is chiral, and the boundary defect that arises from normal anchoring can be either chiral or achiral as we have previously argued.

This is not the only possibility for a director with spherical layers. A cholesteric director reproducing a single spherical layer (toron) can also be constructed from an intrinsically harmonic function ϕ as described in §6.3.3. The required singularity is called P_8 in Arnold's notation [AGZV85], and is given by the function germ

$$\phi = \frac{1}{2}x(y^2 + z^2) - \frac{1}{3}x^3 + r^2x, \tag{9.5}$$

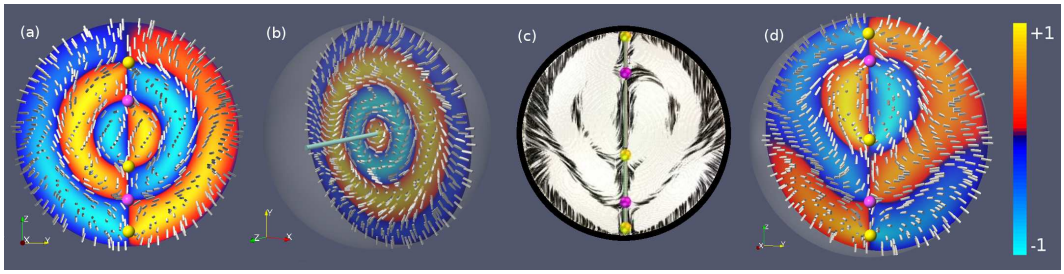

Figure 9.5: Spherical layers in a droplet. (a) Numerical simulation of a DSS structure with two spherical layers, and five point defects. The boundary defect is achiral here, but one can also have a chiral boundary defect. (b) A slice orthogonal to the λ line running through the point defects reveals a similar pattern observed with cylindrical layers, illustrating the need for multiple perspectives when determining the layer structure from slices. (c) An experimental realisation of a structure containing a spherical layer that is different from the DSS. Instead, this structure is obtained by inserting a spherical layer (toron) into a texture with a string of three point defects described by an A_3 singularity. Both boundary defects are achiral, while the three defects in the interior are chiral. (d) Numerical realisation of the same structure.

where $r > 0$ is a parameter that sets the radius of the spherical layer. This function is harmonic with respect to the Euclidean metric, so that the chiral terms can be obtained by the formula $\nabla \times \mathbf{m}_c = \nabla \phi$, and we could perturb into a genuine Beltrami field using the construction in Theorem 6.4 if we wished.

Structures similar to the DSS and containing a toron arise in experiments, Fig. 9.5(c), but there is an important distinction between these structures and the model (9.4): in the experimental structures there are two boundary defects rather than one, and both are achiral hedgehogs. Such a string of three point defects is described by an unfolding of the A_3 singularity, see §7.3. The structure shown in Fig. 9.5(c) arises by displacing the central defect of the A_3 string towards the pole, and then inserting an additional pair of point defects that lie on a spherical layer (a toron) into this structure. The structure of the director inside this spherical layer is given by Eq. (9.4). A numerical realisation built out of this initialisation is shown in Fig. 9.5(d).

Another structure with spherical layers arises from the removal of a χ^{+2} line. This structure is called the radial spherical structure (RSS) [SPRŽ12]. This director results from placing a singular line of winding +2 inside the droplet, and then attempting to remove this line via escape along the radial direction. The way this is achieved is described in detail in §8.7. The model given there is equivalent to the model in Eq. (6) of Ref. [SPRŽ12], where it is suggested to take $R = 0.9$ for the separation between the two λ lines. The structure of the director and the helical λ

lines are also reminiscent of the 'heliknotons,' or linked meron tubes, observed in recent experiments [TS19]; we suggest these may instances of the same phenomenon.

To realise this structure in a droplet we replace the Cartesian coordinates x, y, z in the model in §8.7 with spherical coordinates θ, ϕ, r, and set the parameter $q = q_0/R$. The resulting structure, with $q_0/R = 2$, is shown in Fig. 9.6(a). Although this is the lowest energy structure for a wide range of relative chiralities in planar droplets [SPRŽ12], this structure is not observed in the experiments of Ref. [Pos18c]. Instead there are similar structures, with a double helix of λ lines corresponding to the removal of a χ^{+2} line but without the spherical layer structure. An example of such as texture is shown in panel Fig. 9.6(b). In these experiments, one can detect the λ lines by showing an isosurface of the aFCPM intensity I—I have cropped this surface in Fig. 9.6(b) to expose only the relevant parts of the structure. There are three λ lines. One is short line which connects the point defect to the boundary, which is too small to be picked up by the level set of I but must be present for topological reasons. One is attached at both ends to the boundary, moving from the boundary on the left side of the panel to the right side. The other begins on the left side, moves towards the right, but bends back on itself as it moves towards the point defect (yellow sphere). In Fig. 9.6(c) the director is shown on a slice across the helix structure, coloured according to intensity I, with white corresponding to $I = 0$ and black to $I = 1$. We see the characteristic image of an unfolded $+2$ singularity, showing that this structure corresponds to the escaped χ^{+2} line.

9.4 Hopfions in Droplets

9.4.1 Review of the Hopf and Gompf Invariants

In this section we will look at Hopfion-like structures in droplets. First let us briefly remind ourselves the three-dimensional invariants of plane fields, described in Chapter 2. Homotopy classes of plane fields, equivalently unit vector fields, in $\mathbb{R}^3$ or S^3 correspond to elements of $\pi_3(\mathbb{RP}^2) \cong \mathbb{Z}$. A concrete way of describing this element is the Hopf invariant [Hop31; CAA+13], which is computed in the following manner. A director $\mathbf{n}$ determines a map into the sphere. If we look at the set of points that are mapped to a particular point p on the sphere, this will generically be a line K, which is oriented by pulling back the orientation on the sphere via the map. The Hopf invariant is the linking number $\mathrm{Lk}(K, K')$ of a pair of preimages [Mil65]. For an unoriented nematic it suffices to look at the preimage of a single point in $\mathbb{RP}^2$, and compute its linking number.

It is helpful to think of the Hopf invariant as a four-dimensional version of

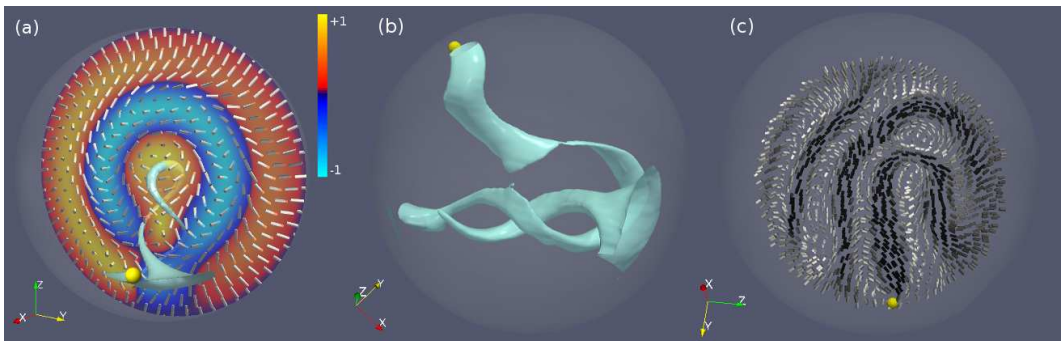

Figure 9.6: (a) RSS structure with $q/R = 2$ in a droplet with normal anchoring. There is a one λ line connecting the defect to the boundary, and then a second λ lines that wraps itself up into a helix. (b) An experimental realisation of a texture containing a double helix of λ lines. The surface shown is an isosurface of the aFCPM intensity I, corresponding to a value $I = 0.5$, which allows us to visualise the λ lines (pale blue). The helix structure is clear. (c) The reconstructed director field shown on a slice across the helix, and coloured according to intensity, with white correspond to $I = 0$ and black to $I = 1$. We see the $+2$ winding where the slice intersects the double helix of λ lines. We also see that the other half of the droplet is filled with flat layers. The experimental data was kindly provided by G. Posnjak.

the defect charge. Consider a director in Euclidean space that is free of defects and uniform at large distances so that we may 'compactify' by adding a point at infinity and regard the director as a unit vector field on the 3-sphere S^3. This is naturally identified with the unit sphere in $\mathbb{R}^4$. We can ask whether it is possible to extend the director over the interior of the 3-sphere without introducing a defect. This extension is possible if and only if the Hopf invariant, an element of $\pi_3(\mathbb{RP}^2)$, vanishes. Conceptually, this is the same problem as specifying a director on the surface of a 2-sphere and asking whether it extends over the interior without defects; the obstruction in this case is the defect charge, an element of $\pi_2(\mathbb{RP}^2)$.

The Hopf invariant is the familiar and classical way of characterising the homotopy group $\pi_3(\mathbb{RP}^2) \cong \mathbb{Z}$. For our purposes it is preferable to describe it in terms of the zero set of a line or vector field everywhere orthogonal to the director, as a cholesteric material has a natural choice for such a direction, the pitch axis. We may compute a homotopy invariant of the director analgous to the Hopf invariant from the defects in the pitch axis, the λ lines. This was described back in §2.4.3 and Eq. (2.12). Let K_j be the set of λ lines in the material, each with strength (winding number) s_j, which is generically a half-integer. Each λ line is endowed with an orientation [MA16b; Mac16], and hence is an oriented knot. Then the total

linking number gives a homotopy invariant, which I will refer to in this section as the *Gompf invariant*.

$$\Gamma^2 = \sum_i s_i^2 \mathrm{SL}(K_i) + \sum_{i \neq j} s_i s_j \mathrm{Lk}(K_i, K_j). \tag{9.6}$$

This type of formula is familiar from helicity and abelian Chern-Simons theory [AK98]. The first term is a self-linking number. Informally, this is defined to be the number of times the 'profile' of the λ line K_i rotates as we move along the line. More concretely, we compute it in the following fashion. Away from the λ lines, the director and the pitch axis define a (possibly unoriented) frame $\mathbf{e}_1, \mathbf{e}_2, \mathbf{n}$. Consider the total rotation $\int_{K'} \mathbf{e}_2 \cdot d\mathbf{e}_1$ of this frame about the director along any push-off K' giving a zero-framing for the λ line. Part of this rotation is an intrinsic Berry phase γ, equal to the area on the unit sphere bound by the curve traced out by $\mathbf{n}$ along K'. The difference $\gamma - \int_{K'} \mathbf{e}_2 \cdot d\mathbf{e}_1 = 2\pi\, \mathrm{SL}(K_i)$ defines the self-linking. In all the concrete examples of textures in spherical droplets that we consider in this article the self-linking number vanishes.

As with the Hopf invariant, Γ^2 has an interpetation as an obstruction to extending a director on the 3-sphere over the interior. We can regard the 4-dimensional Euclidean space as a 2-dimensional complex space $\mathbb{C}^2$ by introducing the obvious complex coordinates. Then S^3 is the unit sphere in this space, comprised of those complex points of magnitude 1. Associated to the director on S^3 is a family of planes, defined by taking the plane orthogonal to the director at each point. These two-dimensional planes become a complex line field on the unit sphere in $\mathbb{C}^2$. The obstruction to extending this complex line field over the interior of S^3 with defects is given by Γ^2.

As an example, consider the χ^{+2} line texture on a solid torus $D^2 \times S^1$ such that the z coordinate is the coordinate on the S^1 factor. We can embed this solid torus in S^3, and match on to a uniform far-field without additional defects. Ignoring constraints on the twist for a moment, we can escape along the singular line to produce a single λ^{+2} line. The framing endows this line with a linking number of q, where q is the number of full rotations of the profile along the χ^{+2} line, and thus for this texture the invariant is $\Gamma^2 = 4q$, as strength of the λ line is $+2$. The Hopf invariant is $2q$. Splitting the χ^{+2} line apart into a pair of helical χ^{+1} lines before escaping as described in §8.7 gives a homotopic texture which is chiral. Each of two λ^{+1} lines has vanishing self-linking number, however, they are linked $2q$ times, and once more we compute $\Gamma^2 = 4q$. In this case it is easier to see that the Hopf invariant is $2q$, because the λ lines themselves are the preimages of appropriately

chosen antipodal points on S^2; I emphasise that the fact that Γ^2 is twice the Hopf invariant here is a happy accident that arises in this particular example, not a general relation.

Both of these descriptions apply to defect-free directors in S^3, however the invariants also amke sense for directors with defects and in domains with boundary, such as a cholesteric droplets, provided we compute the linking numbers 'relative to the boundary.' In this framework, we regard each defect as being a boundary component, along with the droplet boundary itself.

The BS texture with cylindrical layers shown in Fig. 9.4 has linked λ lines, but vanishing Γ^2. Each of the circular λ lines has winding $+\frac{1}{2}$, however the lines are oriented in opposite directions—to see this, observe that the λ lines are oriented out of the orange regions and into the blue regions—and consequently their contributions to the sum cancel each other out.

9.4.2 The Lyre and Yeti Structures

The simplest texture with nonzero Hopf invariant has a pair of λ^{+1} lines that are linked (relative to the boundary) with one another so that they form the Hopf link. In a planar droplet, this occurs when there is a single λ^{+1} line running between the boojums at the poles, which is surrounded by a second circular λ^{+1} line in the interior of the droplet. Textures with this configuration of λ lines occur naturally in cholesteric droplets: they are the so-called Yeti and Lyre textures [SPRŽ12]. In a droplet with normal anchoring, the addition of a boundary layer implies that there is an extra defect of degree $+1$ near the boundary, and now there are two λ^{+1} lines connecting it to the boundary. As the charge of the boundary defect is $+1$ these λ lines must both be oriented from the defect to the boundary, and consequently the λ^{+1} in the interior of the droplet has linking number $+1$ with each of them. Using (9.6), we compute that $\Gamma^2 = +4$. The Hopf invariant is $+1$, which is computed by looking at the linking of preimages in the usual manner.

The Yeti and Lyre textures have a similar structure to the Hopf fibration [Hop31; CAA$^+$13]. They consist of a solid torus $D^2 \times S^1$ linked with a solid cylinder $D^2 \times [0,1]$, where the director is tangent to the level sets $\theta \times S^1$ and $\theta \times [0,1]$, so it has a mix of cylindrical layers and toroidal layers. Concretely, let ρ, ϕ, z be cylindrical coordinates. Choose some $\rho_0 < R$ to be the core, where R is the radius of the droplet. Set $\tau = \sqrt{(\rho_0 - \rho)^2 + z^2}$ and let ψ be the polar coordinate on the disks where $\tau \leq \tau_0$ and ϕ constant, for some fixed τ_0. For $\tau \leq \tau_0$, we define the

director to be

$$\mathbf{n} = -\sin\left(\frac{q_1\pi\tau}{2\tau_0}\right)\mathbf{e}_\psi + \cos\left(\frac{q_1\pi\tau}{2\tau_0}\right)\mathbf{e}_\phi. \tag{9.7}$$

For $q_1 = 1, 2$ this describes a tube of merons – a fractionalisation of a Skyrmion represented by a single λ^{+1} line – along the line $\tau = 0$. For larger q_1 we instead have a tube of Skyrmions. Otherwise, for $\tau > \tau_0$, we take the director to be cylindrical layers aligned along z, as described in §9.3.2,

$$\mathbf{n} = -\sin\left(\frac{q_2\pi\rho}{2\rho_0}\right)\mathbf{e}_\phi + \cos\left(\frac{q_2\pi\rho}{2\rho_0}\right)\mathbf{e}_z. \tag{9.8}$$

Here, q_1, q_2 are positive integers that set the layer number in each separate piece. For the Yeti, we take q_1 to be even, while for the Lyre we take q_1 odd. For director-based simulations we should take $q_2 = q_1 \bmod 4$, so that the directors approximately match up on the boundary between the two regions. Notably, the only difference between the Yeti and Lyre is the whether the director undergoes several full π rotations in the toroidal region encircling the central λ line (Yeti), or whether there is an addional $\frac{\pi}{2}$ rotation (Lyre).

The Yeti texture in a droplet with normal anchoring is shown in Fig. 9.7(a,b) for $q_1 = q_2 = 2$, and the Lyre structure in a droplet with normal anchoring is shown in Fig. 9.7(c,d) for $q_1 = q_2 = 1$. Topologically these variants are the same as Yeti and Lyre structures observed in planar droplets, with the addition of a boundary layer. As with all of these structures, situations where the boundary defect is chiral and achiral are both possible. In each case we see a pair of linked λ^{+1} lines, e.g. Fig. 9.7(a), which witnesses the fact that $\Gamma^2 = +4$. The Hopf invariant is seen by the linking of preimages, e.g. Fig. 9.7(b), where the preimages form the Hopf link in the interior of the droplet. The Lyre structure can be produced by taking $q_1 = 1$ in 9.7. We have also found that in producing numerical simulations that give good agreement with the Lyre structures produced in experiments it helps to explicitly break the symmetry in the droplet, replacing z with $z - z_0$ in the definition of the coordinate τ for some small z_0, and also to choose ρ_0, τ_0 to ensure that the torus filled by (9.7) is very close to the droplet boundary. The resulting structure has a Lyre shape; see Fig. 9.7(c,d). Otherwise, the structure has the same topology as the Yeti structure, with $\Gamma^2 = +4$ and a Hopf invariant of $+1$.

To obtain a texture with Hopf invariant -1 instead of $+1$, we can reverse the sign of the director (9.7). This will also flip the sign of Γ^2, as this will change the orientation of the circular λ line and hence flip the sign of the linking number.

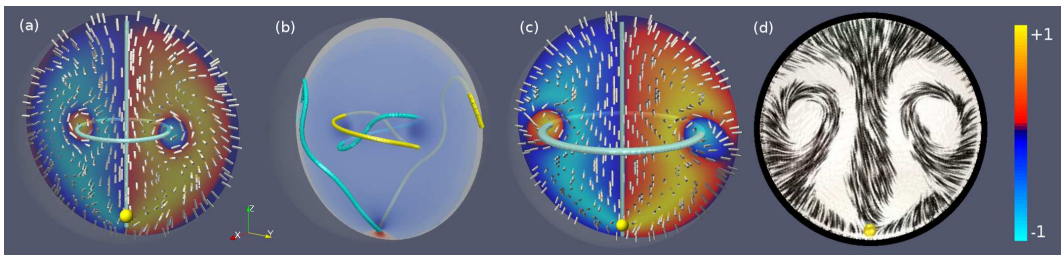

Figure 9.7: (a) The Yeti structure in a droplet with normal anchoring. The director (white rods) is shown on a slice coloured according to the dot product between the director and the layer normal, with λ lines shown in blue. (b) The same texture, this time with the twist, with blue being negative and red being positive. We see that the boundary defect at the south pole, which we have not marked with a yellow sphere so as not to obscure the region of reversed handedness, is achiral. The preimages of $\mathbf{e}_x$ (yellow) and $-\mathbf{e}_x$ also show that the Hopf invariant is nonzero. (c) The Lyre structure, with chiral boundary defect. The texture is visually very similar to the Yeti. (d) An experimental realisation of the Lyre structure, with a chiral boundary defect.

9.4.3 Composite Structures

The textures with strings and high-charge defects described in Chapter 7 can be regarded as 'topological atoms'. The layered structures identified in this chapter also serve as atomic units. Combining multiple atomic structures in a single droplet leads to a composite structure, a 'topological molecule'. I now describe several such structures which combine Hopfions with constellations of defects.

The simplest string of point defects in a cholesteric droplet is described by an unfolding of the A_3 singularity, Fig. 7.3(g,h). The three point defects describe an axis which is a λ^{+1} line, the axis of a double twist cylinder. One can insert a tube of cylindrical layers so that it loops around the λ line. This adds an additional λ^{+1} that links with the first, so that the resting director has Hopf invariant +1. See Fig. 9.8 for a comparison between numerics, panel (a), and with experiment, panel The λ lines (pale blue), illustrate nonzero Γ^2. In panel (c) we show the twist solitons that occur in this droplet. In addition to the regions of reversed handedness pinned to the achiral boundary defects, there is a ring-shaped twist soliton around the equator of the droplet, as well as a stable twist soliton in the interior of the droplet. The latter has similar local structure to those present in the AES texture.

Fig. 9.8(d) shows another composite structure containing a toron and a Hopfion, the latter being witnessed by the linked preimages. The interior of the spherical layer has the same structure as the Yeti texture in a droplet with planar anchoring, as described in Ref. [SPRŽ12]. This differs from the texture shown in panels (a-c)

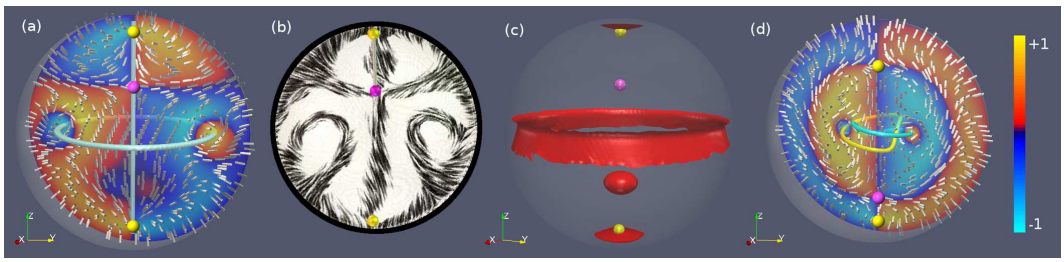

Figure 9.8: (a) A texture combining both the features of a basic string of point defects, and the Lyre structure. The string of three point defects of alternating charge is described by the A_3 singularity. The λ lines (blue tubes) are linked, illustrating the topological nontriviality of the texture. The preimages (not shown) allow us to compute that the Hopf invariant is +1. (b) Experimental realisation of this texture, reproduced from [Pos18a; Pos18b]. (c) This texture has several distinct types of twist soliton. There are two bubbles of reversed handedness pinned to the achiral boundary defects, a ring around the equator, and a stable bubble in the interior of the droplet. (d) An alternative structure with three defects is produced by inserting an extra λ line into a structure with a spherical layer. This differs from the texture shown in panels (a-c) by the fact that one of the +1 defects is chiral. The preimages shown are the lines where $\mathbf{n} = \pm\mathbf{e}_x$

by the fact that one of the +1 defects is chiral. Unlike in the texture shown in panels (a-c), there are no twist solitions besides the one pinned to the achiral boundary defect at the south pole.

Chapter 10

On the Layer Structure of Cholesterics

10.1 Introduction

The homotopy invariants discussed in Chapter 2 and the invariants of tight contact structures introduced in Chapter 3 are quantities invariant under changes that do not produce new defects in the *director*, but say very little about defects in, for example, the bend vector field or the pitch axis. For obvious reasons one may not create a single defect of nonzero winding in either the bend or the pitch axis with moving through a state in which the director has defects, but of course they can be created in pairs without introducing any defects in the director via some homotopy. There is an energy barrier to realising such a change, however, this process does not change the either the nematic homotopy invariants or the contact topological invariants, and consequently this energy barrier is not detected by any of the invariants discussed so far in this thesis.

Conceptually, in a cholesteric the λ lines are singularities in the foliation whose leaves are 'cholesteric layers', surfaces to which the director is tangent. The construction of smectic-like textures at the end of Chapter 5 suggests a similar interpretation for the β lines of twist-bend nematics, except here the director makes a constant (away from the β lines) angle with the layers rather than being tangent to them. The layers don't just play a role in topological considerations, but also energetic ones.

A result of Radzihovsky & Lubensky [RL11], building on foundational work of de Gennes [dGP95], shows that at large scales cholesteric free energy is equivalent to a smectic free energy, with the smectic phase field ϕ chosen so that $\nabla\phi$ is the layer

normal. The argument of Radzihovsky & Lubensky applies both to the cholesteric ground state, where $\phi = z$, but also perturbations $\phi = z - u$ for some function u whose gradients are assumed to be small. The argument goes as follows. On short scales, a cholesteric is characterised by three degrees of freedom: the pitch axis, along which the director breaks translation symmetry, and a pair of nowhere colinear directions orthogonal to pitch axis, which the cholesteric director rotates between as we move along the layers. Consider now a small perturbation around the ground state, so that the layers are defined by the level sets of a slowly varying function u. Taking symmetry constraints into account and neglecting terms that are negligable, the most general coarse-grained form of the energy density of the cholesteric is [dGP95]

$$f = \frac{B}{2}\left(\frac{\partial u}{\partial z}\right)^2 + \frac{K}{2}\left(\frac{\partial^2 u}{\partial x^2} + \frac{\partial^2 u}{\partial y^2}\right), \tag{10.1}$$

where B and K are elastic constants. Thus the three degrees of freedom have been reduced to one, the function u. It follows that the low-energy deformations (Goldstone modes) of the helical state are characterized by a fully rotationally invariant, nonlinear smectic elastic theory [RL11].

In trying to extend this result to arbitrary functions u, and to study cholesteric layers in general, we encounter several difficulties. In chiral materials the pitch axis is defined by the eigendirection of the tensor $-qI + \Pi$ (where q is the twist and $\Pi = J\Delta$) that corresponds to the largest magnitude eigenvalue [EI14]. We do not know what conditions are necessary to ensure that the pitch axis does define a foliation, or what homotopies of the director result in the production of singularities in the foliation. We do not even know what constraints on a singular foliation are necessary to ensure there is a cholesteric director tangent to it.

In this chapter I will address a topological problem which offers some insight into questions of cholesteric layers: when can we construct a contact form η whose Reeb field is tangent to a singular foliation? I will prove that every contact structure is homotopic to one defined by such a contact form; thus, up to homotopy layers exist for every cholesteric director, a global version of the local results proved in §3.9.2. Invariants of layered structures come from the strict contactomorphism group, whose nontrivial elements correspond to functions which play the role of the smectic phase field in the Radzihovsky & Lubensky picture. More work is needed to apply these results to actual physical questions.

10.2 Basic Definitions

Definition 10.1. We will call a contact form η *foliated* if there exists a link L and a singular foliation $\mathcal{F}$ with singular set L such that the Reeb field of η is tangent to $\mathcal{F}$ on the complement of L and also tangent to L itself. If $\mathcal{F}$ satisfies this condition then the pair $(\eta, \mathcal{F})$, is a *foliated contact form (FCF)*, and they define an underlying contact structure $\xi = \ker \eta$. A FCF $(\eta, \mathcal{F})$ is called *minimal* if there is no nontrivial sublink $L' \subset L$ (including L' empty) of the singular set of $\mathcal{F}$ and foliation $\mathcal{F}'$ with singular set L' such that $(\eta, \mathcal{F}')$ is a FCF. A FCF $(\eta, \mathcal{F})$ is called *closed* if $\mathcal{F}$ can be defined by a closed 1-form.

Notice that the singular link L is the zero set of a Legendrian vector (or line, if it is not orientable) field for ξ (the normal to $\mathcal{F}$ for some appropriate metric) and therefore represents the Euler class, $e(\xi) = 2\mathcal{PD}[L]$.

Examples are easy to find. The standard overtwisted contact form $\eta = \cos(r)dz + r\sin(r)d\theta$ is foliated, with $\mathcal{F} = \ker dr$. Even though the standard overtwisted contact form has vanishing Euler class, its Reeb field is not tangent to any foliation without a singular line. In this way, the singular link L of the foliation is capturing something about the topology of the field that is not captured by the Euler class alone, although this property is detected by the dividing curve on a convex surface intersecting L.

The minimality condition asks that we choose the optimal foliation defining the layers, introducing no unnecessary singularties. For example, the standard tight contact form $\eta_{\text{std}} = dz - r^2 d\theta$ has Reeb field $R = \mathbf{e}_z$, and consequently there are many foliations it is tangent to: the level sets of r, θ in a polar coordiate system, which are singular, and the level sets of x, y in a Cartesian coordinate system, which are not. The pair $(\eta_{\text{std}}, \ker \mathbf{e}_r)$ is a FCF by the definition above, but not a minimal FCF as there exist other foliations without singularities that R is tangent to. For any constants a, b, the pair $(\eta_{\text{std}}, \ker (a\mathbf{e}_x + b\mathbf{e}_y))$ is also a minimal FCF.

No definition of a mathematical structure is complete without stating what it means for two such structures to be equivalent.

Definition 10.2. We say two FCFs $(\eta_i, \mathcal{F}_i)$, $i = 0, 1$ are equivalent if there exists an isotopy ϕ_t with $\phi_1^* \eta_0 = \eta_1$ and $\phi_1^* \mathcal{F}_0 = \mathcal{F}_1$.

In particular, for two FCFs to be equivalent it is necessary, but not sufficient, for the foliations to have the same singular link L, up to isotopy. This definition captures the idea that the layers deform along with the director. 'Tearing' of layers corresponds to the creation of new singularities (defects in the 'pitch axis'), and we would like

to understand what new topological invariants exist when we forbid this possibility, extending the ideas of Chapter 2 where we were trying to understand the invariants that arise when we forbid the creation of defects in the director.

Note that if two contact forms η_0, η_1 are isotopic, as is required by the equivalence of foliated contact forms, then their strict contactomorphism groups are equivalent as infinite-dimensional Lie groups. These groups are the novel invariants that appear when we consider the layer structure in addition to the director. One may produce characteristic classes associated with the strict contactomorphism group by way of Chern–Weil theory and an analogy with the symplectomorphism group studied in symplectic geometry [CS16], and it is likely that these characteristic classes will capture information about any layer structure that exists.

The Lie algebra of this group has a simple description for FCFs.

Proposition 10.1. *Suppose $(\eta, \mathcal{F})$ is a FCF on a closed manifold and not every orbit of the Reeb field R of η is closed. Then the Lie algebra of $\mathcal{SC}(M, \eta)$ consists exactly of those functions constant on the leaves of $\mathcal{F}$, and is equivalent to the space of metrics weakly compatible with η for which R is divergence free.*

Proof. Certainly, every function that is constant on the leaves of $\mathcal{F}$ must be preserved by R and hence belongs to the Lie algebra of the strict contactomorphism group. Since by assumption there are orbits of R that are not closed, the only functions that can be preserved by R are those that are constant on the leaves. Any such function can be used to generate a weakly compatible metric for which R is volume-preserving, see §3.11. □

Finally, note that the question of determining whether a contact structure can be defined by a FCF is easily reduced to homotopy data.

Lemma 10.1. *Suppose ξ_0, ξ_1 are homotopic contact structures and ξ_0 is defined by a FCF. Then so is ξ_1. Moreover, these FCFs are equivalent.*

Proof. If ξ_0, ξ_1 are homotopic contact structures defined by contact forms η_0, η_1, then by Gray Stability there exists an isotopy ϕ_t and a positive function λ such that $\phi_1^* \eta_0 = \lambda \eta_1$. If η_0 is foliated then so is $\lambda\eta_1$, as we can choose a foliation $\mathcal{F}$ which the Reeb field of η_0 is tangent to, and pull it back along the isotopy. Thus $(\lambda\eta_1, \psi_1^* \mathcal{F})$ is a FCF defining ξ_1, which is evidently equivalent to $(\eta_0, \mathcal{F})$. □

10.3 Examples of FCFs

Before turning to the general theory I will give several constructions of FCFs to build some intuition about their properties.

10.3.1 Torus Bundles over the Circle

Firstly we will examine when it is possible for the singular link L of a FCF to be empty. The simplest case is when the Reeb field of a contact structure is tangent to a nonsingular foliation defined by a closed 1-form α. This is the most immediate and natural generalisation of the cholesteric ground state. This is studied in Refs. [DR00; DR05], where the following two theorems are proved.

Theorem 10.1. *([DR00]) Let α be a closed nonsingular 1-form on a $2n+1$ dimensional manifold M, and η another 1-form. The following are equivalent:*

1. *The family of 1-forms $\alpha_t = \alpha + t\eta$ is a contact form for every $t > 0$,*
2. *The 1-form η is contact with Reeb field R such that $\alpha(R) = 0$.*

If α is a closed, but singular, 1-form defining a singular foliation $\mathcal{F}$, and $(\eta, \mathcal{F})$ is a FCF, then part of the proof of this theorem given in Ref. [DR00] still applies, and α can still be perturbed into a (nonsingular) contact form $\alpha_t = \alpha + t\eta$ as in the theorem. The contact structure defined by this contact form obviously agrees with that defined by η along the singular link of $\mathcal{F}$, so this singular link still consists of closed orbits of the Reeb field. It follows that all closed FCFs $(\eta, \mathcal{F})$ determine perturbations of the (possibly singular) foliation $\mathcal{F}$ into a (nonsingular) contact structure.

Theorem 10.2. *([DR05]) A closed 3-manifold M has a closed 1-form α satisfying the conditions of Theorem 10.1 if and only if M is a T^2-bundle over S^1.*

This completely classifies the situation where $L = \emptyset$ and the leaves of the foliation are all closed.

10.3.2 Projectively Anosov Reeb Fields

More generally, it is possible for the foliation to be nonsingular but have leaves that are not closed.

A nonsingular vector field X with flow ϕ_t is called *Anosov* if there is a Riemannian metric and a continuous decomposition of the tangent bundle $TM = \{X\} \oplus E^+ \oplus E^-$ into a direct sum of line bundles, such that the splitting is invariant under the flow of X and the differential $d\phi_t$ acts by dilations on E^+ and contractions on E^-. This implies that there exists a constant $C > 0$ such that for all t we have

$$\|d\phi_t v_+\| \geq e^{Ct} \|v_+\| , \tag{10.2}$$

and

$$\|d\phi_t v_-\| \leq e^{-Ct} \|v_-\|, \tag{10.3}$$

for all $t > 0$ and any vector field $v_\pm \in E^\pm$. If the plane fields $\mathcal{F}^\pm = \{X\} \oplus E^\pm$ are smooth, then they are integrable; $\mathcal{F}^+$ and $\mathcal{F}^-$ are called the *unstable and stable foliations* of the Anosov flow. In particular, if X happens to be the Reeb field of a contact form, it defines a FCF.

Mitsumatsu introduced the notion of a *projectively Anosov flow* in Ref. [Mit95]; it was also introduced independently by Eliashberg & Thurston, who call such flows *conformally Anosov* [ET91]. A vector field X is projectively Anosov if there is a Riemannian metric and a splitting $TM = \{X\} \oplus E^+ \oplus E^-$ of the tangent bundle as for the Anosov flow, except we now we require the weaker condition

$$\frac{\|d\phi_t v_+\|}{\|d\phi_t v_-\|} \geq e^{Ct} \frac{\|v_+\|}{\|v_-\|}, \tag{10.4}$$

for all $t > 0$ and any vector fields $v_\pm \in E^\pm$. This is in fact the same as asking that X is Anosov when regarded as a section of the projectivised tangent bundle $\mathbb{P}TM$. As before, if the planes fields $\mathcal{F}^\pm = \{X\} \oplus E^\pm$ are smooth, then they are integrable, and again $\mathcal{F}^+$ and $\mathcal{F}^-$ are called the *unstable and stable foliations* of the projectively Anosov flow. The condition is fairly technical, however there is a nicer condition that shows the relationship with contact structures. Call a pair (ξ^+, ξ^-) of transverse, oppositely-oriented contact structures a *bicontact structure*. Since these contact structures are transverse, we can choose a nonsingular vector field directing their intersection.

Proposition 10.2. *(Misumatsu [Mit95]) A nonsingular vector field X is projectively Anosov if and only if there is a bicontact structure (ξ^+, ξ^-) such that X directs the intersection $\xi^+ \cap \xi^-$.*

If X is projectively Anosov and is also the Reeb field of a contact form, then the contact structure ξ defined by that form is transverse to both the contact structures ξ^+ and ξ^- in the bicontact structure whose existence is implied by Proposition 10.2. The resulting trio of transverse contact structures determine a trivialisation of the tangent bundle, such that two of them have the same handedness and the other has the opposite handedness. Bicontact structures and projectively Anosov flows appear naturally when considering the perturbation of foliations into contact structures, and indeed this is the context in which Eliashberg & Thurston introduce them.

There is an important relationship between Anosov flows, projectively Anosov

flows, and the tightness of the underlying bicontact structure.

Theorem 10.3. *(Mitsumasu [Mit95]) An Anosov vector field on a compact manifold lies in the intersection of a pair of oppositely-oriented tight (in fact, symplectically-fillable) contact structures.*

Little is known about projectively Anosov flows, however there has been some investigation of the topology of the invariant foliations [Nod00]. The most important structural result is the theorem of Noda [Nod00].

Proposition 10.3. *If the invariant foliations are differentiable, then they do not possess Reeb components*[1] *and are therefore taut. Consequently, a projectively Anosov flow with differentiable invariant foliations cannot exist on a manifold whose universal cover is S^3 or $S^2 \times \mathbb{R}$. The invariant foliations have at most finitely many closed integral leaves.*

The invariant foliations of an Anosov flow do not have closed leaves; it is easy to construct projectively Anosov flows that do, see Ref. [Nod00]. Moreover, projectively Anosov flows are far more plentiful than Anosov flows, e.g. T^3 has many projectively Anosov flows but no Anosov flows [ET91]. As Mitsmatsu points out, the contact structures associated to an projectively Anosov flow need not be tight—the construction of the sympletic form on $M \times [-1, 1]$ that allows us to conclude this in the Anosov case fails on closed leaves.

The existence of compatible metrics for contact forms discussed in Chapter 3 allows us to establish the existence of projectively Anosov Reeb fields. Let η be a contact form with Reeb field R and g a compatible metric, and let $J = R\times$ be the almost complex structure on the planes of the contact structure ξ determined by η. Introduce a tensor

$$h = \frac{1}{2}\mathcal{L}_R J. \tag{10.5}$$

When the bend vanishes, which of course it does in a compatible metric, this tensor is equal to $J \circ \Delta$, and as the twist is constant and equal to $+1$ with respect to a compatible metric, $-I + h$ is exactly the 'chirality pseudotensor' used to define the pitch axis in Ref. [EI14].

Theorem 10.4. *(Theorem 11.5 [Bla10]) Suppose h is nowhere-vanishing, and let $\mathbf{e}_1, \mathbf{e}_2 = J\mathbf{e}_1$ be a local orthonormal eigenbasis of h such that $h\mathbf{e}_1 = \lambda\mathbf{e}_1$, where λ is the positive eigenvalue of h. If the sectional curvatures satisfy $K(R, \mathbf{e}_1) < (1 + \lambda)^2$*

[1] A Reeb component is a solid torus with a foliation that has the boundary as a leaf, and foliates the interior with folded-up copies of $\mathbb{R}^2$.

and $K(R, \mathbf{e}_2) < (1-\lambda)^2$, then R is a projectively Anosov flow. In particular, if these sectional curvatures are negative, then R is projectively Anosov.

The standard tight contact structure on $\mathbb{R}^3$ has a projectively Anosov Reeb field.

Let us consider a slightly more general situation, where h is allowed to have zeros. Since its eigendirections are Legendrian line fields of ξ, their zero sets (and consequently the zero set of h) will generically consist of a link L that represents the Euler class [MA16b]. Satisfying the curvature constraints of Theorem 10.4 implies that R is projectively Anosov on the complement of L, and therefore the existence of a compatible metric with those curvature properties implies that R is tangent to a pair of foliations $\mathcal{F}^{\pm}$ on $M - L$, defined by 1-forms $\alpha_{\pm}$. We can extend these over L so they become singular there, by taking 1-forms $\bar{\alpha}_{\pm} = |\lambda|\alpha_{\pm}$, for λ an eigenvalue of h. This gives a FCF, where the foliation may not be orientable. Note these FCFs never have singularities of double-twist type: for this to be the case a neighbourhood of the singular line would have to be foliated by closed torus leaves, and this is not possible in a projectively Anosov flow.

10.3.3 Round Handle Decompositions

Weakly compatible metrics for contact forms η give metrics for which the Reeb field R is Beltrami, $HR = \operatorname{curl} R$ with arbitrary proportionality factor H. If the proportionality factor is not constant, and additionally R is volume preserving, then it must be the case that R is tangent to the level sets of H, and hence the domain is fibered into torii invariant under the flow of R, along with a few 'singular fibers,' which are closed orbits of R. This observation is originally due to Arnold [AK98]. Evidently, if a contact form has a weakly compatible metric with these properties then it is a FCF, with the foliation being defined by the exact singular 1-form dH.

These are perhaps the most natural examples for extending the ideas of Radzihovsky & Lubensky: they fit neatly in the physical picture, with H playing the role of the smectic phase field.

We can easily construct examples of FCFs of this type. Firstly, consider the 1-form

$$\eta_s = r d\theta + \left(1 - \frac{s}{2} r^2\right) dz, \tag{10.6}$$

$s \in (0, \infty)$ fixed, on $D^2 \times S^1$. η_s is contact and has Reeb field $R = \mathbf{e}_z + sr\mathbf{e}_\theta$. This is a vector field tangent to the level sets of the radial coordinate r and defining a linear flow with slope s on the boundary where $r = 1$. Using these 1-forms, we can construct additional examples of FCFs on 3-manifolds using the idea of a round handle decomposition (RHD).

A *round handle* is a solid torus $D^2 \times S^1$ together with an index, either 0, 1, or 2, and an exit set $E \subset \partial D^2 \times S^1$ such that

- If the index is 0, $E = \emptyset$,
- If the index is 1, then either E is a pair of disjoint annuli that each wrap once longitudinally around the torus, or else E is a single annulus wrapping twice longitudinally around the torus,
- If the index is 2, then $E = T^2$.

A *round handle decomposition (RHD)* is a finite sequence of submanifolds $\emptyset = M_0 \subset M_1 \subset \cdots \subset M_n = M$, where each M_{j+1} is formed by adjoining a round handle to ∂M_i along the exit set, in such a way that the handles are adjoined in order of increasing index. For example, the 3-sphere is obtained by taking first an index 0 handle, and then adjoining an index 2 handle. Not all manifolds have an RHD, however any graph-manifold (e.g., a Seifert-fibered space) has one [Mor78]. The *cores* of an RHD, the curves $0 \times S^1$ in each handle, define a finite link L.

Proposition 10.4. *Suppose M has a round handle decomposition $\emptyset = M_0 \subset M_1 \subset \cdots \subset M_n = M$. Then there is a FCF $(\eta, \mathcal{F})$ on M such that the link L consisting of cores of the RHD is the singular link of $\mathcal{F}$, and otherwise the leaves of $\mathcal{F}$ are torii.*

Proof. We construct the FCF via induction. The jth 0-handle may be equipped with the contact form (10.6) for some slope s_j. When M_i consists entirely of 0-handles, this evidently gives the desired FCF. Suppose now we have constructed the desired contact form on M_j, and we now add a round handle h_{j+1} to ∂M_j to obtain M_{j+1}. There is a diffeomorphism $\phi : h_{j+1} \to \partial M_j$ that affects this attachment. Pulling back the characteristic foliation on ∂M_j induced by the contact form we have constructed so far, we obtain a characteristic foliation on the boundary of h_{j+1}. By a diffeomorphism of the handle, we may assume this has constant slope s_{j+1}; we fill h_{j+1} with the contact form η_{j+1}, and then this yields a contact form on M_{j+1} which is evidently still foliated. Continuing this process gives a FCF. □

The Reeb field of the standard tight contact structure on S^3 is of this form, where the RHD is given by the Heergard decomposition of the sphere into a pair of solid torii. In this case, we may take any slope s on the torus T that divides the two handles, and glue η_s into each handle. It is clear when this construction on S^3 yields the tight contact structure: we need to make certain that the 'total twisting' of the slope is such that we never have a Legendrian curve bounding a disk, which would be overtwisted. For this, it is enough to ensure that the Reeb field completes less than a $\pi/2$ rotation.

Proposition 10.5. *a FCF obtained by from a RHD as described in Proposition 10.4 is never equivalent to a FCF determined by a projectively Anosov flow.*

Proof. Close to the singular set of the foliation determined by the RHD, all leaves are closed torii: all singularities are of double-twist type. But no singularities of the invariant foliations of a projectively Anosov flow are of double-twist type, and consequently they cannot be equivalent. □

Physically, these contact forms resemble a collection of double-twist cylinders. Real cholesteric textures that have this form, such as Skyrmion lattices and blue phases, tend not to give a decomposition of space into a RHD; rather, the double-twist cylinders do not quite fill the space, and the director on this space has to match onto the boundaries of the cylinders, which requires disclination lines. It would be interesting to develop a theory of 'almost round handle decompositions' that involve gluing solid torii together to almost fill space but with some space left over, and characterise the structures that can be formed this way, perhaps via the possible symmetry groups. This could be achieved by modifying the ideas of Chapter 4 to bring geometry into the picture, as well as discussing singular foliated contact forms.

In [EG99], Etnyre & Ghrist study vector fields tangent to plane fields. In particular, they study the case where said vector field is the gradient of a function H. The preimage of any regular value of the function must be a disjoint union of torii, while the preimage of the nonregular values gives a link L. Thus such vector fields determine a RHD of M.

Proposition 10.6. *Suppose M has a plane field with a tangent gradient flow $X = \nabla H$. Then there exists a contact form η on M whose Reeb field R preserves H, and a Riemannian metric g such that R is unit length, divergence free, and Beltrami, with proportionality factor H, i.e., R satisfies Euler's equations on (M, g).*

Proof. The first claim is Lemma 3.1 of [EG99]: the foliation by level sets of H agrees with the foliation constructed in Proposition 10.4. Since the Reeb field is tangent to this foliation, it must preserve H. The second claim follows from the existence of weak compatible metrics with arbitrary proportionality factor, §3.11. □

Etnyre & Ghrist study the case where a tight contact structure contains a gradient vector field, and show that there is also an overtwisted contact structure containing that gradient field. One can make a similar argument from the constructions of FCFs in this section: we can modify the contact form on any 0-handle to make it overtwisted there, simply by putting an extra 'turn' into (10.6) while keeping the

boundary slope the same. Etnyre & Ghrist express this in terms of a surgery that mimics the Lutz twist, which is essentially the same idea.

10.4 Constructing FCFs from Open Book Decompositions

In this section, I show that every contact structure is defined by a FCF.

An *open book decomposition* of M is a pair (L, π), where L is a link in M called the *binding* of the open book, and $\pi : M - L \to S^1$ is a fibration such that each fiber $\pi^{-1}(z)$, $z \in S^1$, is the interior of a compact surface with boundary S whose boundary is L. The fibers are called *pages* of the book. By a theorem of Alexander [Ale23], every closed 3-manifold admits an open book decomposition. Examples of practical interest arise by considering the solid angle function ω of a fibered knot L in S^3 [BA18; Bin19]. Whether the solid angle function has singularities depends on the particular embedding of L, but it is not too hard to come up with examples where the level sets of ω fiber the complement of L, e.g by considering a circle of radius R in the $z = 0$ plane in $\mathbb{R}^3$ and compactifying. Two open books are equivalent if they are related by a *positive stabilisation*. This involves glueing a handle onto the pages of the open book, and changing the monodromy by composing with the right-handed Dehn twist.

A contact structure ξ is *supported* by an open book (L, π) if ξ is isotopic to a contact structure ξ' defined by a contact form η such that (1) the restriction of $d\eta$ to each page is a positive area form, and (2) $\eta|_L > 0$. This property can also be stated in terms of Reeb fields.

Lemma 10.2. *(Lemma 3.5 [Etn04b]) Let ξ be a contact structure and (L, π) an open book. The following are equivalent:*

1. *ξ is supported by (L, π),*
2. *ξ can be isotoped to be close to the tangent space to the pages of the open book on compact subsets of those pages, and such that the planes of ξ are transverse to L and to the pages in a neighbourhood of L,*
3. *There is a Reeb field R for a contact structure isotopic to ξ such that R is tangent to L and transverse to the pages of the open book.*

Notice that condition (2) bears a close resemblance to the ideas discussed in §10.3.1. Let $C \subset S$ be the compact subset of the pages implied by this condition. The open

book gives a foliation of $C \times [0,1]$ by the surfaces $C \times z$ that descends to a foliation on $C \times S^1$ by glueing the ends together with the monodromy map. Then, by results of §10.3.1, we can perturb this foliation (which is defined by the closed 1-form dz) into a contact structure by an arbitrarily small perturbation.

The following theorem establishes the converse of the result of Thurston & Winkelnkemper [TW75]: an open book always gives rise to a contact structure.

Theorem 10.5. *(Giroux's Correspondence [Gir02]) There is a bijective correspondence between open book decompositions of M up to positive stabilisation, and homotopy classes of contact structures on M.*

I will not give a full proof of this theorem here. In addition to [Gir02] there are several other references where one can see aspects of the proof, for example Refs. [Gei08; Etn04b]. However, I will make use of the Thurston–Winkelnkemper direction of the proof.

Theorem 10.6. *(Thurston–Winkelnkemper [TW75]) Every open book decomposition supports a contact structure.*

Proof. Let S be a page of the open book and ϕ the monodromy of the fibration. We can write

$$M \cong S_\phi \cup_\psi \prod_{|\partial S|} D^2 \times S^1, \tag{10.7}$$

where S_ϕ is the mapping torus obtained by taking $S \times [0,1]$ and identifying $S \times 0$ and $S \times 1$ using ϕ, and ψ denotes the map that glues the solid torii around the binding to the pages. Now consider the set of 1-forms α that that $\alpha = (1+x)dz$ and $d\alpha$ is an area form on S, where $(z,x) \in S^1 \times [0,1]$ are the coordinates on the pages near the binding L. The set of such 1-forms is nonempty and convex.

Given α in this set $\phi^*\alpha$ is also in this set. Since the set is convex, $t\alpha + (1-t)\phi^*\alpha$ is also in the set. The 1-form $\alpha_K = Kdt + t\alpha + (1-t)\phi^*\alpha$ is contact on $S \times [0,1]$ for K sufficiently large, where t is the coordinate on $[0,1]$. Clearly this gives rise to a contact form on the mapping torus S_ϕ.

Now we extend over the solid torii in the neighbourhood of the binding. On $D^2 \times S^1$ with coordinates z on S^1 and polar coordinates r, θ the map ψ is given by $\psi(r,\theta,z) = (-z,\theta,r-1+\epsilon)$. Pulling back α_K along this map gives $\alpha_\psi = Kd\theta - (r+\epsilon)dz$. We can extend this across the solid torus, for example by taking it to be $f(r)dz + g(r)d\theta$ with $fg' - f'g > 0$ and $f(r) = 1, g(r) = r^2$ near the core. The construction of a 1-form with these properties is similar to the Lutz twist. □

Now I am going to use Theorem 10.5 to prove that every contact structure can be defined by a FCF.

Theorem 10.7. *Let (L, π) be an open book. There exists a foliated contact form η such that the Reeb field of η is tangent to some singular foliation $\mathcal{F}$ with singularity set L, and such that $\mathcal{F}$ agrees with the foliation by pages of the open book outside some neighbourhood N of L. Inside N, the leaves of $\mathcal{F}$ are torii.*

Proof. Let K_j denote the components of L and let $N_j \cong D^2 \times S^1$ be an open neighbourhood of K_j. Set $N = \bigcup_j N_j$. In each component of N, $\mathcal{F}$ agrees with the foliation by level sets of θ, where r, θ, z are the coordinates on $D^2 \times S^1$. Away from L, $\mathcal{F}$ is a taut foliation and consequently there exists a closed 2-form Ω with $\Omega|_{\mathcal{F}} > 0$, such that on each N_j we have $\Omega = rdzdr$.

Using standard facts about open books, we can view $M - N$ as $S \times [0, 1]$, where S is a page of the book, with the endpoints glued together with some monodromy map ψ. Then $\Omega|_{S \times t}$ is a sympletic form on $S \times t$, where t is the coordinate on $[0, 1]$. For any function H we can define a vector field X_H by $\iota_{X_H}\Omega = dH$, which obviously preserves Ω. Since S is compact with boundary we can choose some H so that dH is nonvanishing on S; to see this, take a genus g surface Σ_g such that S is Σ_g with b disks removed, take a Morse function H on Σ_g, and then remove the disks so that the singularities of dH are removed with them.

Since $\Omega = rdzdr$ near the boundary, we can further assume that X_H is independent of t near the boundary of S, $X_H = f(r, z)\mathbf{e}_r + g(r, z)\mathbf{e}_z$. By our method of constructing X_H we can assume that the winding of X_H around each boundary component is some integer $k \leq +1$, and hence that H is (close to the boundary) a harmonic function with the following structure: for coordinates x, y defined by $x = r\cos(z), y = r\sin(z)$, we have $dH = r\sin(kz)dx + r\cos(kz)dy$. Define u by $\star\beta = du$, for $\star$ the Hodge star of a Riemannian metric on the disk whose volume form is Ω. It must be that u is also independent of t.

For a fixed H, this gives a t-parameterised family of vector fields on S, which yields a vector field X on $S \times [0, 1]$ that is tangent to every $S \times t$, preserves Ω, and is also nonsingular. We can choose a smooth family of multicurves Γ_t that divide the foliations on $S \times t$ defined by X, and such that $\Gamma_0 = \phi^*\Gamma_1$, where ϕ is the monodromy of the fibration. Consequently, using the existence result of Lemma 3.7 we can define a contact form $\eta = \beta_t + u_t dt$ where $\beta_t = \iota_{X|_{S \times t}}\Omega$ and we have $\beta_0 = \phi^*\beta_1, u_0 = \phi^* u_1$. The characteristic foliation is directed by X, which preserves an area form, so by Lemma 6.3 the Reeb field of η is tangent to each $S \times t$. By glueing the ends together, this yields a contact form, which we also call η, on $M - N$.

We wish to extend η over each N_j. We can pull back η along the map ψ used to glue the mapping torus $S \times_\phi [0,1]$ onto the neighbourhood of the binding. This map is given by $\psi(r,\theta,z) = (-z,\theta,r-1+\epsilon)$ [Etn04b]. Pulling back η gives

$$\eta_\psi = (\psi^* u)d\theta + \psi^* dz. \tag{10.8}$$

We can extend this over N_j as a 1-form vanishing on $0 \times S^1$ but contact everywhere else, and with Reeb field tangent to the level sets of θ. Now consider the following contact form on $D^2 \times S^1$:

$$\alpha = \cos(\theta)dr + (\epsilon + \sin(\theta))dz \tag{10.9}$$

where $\epsilon < 1$ is a small constant. The Reeb field is

$$R = \frac{\cos(\theta)}{(1+\epsilon\sin(\theta))}\mathbf{e}_r + \frac{\sin(\theta)}{(1+\epsilon\sin(\theta))}\mathbf{e}_z, \tag{10.10}$$

which is tangent to the level sets of θ and also to the line $r = 0$. Take

$$\omega = (1-r)\alpha + Ar\eta_\psi. \tag{10.11}$$

For A sufficiently large this is contact, and it clearly agrees with η_ψ near to the boundary of N_j. Close to $r = 0$, $\eta \approx \alpha$, and therefore the Reeb field is tangent to K_j. This gives our extension of η as a contact form on M with the desired properties. □

We see this is very similar to the construction of a 1-form whose contact structure is supported by the open book. Indeed, it is essentially the same construction, only we take a little more care in choosing the contact form on the mapping torus to ensure the Reeb field is tangent rather than transverse to the pages. By design, all singularities are screw-like.

Theorem 10.8. *Every contact structure ξ on a closed 3-manifold can be defined by a foliated contact form. In particular, there is a FCF with only screw-like singularities in every homotopy class of contact structures.*

Proof. By Lemma 10.1 it suffices to demonstrate the existence of a contact structure defined by a foliated contact form in each homotopy class of contact structures. Let ξ be any contact structure. By Theorem 10.5, there is some open book (L,π) supporting ξ. Let η be the foliated contact form for (L,π) constructed in Theorem 10.7, and let Ω be the closed 2-form, positive on the pages, that is used in the

construction. If we can homotope η into a contact form η' whose Reeb field is tangent to the binding and transverse to the pages, i.e. supported by the open book, then we are done.

We use the fact that a small perturbation of a contact form is again a contact form. Close to the binding, we can write $\eta = adr + bd\theta + cdz$ for some functions a, b, c. AS the Reeb field is tangent to the level sets of θ, $\partial_z a = \partial_r c$. Adding a small r-dependent perturbation to c will destroy this property away from the binding and make the Reeb field of the perturbed contact form transverse to the pages.

The rest of the manifold is diffeomorphic to $S \times [0, 1]$ with the endpoints joined by the monodromy ϕ. Write $\eta = \beta_t + u_t dt$, where β_t is closed. We must perturb β_t so that $d\beta_t > 0$ for each t. Take the function H from the proof of Theorem 10.7. Let J be an almost complex structure associated with Ω. Since dH is nonvanishing by assumption, $dH \wedge JdH > 0$. Let $\alpha_t = tHJdH + (1-t)\phi^*(HJdH)$, and $\beta'_t = \beta_t + \epsilon\alpha_t$. Then $d\beta'_t > 0$. Define a contact form η' such that $\eta'|_{S\times t} = \beta'_t$, and also such that η'_t is homotopic to η. The Reeb field of η' is transverse to each $S \times t$. Clearly η' descends to a contact form on the mapping torus which is homotopic to η.

Thus we have found a contact form η' which is homotopic to η and is supported by the open book (L, π), as required. □

Bibliography

[Abr57] A.A. Abrikosov. On the magnetic properties of superconductors of the second group. *Sov. Phys. JETP*, 5:1174–1182, 1957.

[ACMK10] G.P. Alexander, B.G Chen, E.A. Matsumoto, and R.D. Kamien. Power of the Poincaré Group: Elucidating the Hidden Symmetries in Focal Conic Domains. *Phys. Rev. Lett.*, 104:257802, 2010.

[ACMK12] G.P. Alexander, B.G. Chen, E.A. Matsumoto, and R.D. Kamien. Colloquium: disclination loops, point defects, and all that in nematic liquid crystals. *Rev. Mod. Phys.*, 84:497, 2012.

[AGL05] J. Ahrens, B. Geveci, and C. Law. *ParaView: An End-User Tool for Large Data Visualization*. Visualization Handbook, Elsevier, 2005.

[AGLV88] V. I. Arnold, V. V. Goryunov, O. V. Lyashko, and V. A. Vasil'ev. *Singularity Theory*. Springer, 1988.

[AGZV85] V. I. Arnold, S. M. Gusein-Zade, and A. N. Varchenko. *Singularities of Differentiable Maps, Volume I*. Birkhäuser, 1985.

[AK98] V. I. Arnold and B. A. Khesin. *Topological Methods in Hydrodynamics*. Springer, 1998.

[Ale23] J.W. Alexander. A lemma on systems of knotted curves. *Proc. Nat. Acad. Sci. U.S.A.*, 9:93–95, 1923.

[Ale28] J.W. Alexander. Topological invariants of knots and links. *Trans. Amer. Math. Soc.*, 30:275–306, 1928.

[Ale18] G.P. Alexander. *Topology in Liquid Crystal Phases*. in: S. Gupta and A. Saxena (eds) The Role of Topology in Materials (Springer, Cham), 2018.

[Alt95] S. Altschuler. A geometric heat flow for one-forms on three dimensional manifolds. *Ill. Jour. Math.*, 39:98–118, 1995.

[Arn72] V.I. Arnold. Normal forms for functions near degenerate critical points, the Weyl groups of A_k, D_k, E_k and Lagrangian singularities. *Funct. Anal. Its Appl.*, 6:254–272, 1972.

[Arn78] V.I. Arnold. Index of a singular point of a vector field, the Petrovski–Oleinik inequality, and mixed Hodge structures. *Proceedings of the Internation Congress of Mathematicians, Vancouver*, 12:1–12, 1978.

[Arn89] V. I. Arnold. *Mathematical Methods in Classical Mechanics, 2nd Ed.* Springer, Graduate Texts in Mathematics **60**, 1989.

[Arn90a] V. I Arnold. Contact geometry: the geometrical method of Gibb's thermodynamics. *in: Proceedings of the Gibbs Symposium (Yale, 1989), Amer. Math. Soc., Providence, RI*, pages 163–179, 1990.

[Arn90b] V. I Arnold. Contact geometry and wave propagation. *Enseign. Math.*, 36:215–266, 1990.

[AS16] P.J. Ackerman and I.I. Smalyukh. Static three-dimensional topological solitons in fluid chiral ferromagnets and colloids. *Nature Materials*, 16:426–432, 2016.

[AS17] P.J. Ackerman and I.I. Smalyukh. Diversity of Knot Solitons in Liquid Crystals Manifested by Linking of Preimages in Torons and Hopfions. *Phys. Rev. X.*, 7:011006, 2017.

[AXZ+18] H. Aharoni, Y. Xia, X. Zhang, R.D. Kamien, and S. Yang. Universal inverse design of surfaces with thin nematic elastomer sheets. *Proc. Natl. Acad. Sci. USA*, 115:7206, 2018.

[B+13] V. Borshch et al. Nematic twist-bend phase with nanoscale modulation of molecular orientation. *Nat. Comm.*, 4:2635, 2013.

[BA18] J. Binysh and G.P. Alexander. Maxwell's theory of solid angle and the construction of knotted fields. *J. Phys. A.*, 51, 2018.

[BDP+78a] Y. Bouligand, B. Derrida, V. Poenaru, Y. Pomeau, and G. Toulouse. Distortions with double topological character: the case of cholesterics. *J. Phys. France*, 39:863–867, 1978.

[BDP+78b] Y. Bouligand, B. Derrida, V. Poenaru, Y. Pomeau, and G. Toulouse. Distortions with double topological character: the case of the cholesteric. *Journal de Physique*, 39:863–867, 1978.

[Ben83] D. Bennequin. Entrelacements et équations de Pfaff. *in: IIIe Rencontre de Géométrie du Schnepfenried, Vol. 1, Astérisque*, 107–108:87–161, 1983.

[Ber71] V.L. Berezinskiĭ. Destruction of long-range order in one-dimensional and two-dimensional systems having a continuous symmetry group I. Classical systems. *Sov. Phys. JETP*, 32:493–500, 1971.

[Bin19] J. Binysh. *Construction and Dynamics of Knotted Fields in Soft Matter Systems.* PhD thesis, University of Warwick, 2019.

[Bla10] D. E. Blair. *Riemannian Geometry of Contact and Symplectic Manifolds, 2nd ed.* Birkh auser, Progress in Mathematics **203**, 2010.

[BMČ+14] D.A. Beller, T. Machon, S. Čopar, D.M. Sussman, G.P. Alexander, R.D. Kamien, and R.A. Mosna. Geometry of the Cholesteric Phase. *Phys. Rev. X*, 4:031050, 2014.

[Bou72] Y. Bouligand. Recherches sur les textures des états mésomorphes - 1. Les arrangements focaux dans les smectiques : rappels et considérations théoriques. *J. Phys. France*, 33:525, 1972.

[Bou08] Y. Bouligand. Liquid crystals and biological morphogenesis: Ancient and new questions. *Comptes Rendues Chimie*, 11:281–296, 2008.

[BPA20] J. Binysh, J. Pollard, and G.P. Alexander. Geometry of Bend: Singular Lines and Defects in Twist-Bend Nematics. *Phys. Rev. Lett.*, 125:047801, 2020.

[BT82] R. Bott and L.W. Tu. *Differential Forms in Algebraic Topology.* Springer, Graduate Texts in Mathematics **82**, 1982.

[C+11] M. Cestari et al. Phase behavior and properties of the liquid-crystal dimer 1″,7″-bis(4-cyanobiphenyl-4′-yl) heptane: A twist-bend nematic liquid crystal. *Phys. Rev. E*, 84:031704, 2011.

[C+13] D. Chen et al. Chiral heliconical ground state of nanoscale pitch in a nematic liquid crystal of achiral molecular dimers. *Nat. Comm.*, 110:15931, 2013.

[CAA+13] B. Chen, P.J. Ackerman, G.P. Alexander, R.D. Kamien, and I.I. Smalyukh. Generating the Hopf Fibration Experimentally in Nematic Liquid Crystals. *Phys. Rev. Lett.*, 110:237801, 2013.

[CAK09] B.G. Chen, G.P. Alexander, and R.D. Kamien. Symmetry breaking in smectics and surface models of their singularities. *Proc. Natl. Acad. Sci. U.S.A.*, 106:15577, 2009.

[Cal69] E. Calabi. An intrinsic characterisation of harmonic 1-forms. *Global Analysis, Papers in Honour of K. Kodaira*, page 101, 1969.

[Car04] E. Cartan. Sur la structure des groupes infinis de transformations. *Ann. Éc. Norm.*, 3, 1904.

[Car37] E. Cartan. La théorie des groupes finis et continus et la géométrie différentielle traitées par la méthode du repère mobile. *Gauthier-Villars*, 1937.

[Car45] E. Cartan. Les systèms différentials extérieurs et leurs applications géometriques. *Exposés de Géométrie*, 14, 1945.

[Cay73] A. Cayley. On the cyclide. *Quart. J. Pure Appl. Math.*, 12:148, 1873.

[ČDKŽ13] S. Čopar, M.R. Dennis, R.D. Kamien, and S. Žumer. Singular values, nematic disclinations, and emergent biaxiality. *Phys. Rev. E*, 87:050504, 2013.

[CDTY91] I. Chuang, R. Durrer, N. Turok, and B. Yurke. Cosmology in the Laboratory: Defect Dynamics in Liquid Crystals. *Science*, 251:1336–1342, 1991.

[CK57] S. Chandrasekhar and P.C. Kendall. On force-free magnetic fields. *Astrophys. J.*, 126:457, 1957.

[Cle66] A. Clebsch. Ueber die simultane integration linearer partieller differentialgleichungen. *J. Reine Angew. Math.*, 65:257–268, 1866.

[CM73] N.A. Clark and R.B. Meyer. Strain-induced instability of monodomain smectic A and cholesteric liquid crystals. *Appl. Phys. Lett.*, 22:493, 1973.

[CMPS19] R. Cardona, E. Miranda, and D. Peralta-Salas. Euler flows and singular geometric structures. Preprint available at , 2019.

[CS16] R. Casals and O. Spáčil. Chern–Weil theory and the group of strict contactomorphisms. *Jour. Top. Anal.*, 8:59–87, 2016.

[Cĕ61] G. Călugăreanu. Sur les classes d'isotopie des nœuds tridimensionnels et leurs invariants. *Czechoslovak Math. J*, 11:588–625, 1961.

[ČŽ11a] S. Čopar and S. Žumer. Nematic disclinations as twisted ribbons. *Phys. Rev. E*, 84:051702, 2011.

[ČŽ11b] S. Čopar and S. Žumer. Nematic Braids: Topological Invariants and Rewiring of Disclinations. *Phys. Rev. Lett.*, 106:177801, 2011.

[ČŽ12] S. Čopar and S. Žumer. Topological and geometric decomposition of nematic textures. *Phys. Rev. E*, 85:031701, 2012.

[ČŽ13] S. Čopar and S. Žumer. Quaternions and hybrid nematic disclinations. *Proc. R. Soc. A*, 469:20130204, 2013.

[Dea40] F. Deahna. ber die bedingungen der integrabilitat. *J. Reine Angew. Math.*, 20:340–350, 1840.

[Der64] G.H. Derrick. Comments on nonlinear wave equations as models for elementary particles. *J. Math. Phys.*, 5:1252–1254, 1964.

[DFG+86] T. Dombre, U. Frisch, J. Greene, M. Hénon, A. Mehr, and A. Soward. Chaotic Streamlines in the ABC Flows. *J. Fluid Mech.*, 167:353, 1986.

[dGP95] P.G. de Gennes and J. Prost. *The Physics of Liquid Crystals, 2nd Ed.* Clarendon Press, Oxford, 1995.

[DKJ+10] M.R. Dennis, R.P. King, B. Jack, K. O'Holleran, and M.J. Padgett. Isolated Optical Vortex Knots. *Nat. Phys.*, 6:118, 2010.

[Doz01] I. Dozov. On the Spontaneous Symmetry Breaking in the Mesophases of Achiral Banana-Shaped Molecules. *EPL*, 56:247, 2001.

[DR00] H. Dathe and P. Rukimbira. Foliations and Contact Structures. *Adv. Geom.*, 4:75–81, 2000.

[DR05] H. Dathe and P. Rukimbira. Fibrations and Contact Structures. *Int. Jour. Math. Sci.*, 2005.

[Dzy58] I. Dzyaloshinsky. A Thermodynamic Theory of Weak Ferromagnetism of Antiferromagnetics. *J. Phys. Chem.*, 4:241, 1958.

[EB16] H. Eynard-Bontemps. On the connectedness of the space of codimension one foliations on a closed 3-manifold. *Invent. Math*, 204:605–670, 2016.

[EG99] J. Etnyre and R. Ghrist. Gradient flows within plane fields. *Comm. Math. Helvetici*, 74:507–529, 1999.

[EG00a] J. Etnyre and R. Ghrist. Contact topology and hydrodynamics I: Beltrami fields and the Siefert conjecture. *Nonlinearity*, 13:441–458, 2000.

[EG00b] J. Etnyre and R. Ghrist. Contact topology and hydrodynamics III: Knotted orbits. *Trans. Amer. Math. Soc.*, 352:5781–5794, 2000.

[EG02a] J. Etnyre and R. Ghrist. Tight contact structures and Anosov flows. *Top. & its App.*, 124:211–219, 2002.

[EG02b] J. Etnyre and R. Ghrist. Contact topology and hydrodynamics II: Solid torii. *Ergod. Thy. & Dyn. Sys.*, 22:819–833, 2002.

[EI14] E. Efrati and W. Irvine. Orientation-Dependent Handedness and Chiral Design. *Phys. Rev. X*, 4:011003, 2014.

[EKM12] J. Etnyre, R. Komendarczyk, and P. Massot. Tightness in contact metric 3-manifolds. *Invent. Math.*, 188:621, 2012.

[Eli89] Y. Eliashberg. Classification of overtwisted contact structures on 3-manifolds. *Invent. Math.*, 98:623–637, 1989.

[Eli92] Y. Eliashberg. Contact 3-manifolds twenty years since J. Martinet's work. *Annales de l'institute Fourier*, 42:165–192, 1992.

[Eli93] Y. Eliashberg. Classification of contact structures on $\mathbb{R}^3$. *Internat. Math. Res. Notices*, 3:87–91, 1993.

[ENM+18] P.W. Ellis, K. Nayani, J.P. McInerney, D.Z. Rocklin, J.O. Park, M. Srinivasarao, E.A. Matsumoto, and A. Fernandez-Nieves. Curvature-Induced Twist in Homeotropic Nematic Tori. *Phys. Rev. Lett.*, 121:247803, 2018.

[EPS15] A. Enciso and D. Peralta-Salas. Existence of knotted vortex tubes in steady Euler flows. *Acta. Math.*, 214:61–134, 2015.

[ET91] Y. M. Eliashberg and W. P. Thurston. *Confoliations.* American Mathematical Society, 1991.

[Etn04a] J. Etnyre. Convex surfaces in contact geometry: Class notes. available at `http://people.math.gatech.edu/~etnyre/preprints/papers/surfaces.pdf`, 2004.

[Etn04b] J. Etnyre. Lectures on open book decompositions and contact structures. available at `https://people.math.gatech.edu/~etnyre/preprints/papers/oblec.pdf`, 2004.

[Etn13] J. Etnyre. On knots in overtwisted contact structures. *Quantum Topol.*, 4:229, 2013.

[Far03] M. Farber. *The Topology of Closed One-Forms*. American Mathematical Society, Mathematical Surveys and Monographs **108**, 2003.

[FG10] G. Friedel and F. Grandjean. Observations géométrique sur les liquides à coniques focales. *Bull. Soc. Fr. Minéral.*, 33:409, 1910.

[FLP79] A. Fathi, F. Laudenbach, and V. Poénaru. Traveaux de thurston sur les surfaces. *Asterisque*, 1979.

[Fra58] F. C. Frank. On The Theory of Liquid Crystals. *Disc. Faraday Soc.*, 25:18–25, 1958.

[FS83] H. Friedrich and J.M. Stewart. Characteristic initial data and wave front singularities in general relativity. *Proc. Roy. Soc. Lond*, 385:345–371, 1983.

[Ful71] F. B. Fuller. The writhing number of a space curve. *Proc. Nat. Acad. Sci. USA*, 68:815–819, 1971.

[Gei06] H. Geiges. A brief history of contact geometry and topology. *Expo. Math.*, 19:25–53, 2006.

[Gei08] H. Geiges. *An Introduction to Contact Topology*. Cambridge University Press, 2008.

[Gir91] E. Giroux. Convexité en topologie de contact. *Comm. Math. Helv.*, 66:637–677, 1991.

[Gir00] E. Giroux. Structures de contact en dimension trois and bifurcations des feuilletages de surfaces. *Invent. Math.*, 141:615–689, 2000.

[Gir02] E. Giroux. Géométrie de contact: de la dimension trois vers les dimensions supérieures. *in: Proceedings of the International Congress of Mathematicians, Vol. II, Higher Education Press, Beijing*, pages 405–414, 2002.

[Goo85] S. Goodman. Vector fields with transverse foliations. *Topology*, 24:333–340, 1985.

[Goo86] S. Goodman. Vector fields with transverse foliations II. *Ergod. Th. and Dynam. Sys.*, 24:193–203, 1986.

[Gra59] J. W. Gray. Some global properties of contact structures. *Ann. Math.*, 69:421–450, 1959.

[Gro69] M. L. Gromov. Stable mappings of foliations into manifolds. *Math. USSR Izv.*, 3:671, 1969.

[GS99] R. Gompf and A. Stipsicz. *4-Manifolds and Kirby Calculus*. Graduate Studies in Mathematics **20**, AMS, 1999.

[GV71] C. Godbillon and J. Vey. Un invariant des feuilletages de codimension 1. *C.R. Acad. Sci. Paris*, 273:92–95, 1971.

[Hel71] W. Helfrich. Electrohydrodynamic and Dielectric Instabilities of Cholesteric Liquid Crystals. *J. Chem. Phys.*, 55:839, 1971.

[HH58] H. Hirzebruch and H. Hopf. Felder von flächenelementen in 4-dimensionalen mannigfaltigkeiten. *Acta App. Math.*, 138:156–172, 1958.

[Hob63] R.H. Hobart. On the instability of a class of unitary field models. *Proc. Phys. Soc.*, 82:201–203, 1963.

[Hon98] K. Honda. Confoliations transverse to vector fields. Preprint available at `https://www.math.ucla.edu/~honda/confoliations.pdf`, 1998.

[Hon00a] K. Honda. On the classification of tight contact structures I. *Geom. Topol.*, 4, 2000.

[Hon00b] K. Honda. On the classification of tight contact structures II. *J. Differential Geom.*, 2000.

[Hop31] H. Hopf. ber die Abbildungen der dreidimensionalen Sphre auf die Kugelflche. *Mathematische Annalen*, 104:637–665, 1931.

[Hur73] J.P. Hurault. Static distortions of a cholesteric planar structure induced by magnetic or ac electric fields. *J. Chem. Phys.*, 59:2068, 1973.

[Irv18] W.T.M. Irvine. Moreau's hydrodynamic helicity and the life of vortex knots and links. *C. R. Méch.*, 346:170, 2018.

[Jän87] K. Jänich. Topological properties of ordinary nematics in 3-space. *Acta App. Math.*, 8:65, 1987.

[JLS18] A. Jákli, O.D. Lavrentovich, and J.V. Selinger. Physics of liquid crystals of bent-shaped molecules. *Rev. Mod. Phys.*, 90:045004, 2018.

[Kam96] R.D. Kamien. Liquids with Chiral Bond Order. *J. Phys. II France*, 6:461, 1996.

[Kam02] R.D. Kamien. The geometry of soft materials: a primer. *Rev. Mod. Phys.*, 74:953, 2002.

[Kan97] Y. Kanda. The classification of tight contact structures on the 3-torus. *Comm. Anal. Geom.*, 5:413–438, 1997.

[Kik07] H. Kikuchi. *Liquid Crystalline Blue Phases.* in: Liquid Crystalline Functional Assemblies and Their Supramolecular Structures. Structure and Bonding (Springer, Berlin, Heidelberg), 2007.

[KK18] M. Kleman and K.S. Krishnamurthy. Defects in the twist-bend nematic phase: Stabilities and instabilities of focal conic domains and related topics. *Phys. Rev. E*, 98:032705, 2018.

[KL82] M.V. Kurik and O.D. Lavrentovich. Negative-positive monopole transitions in cholesteric liquid crystals. *JETP Lett.*, 35:444, 1982.

[KL06] M. Kléman and O.D. Lavrentovich. Topological point defects in nematic liquid crystals. *Phil. Mag.*, 86:4117–4137, 2006.

[KL09] M. Kleman and O.D. Lavrentovich. Liquids with conics. *Liq. Cryst.*, 36:1085, 2009.

[KM16] R.D. Kamien and R.A. Mosna. The topology of dislocations in smectic liquid crystals. *New J. Phys.*, 18:053012, 2016.

[KT73] J.M. Kosterlitz and D.J. Thouless. Ordering, metastability and phase transition in two-dimensional systems. *J. Phys. C*, 6:1181–1203, 1973.

[Lie72] S. Lie. Zur theorie partieller differentialgleichungen. *Gottinger Nachrichten*, page 480, 1872.

[LK01] O.D. Lavrentovich and M. Kléman. Cholesteric Liquid Crystals: Defects and Topology. *in: H.S. Kitzerow and C. Bahr (eds) Chirality in Liquid Crystals. Partially Ordered Systems (Springer, New York)*, 2001.

[LMB+11] I.-H. Lin, D.S. Miller, P.J. Bertics, C.J. Murphy, J.J. de Pablo, and N.L. Abbott. Endotoxin-Induced Structural Transformations in Liquid Crystalline Droplets. *Science*, 332:1297–1300, 2011.

[LMP16] H.-G. Lee, S. Munir, and S.-Y. Park. Cholesteric liquid crystal droplets for biosensors. *ACS Appl. Mat. Inter.*, 8:26407, 2016.

[LT86] O.D. Lavrentovich and E.M. Terntjev. Phase transitions altering the symmetry of topological point defects (hedgehogs) in a nematic liquid crystal. *Zhurn. Eksp. Teor. Fiz.*, 91:237–1244, 1986.

[Lut71] R. Lutz. *Sur quelques propriétés des formes differentielles en dimension trois.* Thése, Strasbourg, 1971.

[MA14] T. Machon and G.P. Alexander. Knotted Defects in Nematic Liquid Crystals. *Phys. Rev. Lett.*, 113:027801, 2014.

[MA16a] T. Machon and G.P. Alexander. Global defect topology in nematic liquid crystals. *Proc. R. Soc.*, 472:20160265, 2016.

[MA16b] T. Machon and G.P. Alexander. Umbilic lines in orientational order. *Phys. Rev. X*, 6:011033, 2016.

[Mac16] T. Machon. *Aspects of Geometry and Topology in Liquid Crystalline Phases.* PhD thesis, University of Warwick, 2016.

[Mac17] T. Machon. Contact Topology and the Structure and Dynamics of Cholesterics. *New Journal of Physics*, 19, 2017.

[Mac20a] T. Machon. The Godbillon-Vey invariant as a restricted casimir of three-dimensional ideal fluids. Preprint available at `https://arxiv.org/pdf/2001.01305`, 2020.

[Mac20b] T. Machon. The Godbillon-Vey invariant as topological vorticity compression and obstruction to steady flow in ideal fluids. Preprint available at `https://arxiv.org/pdf/2002.09992`, 2020.

[MAHK19] T. Machon, H. Aharoni, Y. Hu, and R.D. Kamien. Aspects of Defect Topology in Smectic Liquid Crystals. *Comm. Math. Phys.*, 372:525542, 2019.

[Mal76] B. Malgrange. Frobenius avec singularitiés. I. codimension un. *Inst. Hautes Études Sci. Publ. Math.*, 46:163, 1976.

[Mar71] J. Martinet. Formes de contact sur les variétés de dimension 3. *in: Proc. Liverpool Singularities Sympos. II, Lecture Notes in Math.* **209**, *Springer-Verlag, Berlin*, pages 142–163, 1971.

[Max68] J.C. Maxwell. On the cyclide. *Quart. J. Pure Appl. Math.*, 9:111, 1868.

[MD16] C. Meyer and I. Dozov. Local distortion energy and coarse-grained elasticity of the twist-bend nematic phase. *Soft Matter*, 12:574, 2016.

[Mer79] N.D. Mermin. The topological theory of defects in ordered media. *Rev. Mod. Phys.*, 51:591, 1979.

[Mil65] J. W. Milnor. *Topology From The Differentiable Viewpoint.* Princeton University Press, 1965.

[Mil76] J. W. Milnor. Curvatures of left invariant metrics on Lie groups. *Advances in Mathematics*, 21:293–329, 1976.

[Mit95] Y. Mitsumatsu. Anosov flows and non-Stein symplectic manifolds. *Ann. Inst. Fourier*, 45:1407–1421, 1995.

[MKA17] E.A. Matsumoto, R.D. Kamien, and G.P. Alexander. Straight round the twist: frustration and chirality in smectics-A. *Interface Focus*, 7:20160118, 2017.

[MO18] E. Miranda and C. Oms. Contact structures with singularities. Preprint available at , 2018.

[Mor60] T. Moriya. Anisotropic Superexchange Interaction and Weak Ferromagnetism. *Phys. Rev.*, 120:91, 1960.

[Mor78] J. Morgan. Nonsingular Morse–Smale flows on 3-dimensional manifolds. *Topology*, 18:41–54, 1978.

[MR92] H.K. Moffatt and R.L. Ricca. Helicity and the Călugăreanu Invariant. *Proc.R. Soc. A*, 108 439:411–429, 1992.

[MŠT+06] I. Muševič, M. Škarabot, U. Tkalec, M. Ravnik, and S. Žumer. Two-dimensional nematic colloidal crystals self-assembled by topological defects. *Science*, 313:954, 2006.

[Muš17] I. Muševič. *Two-dimensional nematic colloidal crystals self-assembled by topological defects*. Springer International Publishing, Cham, 2017.

[MVP+15] E.A. Matsumoto, D.A. Vega, A.D. Pezzutti, N.A. Garcia, P.M. Chaikin, and R.A. Register. Wrinkling and splay conspire to give positive disclinations negative curvature. *Proc. Natl. Acad. Sci. USA*, 112:12639, 2015.

[MWM17] C. Mostajeran, M. Warner, and C.D. Modes. Frame, metric and geodesic evolution in shape-changing nematic shells. *Soft Matter*, 13:8858, 2017.

[Nab72] F.R.N. Nabarro. Singular lines and singular points of ferromagnetic spin systems and of nematic liquid crystals. *J. Phys. France*, 33:1089, 1972.

[NE18] I. Niv and E. Efrati. Geometric Frustration and Compatibility Conditions for Two-Dimensional Director Fields. *Soft Matter*, 14:424–431, 2018.

[NFO+17] A. Nych, J.-I. Fukuda, U. Ognysta, S. Žumer, and I. Muševič. Spontaneous formation and dynamics of half-skyrmions in a chiral liquid-crystal film. *Nat. Phys.*, 13:1215–1220, 2017.

[Nod00] T. Noda. Projectively Anosov flows with differentiable (un)stable foliations. *Ann. Inst. Fourier*, 50:1617–1647, 2000.

[NV12] G. Napoli and L. Vergori. Extrinsic Curvature Effects on Nematic Shells. *Phys. Rev. Lett.*, 108:207803, 2012.

[Nye83] J.F. Nye. Lines of circular polarization in electromagnetic wave fields. *Proc. R. Soc. A.*, 389:279, 1983.

[Olv95] P. J. Olver. *Equivalence, Invariants, and Symmetry*. Cambridge University Press, 1995.

[OS98] A.A. Oshemkov and V.V. Sharko. Classification of Morse–Smale flows on two-dimensional manifolds. *Sb. Math.*, 189:1205, 1998.

[P+16] Z. Parsouzi et al. Fluctuation Modes of a Twist-Bend Nematic Liquid Crystal. *Phys. Rev. X*, 6:021041, 2016.

[PČM16] G. Posnjak, S. Čopar, and I. Muševič. Points, skyrmions and torons in chiral nematic droplets. *Sci. Rep.*, 6:26361, 2016.

[PČM17] G. Posnjak, S. Čopar, and I. Muševič. Hidden topological constellations and polyvalent charges in chiral nematic droplets. *Nat. Commun.*, 8:14594, 2017.

[Po1] V. Poénaru. Some aspects of the theory of defects of ordered media and gauge fields related to foliations. *Commun. Math. Phys.*, 80, 1981.

[Pon55] L. Pontryagin. Smooth manifolds and their applications in Homotopy theory. *Trudy Mat. Inst. im Steklov, No 45, Izdat. Akad. Nauk. USSR, Moscow*, 1955.

[Pos18a] G. Posnjak. *Experimental Inspection of Director Fields.* in: Topological Formations in Chiral Nematic Droplets (Springer, Cham), 2018.

[Pos18b] G. Posnjak. *Simulated Annealing for Determination of z-Component Sign.* in: Topological Formations in Chiral Nematic Droplets (Springer, Cham), 2018.

[Pos18c] G. Posnjak. *Structures in Chiral Nematic Droplets with Homeotropic Anchoring.* in: Topological Formations in Chiral Nematic Droplets (Springer, Cham), 2018.

[PPČ+19] J. Pollard, G. Posnjak, S. Čopar, I. Muševič, and G.P. Alexander. Point Defects, Topological Chirality, and Singularity Theory in Cholesteric Liquid-Crystal Droplets. *Phys. Rev. X*, 9:021004, 2019.

[PSLW97] P. Poulin, H. Stark, T.C. Lubensky, and D.A. Weitz. Novel colloidal interactions in anisotropic fluids. *Science*, 275:1770, 1997.

[PSWZ76] J. Patera, R. T. Sharp, P. Winternitz, and H. Zassenhaus. Invariants of real low dimension lie algebras. *Jour. Math. Phys.*, 17, 1976.

[PT77] V. Poenaru and G. Toulouse. The crossing of defects in ordered media and the topology of 3-manifolds. *Journal de Physique*, 38:887–895, 1977.

[PTY91] A. Pargellis, N. Turok, and B. Yurke. Monopole-antimonopole annihilation in a nematic liquid crystal. *Phys. Rev. Lett.*, 67:1570, 1991.

[PV20] A. Pedrini and E.G. Virga. Liquid crystal distortions revealed by an octupolar tensor. *Phys. Rev. E*, 101:012703, 2020.

[PVK+13] E. Pairam, J. Vallamkondu, V. Koning, B.C. van Zuiden, P.W. Ellis, M.A. Bates, V. Vitelli, and A. Fernandez-Nieves. Stable nematic droplets with handles. *Proc. Natl. Acad. Sci. USA*, 110:9295–9300, 2013.

[RL88] S.R. Renn and T.C. Lubensky. Abrikosov dislocation lattice in a model of the cholesteric–to–smectic-A transition. *Phys. Rev. A*, 38:2132, 1988.

[RL11] L. Radzihovsky and T.C. Lubensky. Nonlinear smectic elasticity of helical state in cholesteric liquid crystals and helimagnets. *Phys. Rev. E*, 83:051701, 2011.

[RS99] A. Rudinger and H. Stark. Twist transition in nematic droplets: a stability analysis. *Liquid Crystals*, 26:753–758, 1999.

[RW73] B. Reinhart and J. Wood. A Metric Formula For The Godbillon–Vey Invariant For Foliations. *Proc. Amer. Math.*, 38, 1973.

[RŽ09] M. Ravnik and S. Žumer. Landau-de Gennes modelling of nematic liquid crystal colloids. *Liq. Cryst.*, 36:1201–1214, 2009.

[S+91] T. Beng Saw et al. Topological defects in epithelia govern cell death and extrusion. *Nature*, 544:212–216, 1991.

[SDS13] S. Shamid, S. Dhakal, and J.V. Selinger. Statistical mechanics of bend flexoelectricity and the twist-bend phase in bent-core liquid crystals. *Phys. Rev. E*, 87:052503, 2013.

[Sel18] J.V. Selinger. Interpretation of saddle-splay and the Oseen–Frank free energy in liquid crystals. *Liq. Cryst. Rev.*, 6:129, 2018.

[SL01] I.I. Smalyukh and S.V. Shiyanovskii O.D. Lavrentovich. Three-dimensional imaging of orientational order by fluorescence confocal polarizing microscopy. *Chem. Phys. Lett.*, 336:88–96, 2001.

[SLH+13] B. Senyuk, Q. Liu, S. He, R.D. Kamien, R.B. Kusner, T.C. Lubensky, and I.I. Smalyukh. Topological colloids. *Nature*, 493:200, 2013.

[SMS20] J-F Sadoc, R. Mosseri, and J.V. Selinger. Liquid crystal director fields in three-dimensional non-euclidean geometries. Preprint available at arXiv:2006.12668, 2020.

[SPRŽ12] D. Seč, T. Porenta, M. Ravnik, and Slobodan Žumer. Geometrical frustration of chiral ordering in cholesteric droplets. *Soft Matter*, 8:11982, 2012.

[ŠRŽ+07] M. Škarabot, M. Ravnik, S. Žumer, U. Tkalec, I. Poberaj, D. Babič, N. Osterman, and I. Muševič. Two-dimensional dipolar nematic colloidal crystals. *Phys. Rev. E*, 76:051406, 2007.

[Ste74] P. Stefan. Accessible sets, orbits and foliations with singularities. *Proc. London Math. Soc.*, 29:699–713, 1974.

[Sus73] H.J. Sussmann. Orbits of families of vector fields and integrability of distributions. *Trans. Amer. Math. Soc.*, 180:171–188, 1973.

[Sut07] P. Sutcliffe. Knots in the Skyrme–Faddeev model. *Proc. R. Soc. A*, 463:3001–3020, 2007.

[SWM83] J.P. Sethna, D.C. Wright, and N.D. Mermin. Relieving Cholesteric Frustration: The Blue Phase in a Curved Space. *Phys. Rev. Lett.*, 51, 1983.

[Tau07] C. H. Taubes. The SeibergWitten equations and the Weinstein conjecture. *Geom. Topol.*, 11:2117–2202, 2007.

[Tay34] G.I. Taylor. The mechanism of plastic deformation of crystals. Part I.–Theoretical. *Proc. R. Soc. A*, 145:362–387, 1934.

[Tho54] R. Thom. Quelques propriétés globales des variétés différentiables. *Comm. Math. Helv.*, 28:17–86, 1954.

[TK76] G. Toulouse and M. Kléman. Principles of a classification of defects in ordered media. *Jour. Phys. Lett.*, 37:149–151, 1976.

[TLB+16] L. Tran, M.O. Lavrentovich, D.A. Beller, N. Li, K.J. Stebe, and R.D. Kamien. Lassoing saddle splay and the geometrical control of topological defects. *Proc. Natl. Acad. Sci. USA*, 113:7106, 2016.

[Tri04] J.J. Tripp. *Contact Structures on Open 3-Manifolds*. PhD thesis, University of Pennsylvania, 2004.

[TS19] J-S.B. Tai and I.I. Smalyukh. Three-dimensional crystals of adaptive knots. *Science*, 365:1449, 2019.

[TW75] W.P. Thurston and H.E. Winkelnkemper. On the existence of contact forms. *Proc. Amer. Math. Soc.*, 52:345–347, 1975.

[VAG+18] G.T. Vu, A.A. Abate, L.R. Gómez, A.D. Pezzutti, R.A. Register, D.A. Vega, and F. Schmid. Curvature as a Guiding Field for Patterns in Thin Block Copolymer Films. *Phys. Rev. Lett.*, 121:087801, 2018.

[VI13] V. Vitelli and W.T.M. Irvine. The geometry and topology of soft materials. *Soft Matter*, 9:8086, 2013.

[Vir19] E.G. Virga. Uniform distortions and generalized elasticity of liquid crystals. *Phys. Rev. E*, 100:052701, 2019.

[VL83] G.E. Volovik and O.D. Lavrentovich. Topological dynamics of defects: boojums in nematic drops. *Zh. Eksp. Teor. Fiz.*, 85:1997, 1983.

[VM77] G.E. Volovik and V.P. Mineev. Particle-like solitons in superfluid 3He phases. *Zh. Eksp. Teor. Fiz,*, 73:767–773, 1977.

[WB15] T.J. White and D.J. Broer. Programmable and adaptive mechanics with liquid crystal polymer networks and elastomers. *Nat. Mater.*, 14:1087, 2015.

[WMB+16] X. Wang, D.S. Miller, E. Bukusoglu, J.J. de Pablo, and N.L. Abbott. Topological defects in liquid crystals as templates for molecular self-assembly. *Nat. Mater*, 15:106–112, 2016.

[Zhi93] M. Zhitomirskiĭ. *Typical Singularities of Differential 1-Form and Pfaffian Equations.* AMS Translations of Mathematical Monographs, 1993.